Physical Modeling of the Downwash Effect of Rooftop Structures on Plume Dispersion

Amit Gupta

A Thesis

in

The Department

of

Building, Civil and Environmental Engineering

Presented in Partial Fulfillment of the Requirements
for the Degree of Doctor of Philosophy (Building Engineering) at
Concordia University
Montreal, Quebec, Canada

Feburary 2009

Your file Votre référence
ISBN: 978-0-494-63441-7
Our file Notre référence
ISBN: 978-0-494-63441-7

ABSTRACT

Physical Modeling of the Downwash Effect of Rooftop Structures on Plume Dispersion

Amit Gupta, Ph.D.
Concordia University, 2009

One of the major causes of poor indoor air quality in buildings is exhaust re-ingestion at fresh air intakes. The downwash effect of an RTS on plume may lead to significantly increased levels of re-ingestion. The present study aims to quantify the downwash effect of an RTS located upwind of a stack.

Wind-tunnel modeling is used to model the flow and dispersion associated with various building/RTS arrangements with a focus on "micro-scale" urban dispersion; that is, modeling dispersion within a range of 100 m of the building exhaust. Wind-tunnel techniques include flow visualization and tracer gas experiments. The influence of various key parameters, such as building height, RTS crosswind width, stack height, exhaust momentum ratio, stack location, and wind direction is considered. Concentration measurements were obtained at sampling locations downwind of the RTS on the building roof. It was found that the downwash effect of RTS on plumes could increase roof -level concentrations by a factor of 2 to 100. The RTS downwash effect was intensified with an increase in RTS crosswind width and was generally stronger for an oblique wind than for a normal wind. The results also showed that an RTS engulfed inside the building recirculation zone may not have a significant effect on plume dispersion for winds approximately normal to the building face.

The minimum dilution models recommended by ASHRAE (2003, 2007) as well as the ASHRAE Geometric Stack Design Method (AGM) were evaluated. It was found that the ASHRAE models do not account for the downwash effect of the RTS on plumes and result in either overly conservative or un-conservative predictions. Therefore, a new empirical model, which takes into consideration the downwash effect of RTS was proposed. A validation study of the proposed model using results from previous experimental studies showed that the model is more accurate than the ASHRAE dilution models. Thus the proposed model will be very useful to practicing engineers. In addition, some modifications to the ASHRAE (2007) dispersion model and the AGM are also proposed.

ACKNOWLDGEMENTS

I would like to thank my supervisors Dr. T. Stathopoulos and Dr. P. Saathoff for their advice, direction and continued support throughout the study.

Many, many thanks and loving appreciation is due to my parents for all their caring and love. In particular, to my dearest wife Suniti for putting up with it all and supporting me regardless...!

Finally yet importantly, I am thankful to my dear friend and colleague B. Hajra for his support and to all of them who directly or indirectly helped me to complete thesis.

TABLE OF CONTENTS

LIST OF FIGURES

LIST OF TABLES

NOMENCLATURE

A	area of building upwind face	(m^2)
A_e	cross-sectional areas of exhaust stack	(m^2)
A_m	projected area of wind tunnel model	(m^2)
A_o	cross-section area of wind tunnel	(m^2)
B_l	distance dilution parameter in Wilson and Lamb D_{min} model	(-)
B_L	larger of two upwind face dimensions (height and width)	(m)
B_s	smaller of two upwind face dimensions (height and width)	(m)
C	contaminant concentration at receptor	(-)
C_e	exhaust concentration	(-)
C_{max}	maximum contaminant concentration at a receptor	(-)
C_N	normalized concentration	(-)
C_y	concentration at lateral distance y from stack	(-)
D	dilution factor	(-)
D_d	distance dilution	(-)
d_e	stack diameter	(m)
D_h	plume height factor	(-)
D_{min}	minimum dilution D at the receptor	(-)
$(D_{min})_{WL}$	minimum dilution D with Wilson and Lamb (1994) model	(-)
D_o	initial dilution	(-)
D_N	normalized dilution	(-)
D_r, D_s	ASHRAE (2003) and ASHRAE (2007) minimum dilution models	(-)
F_m	momentum flux	(m^4/s^2)

F_r	Froude number	(-)
H	building height	(m)
H_p	plume centerline height from classical Gaussian model	(m)
h	height of rooftop structure (RTS)	(m)
h_{AGM}	stack height estimated using ASHRAE Geometric Method (AGM)	(m)
h_{MAGM}	stack height estimated using modified AGM (MAGM)	(m)
h_c	height of roof recirculation zone	(m)
h_d	stack tip downwash correction factor	(m)
h_p	plume height	(m)
h_r	plume rise of uncapped vertical exhaust	(m)
h_{req}	stack height required to escape downwash due to RTS	(m)
h_s	physical exhaust stack height (above roof level)	(m)
h_{small}	maximum plume height required to avoid critical receptor	(m)
h_{top}	height of highest of intake, active obstacle, or recirculation zone on a rooftop between stack and intake	(m)
Δh	effective plume rise	(m)
h_f	final plume rise height of the fully bent over plume	(m)
h_m	jet momentum rise	(m)
$h_{f.m}$	final momentum rise height	(m)
I_u	turbulence intensity	(-)
i	sample number	(-)
l	smaller of building crosswind width and building height	(-)
ΔT	change in temperature	(°C)

k^*	normalized concentration from Schulman and Scire (1991)	(m^2)
k	normalized concentration from Halitsky (1995)	(-)
l	along-wind length of Rooftop structure	(m)
L	along-wind length of building	(m)
L_c	length of separation bubble at the leading edge of the building	(m)
L_r	length of separation bubble downwind of the leading edge of the building	(m)
l_c	length of separated flow region on RTS leading edge	(m)
l_r	length of separated flow downwind of the leading edge of the RTS	(m)
M	exhaust momentum ratio (w_e/U_H)	(-)
ME	measured dilution	(-)
N	number of samples	(-)
P	predicted dilution with proposed model	(-)
Q	exhaust flow rate	(m^3/s)
R	recirculation length scale	(m)
Re_b	building Reynolds number	(-)
Re_s	stack Reynolds number	(-)
R_i	Richardson number	(-)
S(#)	stack location	(-)
S	exhaust to intake stretch-string distance	(m)
S(n)	power spectral density function	(-)
T_a	ambient temperature	(°C)
T_s	exhaust temperature at stack tip	(°C)

t_{avg}	averaging time	(s)
u	fluctuating components of wind speed	(m/s)
U	mean components of wind speed	(m/s)
U_g	wind speed at gradient height	(m/s)
U_H	wind speed at height H	(m/s)
U_s	wind speed at stack tip	(m/s)
U(z)	mean velocity at height z	(m/s)
U*	friction velocity	(m/s)
W	crosswind width of building	(m)
w	crosswind width of RTS	(m)
w_e	exhaust velocity	(m/s)
X_c	distance from upwind edge of the roof to H_c	(m)
$X_{m,f}$	plume rise final distance	(m)
x_c	distance from upwind edge of the roof to h_c	(m)
x_s	separation between stack and rooftop structure	(m)
x_o	virtual origin upstream distance	(-)
x, y, z	distances [x – downwind, y – lateral and z – vertical distances]	(m)
y_c	lateral displacement of plume	(m)
Z	receptor height	(m)
Z_g	gradient height	(m)
z_o	roughness length	(m)

Greek Symbols

α	power law exponent	(-)
β	capping factor	(-)

βj	jet entrainment	(-)
θ	wind direction	(degrees)
ν	kinematic viscosity	(m^2/s)
ξ	vertical separation above h_{top}	(-)
ρ_a	density of air	(kg/m^3)
ρ_e	density of exhaust gas	(kg/m^3)
σ	standard deviation	(-)
σ_o	standard deviation of initial plume spread	(m)
σ_u	standard deviation of wind velocity in along-wind direction	(m/s)
σ_y	standard deviation of crosswind plume spread	(m)
σ_z	standard deviation of vertical plume spread	(m)
σ_θ	standard deviation of wind direction	(m)
φ	ratio of ASHRAE estimated D_N with measured D_N	(-)
φ_r	ratio of normalized D_r estimated with ASHRAE (2003, 2007) to measured D_N	(-)
φ_s	ratio of normalized D_s estimated with ASHRAE (2003, 2007) to measured D_N	(-)
φ_{mod}	ratio of normalized D_N estimated with modified ASHRAE to measured D_N	(-)

Chapter 1

INTRODUCTION

1.1 General

One of the major causes of poor indoor air quality in buildings is the sporadic occurrence of exhaust reingestion at fresh air intakes. Universities, hospitals, and industrial laboratories, as well as manufacturing facilities, are particularly susceptible to this phenomenon since they emit a wide range of toxic and odorous chemicals. Unfortunately, the state-of-the-art is not sufficiently advanced to allow building engineers to apply appropriate design criteria to avoid this problem. Consequently, numerous incidents of poor indoor air quality have been recorded and documented [Meroney (1999), Petersen (2002a)].

The most fundamental and effective way to minimize the problem of exhaust re-ingestion is the suitable design and placement of exhaust stacks and air intakes in buildings. However, due to practical limitations, it is not always possible to avoid exhaust reingestion problems all the time. The job of the designer is to reduce the risk of exhaust reingestion to acceptable levels at a reasonable cost.

The designer must choose an appropriate method to estimate the dilution of building exhausts. In general, six methods are available: wind tunnel simulations, full-scale measurements, the classical Gaussian model, modified Gaussian models, semi-

empirical models and numerical modeling techniques, such as computational fluid dynamics (CFD), puff models, and lagrangian models.

i) Fluid modeling, either by wind tunnel or water flume, can give relatively accurate predictions of exhaust dilution around buildings if the required dispersion modeling criteria are satisfied. Fluid modeling is especially useful for modeling the effects of surrounding buildings and topography, which are difficult to consider in some of the other modeling methods discussed below. Wind tunnel and water flume simulations are reliable, repeatable, and can be conducted at the designer's convenience. The discussion on fluid modeling is presented in Section 2.4.1.

ii) Full-scale or field testing provides the most accurate assessment of the plume dispersion for existing facilities. However, field studies are very expensive, time-consuming and labor intensive. Therefore, full-scale studies are used primarily for validating empirical dispersion models or fluid modeling methods. The discussion on full-scale studies with a focus on building-exhaust dispersion is presented in Section 2.4.2.

iii) The only analytical model to predict pollutant dispersion in the urban environment that is available in the literature is the "Gaussian Model." The classical Gaussian plume model is one of the most commonly used methods for estimating the plume dispersion downstream of a continuous source. It is based on the assumption that the lateral and vertical plume spreads follow a Gaussian distribution. The major advantages of the

Gaussian model are that it is a good representation of the random nature of the atmospheric turbulence with a solution that can be acquired by mathematical operations. However, the main disadvantage of the Gaussian model is that it does not take into consideration the turbulence generated by the surrounding buildings or the building itself—especially when the exhaust sources are located downwind of an obstruction such as buildings or rooftop structures. This model is presented in Section 2.4.5.1.

iv) Various researchers have modified the basic Gaussian plume model to simulate micro-scale dispersion near a structure. A few popular modified Gaussian approach-based plume dispersion models are presented in Section 2.4.5.2.

v) Another important dispersion modeling technique uses semi-empirical models. These models are based on concentration measurements obtained either in full-scale, wind tunnel, or water flume simulations. These were developed to provide the plume centerline dilutions and are generally based on the exhaust/intake characteristics, such as exhaust speed, stack diameter, and intake locations. However, these models, which are presented in Section 2.4.5.3, do not take into consideration the general structure of the flow around buildings.

vi) In the past decade, significant progress has been made in numerical modeling methods using more sophisticated techniques, such as CFD,

puff models, and lagrangian approach models. Computer simulation of wind flow around buildings may eventually be more cost effective and convenient than all other methods listed above. However, due to the complexity of flow around buildings, the success of numerical modeling techniques for building-scale dispersion has so far been rather limited and these models are recommended primarily for far-field dispersion. Further discussion on numerical modeling methods is outside the focus of this paper

1.2 Present study

The main motivation behind this research lies in the need to improve current plume dispersion models that are recommended for building-scale dispersion; i.e. ASHRAE (2003) and ASHRAE (2007) minimum dilution models. Although dispersion around buildings with flat roofs has been the focus of most of the previous building-scale dispersion studies, buildings are generally not flat-roofed. In fact, most of the buildings have some type of rooftop structure (RTS), which could be in the form of a skylight, penthouse, elevator rooms, or any other temporary or permanent structure. The shape of the structure can also vary depending on its use. Very few studies have examined the effect of rooftop geometry on plume dispersion [for e.g. Wilson (1979)], Schuyler and Turner (1989), Saathoff et al. (2002, 2008), and Gupta et al. (2005a)].

The focus of the present research is on "micro-scale" urban dispersion; that is, modeling dispersion within 100 m of the building exhaust. Wind tunnel modeling is used to investigate the influence of RTS on building-exhaust dispersion. In particular, the

downwash effect of an RTS on plume dispersion is investigated and quantified for typical low-rise and high-rise buildings. In addition, the research intends to evaluate ASHRAE dispersion models, and develop and validate an empirical plume dispersion model that takes into account the downwash effect of RTS of plume dispersion.

Figure 1.1 schematically shows the cause of plume downwash for a typical building. Far upwind of the building, the streamlines are horizontal. However, as the flow reaches the building, the streamlines begin to slope upwards and the flow accelerates. On the leeward side of the building, the streamlines descend and the flow eventually reattaches to the ground. This reattachment location separates the near- and far-wake regions. The trajectory of a plume will depend on the emission location. A plume emitted in the near wake (outside of the high turbulence region) of an RTS will be in the descending flow region and downwash will occur. On the other hand, a plume emitted in the far wake of the RTS will experience little downwash since the mean flow streamlines are nearly horizontal.

The main objectives of the present study are to:

i. conduct a preliminary wind-tunnel study to determine the key parameters and building/RTS configurations that influence RTS downwash;

ii. conduct a comprehensive wind-tunnel study for several building/RTS configurations;

iii. evaluate ASHRAE (2003) and ASHRAE (2007) plume dispersion models and provide recommendations to improve their performance;

iv. evaluate the ASHRAE Geometric Stack Design Method (AGM) and provide recommendations to improve its performance;

v. develop and validate an empirical micro-scale plume dispersion model to estimate dilutions within 100 m from exhausts located on the roof of a building. The model also considers the downwash effect of an RTS on plume dispersion.

1.3 Outline of the thesis

The thesis is organised in the following manner: Chapter 2 presents the fundamentals of atmospheric dispersion and a brief review of past research on micro-scale dispersion modeling. Chapter 3 discusses in detail the experimental methodology, while Chapter 4 discusses the main findings from wind tunnel simulations. Chapter 5 demonstrates the performance and provides recommendations to improve the ASHRAE (2003) and ASHRAE (2007) dispersion models and AGM. In Chapter 6 the proposed micro-scale plume dispersion model is discussed and results of validation tests are presented. Finally, the conclusions, new developments, limitations and recommendations of the present study, and suggestions for future research are presented in Chapter 7.

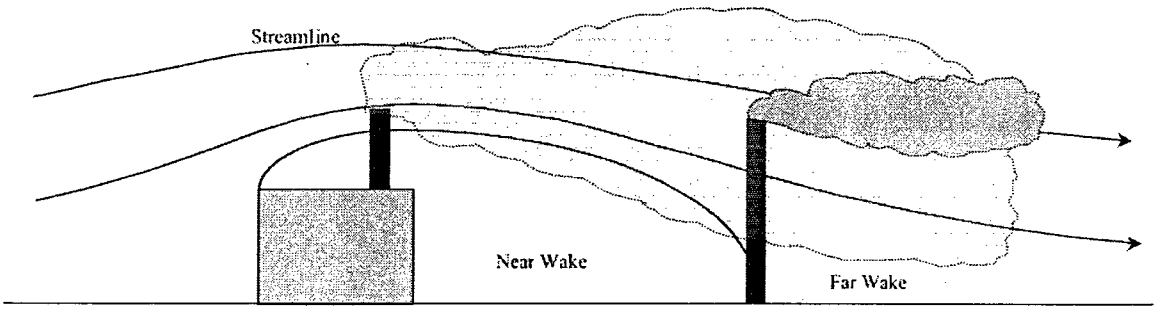

Figure 1.1 Schematic representation of two identical emission sources showing the dependence of plume dispersion on stack proximity to a structure [from Schulman et al. (2000)].

Chapter 2

LITERATURE REVIEW

2.1 Introduction

This chapter discusses the fundamental aspects involved in the aerodynamics of buildings and the dispersion of pollutants around structures. Various experimental works related to micro-scale dispersion are discussed with special attention to building/RTS downwash. Finally, various plume dispersion models relevant to building-scale dispersion are also discussed.

2.2 Urban dispersion

Modeling urban dispersion is an active area of research, which combines various disciplines, such as wind engineering, building physics, applied meteorology and environmental engineering. In simple terms, dispersion modeling is the estimation of the concentration of a pollutant coming out from an exhaust source at any distance from that source.

Due to the nature of the air flow around buildings, urban dispersion is difficult to model using mathematical techniques. Along with the atmospheric conditions, other factors, such as topography, building shape, source location, and exhaust characteristics must be considered. Figure 2.1, taken from Robins and Macdonald (1999) shows typical dispersion patterns for ground level emissions upwind or downwind of a building. For instance, Figure 2.1(k) shows how a small building downwind of a source may force

most of the exhaust to pass to one side of the building, thus breaking the symmetry that would otherwise exist. Other cases in Figure 2.1 (Figure 2.1f–2.1j) indicate the wide range of possible dispersion patterns for elevated sources.

A plume originating from sources on or near a building has a width much smaller than the length-scale of building-generated turbulence. Consequently, the dispersion for such building/source configurations is particularly sensitive to the building shape, rooftop obstructions, and small changes in incident wind speed and direction. The present research corresponds to dispersion at micro-scale since it involves plume dispersion within 100 m from the source. However, this regime is the most difficult to model because the dispersion patterns are highly complex. In order to model micro-scale dispersion, it is important to understand the nature of flow around buildings. The following section describes the flow characteristics of the simplest case: an isolated, prismatic building.

2.3 Nature of flow: Flow patterns around an isolated building

Although the majority of buildings are surrounded by other buildings, most building aerodynamics research has been carried out for isolated buildings of relatively similar shape. But even for an isolated building, the flow patterns are extremely complex and best understood using a fluid modeling technique such as a boundary layer wind tunnel or water flume. A number of wind-tunnel studies have been carried out on bluff structures to investigate flow patterns and dispersion [for e.g. Cermak (1976, 1995), Castro and Robins (1977), Hunt et al. (1978), Wilson (1979), Ogawa et al. (1983), Snyder and Lawson (1994), and Snyder (2005)].

The flow around a bluff body considerably depends on its shape and its orientation to the approaching wind. The following are the general mean flow characteristics in the various regions around an isolated obstacle:

1) flow displacement

2) separated flow (rooftop, sides, and wake cavity)

3) ground-based horseshoe vortex

4) rooftop trailing vortices

Figure 2.2 shows these flow regions as presented by Hunt et al. (1978). These flow patterns are described in detail below to provide the background for understanding the dispersion behavior around buildings.

1) Flow Displacement

Flow displacement occurs when mean streamlines in the approach flow are deflected over the building, as shown in Figure 2.2a. They may cause the plume from an upwind source to be carried over the building, thus avoiding contamination of the building. Flow displacement may also cause increased ground-level concentrations by forcing the elevated plume towards the ground in the near-wake recirculation region of the building (building downwash) as shown earlier in Figure 1.1.

2) Separated flow

Separated flow regions occur where the flow detaches at the building surface. The separation could occur around the building edges forming a re-circulating wake on

the roof, and on the sides or down wind of the building (near-wake), as shown in Figure 2.2b. These regions are characterized by low mean velocity and high turbulence. The recirculation zone formed on the roof is typically known as 'separation bubble'. The bubble can either re-attach or merge with the downwind near-wake. The dimensions of the bubble depend on two factors: 1) building dimensions and, 2) upstream atmospheric turbulence. Pollutants emitted into such regions (separation bubble and near-wake) could get entrained producing high concentrations on building roofs or at ground level.

Beyond the near wake region is the 'far-wake'. In this region, the turbulence is less intense than the near-wake but is enhanced compared to the approach flow and decays gradually with distance. The effect of far-wake region on exhausts discharged downwind of a building could extend downwind up to 3H–6H and for a narrow building and up to 10H-30H downwind for wider buildings, where H is the building height, [Peterka et al. (1985)].

3) Ground-based horseshoe vortex

For a flow normal to face of a building, a ground-based horseshoe vortex forms at around the upwind face of a building. This is driven by the vorticity in the approaching boundary layer, which causes the flow to curl downward on the upwind face and roll around the sides of the building – see Figures 2.2b and 2.2c. For an oblique wind the stagnation point cannot remain on the edge since the flow tends to flip from side to side with "vortex shedding" on alternate sides. Pollutants captured in this region could spread laterally around the building instead of over the building.

4) Roof edge trailing vortices

Roof-edge trailing vortices are formed along the building roof edges for winds approaching the building leading edge at oblique angles, as shown in Figure 2.2c. The size and strength of these vortices depend on the approaching wind angle and cross-sectional shape of the building.

Figure 2.3 illustrates the flow regimes around a tall building for normal and oblique winds as suggested by Wilson (1979). He notes that when the angle between the upwind face of a building and the approaching wind direction is less than 70°, the recirculation cavities become very small and intense roof-edge trailing vortices develop along the upwind edges of the roof. The dimensions of the vortices depend on the building geometry, wind direction and upstream turbulence. These vortices can have a strong influence on plume trajectories, by bringing a plume to the roof and producing high concentrations at the roof level.

An extensive wind tunnel study was conducted by Snyder and Lawson (1994) to illustrate the mean flow fields in the wake of buildings with various shapes and for wind direction varying from 0° to 60°. Velocity measurements were obtained around buildings using pulse-wire anemometry. The crosswind dimensions of the building were W, 2W, 4W and 10W, with L = W = H. The authors also looked into the effect of building height and along-wind length on the downwind wake. Figure 2.4 shows the flow fields in a vertical plane along the building centerline with widths varying from W to 10W. The most prominent effect was the lifting of streamlines with the increase in building width. The length of the downwind wake significantly increased from 1.5H to 5.5H, with a ten-

fold increase in building width. The height of the cavity increased from H to 1.5H. Moreover, for a normal wind, the separation bubble reattached to the roof of the cubical building (W/H = 1). The authors noted that the height and along wind length of the building did not have a significant effect on the stream-wise length of downwind wake cavity compared to the crosswind width.

Wilson et al. (1998) used water flume simulations to investigate flow patterns around various building configurations. Figure 2.5 illustrates the flow patterns for a particular configuration in which a low-rise building is located in the wake of a taller building. Note that the plume discharged from the roof of the low-rise building is entrained within the wake of the taller upwind building and as a result, the leeward wall of the upwind building and the entire roof of the lower emitting building are exposed to the plume. Saathoff et al. (2003b) showed similar findings from full-scale tests in which exhaust was released from the roof of a low-rise building located adjacent to a tall upwind building.

2.4 Dispersion modeling

Estimating pollutant concentration around buildings can be done by using different methods. These include wind-tunnel/water flume modeling, full-scale experiments, and, empirical, analytical, or computational modeling. Of these methods, wind-tunnel modeling is the most popular method. It is a fast, reliable, and cost-effective solution in comparison to a full-scale study or by CFD. Figure 2.6 shows a wind tunnel set-up at a model scale of 1:200 [from Stathopoulos (2003)], indicating the level of detail involved in wind-tunnel modeling. The most comprehensive reviews of wind-tunnel

research on dispersion around buildings are those of Meroney (1982, 1990) and Hosker (1984, 1985).

In the wind tunnel, the most common method to simulate dispersion from building exhausts is by releasing a tracer gas of know concentration and sampling it at required locations. In past, researchers have used different gases (tracer) to simulate dispersion of exhaust. For example, previous studies such as Snyder and Lawson (1976) used a methane-air mixture, Robins and Castro (1977) used helium-propane, Snyder (1994) used air-helium-methane mixture, and Schulman and Scire (1991) used ethane as a tracer gas. The tracer concentrations were determined by flame ionization detector. However, other researchers such as Lamb and Cronn (1986), Stathopoulos et al. (2002, 2003), and Saathoff et al. (2002, 2008) used sulfur hexafluoride as a tracer gas in the wind tunnel with sample concentrations determined by a gas chromatograph.

As discussed previously, fluid modeling can also be carried out in a water flume. Wilson et al. (1998) used laser induced fluorescence technique to quantify building exhaust dispersion in water flume. Wilson used a fluorescent dye as a tracer, which was illuminated with laser sheet lighting. The concentrations were obtained by detecting the fluorescent light with a video camera, which was calibrated against known concentrations of the tracer.

The following sections summarize a few significant wind-tunnel and full-scale studies with consideration to building-exhaust dispersion. A few popular empirical and analytical dispersion models will also be discussed.

2.4.1 Wind-tunnel studies

The majority of the previous research on building-scale dispersion has been conducted for isolated buildings [for e.g. Halitsky (1961, 1962, and 1963), Wilson (1976, and 1977), Robins and Castro (1977), Thompson (1993), Wilson and Britter (1982), and Wilson and Chui (1994)]. Although isolated buildings are not typical, such studies allow the investigation of fundamental processes. This section discusses a few studies, which shows the effect of stack height, wind direction, exhaust momentum ratio, and upstream turbulence on building exhaust dispersion.

Wilson (1976) investigated dispersion from exhausts released from the roof of isolated buildings. Rooftop concentrations were obtained for low values of exhaust momentum ratio ($M < 1$) and flush stacks. Exhaust momentum ratio is defined as $(\rho_e/\rho_a)^{0.5}(w_e/U_H)$, where w_e is the exhaust speed, U_H is the wind speed at the building height, ρ_e and ρ_a are the exhaust and ambient air densities. Note that for ρ_e and ρ_a, $M = w_e/U_H$. He developed a dispersion model to estimate pollutant concentration on roof of buildings for exhausts and intakes located on same building roof.

$$D_{min} = 0.11\ (U_H S^2)/Q \qquad \text{[Eq 2.1]}$$

where U_H is the mean wind speed at building height, S is defined as the stretch-string distance or the minimum distance between exhaust and vent location, and Q is the flow rate of the exhaust released from the vent. The model did not take into consideration the effect of stack height and exhaust momentum ratio. Moreover, the results are not of much use for practical stack design purpose because the concentration data were obtained for such low M values.

The model was extended by Wilson (1977). He investigated the effect of building shape and vent location on the dispersion of a non-buoyant building exhaust in a boundary layer wind tunnel. Concentration measurements were obtained on the walls of two buildings with aspect ratio (W/H) 0.3 and 0.6 representing typical medium- to high-rise structures. For both buildings, L = 2W. He suggested that based on the appropriate scale factors for the wind tunnel, the 7.5 cm tall model will correspond to full-scale building height of 40 m to 150 m. Wilson showed that the model worked reasonably well for estimating concentrations on building surfaces from exhausts released from vents located on building surfaces.

The effect of wind direction on building exhaust dispersion was studied by Li and Meroney (1983), Wilson and Chui (1985), and Chui and Wilson (1988). Li and Meroney (1983) investigated the dispersion of exhausts from roof vents of a cubical building for different exhaust locations and wind directions (0°–45°). Vertical and horizontal concentration profiles were obtained on the cube surfaces and at ground level in the wake of building. The experiments were performed with a very low exhaust momentum ratio. Li and Meroney (1983) found that for low M values ($M < 0.07$) a change in wind direction from $\theta = 0°$ to 45° could decrease the roof-level concentrations by a factor of 3–9 and suggested a correction factor (f) for equation 2.1.

$$f(\theta) = 1/(1+4\,\theta/\pi) \qquad \text{[Eq 2.2]}$$

where θ is the incidence angle varying between 0 and $\pi/4$

Wilson and Chui (1985) found that roof level dilutions are independent of wind direction contradicting Li and Meroney (1983) finding. Chui and Wilson (1988) later

clarified this contradiction between the earlier two studies and demonstrated that for large exhaust momentum (M > 1) roof level dilutions are independent of wind direction up to 30°. For wind angles greater than 30° and low exhaust momentum ratios, the dilutions were found to be 2–8 times higher than those found for normal wind ($\theta = 0$).

Schulman and Scire (1991) conducted wind-tunnel experiments on an isolated building to investigate the effect of stack height and exhaust speed on rooftop concentration for wind directions 0° and 45°. The 15 m tall building has a square plan with the length and width equal to 75 m. Plume centerline concentrations were obtained on the building roof, leeward wall, and at ground level for stack height (h_s) varying from 0 to 7.5 m and for w_e/U_H (or M if ρ_e and ρ_a)values ranging from 0.75 to 5. The concentration measurements were presented in the form of normalized concentration 'k*', which is calculated using the expression CU_H/Q, where C is the ratio or the source concentration to receptor concentration, U_H is the wind speed at building height H, and Q is the flow rate of the tracer. Schulman and Scire (1991) found that increasing the stack height or exhaust speed by a factor of 3 decreases the roof-level concentration near the stack by a factor of 100, as shown in Figures 2.7a and 2.7b. However, the results also indicated that the influence of exhaust speed and stack height starts diminishing rapidly with the increase in distance from the stack. Wilson (1998), Wilson and Winkel (1982), Petersen et al. (1999), and Petersen (2002b) reported similar findings from wind-tunnel or water flume tests carried out on isolated buildings.

Wilson and Netterville (1978) and Saathoff et al. (1995) studied the effect of turbulence on near-field dispersion by carrying out wind-tunnel experiments for buildings

with different model scales. Wilson and Netterville (1978) conducted experiments for three model scales (1:500, 1:1000, and 1:2000) by measuring building surface concentration around a rectangular model building in a simulated atmospheric boundary layer with model scale dimensions as H = 7 cm and L = W = 5 cm. They noted that modeling of mean concentrations is not particularly sensitive to the model-scale. Thus, the wind-tunnel results are applicable to a wider range of applications in the full-scale than indicated by an examination of strict turbulence modeling. Saathoff et al. (1995) concurred with the above finding. Saathoff et al. (1998) conducted wind tunnel tests for exhaust released from building roof. Roof level dilutions were obtained with two upstream exposures – open country and urban terrain - to quantify influence of free-stream turbulence on near-field dilution of exhaust from building vents. They noted that the roof level dilutions increased by a factor of about 2 by changing the upstream exposure from open country terrain to urban country terrain.

2.4.2 Full-scale studies

Full-scale testing avoids difficulties and assumptions encountered in wind-tunnel simulations. However, field studies are very expensive, time consuming, and labor intensive. Nonetheless, they are most useful for understanding complex dispersion processes and for validating dispersion models. A number of field studies have investigated building-exhaust dispersion. Many of the previous full-scale studies have used idealized, isolated and relatively smaller building sizes to evaluate various atmospheric and exhaust parameters [for e.g. Ogawa et al. (1983), Higson et al. (1994 and 1995), Okiawa and Meng (1997)].

The most extensive set of tracer data from rooftop emissions was provided by Lamb and Cronn (1986) for a building located on the campus of Washington State University (WSU) campus. Concentration measurements on the roof and at ground level were taken for various stack heights and exhaust flow rates over a sampling time of 1 hour. Therefore, an averaging time correction is required to allow comparison with model estimates. The concentration data from Lamb and Cronn (1986) is more appropriate for evaluating dispersion models than the data of many previous studies for a variety of reasons: (i) there were a large number of measurement locations; (ii) there were reliable wind records for all tests; and (iii) the test building was a typical laboratory building (i.e. not a reduced size model). Wilson and Lamb (1994) analyzed the WSU data set and concluded that an increase in atmospheric turbulence tends to increase plume dilution. The Wilson and Chui (1994) minimum dilution model (discussed in later sections) was revised to take into account the influence of upstream turbulence. Further details on these models are provided later in section 2.4.5.3.

Georgakis et al. (1995) carried out a series of tracer gas experiments using two buildings at the University of Toronto in Canada. A number of different stacks of varying height and diameter were used in the study. The sampling period was 15-minutes, which is appropriate to evaluate minimum dilution models. However, the wind direction was often not in direct line with the stack/receptor pairs. As a result, most of the dilution measurements were not appropriate for evaluation of the models.

2.4.3 Wind-tunnel and full-scale comparison studies

Although many researchers have investigated the accuracy of wind-tunnel modeling of atmospheric dispersion, only a few have dealt with micro-scale dispersion.

For example, Petersen (1986) obtained excellent agreement between wind-tunnel and field concentrations measured far downwind (6 km) of a stack on an offshore oil rig. Petersen and Ratcliff (1991) noted that wind-tunnel simulations of dense gas dispersion have generally compared well with field results. Bachlin et al. (1991) found that wind-tunnel concentrations were within a factor of 2 of field values for a ground-level source located in a chemical plant.

Saathoff et al. (1996) compared wind tunnel results with those obtained in the WSU field study [Lamb and Cronn (1986)]. The evaluation was limited to field tests conducted with moderate to strong winds, since light winds cannot be modeled well with the wind tunnel. In general, wind tunnel dilution values compared well with the field data; dilution measurements at most receptors were within a factor of two of the field data.

Ogawa et al. (1983) conducted full-scale tests on a 1.8 m cube with the exhaust located on the center of the building roof. Wind-tunnel simulations were done for four roughness cases and for five different wind directions (0°–45°). The results are presented in the form of concentration contours on the surface of the cube and at ground level. Ground-level concentrations measured in the wake of the model generally compared well with the field results. However, concentrations obtained on the model surfaces did not compare well. Consequently, it was recommended that concentrations measured on the roof and walls of a model building be used only as qualitative indicators of the dispersion of emissions from a rooftop source. Results obtained by Ogawa et al. (1983b) may have been influenced by turbulence scale effects because of the small size of the structure used

in the field tests. The size of turbulent eddies relative to the building dimension was much larger in the field tests than in the wind tunnel experiments.

Higson et al. (1994) conducted full-scale and wind-tunnel tracer gas experiments with a stack located at varying distances upwind of a small building. They found that the maximum concentrations were generally overestimated in the wind tunnel tests and the minimum concentrations were underestimated. The authors suggested that the wind tunnel plume was narrower than the plume formed in field due to the absence of large-scale turbulence in the wind tunnel.

Figure 2.8 shows a typical wind velocity spectrum from Van der Hoven (1957). The spectra indicates that there are two peaks: the macrometeorological peak at a period of approximately 4 days corresponds to the passage of large-scale weather systems; and the micrometeorological peak at a period of 1 minute corresponds to the small scale turbulence generated by differential surface heating in the boundary layer, roughness elements, and topographical features. In the wind tunnel, only the longitudinal turbulence (I_u) corresponding to only the micrometeorological range can be simulated as highlighted by Ogawa et al. (1983) and Higson et al. (1994).

Stathopoulos et al. (2003) conducted an extensive full-scale and wind-tunnel study to quantify building-roof dispersion. The exhaust gas sulfur hexafluoride (SF_6) was released from an isolated stack located on the roof of a 13.5 m tall building, located in an urban environment. A total of 21 tests (of 50 minutes duration each) were carried out; 13 with open fetch and 7 with the emitting building downstream of a tall building. The field experiments were carried out for four different stack locations, two stack heights, h_s = 1

m and 3 m, and different M values and wind directions. The authors found that the wind tunnel predictions of concentration were generally within a factor of 2 of the field values and often within 10–20%. However, for cases with the emitting building downstream of a tall building, some discrepancies between wind-tunnel and field data occurred for the sampling locations on leeward wall of the tall building. The results showed that the concentrations on the leeward wall of the tall building were consistently too large by factor of about 3 in the wind tunnel. Saathoff et al. (2003b) later suggested that that this might have been due to the low level of turbulence in the approaching flow in the wind tunnel.

Stathopoulos et al. (2003) used field results to evaluate the ASHRAE (1999) and ASHRAE (2003) dispersion models. The authors noted that for the open fetch configurations tested, the ASHRAE (1999) D_{min} model predictions were more accurate compared to the ASHRAE (2003) D_r model.

2.4.4 Downwash effect of building/RTS on plume dispersion

As outlined in Chapter 1, downwash occurs when plumes released from a stack near a building are brought downward by the flow of air on the leeward side of the building [Schulman et al. (2000)]. As a result, the plume rise decreases significantly, leading to high roof-level or ground-level concentrations depending on the source location (see Figure 1.1). The potential for downwash is one of the most important factors in determining the acceptable stack height for sources near the structures, [Schultz (1995)].

A significant amount of research has been carried out on building downwash, [for e.g. Halitsky (1995), Huber (1982, 1988, and 1991), Thompson (1993), Snyder and Lawson (1994), Snyder (2005)]. A review of some recent building downwash related studies was provided by Canepa (2004). However, very few studies have examined the downwash due to RTS. This section presents a brief review of studies, which highlight downwash due to building and RTS on plume dispersion.

2.4.4.1 Building downwash

A frequently cited "rule of thumb" for the determination of necessary height for a stack downwind of a tall building is the Lucas (1972) "two-and-a-half times rule". According to this rule, the stack must be 2.5 times the height of the nearest upstream tall building in order to avoid the downwash in the wake of the building, which could result in high concentrations of pollutant at ground level.

Snyder and Lawson (1976) note that "*Lucas rule is merely a rule of thumb, yet it is frequently applied across-the-board under unwarranted circumstances*". The authors highlight that for a proposed electric plant building 100 m in height, which was to use lignite as a fuel, application of Lucas rule will result in a stack height of 250 m. However, in presence of building downwash, it was found that a stack height of 150 m was adequate to meet the ambient air quality standards. Therefore, it is important to understand the limitations of Lucas rule. Snyder and Lawson (1976) conducted wind tunnel tests to evaluate Lucas rule. The authors suggested that for wider buildings (W/H > 2.5), with height H and crosswind width W, the Lucas rule is justified. However, for

tall slender structures (W/H < 2.5), the Lucas rule could be relaxed to H + 1.5*l*, where *l* is the smaller either of W and H.

One of the earliest studies to examine building downwash was by Castro and Robins (1977), who performed wind-tunnel dispersion tests with a cubical building. The experiments were conducted for various stack heights and wind directions. The study indicated that there was greater downwash for a wind direction of 45°, resulting in increased ground-level concentrations compared with the normal wind. It was suggested that the Lucas (1972) "two-and-a-half times rule" for determining stack height tends to be unconservative and should be modified to "three-times rule".

Barret et al. (1978) also highlighted the significance of building downwash for oblique winds. Wind-tunnel experiments were conducted for a stack located upwind and downwind of a cubical building with height H. Ground-level concentration measurements were obtained for an oblique wind ($\theta = 45°$) for different stack heights. The authors noted that for $\theta = 45°$, the effect of the building on ground-level concentrations was noticeable up to a distance of about 20H downwind of the building. The authors concluded that the Lucas 2.5H rule might not be sufficient to avoid building-downwash effects.

Huber (1989) evaluated the influence of building width (W) and orientation on plume downwash. Concentration measurements were obtained in the wake of the building with W/H varying from 2 to 22 and orientation angles from -30° to 60°. The presence of building increased the downwind concentrations. The results showed an enhanced plume spread and decrease in ground-level concentrations with increase in building width. The study concluded that the shape, size, and orientation of a building

have a significant role in the dispersion of pollutants at both roof level and in the wake of the building. Mirzai et al. (1994) supported this finding.

Thompson (1993) carried out wind-tunnel experiments for stacks located downwind of buildings with different aspect ratios. Four building geometries were considered. Concentration measurements were obtained with and without buildings for stack heights ranging from 0.5H to 3H, where H is the height of the building. Measurements were obtained for stack located upwind of the building, on top of the building, and downwind of the building for a normal wind. Results were presented in the form of "amplification factors" (the ratio of pollutant concentration with building to the concentration without building). The author concluded that increasing the building width or decreasing stack height increased the building amplification factors, which indicated a stronger downwash.

2.4.4.2 Downwash due to RTS (for e.g. architectural screen walls, roof parapets, and penthouse)

Petersen et al. (1999) conducted a wind-tunnel study to determine the effect of architectural screens surrounding a rooftop stack on roof-level concentrations. The authors noted a significant increase in roof-level concentrations in the presence of architectural screens. The measured concentrations were also sensitive to the size and porosity of the screen. A stack height reduction factor (SHR), similar to Thomson's amplification factor for concentrations was proposed, which is defined as the ratio of stack height without screen divided by stack height with screen. It was shown that, depending on the porosity of the screen, the stack height reduction factor could be as

small as 0.2. For example, a 3-m stack surrounded by solid architectural screens (no porosity) will behave as a 0.6 m stack without the screens.

A common practice for architects is to hide stacks with the use of a parapet in order to make industrial buildings more aesthetically pleasing. Lowrey and Jacko (1996) conducted a wind-tunnel study to quantify the effect of roof parapets on plume from a stack located downwind of the parapet. The minimum dilution models proposed by Halitsky (1963), and Wilson and Chui (1985) were also evaluated. Wind tunnel tests were conducted with a model building which had a full-scale height of 7 m with length and width equal 100 m. All measurements were obtained for M = 2, for a normal wind (θ = 0°). Tests were conducted with two parapet heights – 1.5 m and 3 m. Concentration measurements were obtained along the plume centerline with and without a parapet for h_s ranging from 0 (flush with roof) to 6 m stacks, downwind of the parapet. The authors noted that that a separation bubble about two times the height of the parapet was formed at the leading edge. Consequently, stack height had little effect on dispersion for stacks shorter in height than the separation bubble height. The authors concluded that the widely accepted view that the effect of parapet is simply to decrease the effective stack height by the parapet itself may provide conservative estimates. The authors also showed that the empirical models proposed by Halitsky (1963), and Wilson and Chui (1985) cannot predict the effect of stack height in presence of a rooftop parapet.

Saathoff et al. (2002) conducted full-scale and wind-tunnel experiments on the roof of a 13.5 m tall building in an urban environment to study the downwash effect of an RTS on plume dispersion. The tracer gas was emitted from a 3.1 m tall stack with a diameter of 0.9 m. The stack was located approximately 1 m downwind of the RTS,

which had a height of 2.2 m and crosswind width of 35 m. The results indicated a significant decrease in dilutions for all sampling locations in the presence of an RTS. In general, the roof-level dilutions decreased by a factor of 10 for typical values of exhaust momentum ratio (M = 2 to 3).

Saathoff et al. (2003a) conducted a wind-tunnel study to identify the building configurations with significant RTS influence. The results were used to evaluate the ASHRAE (2003) dispersion models and the ASHRAE geometric stack design method. The wind-tunnel experiments were conducted with four isolated buildings with a square plan and full-scale heights of 15 m, 30 m, 50 m, and 70 m and a cross-wind width of 30 m. A stack with a full-scale diameter of 0.6 m and a height of 4 m was located at the center of the roof. An RTS, 4 m in height (h), was located upwind of the stack. The structure had an along-wind length (l) of 4 m and a crosswind width (w) that varied from 4 m to 24 m. Experiments were carried out for two wind directions ($\theta = 0^{\circ}$, $\theta = 45^{\circ}$) and for two locations of the rooftop structure, $x_s = 2$ m and 4 m, where x_s is the distance from the structure to the stack. Concentration measurements were obtained on the building rooftop in the lee of the stack, All experiments in the preliminary study were conducted for M = 2 and $h_s = h = 4$ m.

The major conclusions of the study were:

i) The downwash caused by an upwind RTS can greatly reduce the dilution values on the building roof up to 10 times and reduce the effectiveness of stacks in dispersing pollutants away from critical receptors such as fresh air intakes. Such problems appear to be particularly severe for wind at an

oblique angle to the rooftop structure as noted previously in building/RTS downwash studies [RTS downwash - Saathoff et al. (2002, 2008), and building downwash - Huber (1989, 1991), Thompson (1993)]

ii) The downwash effect of RTS was found to be significant for low-rise buildings and negligible for high-rise building. For the latter case, the RTS is engulfed within the building re-circulation zone.

iii) The downwash effect of an RTS is not considered in the ASHRAE (2003) D_r dispersion model. The wind tunnel results from the preliminary study showed that the dilution at rooftop receptors may be significantly overestimated by the D_r model when the RTS is upwind of the stack.

2.4.5 Plume dispersion models

Various analytical and empirical models have been developed to model near-field dispersion and building downwash effects. Until recently, the most popular approaches have been the empirical methods [ASHRAE (1997, and 1999], and Gaussian or modified Gaussian-model [Industrial Source Complex Model with Plume Rise Enhancements (ISC-PRIME), Atmospheric Dispersion Modeling System (ADMS), Huber (1988), Ramsdell (1990), ASHRAE (2003), and ASHRAE (2007)]. These models are summarized in the following sub-sections.

2.4.5.1 Classical Gaussian plume dispersion model

The classical Gaussian plume dispersion model is one of the most commonly used methods for estimating plume dispersion downstream of a continuous source. The major

reasons for using the Gaussian model are that it represents the random nature of the turbulence and the solution can be acquired by mathematical equations. Considering a continuous source with exhaust concentration C_e, and exhaust flow rate Q as shown in Figure 2.9, the concentration C at a certain location (x, y, z) downwind of the stack with height h_s is:

$$C(x,y,z;h_S) = \frac{C_e Q}{2\pi U_s \sigma_y \sigma_z} \exp\left[-\frac{y^2}{2\sigma_y^2}\right]\left\{\exp\left[-\frac{(h_p - z)^2}{2\sigma_z^2}\right] + \exp\left[-\frac{(h_p + z)^2}{2\sigma_z^2}\right]\right\} \qquad \text{[Eq 2.3]}$$

where U_s is wind speed at the tip of the stack, x is the downwind distance, y is the crosswind position, z is the vertical position above the ground, and h_p is effective height of the plume centerline. For example, to calculate concentrations along the plume centerline at ground level from a ground level release, y = 0, z = 0, h_s = 0, Eq 2.3 becomes:

$$C(x,0,0;0) = \frac{C_e Q}{\pi U_S \sigma_y \sigma_z} \qquad \text{[Eq 2.4]}$$

Wilson and Britter (1982) reported that the Gaussian plume model performed well for simple building shapes and predicted maximum building surface concentrations within a factor of 2–5. Due to complex flow patterns around buildings, the Gaussian model is not so effective in predicting pollutant concentrations for exhausts located on the roof or in the wake of buildings. In general, the classical Gaussian model is more applicable and recommended for far-field dispersion applications.

2.4.5.2 Modified Gaussian plume models

The classical Gaussian plume is not applicable for predicting pollutant concentrations around buildings, especially when building downwash is a contributing factor. Some researchers have modified the basic Gaussian plume models to consider building effects. The modifications usually deal with plume-spread factors, σ_y and σ_z, to account for the enhanced plume spread due to building generated turbulence. Simple methods for estimating σ_y and σ_z downwind of buildings were reviewed by Fackrell (1984).

Huber (1988) developed a modified Gaussian plume model to estimate pollutant concentrations in the wake of building. Derived from an extensive field data set, this model is based on two simple concepts: (i) in the immediate lee of the building, rapid dispersion occurs as the pollutant is mixed within the recirculating flow; (ii) further downwind, where flow is re-establishing itself to background conditions, plume dispersion is controlled by decaying turbulence. The model performed reasonably well although Huber concluded that "*Until the understanding of building-wake effects is more complete, it may not be appropriate to extend a generalized Gaussian plume model for all situations*".

Ramsdell (1990) developed a modified Gaussian dispersion model for predicting ground level centerline concentrations in the wake of buildings for exhausts released downwind of the building. This model predicted concentrations reasonably well in comparison to the other building wake models, but significantly over-estimated the concentrations at low wind speeds. Ramsdell and Fosmire (1998a) proposed a new

building-wake-dispersion model, which incorporated the effect of low and high wind speeds following the comments of Briggs et al. (1992). Comparisons were also made with other non-Gaussian models [Ramsdell and Fosmire (1998b)], such as Wilson and Chui (1994) and Wilson and Lamb (1994). The authors showed that the performance of the new model was significantly better than that of the previous model.

Huber (1991) carried out wind-tunnel studies to characterize the dispersion of a neutrally buoyant tracer released in the wake of a model rectangular building and proposed a modified Gaussian plume model. The experiments evaluated the effects of boundary-layer turbulence on tracer gas concentrations. It was observed that the concentrations were about the same within each of the two boundary layers developed in the wind tunnel (a low and high turbulence boundary layer) at distances $x < 10H$ downstream of the building. Beyond this near-wake region, concentration values were similar to those obtained without the building. The distance where the effect of the building becomes insignificant is influenced by the boundary-layer characteristics and the size of the building. The model estimated the ground-level plume centerline concentrations reasonably well.

The ADMS model developed by Carruthers et al. (1994) is used by the UK environmental agency for urban dispersion applications. This model incorporates the influence of the turbulence and mean velocity field in an extensive downstream wake. A simplified flow field is defined, based on a well-mixed cavity (or recirculating flow region) and a downstream turbulent wake (see Figure 2.10). The model also considers the source position and allows for complete or partial entrainment into the recirculating flow

region, where a uniform concentration distribution is assumed. The ADMS model has been primarily used for far-field dispersion.

The ISC-PRIME model by Schulman et al. (2000) is another modified Gaussian model used for predicting concentrations in the near wake and far wake of a building. This model is used by the U.S. Environmental Protection Agency (EPA) to estimate the dispersion of pollution from sources near isolated large buildings. It is based on two fundamental features associated with building downwash: i) reduced plume rise caused by a combination of the descending streamlines in the lee of the building and increased entrainment in the wake; and ii) enhanced plume dispersion coefficients due to the turbulent wake. A cavity module calculates the fraction of plume mass captured and recirculated within the near wake. The captured mass is re-emitted to the far wake as a volume source and added to the uncaptured plume contribution to obtain the far wake concentrations. The ISC-PRIME model is primarily recommended for far-field dispersion.

ASHRAE (2003) recommends a modified Gaussian plume dispersion model for exhaust emissions from rooftop stacks, based on water flume simulations of Wilson et al. (1998). The model predicts plume center-line (worst-case) dilution at roof level, D_r, assuming that the plume has a Gaussian concentration profile in both the vertical and lateral directions (see Figure 2.9). Roof level dilution at a receptor distance x from the stack is given as,

$$D_r = 4\frac{U_H}{w_e}\frac{\sigma_y}{d_e}\frac{\sigma_z}{d_e}\exp\left[\frac{h_p^2}{2\sigma_z^2}\right]$$

[Eq 2.5]

where U_H is the wind speed at the building height d_e is stack diameter, w_e is the exhaust speed, σ_y and σ_z are the plume spreads in the lateral and vertical directions, and h_p is the plume height. The value of h_p is determined from the following expression:

$$h_p = h_s + h_r - h_d \qquad \text{[Eq 2.6]}$$

where h_s is the stack height, h_r is the plume rise and h_d is the stack wake downwash. The plume rise, which is assumed to occur instantaneously, is calculated using the formula of Briggs (1984):

$$h_r = 3\beta d_e (w_e/U_H) \qquad \text{[Eq 2.7]}$$

where β is known as the capping factor. For un-capped stacks, $\beta = 1$; for capped stacks, $\beta = 0$.

To account for the stack downwash caused by low exit velocities, when $w_e/U_H < 3.0$, Wilson et al. (1998) recommended a stack wake downwash adjustment h_d, which is defined as,

$$h_d = d_e (3.0 - \beta w_e/U_H) \qquad \text{[Eq 2.8]}$$

For $w_e/U_H > 3.0$ there is no stack downwash ($h_d = 0$).

The equations for σ_y and σ_z are the equations used in the Industrial Source Complex Screening Tool (ISCST) dispersion model, which was developed by the U.S. EPA [EPA (1995)]. The sigma values are adjusted from a 60-minute averaging time to a 2-minute averaging time using the 0.2 power law applied to both vertical and crosswind spreads. The normalized crosswind and vertical spreads are given by the following equations,

$$\frac{\sigma_y}{d_e} = 0.071\left(\frac{t_{avg}}{2.0}\right)^{0.2}\frac{x}{d_e} + \frac{\sigma_o}{d_e} \qquad \text{[Eq 2.9]}$$

$$\frac{\sigma_z}{d_e} = 0.071\frac{x}{d_e} + \frac{\sigma_o}{d_e} \qquad \text{[Eq 2.10]}$$

where t_{avg} is the concentration averaging time in minutes, and σ_o is the initial source size that accounts for stack diameter and for dilution due to jet entrainment during plume rise.

$$\frac{\sigma_o}{d_e} = \left[0.125\beta\frac{w_e}{U_H} + 0.911\beta\left(\frac{w_e}{U_H}\right)^2 + 0.250\right]^{.5} \qquad \text{[Eq 2.11]}$$

The Gaussian dilution model should not be used when h_p is less than the maximum height of the roof recirculation zones that are in the path of the plume. This critical height is referred to as h_{top} and is shown in Figure 2.11. For building/stack configurations in which h_p is greater than h_{top} but less than the height required to escape all critical recirculation zones, the physical stack height should be set at 0 when calculating h_p [ASHRAE (2003)].

Another dilution model recommended by ASHRAE (2003) is the D_s model. The D_s model is used for wall vents or for cases in which the plume height is below the maximum height of recirculation zones. The D_s model is similar in form to the D_r model except that the plume height is set equal to zero and 'x' is replaced by the stretched-string distance S, which is the distance between the nearest edge of the exhaust to the nearest edge of the intake. Because plume height is not considered, the D_s model provides very conservative estimates of dilution at rooftop receptors. It should be noted that the D_s model is similar to the earlier ASHRAE dilution models which used stretched-string distance rather than horizontal distance.

The D_r model was revised in ASHRAE (2007). The primary reason was to simplify the ASHRAE (2003) D_r model. Equation 2.5 was replaced with,

$$D_r = 4\frac{U_H}{w_e}\frac{\sigma_y}{d_e}\frac{\sigma_z}{d_e}\exp\left[\frac{\xi^2}{2\sigma_z^2}\right] \qquad \text{[Eq 2.12]}$$

where h_p is replaced by the vertical separation factor, ξ. The vertical separation depends upon h_p and h_{top}. The vertical separation factor is defined as

$$\xi = h_p - h_{top} \qquad h_p > h_{top}$$

$$= 0 \qquad h_p < h_{top} \qquad \text{[Eq 2.13]}$$

Bahloul et al. (2008) compared results of the ADMS and ASHRAE (2007) models with the wind tunnel results from Gupta et al. (2005), for exhausts released from the roof of a low-rise and a high-rise building. Normalized roof-level dilutions were compared for h_s = 1 m and 7 m, M = 1, 2, 3 and 5 for $\theta = 0^0$ and 45^0. The study showed

that the measured data compared well with ADMS for the low-rise building for low h_s (1 m) and low M values (1, 2). However, considerable deviation in dilutions was observed for the high-rise building. For $\theta = 45^0$, the ADMS estimates compared well with the wind tunnel data for both the low-rise and high-rise building.

The authors found that ASHRAE (2007) minimum dilution models were significantly conservative for all the cases evaluated compared to the ADMS-model estimates and the wind-tunnel data.

2.4.5.3 Empirical dispersion models

Another practical and cost-effective method to estimate the concentration of pollutant from building-roof exhausts is the semi-empirical model. In past researchers have proposed semi-empirical equations to estimate minimum dilutions (D_{min}) for a wide variety of cases. A few of these models are presented below.

Wilson and Chui (1985, 1987) developed a minimum dilution model, referred to as the WC model, through a series of wind-tunnel experiments. The WC model is limited to flat-roofed buildings with flush stacks (i.e. $h_s = 0$). Minimum dilution along the plume centerline is given as:

$$D_{min} = (D_o^{0.5} + D_d^{0.5})^2 \qquad \text{[Eq 2.14]}$$

where D_o is the initial dilution at the exhaust location that takes into account the entrainment of ambient air into the exhaust jet and D_d is the distance dilution.

The initial dilution is given by the following expression:

$$D_o = 1 + 7\beta M^2 \qquad \text{[Eq 2.15]}$$

The distance dilution factor D_d is associated with atmospheric and building turbulence and is given by:

$$D_d = B_1 S^2 / M A_e \qquad \text{[Eq 2.16]}$$

B_1 is the distance dilution parameter and M is the exhaust momentum ratio. The parameter, β, is the stack-capping factor and is set equal to 1.0 for uncapped stacks and 0 for capped stacks. The parameter, B_1, is set at a constant value with its magnitude dependent on the location of the receptors: $B_1 = 0.0625$ for rooftop receptors and $B_1 = 0.2$ for wall receptors.

Wilson and Lamb developed another minimum dilution model based on the WC model, referred to as WL model. A significant revision was the initial dilution calculation. In the WC model D_o is proportional to M^2, while in the WL model D_o is proportional to M and is given by,

$$D_o = 1 + 13\beta M \qquad \text{[Eq 2.17]}$$

Also from the dilution data obtained in a field study [Wilson and Lamb (1994)] and a wind tunnel study [Wilson and Chui (1987)], it was shown that B_1 was strongly affected by the level of atmospheric turbulence in the approaching flow. To incorporate the effect of upstream turbulence, the distance dilution parameter was defined as:

$$B_1 = 0.027 + 0.0021\sigma_\theta \qquad \text{[Eq 2.18]}$$

where σ_θ is the standard deviation of wind direction fluctuations in degrees. The model suggests that distance dilution has two components: the dilution due to building-generated turbulence and that due to atmospheric turbulence. For an urban environment, ASHRAE (1997) recommends a typical value of σ_θ =15°, which yields B1 = 0.027 + 0.032 = 0.059. Thus, more than 50% of D_d is assumed to be due to upstream turbulence.

2.4.5.4 ASHRAE Geometric Stack Design Method (AGM)

ASHRAE (2003, 2007) provides a "Geometric Stack Design" method for estimating the minimum stack height to avoid plume entrainment in the flow recirculation zones of a building. The AGM is based on the water flume study conducted by Wilson (1979). Even though it is not a quantitative dispersion model, it allows designers to determine the minimum required stack height by avoiding plume entrainment.

The AGM requires the dimensions of the building recirculation zones. These are expressed in terms of the scaling length, R, which is defined as:

$$R = B_s^{0.67} B_L^{0.33} \quad \text{[Eq 2.19]}$$

where B_s is the smaller of upwind building height or width and B_L is the larger of these dimensions. The dimensions of flow re-circulation zones that form on the building and rooftop structures are:

$$H_c = 0.22R \quad \text{[Eq 2.20]}$$

$$X_c = 0.5R \quad \text{[Eq 2.21]}$$

$$L_c = 0.9R \quad \text{[Eq 2.22]}$$

$$L_r = 1.0R \qquad \text{[Eq 2.23]}$$

where H_c is the maximum height of the roof recirculation zone, X_c is the distance from the leading edge to H_c , L_c is the length of the roof recirculation zone, and L_r is the length of the building wake zone. Figure 2.12 shows the recirculation zones for a typical building.

The design method assumes that the boundary of the high turbulence region is defined by a line with a slope of 10:1 extending from the top of the leading edge separation bubble. The location of the plume relative to the recirculation zones is determined by taking into account plume rise due to exhaust momentum and assuming a conical plume with a slope of 5:1. The required stack height is obtained by rearranging Eq 2.6.

$$h_s = h_p - h_r + h_d \qquad \text{[Eq 2.24]}$$

AGM is a simple method to estimate the design stack height and applies to rectangular buildings that do not have tall adjacent buildings. Stathopoulos et al. (2003) evaluated the AGM with concentration measurements obtained from full-scale tests for stacks located on the roof of a low-rise building in an urban environment. The authors noted that AGM could lead to an un-conservative stack design.

2.5 Summary

A detailed review of past work in micro-scale dispersion is presented in this chapter and shows that deficiencies exist in a number of areas:

1. A detailed understanding towards the downwash effect of rooftop structures on plume dispersion remains unexplored.

2. No specific guidelines are available to locate fresh air intakes for buildings to avoid potential re-ingestion.

3. Present ASHRAE dispersion models need improvement. They are sometimes overly conservative and sometimes un-conservative and most importantly, do not properly address the downwash effect of RTS.

This study deals mainly with the influence of rooftop structures on the dispersion process. The experimental approach that was used is described in detail in the next chapter.

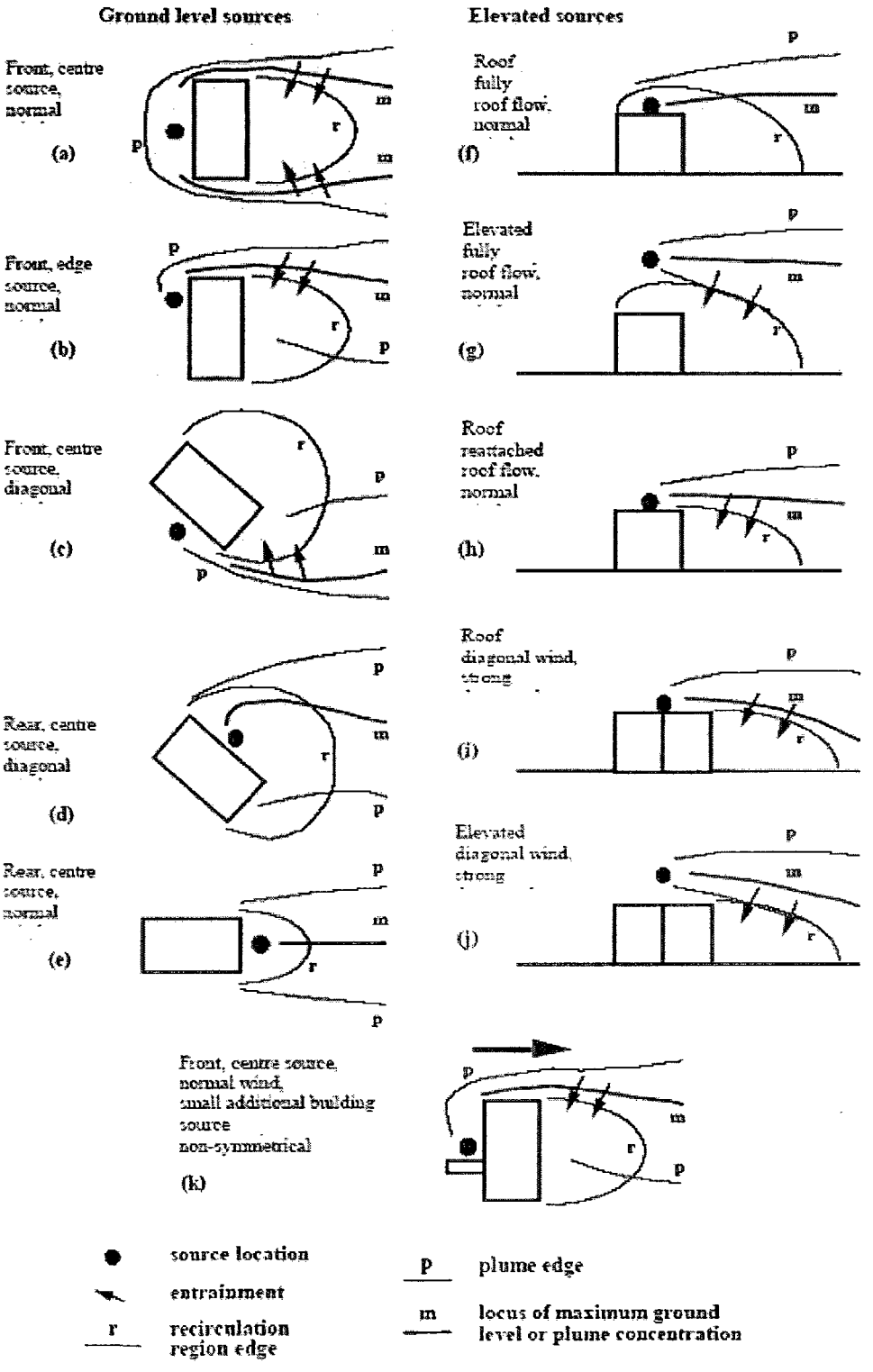

Figure 2.1 Dispersion patterns for emissions above and to the side of cuboids showing regions of entrainment [from Robins and Macdonald (1999)]

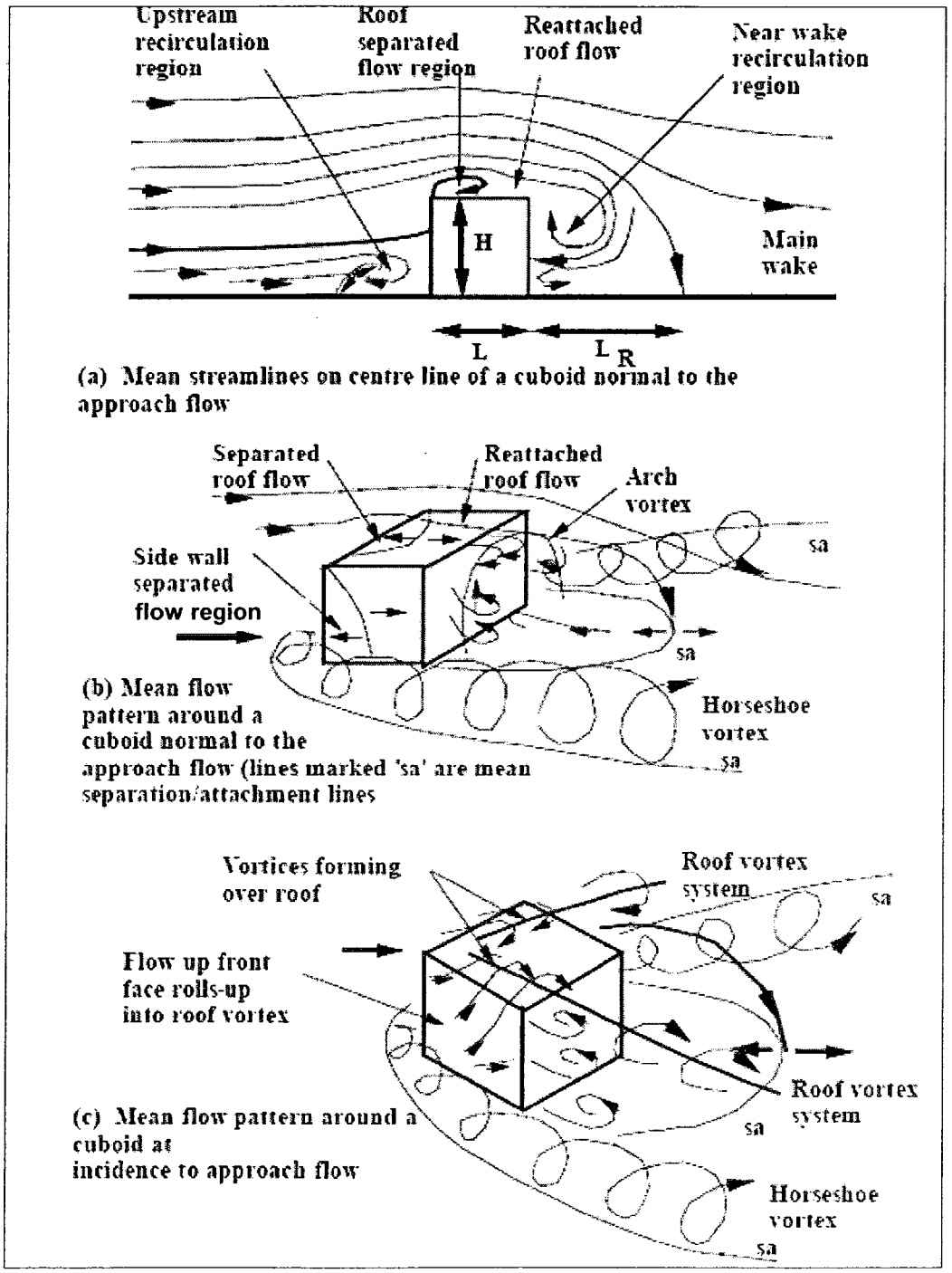

Figure 2.2 A three-dimensional (3-D) illustration of flow patterns around a cuboids at a wind incidence of 0 and 45 degrees in an atmospheric boundary layer [from Hunt et al. (1978)].

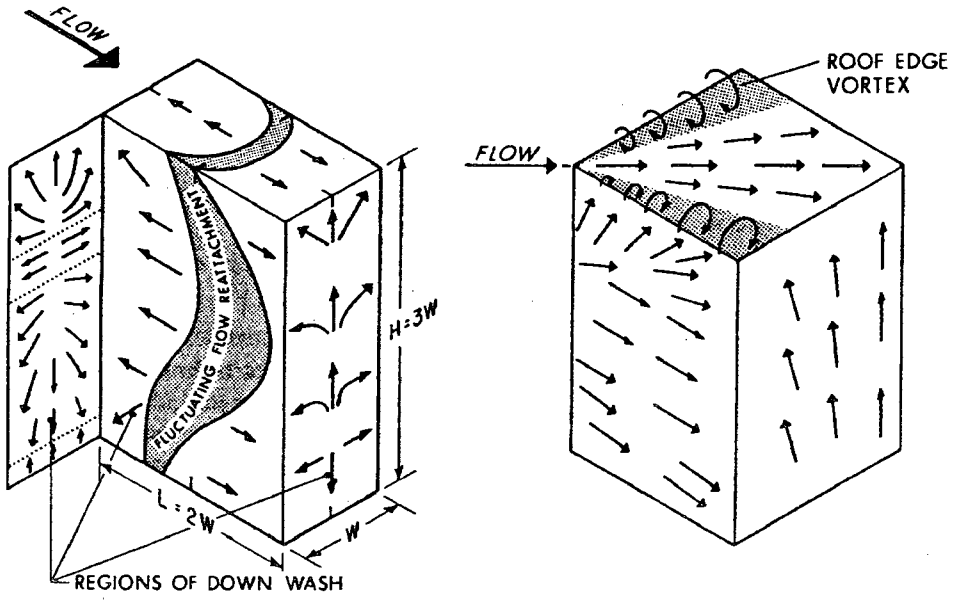

a) Normal wind b) Oblique wind

Figure 2.3 Mean flow patterns for wind incident to a tall building [from Wilson (1979)].

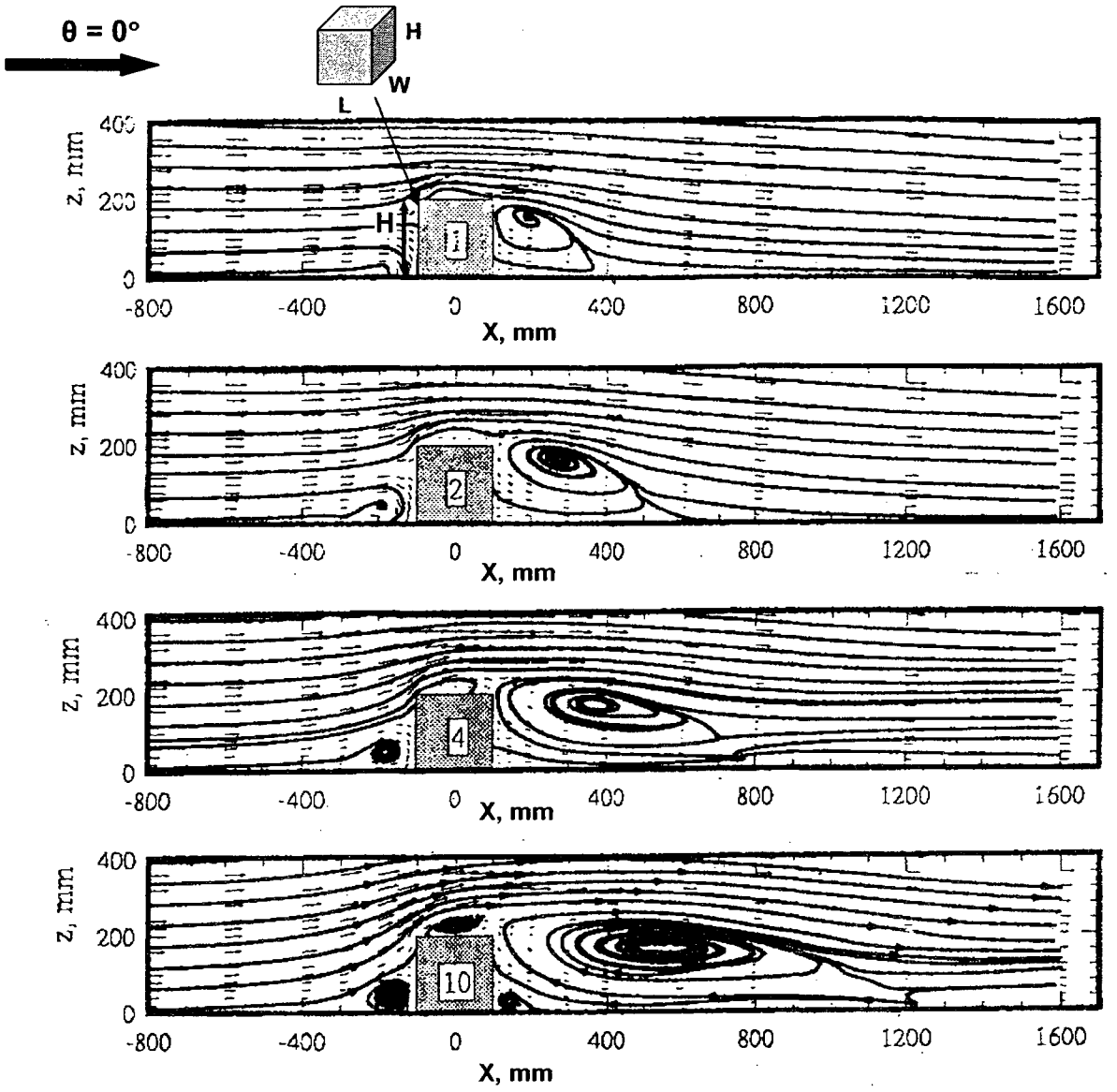

Figure 2.4 Flow fields in the wake of a building with varying widths [from Snyder and Lawson (1994)]. The number shown inside the building represents W/H.

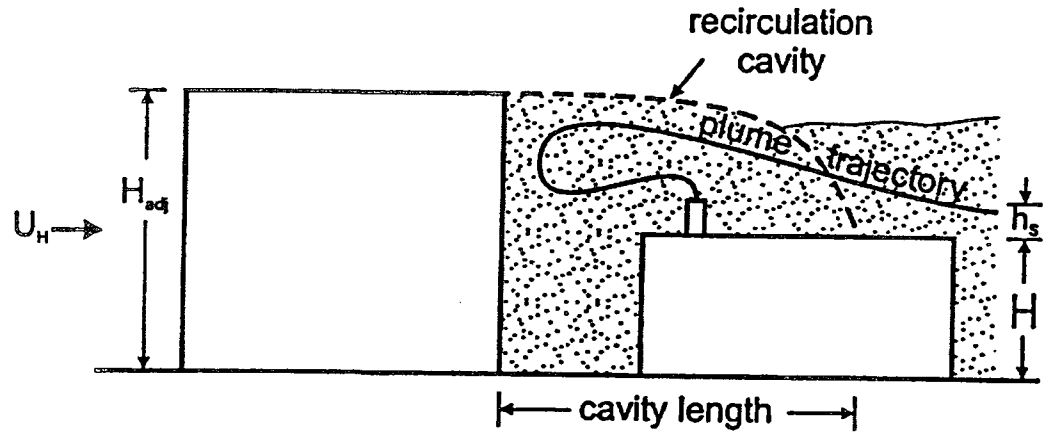

Figure 2.5 Flow recirculation pattern for a small emitting building lying in the wake of taller building [from Wilson et al. (1998)].

Figure 2.6 Photograph of wind tunnel set-up [from Stathopoulos et al. (2003)].

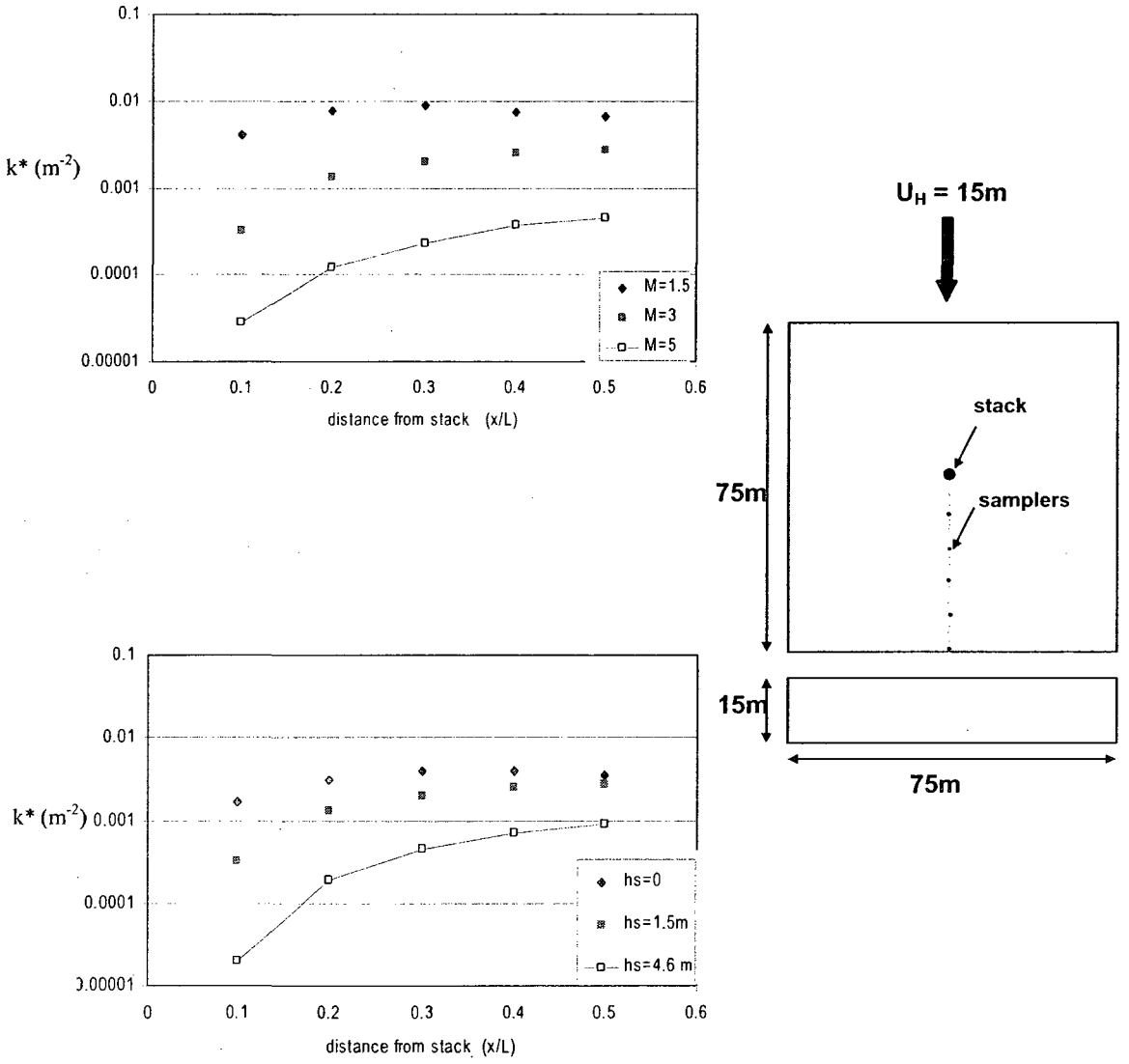

Figure 2.7 Effect of exhaust momentum ratio and stack height on normalized concentration measured on the plume centerline [from Schulman and Scire (1991)].

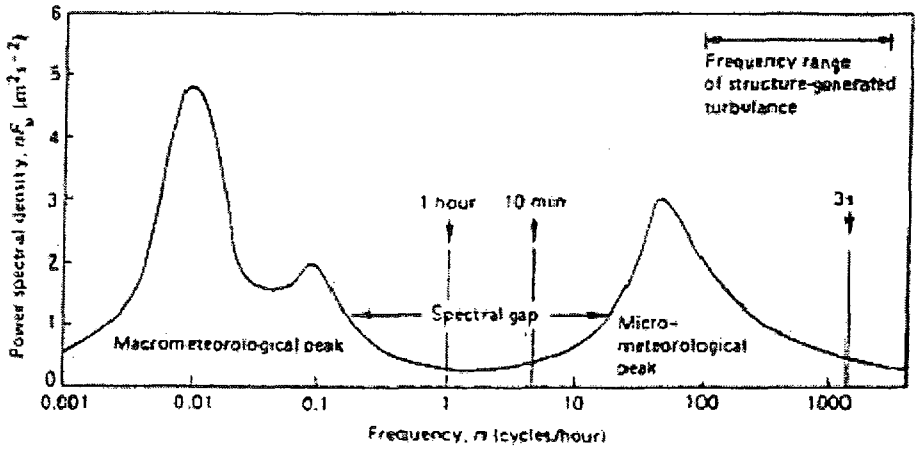

Figure 2.8 Spectrum of horizontal wind speed [from Van der Hoven (1957)]

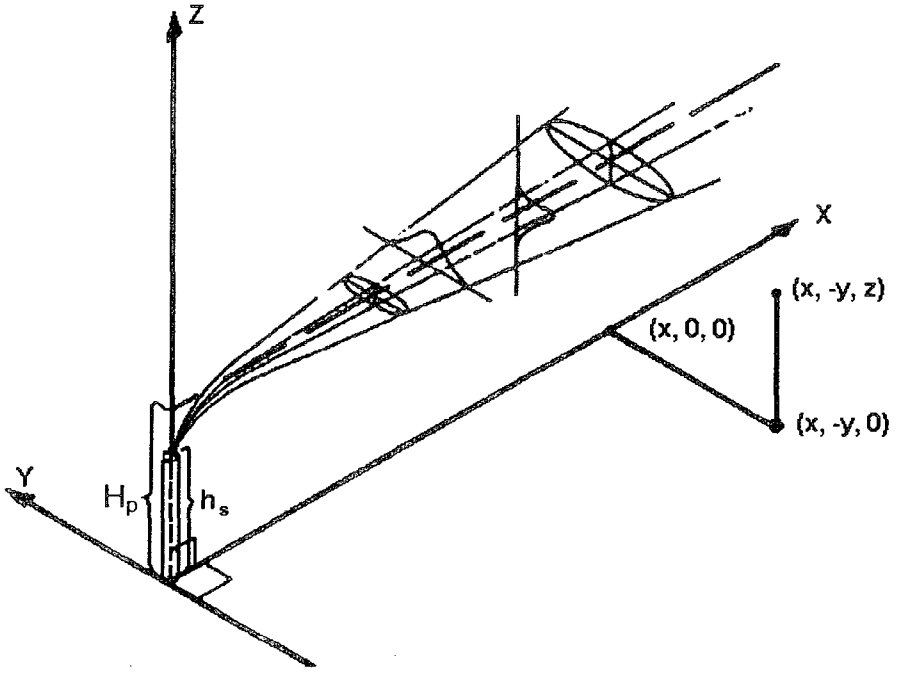

Figure 2.9 Coordinate system showing Gaussian plume spreads in the horizontal and vertical direction [from Turner (1994)].

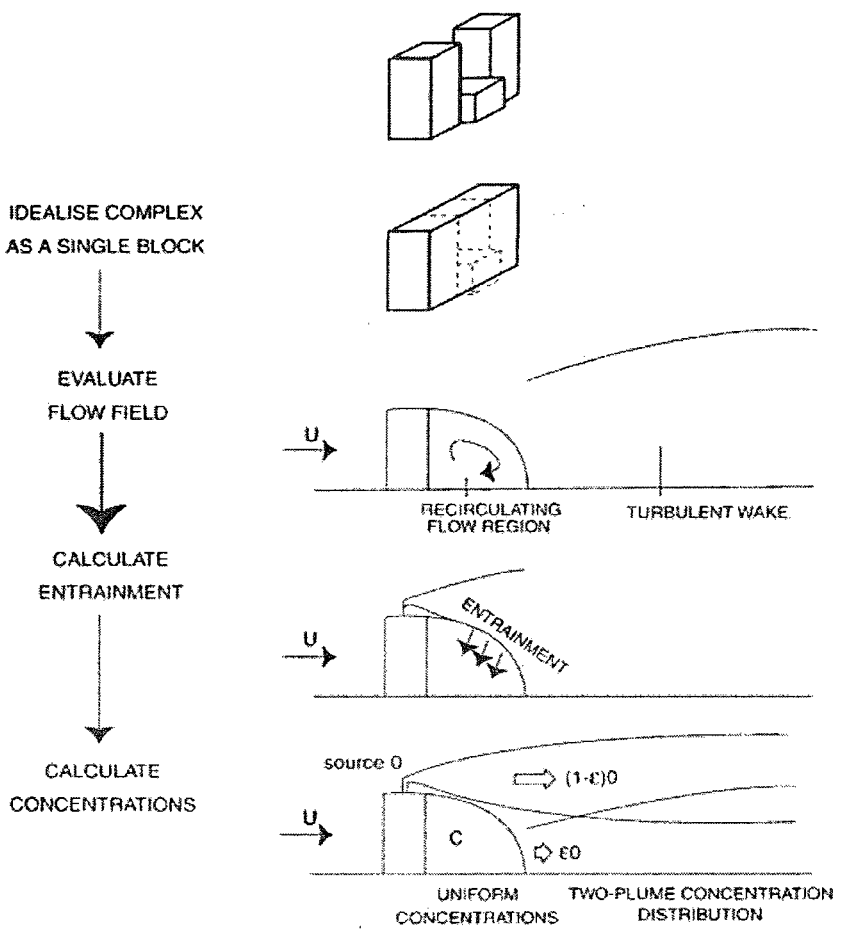

Figure 2.10 Stages in the analysis of the ADMS building effects module [from Carruthers et al., 1994)].

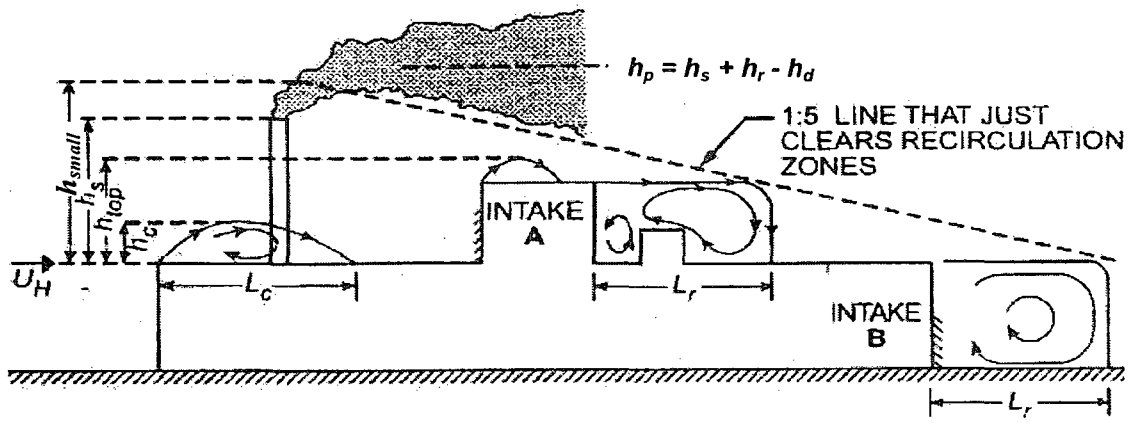

Figure 2.11 Flow recirculation regions and exhaust-to-intake stretched-string distances [from ASHRAE (2003)].

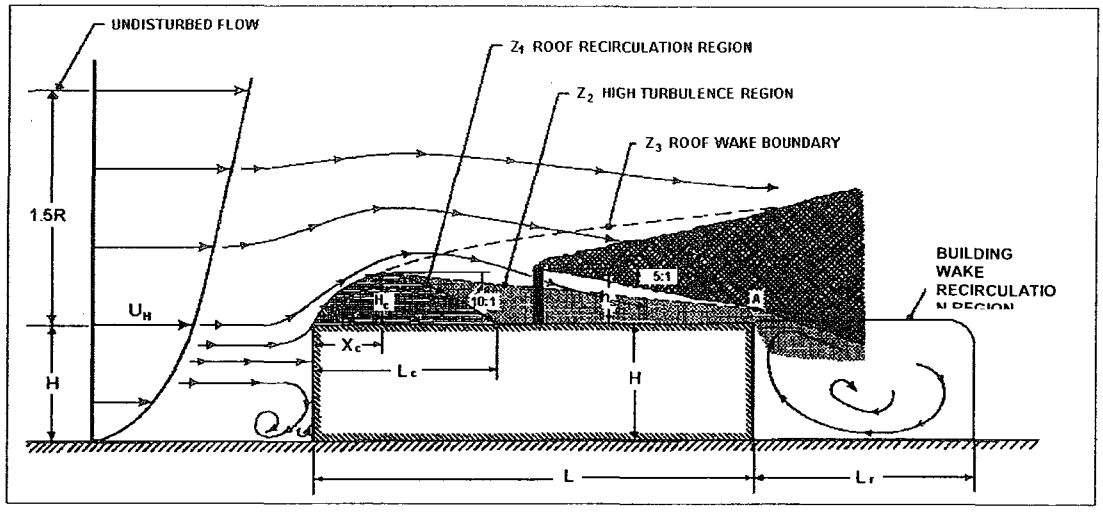

Figure 2.12 Design procedures for required stack height to avoid contamination [from Wilson (1979)].

Chapter 3

EXPERIMENTAL METHODOLOGY

3.1 Introduction

This chapter describes the experimental methodology used in the present study. As highlighted in Chapter 2, the boundary layer wind tunnel is an ideal tool for modeling dispersion around buildings and is used in the present study. The scope of the study is confined to modeling non-buoyant exhaust discharged from the roof of the building.

This study uses tracer gas measurements to investigate plume dispersion, which involves discharging a known concentration of tracer gas from an exhaust source and measuring the concentration of the released gas at the required location. Before describing the experimental details, a brief discussion is provided on the formation of atmospheric boundary layer and dispersion modeling criteria.

3.2 Atmospheric boundary layer

The "atmospheric boundary layer" forms when the air flow interacts with the upstream roughness generated by buildings or any other kind of obstructions. Figure 3.1 shows the formation of boundary layer for different roughness categories: urban, suburban and open country [from Davenport (1963)]. As shown in Figure 3.1, the wind speed increases with height up to the top of the boundary layer (also called "gradient height") where it reaches a constant value. As the terrain becomes rougher, the friction forces increase. Consequently, the boundary layer height is maximum for an urban

exposure and minimum for an open exposure. The height of the boundary layer can vary from a few hundred to several hundred meters, [Holmes (2001)]. A typical value for a neutral boundary layer for a city varies from 500 m to 600 m.

A model widely used to describe the mean velocity profile in atmospheric boundary layer in neutral conditions is the power law, which is given by the following expression:

$$\frac{U(Z)}{U(Z_g)} = \left(\frac{Z}{Z_g}\right)^{\alpha} \qquad \text{[Eq 3.1]}$$

where α is the power law exponent and U(Z) is the wind speed at any desired height Z and $U(Z_g)$ is the wind speed at the top of the boundary layer, or gradient height (Z_g). The value of α varies from 0.10 for very smooth terrain to approximately 0.35 for an urban terrain.

The wind speed (U) and wind direction (θ) vary randomly with time due to the atmospheric turbulence. The wind speed at any instant can be expressed in terms of a mean (averaged over 10 minutes to 1 hour) and fluctuating component. Figure 3.2 shows a typical wind speed time history measured during a field test [from Stathopoulos et al. (2003)]. At any instant the total wind speed (U) can be expressed as:

$$U = \bar{U} + u \qquad \text{[Eq 3.2]}$$

where $\bar{U}$ and u are the mean and fluctuating components of wind speed. The ratio of the standard deviation of the fluctuating component to the mean value of the wind speed is

known as turbulence intensity (I) of that component. The longitudinal turbulence intensity $I_u(Z)$ at height Z can be estimated with the following expression.

$$I_u(Z) = \sigma_u(Z)/U(Z) \qquad \text{[Eq 3.3]}$$

where σ_u is the standard deviation of longitudinal component of wind speed.

The turbulence intensity is also related to the surface roughness length (z_o) which is a measure of eddy size at the ground. The variation of longitudinal turbulence intensity with height can also be estimated using the following expression [EPA (1981)]:

$$I_u = \alpha \frac{\ln(30/z_0)}{\ln(Z/z_0)} \qquad \text{[Eq 3.4]}$$

where all heights are in full-scale meters.

3.3 Dispersion modeling criteria

Various criteria are required for modeling dispersion in a wind tunnel. These requirements are provided in the ASCE (1999) - Manual of Practice No. 67 on "Wind Tunnel Studies of Buildings and Other Structures". As discussed by ASHRAE (1993), Isyumov and Tanaka (1979), Cermak (1976), and Snyder (1981), the following criteria are generally recommended in wind tunnel dispersion studies:

i) similarity of wind tunnel boundary layer with the atmospheric surface layer (i.e. similar mean velocity and turbulence intensity profiles);

ii) similar geometric dimensions in model and full-scale;

iii) building Reynolds number (Re_b) should be greater than 11,000 for sharp edged structure to ensure the flow patterns around the building are similar to the full-scale structures, where $Re_b = U_H W/\nu$, W is the smaller of building upwind height or cross-wind width, ν is the kinematic viscosity of air;

iv) stack Reynolds number (Re_s), should be greater than 2,000 to ensure the flow is turbulent where $Re_s = w_e d_e/\nu$, d_e is the stack inside diameter and w_e is the exhaust speed;

v) similar exhaust momentum ratio, $M = (\rho_e/\rho_a)^{0.5}(w_e/U_H)$, where ρ_e is the density of the exhaust gas and ρ_a is density of air;;

vi) equivalent atmospheric stability as characterized by the Richardson number Ri $= (\Delta T/T)(gl/U_H^2)$, where ΔT is the change in temperature, T is the ambient temperature, g is acceleration due to gravity and l is building characteristic length;

vii) similar density ratio (ρ_e/ρ_a) in model and full-scale;

viii) Equivalent buoyancy ratio, $B = (w_e/U_H)^3(d_e)/(lF_r^2)$, where Froude Number, $F_r = w_e\rho_e/(\Delta\rho g d_e)^{0.5}$, and $\Delta\rho = \rho_e - \rho_a$

For accurate simulation of the flow around a building, it is essential to match the full-scale longitudinal mean velocity and turbulence intensity profiles. To achieve closest match between the simulated and full-scale boundary layer, the simulated boundary layer should be as thick as possible. To generate a deep boundary layer a wind tunnel needs to have a long development length and a sufficiently large cross-section. Devices such as vortex generators [Counihan (1969)] are used for the development of a thick boundary

layer and the roughness elements on the wind tunnel floor maintain the boundary layer structure along the length of the tunnel. Roughness elements are small cubical pieces of foam, wood, or any other material that are placed along the development length inside the wind tunnel. The size and density of roughness elements will vary depending on the type of boundary layer required (open, suburban, and urban). The boundary layer thickness can be controlled by using different combinations of roughness and/or other passive devices placed at the entrance of the test section, such as grids, barriers, and fences.

To ensure the flow patterns around the building are similar to the full-scale structures ASHRAE (2001) recommends that Re_b should be greater than 11,000 and to maintain a turbulent flow from the stack, Re_s should be greater than 2,000.

It is generally rather difficult to satisfy all the criteria. Researchers such as Cermak (1976), and Snyder (1981) demonstrated that accurate simulation of plume dispersion can be achieved by satisfying a few important modeling criteria. For example, if the stack is engulfed within the building recirculation zone, correct matching of atmospheric turbulence intensity may not be that significant. If the exhaust discharged from stacks is neutral, a matching Froude number is not necessary. Similarly, if the experiments were conducted for neutral stability (i.e. no temperature gradient with height) then Richardson number scaling is not required.

Another important criterion for dispersion modeling is wind-tunnel blockage. Wind-tunnel blockage is defined as the ratio of the projected area of the model normal to the flow with the cross-sectional area of the wind tunnel. According to ASCE (1999), the wind-tunnel measurements should be corrected for blockage effects if the blockage ratio,

A_m/A_o, exceeds 5%, where A_m is the projected area of the model normal to the flow and A_o is the cross-sectional area of the wind tunnel. Snyder (1981) recommends a maximum allowable blockage of 4%.

3.4 Experimental Strategy

The primary objective of the present study is to quantify the downwash effect of an RTS on plume dispersion by means of wind-tunnel modeling. To achieve this objective, the present study was conducted in two phases.

i) Phase One: a preliminary wind-tunnel study to identify the building configurations with significant RTS influence; and

ii) Phase Two: a comprehensive wind-tunnel study to quantify the effects of RTS based on the results obtained from the preliminary study.

The preliminary study details are provided in Saathoff et al. (2003a). The experimental details for the comprehensive wind-tunnel study are outlined in the current chapter, which include the following:

i) selection of building and RTS configurations

ii) selection of experimental parameters

iii) boundary layer simulation

iv) flow visualization

v) tracer gas dispersion.

3.4.1 Building and RTS configurations

An important consideration in the case of an RTS is its exposure to the approaching flow. If the RTS is located outside the separated flow region that forms on the building roof, the RTS will be exposed to the approaching flow and downwash effects may be important. On the other hand, if the RTS is located inside the separated flow region, the RTS will not be exposed to the approaching flow and consequently, downwash effects will be relatively minor.

Whether or not the RTS is exposed to the approaching flow depends on the shape and orientation of the building and the location of the RTS on the roof. Winds approximately normal to the building will produce a separated flow region near the leading edge characterized by high turbulence and intermittent flow reversal. For low-rise buildings with large along-wind length, flow reattachment will occur relatively close to the leading edge, as shown in Figure 2.12. In this case, an RTS located near the center of the roof will be exposed to the approaching flow and may produce significant downwash effects. On the other hand, for tall buildings and those with small along-wind length, the separated flow region may encompass the entire roof. For this case, the RTS is not exposed to the approaching flow and consequently will not have a significant impact on plumes emitted from rooftop stacks.

Building Dimensions: along-wind length (L), crosswind width (W) and height (H): To obtain a significant variation of dilution with distance from the stack, an along-wind length of L = 50 m was used for all test buildings. Two building heights, H = 15 m

representing the low-rise building and H = 60 m representing the high-rise building were considered.

Measurements for the low-rise building were obtained for two crosswind widths, W = 30 m and 50 m. However, measurements for the high-rise building were obtained for a fixed crosswind width of W = 50 m.

In the present study the buildings will be categorized as either low-rise or high-rise. Therefore, before discussing the building dimensions used in the present study, a brief description is presented which provides the basis for categorizing the building type: low, medium and high-rise.

For wind loading applications, the ASCE 7 (2005) suggests that for $H < 60$ ft (18 m) the building is a low-rise building and for $H \geq 60$ ft the building is a high-rise building. However, for building exhaust re-entrainment applications, there are no specific standards available which categorizes buildings into different groups such as low-rise, medium-rise, and high rise.

Saathoff et al. (2003a) conducted wind-tunnel experiments with four isolated buildings to quantify the downwash effect of a 4 m tall RTS on a downwind stack. The buildings had a square plan with full-scale heights of 15 m, 30 m, 50 m, and 70 m and a crosswind width of 30 m. They showed that the downwash effect of the RTS is negligible for buildings taller than 30 m and $W/H \leq 1$. The results obtained in the present study for the buildings with height 15 m and 60 m are similar with Saathoff et al. (2003a) results for buildings with same or similar heights. Therefore, in the present study, buildings with heights generally less than 30 m with $W/H > 1$ are considered as low- to mid-rise

buildings where the downwash effect of RTS is expected to be significant. On the other hand, buildings generally taller than 30 m with W/H $\leq$ 1 are classified as high-rise buildings.

RTS Dimensions: along-wind length (l), crosswind width (w) and height (h): A survey of different buildings with RTS showed that typical heights of RTS range from 2.5 m to 5 m, with the majority approximately 4 m tall, representing a penthouse. However, the RTS width is highly variable, ranging from 5 m to 50 m. Given this, the present study focused on the effect of RTS crosswind width rather than RTS height or along-wind length. RTS crosswind widths of 10 m, 20 m, 30 m, 40 m, and 50 m were used in the comprehensive study. The majority of concentration measurements were obtained for an RTS with h = 4 m and l = 8 m. A few additional measurements were also conducted for l = 1 m and 4 m.

Previous researchers such as Wilson and Netterville (1978) and Saathoff et al. (1995) suggested that the effect of upstream turbulence on near-field dispersion for buildings is not that significant. Saathoff et al. (1995) showed that a change in model scale by a factor of 4 could cause mean concentration at the roof level to vary by a factor of two. Wilson et al. (1998) notes that the model experiments can be scaled up or scale down by a factor of 4 higher or lower. This suggests that the building/RTS dimensions used in the present study can be scaled up or scale down by a factor of at least 2 higher or lower.

A schematic presentation of the building and RTS models are shown in Figure 3.3 and the photographs of the building models are shown in Figure 3.4.

3.4.2 Experimental parameters

The experimental parameters (h_s, M, x_s and θ) considered in the present study are discussed in this section. Note that this study is limited to neutral conditions, which are associated with moderately high wind conditions where the wind speed is greater than 4 m/s.

Stack height (h_s), exhaust momentum ratio (M) and stack location (x_s): The stack height ranged from 1 m to 7 m. Stack heights greater than 7 m are generally considered as impractical and difficult to implement. M values ranged from 1 to 5 representing strong (12 m/s) to moderately weak (3 m/s) wind speeds.

The RTS downwind edge was located at a distance of 18 m from the building leading edge. Six different stack locations were tested, as shown in Figure 3.5. The x, y, and z coordinates of the stack outlet are listed in Table 3.1. Five stack locations, S1 to S5, were downwind of the RTS on the building centerline and symmetric with respect to the RTS. Stack location A1 was off the building centerline and asymmetric with respect to the RTS. The majority of measurements were obtained for stack S1, $x_s = 0.5h$, where x_s is the separation distance between the stack and the RTS.

Wind direction (θ): In the comprehensive study concentration measurements were obtained for θ ranging from 15° to 60°. However, the majority of measurements were obtained for $\theta = 0°$ and $\theta = 45°$.

Due to the dependence of building exhaust dispersion on several parameters, it was neither practical nor feasible to test all possible combinations of the different

variables. Based on judgment and results obtained from about 200 wind tunnel tests conducted for the preliminary study and about 600 selected wind tunnel tests were carried out for different RTS/building configurations in the comprehensive study. A list of experimental parameters is provided in Table 3.2 and a brief summary of different cases tested in the comprehensive wind-tunnel study are summarized in Tables 3.3 and 3.4, respectively. A detailed list of individual tests is also presented in Appendix A.

3.4.3 Boundary layer simulation

The wind-tunnel experiments were conducted in Concordia University's boundary layer wind tunnel (BLWT). Complete details for the BLWT can be found in Stathopoulos (1984). The wind tunnel has a working section of 1.8 m by 1.8 m and the length of the boundary layer development region is 12 m, as shown in Figure 3.6. The wind tunnel can generate a maximum wind speed of 12.5 m/s at the gradient height (Z_g) of 850 mm for an urban exposure and is capable of generating a neutral atmospheric boundary layer.

An urban boundary layer was simulated for the present study for neutral conditions. Since temperature change with height in the wind tunnel is small, the simulated atmospheric conditions are neutral to slightly unstable, which correspond to the Pasquill-Gifford C and D stability classes as described in Table 3.5, [from Turner (1994)]. Stability classes C and D are associated with moderate to strong wind speeds and generally occur when the surface wind speed exceeds 4 - 5 m/s. For the urban exposure, a mix of various roughness panels was used. The roughness elements consisted of egg boxes and styrofoam cubes arranged in a staggered way. Steel tubes of varying diameter

were used near the fan outlet section to generate turbulence. Photographs of the wind tunnel section for the urban profile simulation are shown in Figure 3.7.

Vertical profiles of mean velocity and turbulence intensity were obtained with a TSI hot-wire anemometer (see Figure 3.8a). In brief, hot-wire anemometry is a technique for measuring fluid speed by measuring heat transfer from a small, thin (5μm) wire that is immersed in the fluid. The rate of heat removal is directly related to the speed of the fluid flowing over the sensor. The mean and RMS voltage from the anemometer were measured with an ANALOGIC Data 6100 "Universal Waveform Analyzer," shown in Figure 3.8b. The vertical profiles of mean velocity and longitudinal turbulence intensity for the urban exposure for a model scale of 1:200 are presented in Figures 3.9a and 3.9b, respectively. Using Eq 3.1, the mean velocity profile for the urban exposure had a power law exponent (α) of 0.31.

The estimated model-scale roughness length (z_o) was approximately 5.5 mm. For a model scale of 1:200, the equivalent full scale z_o is 1.1 m, which is within the expected range for an urban environment (0.5 m $< z_o <$ 1.5 m) recommended by Wieringa (1992).

Another consistency check is to relate the power law exponent, α, to the surface roughness z_o. Counihan (1975), showed that α and z_o are related by the following expression:

$$\alpha = 0.24 + 0.96\log_{10}z_o + 0.016\,(\log_{10}z_o)^2 \qquad \text{[Eq 3.5]}$$

For z_o = 1.1 m, Eq. 3.5 gives an α value of 0.26. The estimated value is close to the measured values of 0.31, indicating an acceptable agreement between the power law approximation and the measured velocity profile.

The turbulence intensity values measured at the model building heights for the urban profile were 27% for the low-rise building (H = 15 m) and 18% for the high-rise building (H = 60 m), as shown in Figure 3.9a. The estimated values obtained with Eq 3.4 are 31% at H = 15 m and 20% at H = 60 m. The estimated I_U values are approximately 10-15% higher than the measured values for both the low- and high-rise buildings.

In summary, the mean velocity and turbulence intensity profiles obtained in the wind tunnel are representative of those expected at full scale, and thus satisfy the boundary layer similarity requirements for wind-tunnel modeling.

3.4.4 Flow visualization

Flow visualization was used in the comprehensive study to explore the effects of various parameters on building exhaust dispersion. In particular, these experiments provided a qualitative assessment of the size of recirculation zones and the downwash effect of RTS. Flow visualization was carried out for various values of w, h_s, θ and x_s.

A Dantec fog generator, as shown in Figure 3.10, was used to produce smoke using a water-based fluid specially formulated for exhaust dispersion applications. Smoke was released from the building roof stack and photographs were taken for different configurations with a Casio 10.2 mega pixel digital camera. Note that the visualization photographs are snap shots in time and therefore may not represent the steady state

conditions. However, as mentioned previously, the purpose of flow visualization was to obtain only a qualitative assessment of the flow around RTS.

All flow visualization tests were conducted for a constant upstream wind speed of 5 m/s at the building height. The upstream exposure represented an urban terrain. The exhaust speed was not measured. However, it was kept low to ensure that the plume rise was negligible (i.e. worst-case condition).

3.4.5 Tracer gas dispersion

The tracer gas experiments were conducted by releasing a tracer gas into the flow through an adjustable brass stack fitted in the model roof. Air samples were collected at selected locations on the roof. Each sample was analyzed with a gas chromatograph (GC) to obtain mean concentration. A schematic diagram of the tracer gas measurement system is shown in Figure 3.11.

A certified mixture of sulfur hexafluoride (SF_6) and nitrogen was emitted from the stack. SF_6 was used because it is inert, stable, easily detectable, and a non-toxic gas. The flow from the stack was regulated using a Matheson mass flow controller, as shown in Figure 3.12. Air samples with duration of 1 minute were obtained simultaneously at multiple sampling locations using a Cole-Parmer multi-syringe sampler, as shown in Figure 3.13. Plastic tubes with an inner diameter of approximately 1 mm were used to collect the samples and were purged between collections to eliminate any traces of previous samples. The 1-minute mean concentrations obtained in the wind tunnel were assumed to be equivalent to full-scale data averaged over a period of 10–15 minutes, [Britter and Wilson (1982)].

The air samples were analyzed using a VARIAN Gas Chromatograph (GC Model 3400), as shown in Figure 3.14 and is specially designed for detecting SF_6. The settings used for GC are provided in Appendix B. For each sample, three GC readings were obtained by injecting a portion of the sample into the GC. Only the last measurement of the three was used for measuring concentration to prevent any contamination from the previous samples. The raw data obtained from the GC were converted into concentrations by using formulae of curves fitted to calibration data. A typical set of calibration curves used for the GC and Mass-flow meter used in the present study are also provided in Appendix B.

3.4.5.1 Sampling locations

The coordinate system used in the present study is shown in Figure 3.15. The origin is located at the base of the stack. The positive x direction is along-wind downstream of the stack; the y direction is in the crosswind direction; and z is the vertical direction. The concentration measurements were obtained in the along-wind, crosswind and vertical directions.

Along-wind concentration measurements were obtained at seven sampling points stretching from near the stack to the downwind edge of the building as shown in Figure 3.16. For a normal wind the plume centerline is expected to be along the wind direction approaching the building leading edge. However, due to complex flow on the building roof for oblique winds, it was difficult to accurately determine the plume centerline. For both normal and oblique winds, the sampling locations were in line with the wind

directions tested and spaced 1.25h (5 m) apart with the exception of the first sampler, which was located at a distance of 0.6h (2.5 m) from the stack.

The crosswind and vertical measurement planes for normal and oblique winds are shown in Figures 3.17a and 3.17b, respectively. The crosswind and vertical concentration profiles were obtained at a distance of 2h and 5h from stack S1 (x_s = 0.5h). For the crosswind profile, the concentration measurements were obtained in positive and negative y directions at seven sampling locations separated by a distance of 1.25h (5 m). The vertical dilution profiles were obtained in using a thin vertical brass tube with sampling tubes attached at different heights. Concentration measurements were obtained for z values of from 0.05h (0.2 m) to 2.75h (11 m).

3.4.5.2 Simulation of exhaust momentum ratio (M)

A key factor in stack dispersion modeling is exhaust momentum ratio, which is defined as $(\rho_e/\rho_a)^{0.5}(w_e/U_H)$. Since the scope of the present study is limited to only neutral exhausts ($\rho_e = \rho_a$), $M = w_e/U_H$. However, if the exhaust is colder or warmer than the ambient air, actual densities of exhaust must be used to simulate M values.

The value of M can be varied using the following two options:

Option i) varying w_e while keeping U_H constant

Option ii) varying U_H while keeping w_e constant

In general, Option (ii) is more realistic than Option (i) since most building stacks have a constant flow rate. One major disadvantage with Option (i) is that it is often

difficult to satisfy the stack Reynolds number criterion for stacks with low exhaust flow rates. However, option (ii) has several disadvantages such as (1) the boundary layer parameters may vary at different wind speeds, and (2) need more experimental time because additional time is required to reach equilibrium when the wind speed is changed. Therefore, option (i) was opted for the present study.

The exhaust speed ranged from a minimum of 5.4 m/s to a maximum 27 m/s, which correspond to M values ranging from a minimum of 1 to a maximum of 5. The corresponding range of stack Reynolds number is 1,100 - 5,500. The criterion of $Re_s >$ 2,000 [ASHRAE (2001)] for stack Reynolds number independence was not met for M = 1, indicating that the flow was laminar for this case. Wilson et al. (1998) suggested a correction factor, which could be used to determine the full-scale equivalent M corresponding to the model value. He suggested that for laminar flows from stacks:

$$M_{full\text{-}scale} = 1.414\, M_{model} \qquad \text{[Eq 3.6]}$$

Therefore, according to Eq 3.6, $M_{model} = 1$ in the present study is equivalent to $M_{full\text{-}scale}$ of 1.4. Such small variation in M value is not expected to produce significant discrepancies. Therefore, no attempt was made to modify the exhaust to increase the Re_s.

3.5 Quality assurance of the wind-tunnel data

Various building/RTS configurations were re-tested after a few months to assess the repeatability of the wind-tunnel data. Discrepancies in the results may be a result of a combination of various factors, which include: calibration of GC, and consistency in experimental conditions.

Figure 3.18 shows a comparison between the D_N values obtained at different times for the flat-roofed low-rise building for two wind directions: $\theta = 0°$ and $\theta = 45°$. Results are shown for $h_s = 3$ and $M = 2$. In the present study, the repeatability of concentration measurements generally ranged between 10% and 20%. Previous studies, such as Schulman and Scire (1991), Wilson and Chui (1994), and Petersen et al. (1999) have also reported the repeatability error factors ranging from 10% to 20%. Wilson et al. (1998) reported the repeatability error of about 30%.

3.6 Normalized dilution

A brief discussion on the normalization technique used in this study is presented in this section. In general, for the same building configuration, stack height, and wind direction, the concentration at any receptor on the building roof depends mainly on the exhaust momentum ratio, which is a function of stack diameter and exhaust speed, and wind speed.

Halitsky (1995) showed a 'concentration coefficient technique' for calculating the concentration field around a building when an exhaust is released from or near the building. According to Halitsky: "*A concentration coefficient is a nondimensional representation of a real concentration in the same sense that a pressure coefficient is a nondimensional representation of a real pressure.*" In both cases, the coefficient is found by dividing the measured quantity by an artificial reference quantity obtained from the field conditions.

The nondimensional concentration k as proposed by Halitsky (1990) is given by the following expression:

$$k = (C_e/C)AU_H/Q \qquad \text{[Eq 3.7]}$$

where C_e/C is the ratio of the exhaust concentration to the receptor concentration, Q is the exhaust flow rate, U_H is the wind speed at building height, and A is the area of the building upwind face or square of any suitable building characteristic length. Halitsky showed that the 'concentration coefficient technique' is quite accurate for predicting full-scale concentrations from scale-model test measurements.

A technique similar to Halitsky's 'concentration coefficient technique' is used in the present study. However, instead of calculating normalized concentration k, concentration values measured in the wind tunnel were converted to normalized dilution D_N, as suggested by Wilson et al. (1998). The usefulness of D_N derives from the fact that, it remains relatively constant for a variety of full-scale atmospheric conditions and varying ratio of exhaust velocity to wind speed. The dilutions were normalized by using exhaust flow rate, wind speed at the building height, and the building height.

Normalized dilution was derived assuming the roof level concentrations follow a Gaussian concentration profile, as suggested by Wilson et al. (1998). The present study is only concerned with roof level concentrations and in particular concentrations on the plume centerline, where maximum concentrations occur. The plume center line concentration at roof or ground level with the standard Gaussian equation is given by the following expression [from Turner (1994)]:

$$C = \frac{C_e Q}{\pi U_H \sigma_y \sigma_z} \left\{ \exp\left[-\frac{(h_s + \Delta h)^2}{2\sigma_z^2} \right] \right\} \qquad \text{[Eq 3.8]}$$

where σ_y and σ_z are the plume spreads in the crosswind and vertical directions, h_s is the stack height, and Δh is the effective plume rise (h_r - h_d).

Re-arranging Eq 3.8 and substituting minimum dilution $D_{min} = C_e/C$ gives:

$$\frac{D_{min}Q}{U_H} = \frac{\pi\sigma_y\sigma_z}{1}\left\{\exp\left[\frac{(h_s+\Delta h)^2}{2\sigma_z^2}\right]\right\} \qquad \text{[Eq 3.9]}$$

The left hand side of Eq. 3.9 will be non-dimensional, if divided by the square of any length scale. An appropriate length scale could be any of the building dimensions or length scales obtained from the ASHRAE Geometric Method. The height of the low-rise building (H = 15 m) was used for non-dimensionalizing Eq 3.9. Thus, the normalized dilution D_N is calculated by the following equation:

$$D_N = \frac{D_{min}Q}{U_H H^2} = \frac{\pi\sigma_y\sigma_z}{H^2}\left\{\exp\left[\frac{(h_s+\Delta h)^2}{2\sigma_z^2}\right]\right\} \qquad \text{[Eq 3.10]}$$

In the present study, a single value of U_H was used for all tests carried out in the wind tunnel. However, the results are applicable for different wind speeds since plume rise only depends on the exhaust momentum ratio, which is the ratio of exhaust speed to wind speed.

Table 3.1 Co-ordinates for different stack locations used in the comprehensive wind-tunnel study.

Stack location	x_s	y_s
S1	0.5h	0
S2	1.0h	0
S3	1.5h	0
S4	2.0h	0
S5	2.5h	0
A1	0.5h	2.5h

* h = 4 m

Table 3.2 Experimental parameters used for the comprehensive wind tunnel study

Parameters (full scale)	**Present study**
Model scale	1: 200
Boundary layer height (m)	170
Maximum reference wind speed (m/s)	12.5
Wind speed at building height U_H (m/s)	5.4
Upstream terrain	Urban
Power law exponent (α)	0.31
Upstream roughness (m)	1.1
Upstream turbulence at building height (%)	27[a], 18[b]
Stack diameter d_e (m)	0.60
Wind direction ($\theta°$)	0°, 45°
Stack height h_s (m)	1, 3, 5, and 7
Exhaust momentum M	1, 2, 3, and 5
Building along wind length L (m)	50
Building crosswind width W (m)	30, 50
Building height H (m)	15[a], 60[b]

a – Low-rise building
b – High-rise building

Table 3.3 Plume dispersion test cases in the comprehensive wind-tunnel study to obtain along-wind concentration profiles.

Building type	Building dimensions L x W x H (m)	Exhaust momentum (M)	Stack height h_s (m)	Wind direction (θ)	Stack location	RTS (w/h) h = 4m, l = 8m
Low-rise	50 x 5 0 x 15	1, 2, 3, 5	1, 3, 5, 7	0°, 45°	S1	2.5, 5, 7.5, 10, 12.5
		2	3, 5	0°, 45°	S2, S3, S4	2.5, 7.5
		1, 2, 3, 5	3, 5	0°,15°, 30°, 45°, 60°	S1, S2, S3, S4, S5	2.5, 7.5
	50 x 5 0 x 15*	1, 2, 3, 5	6, 8, 9, 10, 11, 12	0°, 45°	S1, S2, S3, S4, S5, A1	2.5, 7.5
	50 x 30 x 15	1, 2, 3, 5	1, 2, 3	0°	S1	2.5, 7.5
	50 x 5 0 x 15	2	3, 5	0°, 45°	S1	2.5, 7.5
High-rise	50 x 50 x 60	1, 2, 3, 5	1, 3, 5, 7	0°, 45°	S1	2.5, 5, 7.5, 10, 12.5
		2	3, 5	0°, 45°	S2, S3, S4	2.5, 7.5

* - Data was obtained at only a few sampling points.

Table 3.4 Plume dispersion test cases to obtain vertical and across-wind concentration profiles at x = 2h and 5h from stack.

Building type	Building dimensions L x W x H (m)	Exhaust momentum (M)	Stack height h_s (m) h = 4m	Wind direction (θ)	Stack location	RTS (w/h) h = 4m, l = 8m
Low-rise	50 x 5 0 x 15	2	1, 3, 5	0°, 45°	S1	0, 2.5, 7.5
High-rise*	50 x 5 0 x 60	2	3, 5	0°, 45°	S1	0, 2.5, 7.5

* - Only lateral concentration measurements were obtained.

Table 3.5 Key to stability categories [from Turner (1994)].

Surface Wind Speed (at 10 m),		Day			Night	
		Incoming Solar Radiation			Thinly Overcast or 4/8 Low Cloud	3/8 Cloud
m sec^{-1}	$Km.h^{-1}$	Strong	Moderate	Slight		
< 2	< 7	A	A-B	B		
2-3	7-11	A-B	B	C	E	F
3-5	11-18	B	B-C	C	D	E
5-6	18-22	C	C-D	D	D	D
> 6	> 22	D	D	D	D	D

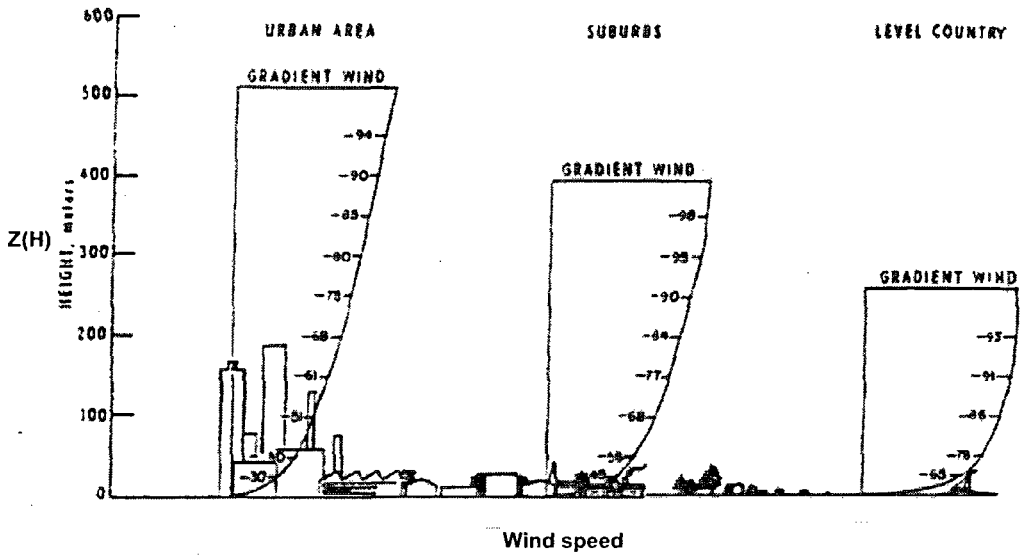

Figure 3.1 Boundary layer formation for different exposure categories [from Davenport (1963)].

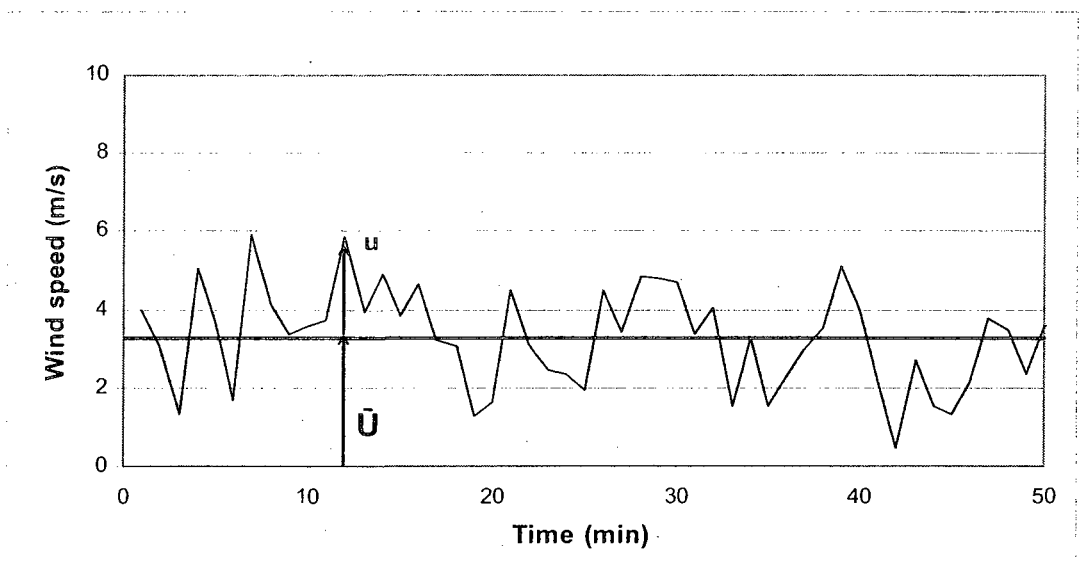

Figure 3.2 Typical wind-time history [from Stathopoulos et al. (2003)].

H = 15 m (full-scale)
L = W = 50 m (full-scale)

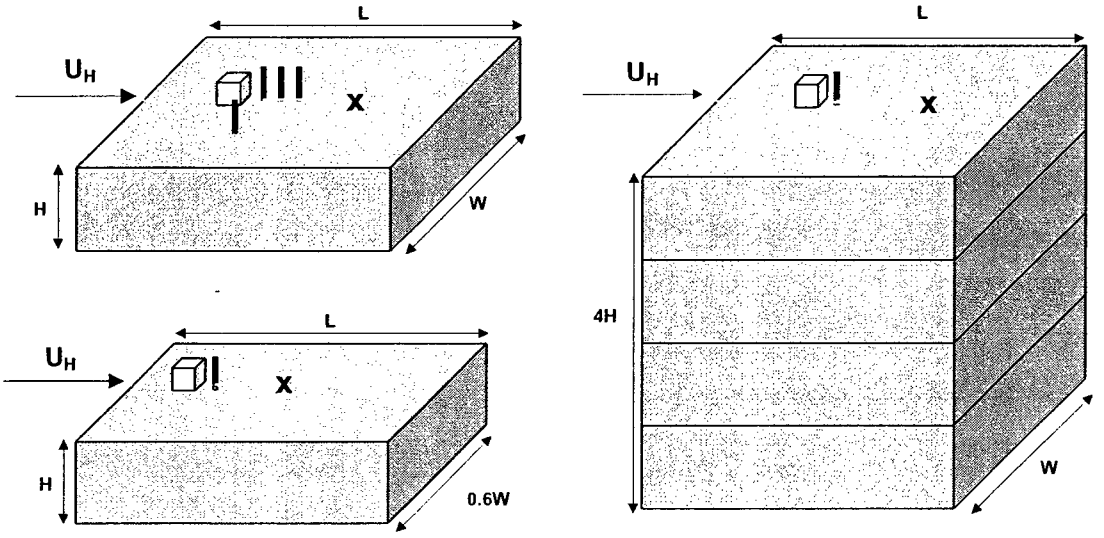

a) Low-rise buildings

a) High-rise building

h = 4 m (full-scale)
w = 10 m, 20 m, 30 m, 40 m, 50 m (full-scale)
l = 8 m (full-scale)

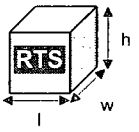

Figure 3.3 Full-scale dimensions of the model buildings and RTS used for the present study.

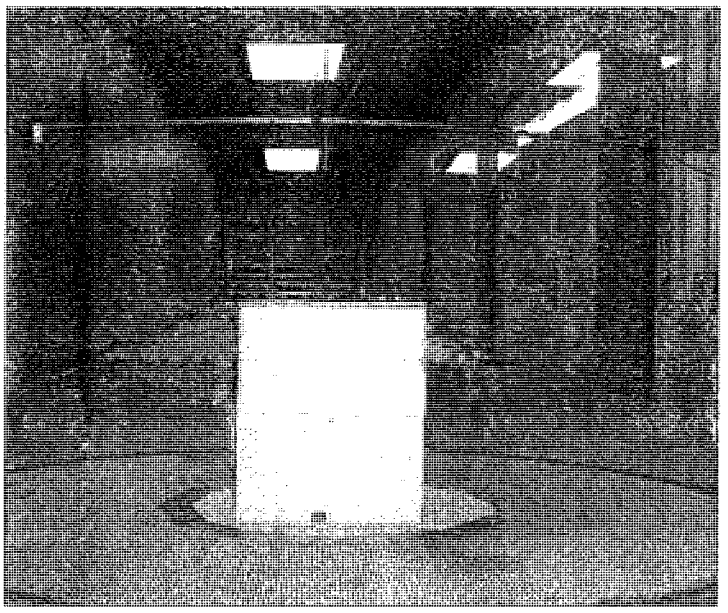

a) Tall building with wind approaching normal ($\theta = 0^{\circ}$) to the building upwind face.

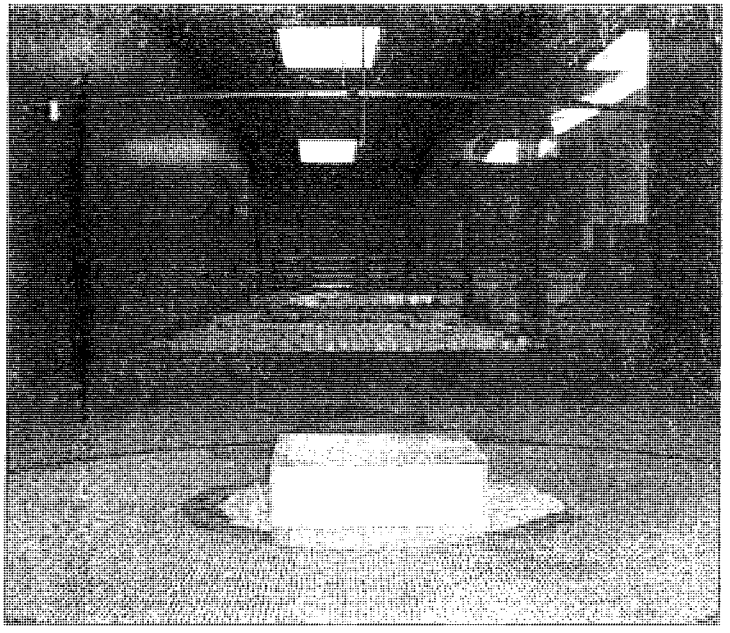

b) Low-rise building with wind approaching normal ($\theta = 0^{\circ}$) to the building upwind face.

Figure 3.4 Photograph of the wind-tunnel model used for the comprehensive study.

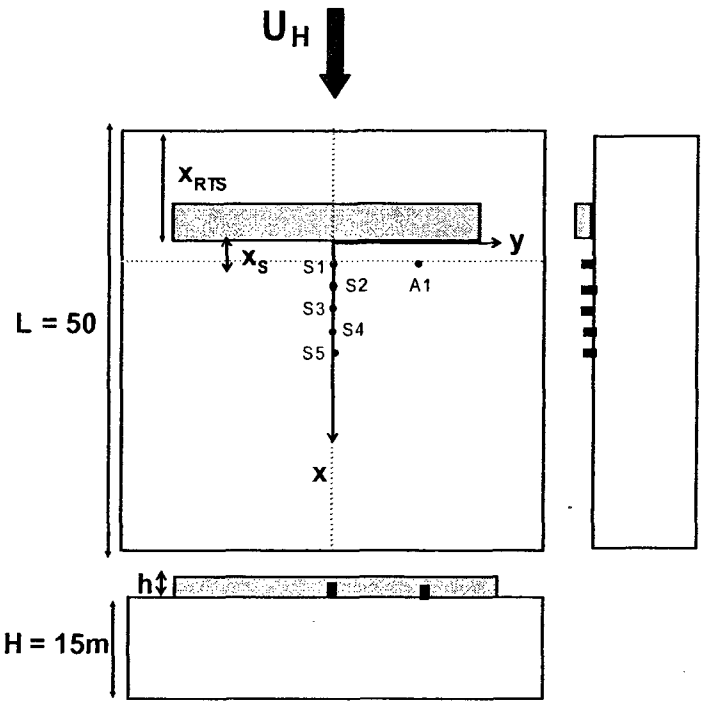

Figure 3.5 Stack locations tested in the comprehensive study.

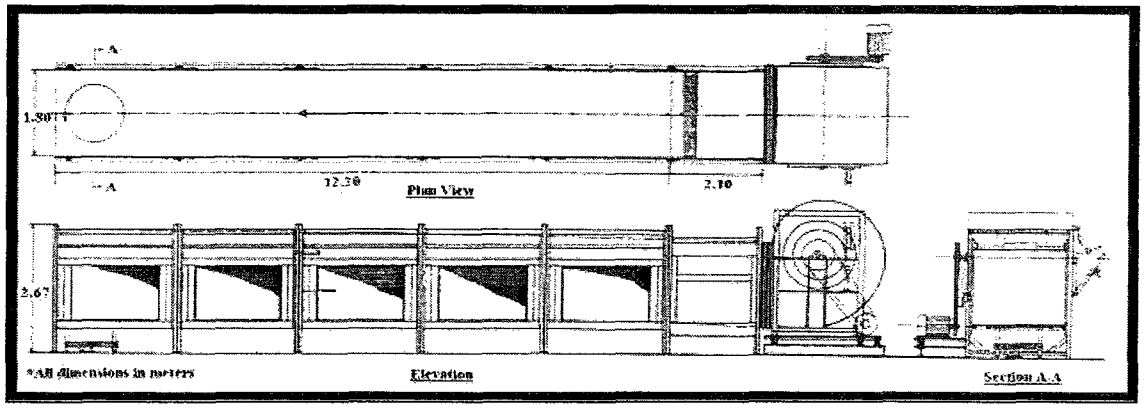

Length (m)	12
Width (m)	1.8
Height (m)	1.8
Max. U at reference height (m/s)	12.5

Figure 3.6 Concordia University's boundary layer wind tunnel.

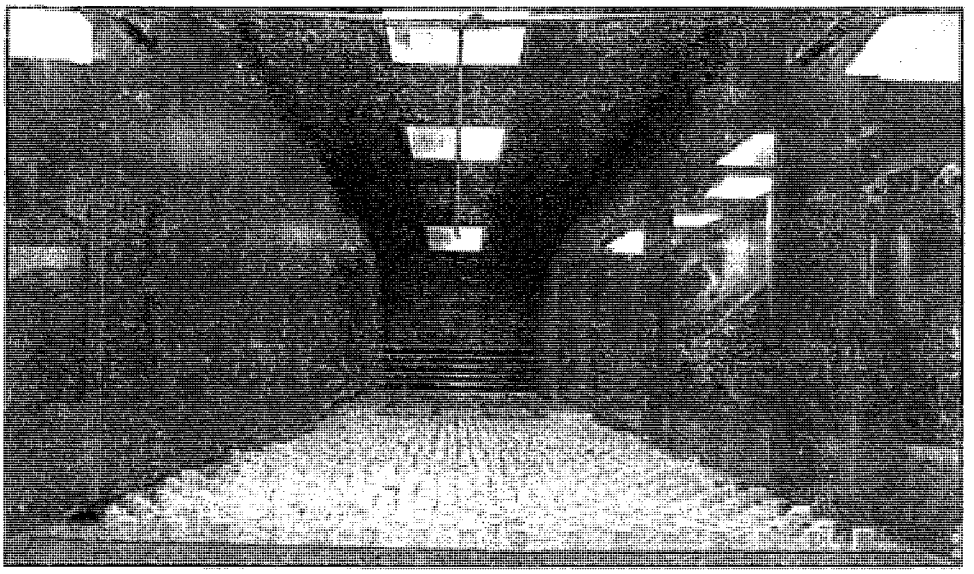

Figure 3.7 Upstream view of Concordia University's boundary layer wind tunnel for an urban exposure.

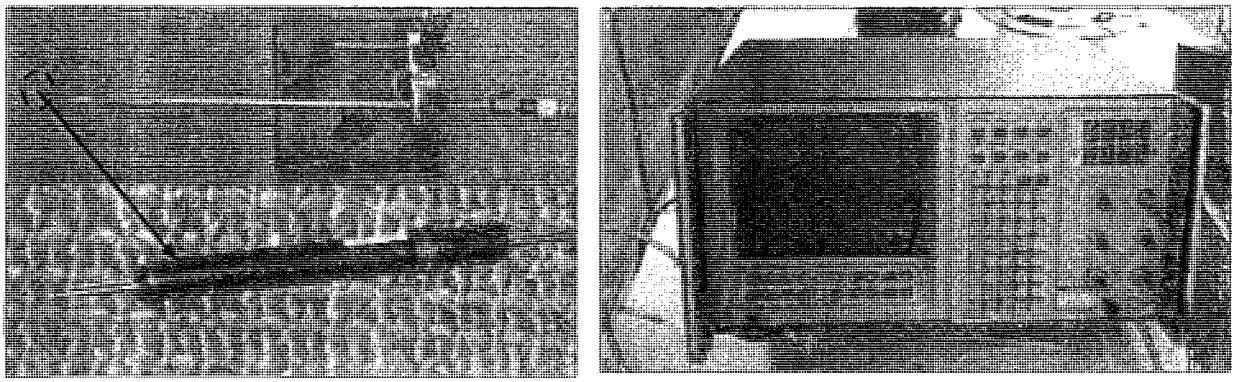

a) hot-wire anemometer

b) Data 6100

Figure 3.8 Photograph of instrumentation used for measuring mean velocity and turbulence intensity profiles: a) hot-wire anemometer and b) Data 6100.

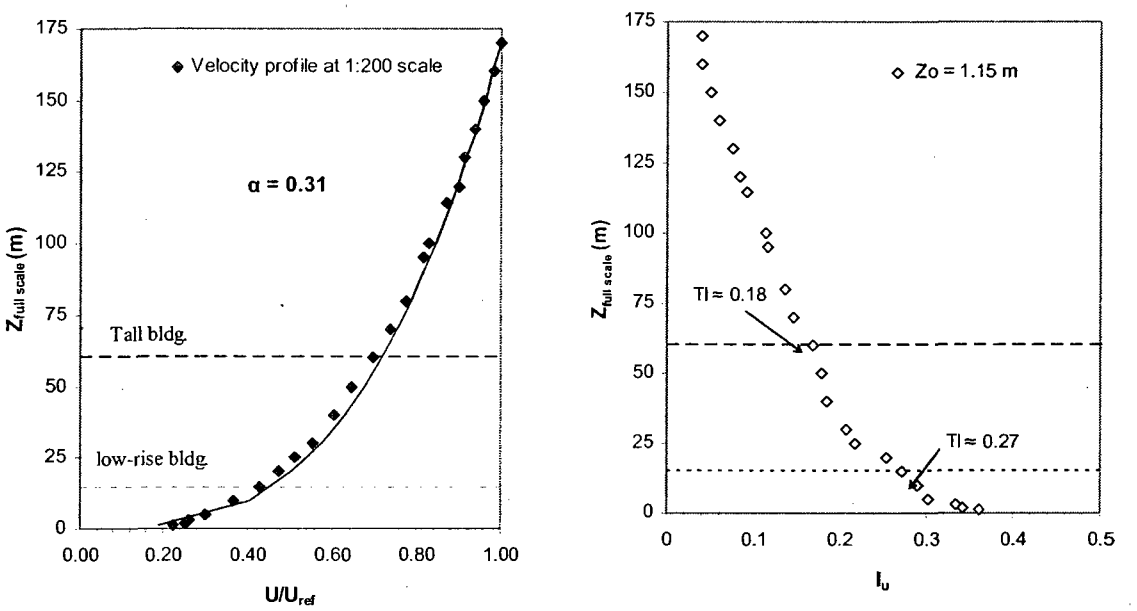

a) Mean velocity profile

b) Longitudinal turbulence intensity profile

Figure 3.9 Mean velocity and longitudinal turbulence intensity profiles.

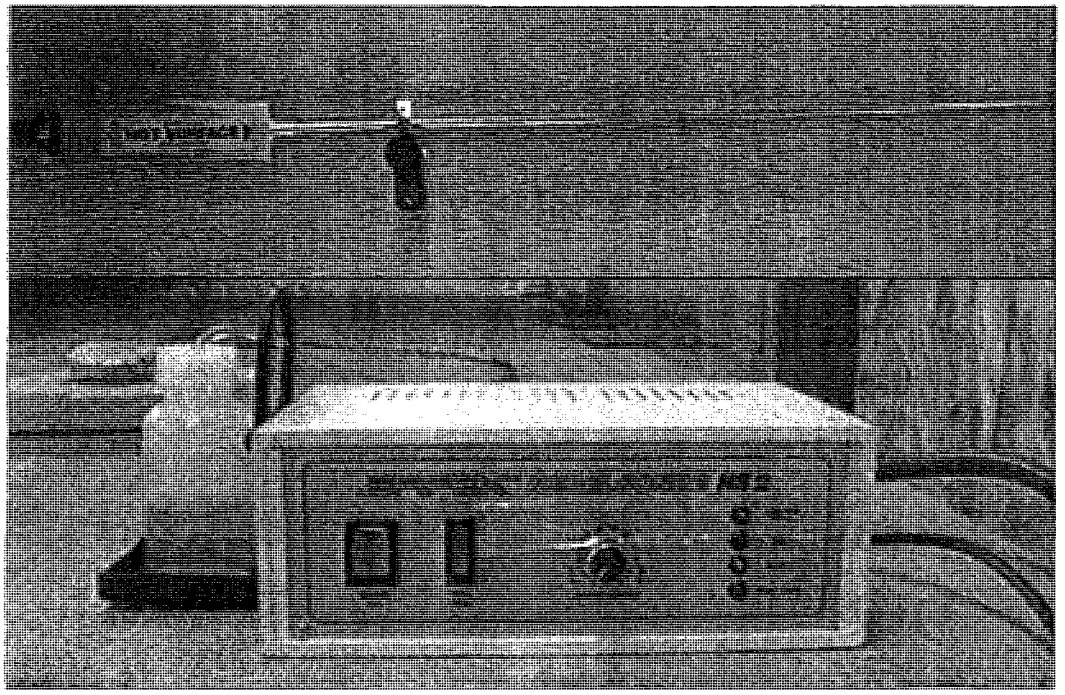

Figure 3.10 Dantec fog generator.

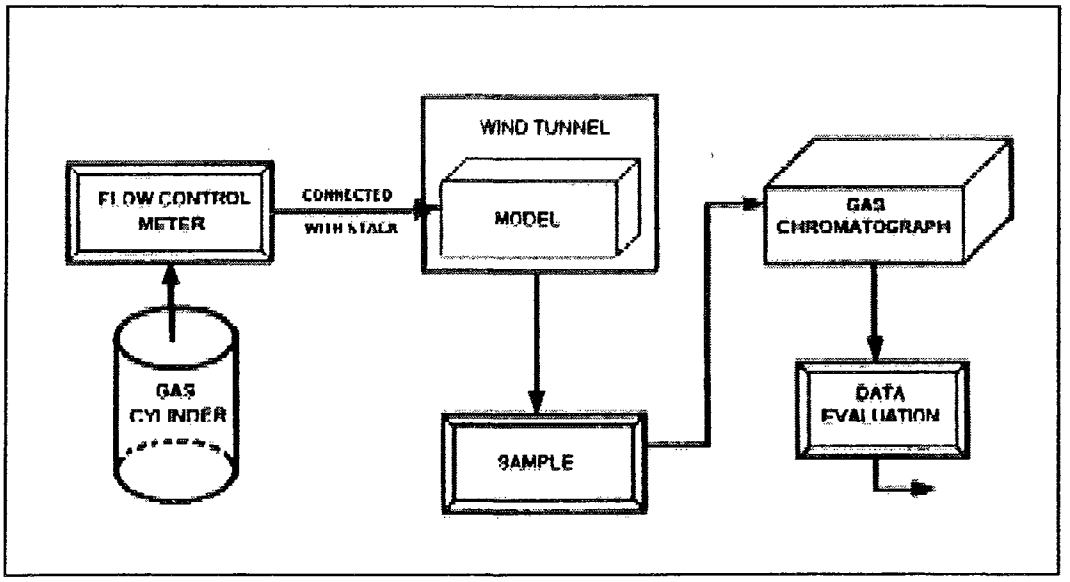

Figure 3.11 Tracer gas experiment system.

Figure 3.12 Mass flow meter.

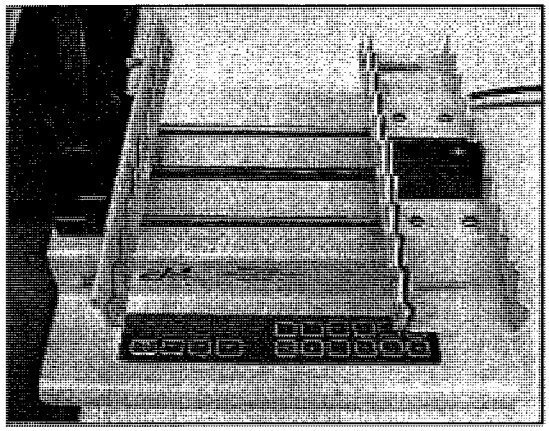

Figure 3.13 Multi-syringe sampler.

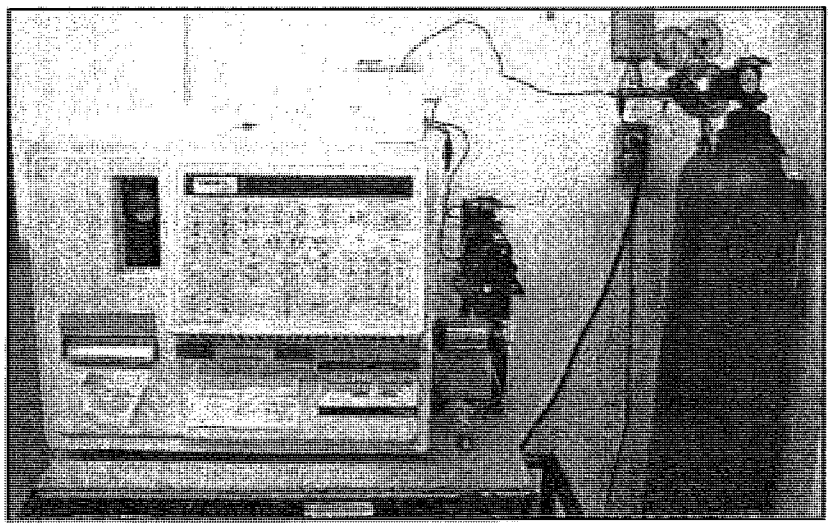

Figure 3.14 Gas chromatograph.

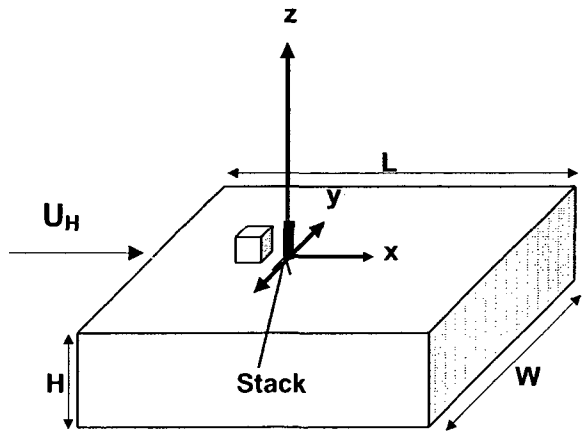

Figure 3.15 The local coordinate system used in the comprehensive wind-tunnel study.

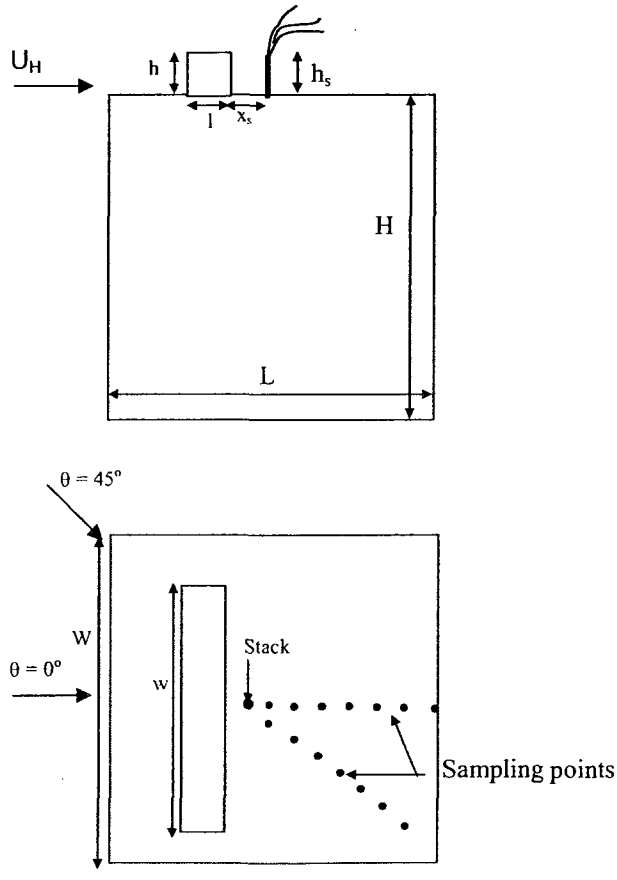

Figure 3.16 Sampling locations considered for along-wind concentration measurements in the comprehensive wind-tunnel study.

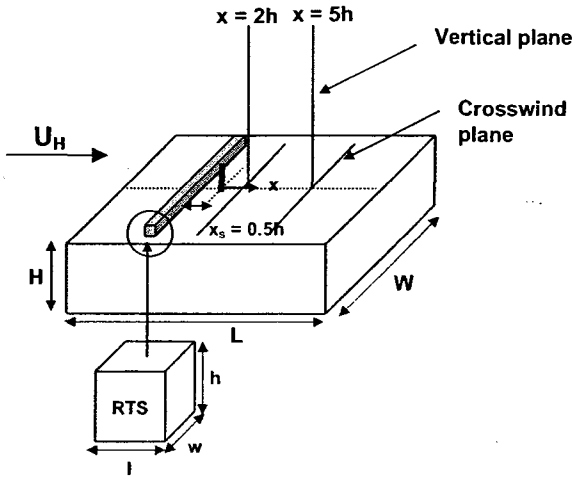

a) Normal wind ($\theta = 0°$)

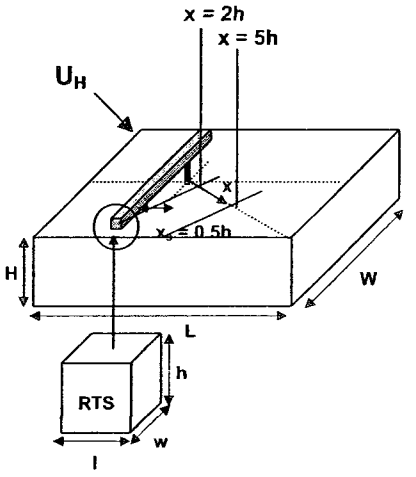

b) Oblique wind ($\theta = 45°$)

Figure 3.17 Crosswind and vertical concentration measurement planes for the normal and oblique wind directions considered in the comprehensive wind-tunnel study.

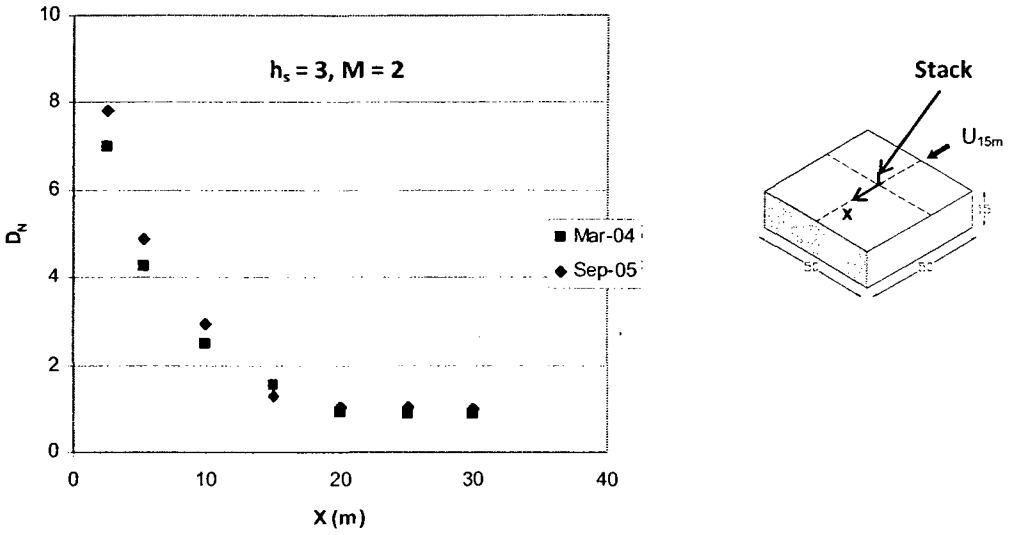

a) Normal wind (θ = 0°)

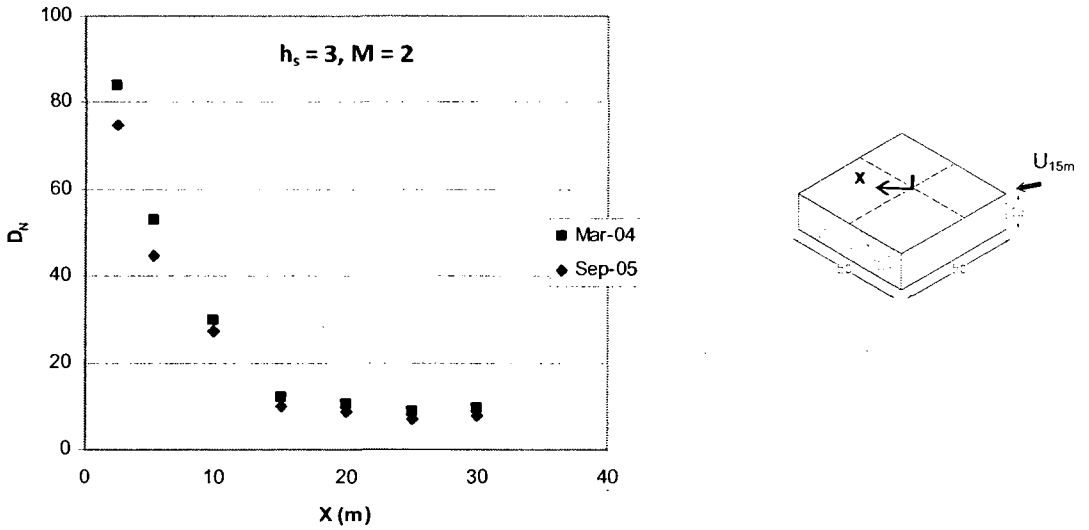

b) Oblique wind (θ = 45°)

Figure 3.18 Repeatability measurements for the low-rise building with no RTS.

Chapter 4

WIND TUNNEL RESULTS

4.1 Introduction

Wind tunnel experiments were carried out for a typical low- and high-rise building to quantify the downwash effect of an RTS located upstream of an emitting stack. The study will focus on the effect of a few critical experimental parameters on plume dispersion, which include:

i) RTS crosswind width (w);

ii) exhaust momentum ratio (M);

iii) stack height (h_s);

iv) wind direction (θ);

v) separation distance between stack and RTS (x_s).

vi) building height (H)

vii) building width (W)

The preliminary study [Saathoff et al. (2003a)] showed that the downwash effect of an RTS was insignificant for high-rise buildings for the normal wind direction ($\theta = 0°$). For $\theta = 45°$, the downwash effect of RTS was similar to that found for the low-rise buildings. The preliminary study was limited to one value of M (M = 2) and h_s ($h_s = 4$ m). Similar observations were made during the comprehensive study in which measurements were obtained for a wide range of M and h_s. The focus of the present study is to quantify

the downwash effect of an RTS on plume dispersion. Therefore, this chapter will focus only on concentration measurements obtained for the low-rise building for which RTS downwash effect on plume was significant. The concentration measurements obtained for the high-rise building for all cases tested are summarized in Appendix C.

4.2 Flow visualization

Flow visualization was conducted primarily to obtain a qualitative assessment of the downwash effect of an RTS on dispersion from isolated stacks on a building roof. Figure 4.1 shows a schematic representation of the flow visualization setup. The stack was located at a distance of 0.4L from the building leading edge and 0.5h from the RTS, where L = 50 m and h = 4 m are the building along-wind length and RTS height, respectively. The RTS leading edge was located 0.2L from the building leading edge. The height of the low-rise and high-rise buildings was 15 m and 60 m.

The flow visualization tests qualitatively assessed the following:

i) The size of separation bubble for the low-rise and the high-rise building for θ = 0°;

ii) The downwash effect of an RTS on the plume from a downwind stack for the low-rise building for θ = 0° and θ = 45°;

iii) The effect of separation distance between RTS and stack on the severity of downwash.

4.2.1 Building roof recirculation zone

To determine the size of the separation bubble that forms at the leading edge of the low-rise building for $\theta = 0°$, smoke was released from a flush stack ($h_s = 0$) located at x/H = 0.7 m, where x is the distance from building leading edge. To obtain a qualitative assessment of the flow fields around the test buildings, the size of recirculation zones estimated from flow visualization photographs were compared with the estimated recirculation zones using Wilson's (1979) method, previously discussed in section 2.4.5.4. ASHRAE (1999) notes that the dimensions of the recirculation zones are sensitive to the intensity and scale of turbulence in the approaching wind. High levels of turbulence generated from upstream buildings could decrease the dimensions of the bubble by up to half.

In brief, Wilson's model predicts the height and length of the building roof recirculation zone as $H_c = 0.22R$, and $L_c = 0.9R$. The parameter R is known as the scaling length and is given by, $R = B_s^{0.67} B_L^{0.33}$, where B_s is the smaller of the building upwind face dimensions (height or width) and B_L is the larger dimension. For the low-rise building $B_s = 15$ m and $B_L = 50$ m, producing R = 22.3 m. For the high-rise building $B_s =$ 50 m and $B_L = 60$ m, producing R = 53.1 m.

As outlined in Chapter 2, when the flow impinges on the windward wall of a building, it separates at the roof edge and forms a recirculation zone (separation bubble). Figure 4.2a shows the estimated dimensions of the separation bubble from the flow visualization photograph for the low-rise building with no RTS for $\theta = 0°$. Even though the re-attachment point of the flow is not clearly visible, estimation was made using the

curvature of the bubble. Values of H_c and L_c were approximately equal to 5.3 m and 22 m, respectively. Corresponding values predicted by the Wilson model are H_c = 4.9 m and L_c = 20.1 m and are also shown in Figure 4.2b. The estimated values of H_c and L_c are approximately 10% larger than the predicted values.

Figure 4.2c shows the flow visualization results for the low-rise building with an RTS. The crosswind width to height ratio of the RTS (w/h) was 7.5 in this case. The H_c valued estimated from the flow visualization photograph increased from 5.3 m for the flat-roof case to 6.8 m for the building with the RTS. More importantly, the smoke plume is bending downstream of the RTS. The phenomenon of downwash, due to the RTS, is quite apparent. The value of L_c obtained with the RTS was 36 m, which is 50% larger than the flat-roof value.

Figure 4.2d shows the predicted dimensions of separation bubble for the building and the RTS obtained with Wilson's formula. Note that the maximum height of the recirculation zone increased from 4.9 m to 5.7 m, due to the formation of the recirculation bubble on the top of the RTS roof. The along-wind length of the turbulence zone, L_c, of the building and RTS also increased from 20 m for the building with no RTS to 31.5 m with RTS. Values of H_c and L_c estimated from flow visualization photograph were approximately 15% greater than the values predicted by Wilson's model.

Figures 4.3a and 4.3b show the estimated dimensions of the separation bubble from the flow visualization photograph and from Wilson's model for the high-rise building. In this case, the entire roof was engulfed by the bubble. The predicted values of L_c and H_c were 47.8 m and 11.7 m respectively, which are similar (with a difference of <

5%) to the values estimated from the flow visualization photograph. Similarly, Figures 4.3c and 4.3d show the separation bubble for the high-rise building with an RTS. It is evident that a 4 m tall RTS does not significantly affect the flow over the building. The separation bubble for the building with RTS is similar in size to that of the building with no RTS. This indicates that an RTS totally engulfed by the building recirculation zone may not see the approaching flow. Therefore, the RTS may have little or no effect on plume dispersion.

4.2.2 Downwash effect of RTS on a plume for the low-rise building

This section will qualitatively assess the downwash effect of an RTS on a typical stack with h_s = 5 m (1.25h). The smoke visualization patterns obtained for a low-rise building for two RTS crosswind widths w/h = 5 and w/h = 12.5 for $\theta = 0°$ and $\theta = 45°$ are shown in Figure 4.4. For all cases shown, x_s = 0.5h.

Flow visualization results for the normal wind case ($\theta = 0°$) are shown in Figure 4.4a. Note that for the building with no RTS, the plume did not make any significant interaction with the building roof. With an RTS, w/h = 5, the plume was entrained within the turbulent wake of the RTS and a significant portion of it made contact with the roof. The smoke intensity and portion of the plume that is impacting the building roof appears to increase as the RTS crosswind width increases from w/h = 5 to w/h = 12.5. This indicates that downwash effect of RTS is stronger for a wider RTS.

Flow visualization results for the oblique wind case ($\theta = 45°$) are shown in Figure 4.4b. The downwash effect of RTS is clearly visible and the bending of the plume appears to be greater than that for $\theta = 0°$.

4.2.3 Effect of separation distance between stack and RTS

The distance between the stack and the RTS was gradually increased from x_s = 0.5h to 1.5h to assess the effect of stack-RTS separation on the plume. Smoke was released from a 4 m (1.0h) tall stack at a constant exhaust speed. Figures 4.5a and 4.5b show the flow patterns observed for normal and oblique wind directions for different stack/RTS separation distances. In all cases, w/h = 7.5.

For the normal wind case (see Figure 4.5a), the maximum downwash effect of the RTS was observed for the stack placed closest to the RTS (x_s = 0.5h). It is quite evident in the photographs that the plume was entrained inside the wake of the RTS. Smoke concentration is high close to the stack. As x_s increased to 1.0h and 1.5h, the entrainment downwind of the RTS reduced significantly. The downwash caused by the RTS appears to weaken as the separation distance increases. Similar results were obtained for the oblique wind case, as shown in Figure 4.5b.

4.3 Concentration measurements

This section will present the results of the tracer gas experiments. Before discussing the RTS downwash results, dilution data obtained for the low-rise building with no RTS in the present study will be compared with results from a few previous studies conducted on similar sized buildings.

4.3.1 Present study and previously published dilution data

It is important to compare data from the present study with results of previous studies to check the reliability of the concentration measurements and the experimental methodology. The comparisons presented are limited to low-rise buildings with no RTS. Few previous studies have been carried out for high-rise buildings or buildings with RTS. However, it can be assumed that if the results compare well for the low-rise case, the methodology is acceptable. The different studies used for the comparison are Lowrey and Jacko (1996), Schulman and Scire (1991), Wilson et al. (1998), and Petersen et al. (1999).

Lowrey and Jacko (1996) conducted a wind-tunnel study to quantify the effect of roof parapets on plume from a stack located on the roof of a 7 m tall building. The building has a square plan with the length and width equal to 100 m. Concentration measurements were obtained with and without a parapet for stacks located on the building centerline downwind of the parapet. The results obtained without the parapet are used for comparison with the present study wind-tunnel results. The h_s values ranged from 0 to 6 m. All measurements were obtained for M = 2 and for a normal wind ($\theta = 0°$).

Schulman and Scire (1991) conducted wind-tunnel experiments to investigate the effect of h_s and M on dispersion of exhaust from a rooftop stack on an isolated flat-roofed building. Tracer gas was released from the roof of a 15 m tall building for two wind directions, $\theta = 0°$ and $\theta = 45°$. The building has a square plan with the length and width equal to 75 m. Plume centerline concentrations were obtained on the building roof, leeward wall, and at ground level for h_s varying from 0 to 7.5 m and for M values ranging

from 0.75 to 5. The results obtained on the building roof are used for comparison with the present study wind-tunnel results.

Wilson et al. (1998) conducted extensive measurements in a water flume to evaluate the effect of adjacent buildings on dispersion of emissions from a stack located on the roof of a low-rise flat-roofed building. Concentration measurements were also obtained on the roof of a 12.2 m tall isolated flat-roofed building located in a suburban exposure, which are used for comparison with the present study wind-tunnel result. The length and width of the study building were 72 m and 30 m. The experiments were conducted for h_s = 2.1 m, 3 m, and 6 m and M values ranging from 1 to 8. All measurements were obtained for the flow normal to the upwind face of the test building.

Petersen et al. (1999) conducted a wind-tunnel study to determine the effect of architectural screens of different height, width, and porosity on plume dispersion from a rooftop stack. Concentration measurements were obtained along the plume center line on the roof of 15 m tall building for wind directions, $\theta = 0°$ and $\theta = 45°$. The length and width of the study building were 30 m and 15 m, respectively. The experiments were conducted for h_s ranging from 0.3 m to 6 m and M values ranging from 1 to 5. All measurements were obtained with and without architectural screens. The results obtained without the screens are used for comparison with the present study wind-tunnel results.

The results obtained from Schulman and Scire (1991) are in the form of normalized concentrations (k*) and data from Lowrey and Jacko (1996) and Petersen et al. (1999) are in the form of minimum dilutions (D_{min}). Wilson et al. (1998) data is in the form of normalized dilutions (D_N), similar to the present study. To make the data

obtained from previous studies comparable with the present study results, the data from previous studies other than Wilson et al. (1998). Equations 3.8 to 3.10 were used to convert normalized concentration and minimum dilutions to normalized dilution.

Comparisons with data from previous studies were made for different M and h_s for $\theta = 0°$. Typical examples will be shown for $h_s = 2$ m and 7 m, M = 2 and $\theta = 0°$. The comparisons for other M and h_s values showed similar trends and are provided in Appendix D. The experimental parameters and boundary conditions for the present and previous studies are summarized in Table 4.1. Some variation between experimental parameters is noted; for example, most of the studies were conducted with suburban exposure. However, the present study was carried out for urban exposure. The stack locations with respect to the building leading edge are also different in the separate studies. However, the most important experimental parameters (θ, h_r, h_p and x) have been matched as close as possible.

Wilson et al. (1998) showed that for a typical low-rise building, normalized dilution (D_N) values on the plume center line for stacks with different diameters producing the same plume rise should be comparable if, stack location, and stack heights are similar. Since, the stack diameters for the different studies varied (see Table 4.1), a similar approach is used for the validations presented.

Figure 4.6a shows the along-wind D_N profiles obtained for $h_s = 2$ m. Estimated D_N values obtained with the ASHRAE (2003) D_r dispersion model are also shown. Note that the present study results are shown with an error bound of ± 20%, representing the repeatability error found in the present study. The D_N profiles obtained from all studies

are very similar for this case. The D_N values from Schulman and Scire (1991) and Petersen et al. (1999) are towards the lower side compared with the other studies. This was probably because the plume rise for these studies was about 10–20% smaller than that for the other studies. The estimated plume rise values for different studies are shown in Table 4.2. The ASHRAE (2003) D_r model predicted reasonable dilutions for this particular case.

Figure 4.6b shows a similar comparison for a significantly taller stack ($h_s \sim 7$ m) and $M \sim 2$. The D_N values from the previous studies generally agree with the present study findings, except for the results of Wilson et al. (1998) obtained close to the stack ($x < 15$ m), which are significantly lower than those obtained in the other studies. Since the ASHRAE (2003) D_r model is based on the results of Wilson et al. (1998), predicted dilutions obtained with this model are also significantly conservative for $x < 15$ m.

Dilution values near the stack for this case should be large due to the height of the plume. The estimated plume height (h_p) from Briggs (1984) plume rise equation for neutral exhausts (see Eq 2.7) for $h_s = 7$ m and $M = 2$ is 10 m. Due to the large plume height and small vertical plume spread near the stack, the dilutions near the stack should be high. Thus, the results of the present study and those from Petersen et al. (1999), Schulman and Scire (1991) are as expected.

The discrepancy between Wilson's data and results of the other studies for the tall stack is unclear but it may be due to Wilson's methodology. Concentrations were obtained using analysis of video images of the dispersion of dye in a water flume.

In general, the dilution data from previous studies were within ± 30% of the present results for cases with similar plume rise values, with the exception of Wilson et al. (1998). Considering the difference in the boundary conditions for the various studies discussed above, and a repeatability error of ± 20% for the present study results, such differences are acceptable.

4.3.2 Effect of RTS on concentration measurements for the low-rise building

The following section will demonstrate the effect of RTS on along-wind, crosswind and vertical D_N profiles for the low-rise building with crosswind width W = 50 m. Note that the results for the low-rise building with W = 30 m were similar to the building with W = 50 m, with and without RTS. Along-wind D_N profiles for 30 m wide building are presented in Appendix E.

Minimum D_N values for the flat-roof building were obtained for $\theta = 0°$. On the other hand, $\theta = 45°$ was the critical wind direction for the building with RTS. From a stack design perspective the worst-case results are of primary concern. Therefore, the following section will focus on $\theta = 0°$ and 45°. Concentration data were obtained for θ values of 0° to 60° and are shown in Appendix E.

The downwash effect of RTS crosswind width on D_N values will be presented for $h_s = 0.75h$ (3 m) and M = 2. The effect of RTS crosswind width on D_N values was generally similar for other h_s and M values. However, the downwash effect reduced with the increase in h_s and M and decrease in w/h.

A key parameter in the stack design process is the exhaust momentum ratio, $M = w_e/U_h$. ASHRAE (2003, 2007) recommend designing stacks for $M > 1.5$ in order to avoid stack tip downwash. Although the experiments were conducted for different M values (M = 1, 2, 3 and 5), as a representative practical worst-case scenario, the effect of RTS width on D_N values will be presented for M = 2, which corresponds to relatively strong wind conditions for which plume rise is relatively small. It should be noted that M-values for high-flow stacks ($w_e > 15$ m/s) may range from 3 to 5 during more moderate wind conditions. At these higher M-values, plume downwash will be less severe.

4.3.2.1 Effect of RTS crosswind width on along-wind D_N profiles

Figure 4.7 shows the effect of RTS crosswind width on along-wind DN profiles for the low-rise building. Results are presented for non-dimensional RTS width (w/h) ranging from 2.5 to 12.5. Tracer gas was emitted from stack S1 located at 2 m (xs = 0.5h) from the leeward wall of the RTS. Data for the flat-roof building are also shown for comparison.

For the case of $\theta = 0°$ (Figure 4.7a), the addition of RTS produced the following impacts:

(1) D_N values reduced significantly near the stack compared to flat-roof case. It is important to note that significant downwash occurred even with the smallest RTS (w/h = 2.5).

(2) For the smallest RTS, D_N values reduced nearly 10 times at the sampler located closest to the stack. However, D_N reduced by a maximum of about 20 times for the RTS with $w/h \geq 7.5$.

(3) D_N values obtained with the RTS did not change much with x. The reduction in D_N values due to the downwash effect of the RTS was more pronounced for samplers placed close to the RTS ($x < 2.5h$).

(4) The D_N values reduced with increase in w/h up to w/h = 7.5. A further increase in w/h had little effect on D_N values.

It should be noted that additional configurations were tested. Reduction in D_N varied depending on h_s and M values. The results for other h_s and M values tested are presented in Appendix E. In general, the reduction in D_N could vary from 2 to 100 times depending on x, h_s, θ and M values.

The above findings can be explained from the building wake velocity measurements of Snyder and Lawson (1994). Their results showed that the along-wind length of the near wake increases significantly with increase in building crosswind width (see Figure 2.4). Results are expected to be similar for an RTS for the cases when the RTS is exposed to the flow (e.g. for the low-rise building). The predicted characteristic lengths of recirculation zones (see Figure 2.12) for the different RTS tested are summarized in Table 4.3. Results shown in Table 4.3, which were determined using equations from Wilson (1979), indicate that the height and length of the RTS downwind cavity (h_c, l_c) nearly doubled with a five-fold increase in RTS crosswind width from w/h = 2.5 to 12.5. A higher and longer downwind cavity will entrain more of the plume and reduce plume height, which causes lower dilutions for the wider RTS as shown earlier in Figure 4.7a.

Figure 4.7b shows similar plots for $\theta = 45°$. For this case, D_N values for the flat-roof building are, on average, 10 times higher than dilutions obtained for $\theta = 0°$. Similar

results have been reported by Wilson and Winkel (1982), Petersen et al. (2002c), and Schulman and Scire (1991) for typical low-rise flat-roofed buildings. High D_N values for $\theta = 45°$ occur due to the absence of the separation bubble that form at the roof leading edge for $0° \leq \theta < 30°$. For $\theta > 30°$, delta wing vortices are formed around the building upwind edges (see Figure 2.3). Petersen et al. (2002c) showed that for diagonal wind directions, the ratio of the wind speed over the building roof to the approach wind speed is relatively constant. This indicates that for an oblique wind, flow over building roof is not significantly affected by building-generated turbulence. Consequently, for an oblique wind, the plume rise may be greater than that for the normal wind case, which produces higher dilutions.

Similar to the normal wind case, D_N values were significantly reduced with the addition of the RTS for $\theta = 45°$. However, the D_N values did not depend significantly on x and w/h. In general, the D_N values for $\theta = 45°$ were approximately half of those obtained for $\theta = 0°$, indicating a stronger downwash effect for the oblique wind direction. This was generally true for other h_s and M values tested.

For an oblique wind, the crosswind width of the RTS exposed to the approaching flow is greater than that for $\theta = 0°$. This will produce a longer and wider downwind wake cavity for $\theta = 45°$. As indicated previously, a longer and wider wake entrains more of the plume, which produces lower D_N values at the roof level.

4.3.2.2 Effect of RTS on crosswind concentration (C_N) profiles

Span-wise concentration measurements were obtained for the low-rise building to demonstrate the effect of RTS on crosswind plume spread. The results are expressed as normalized concentration (C_N), which is defined as:

$$C_N = CU_H H^2/C_e Q = 1/ D_N \qquad \text{[Eq 4.2]}$$

where C is the receptor concentration and C_e is the exhaust concentration. Normalized concentration is used instead of dilution so that the results can be compared with the classical Gaussian model.

Figure 4.8 shows the lateral C_N profiles for the low-rise building measured at x = 2h and x = 5h, where x is the distance downwind of the stack. The results are shown for M = 2 and h_s = 0.75h for $\theta = 0°$. The lateral plume spread (σ_y) values are also presented. The σ_y values were estimated by assuming that the lateral concentration profile follows a Gaussian distribution.

The expression used to fit a Gaussian distribution is:

$$c(y) = c_{max}\left\{\exp\left[-\frac{(y + y_c)^2}{2\sigma_y^2}\right]\right\} \qquad \text{[Eq 4.3]}$$

where c(y) is the concentration at lateral distance y, c_{max} is the maximum concentration and y_c is the lateral displacement of the plume.

The results presented in Figure 4.8a for $\theta = 0°$ show that the lateral C_N profiles are symmetrical along the y-axis; therefore $y_c = 0$. Note that at x = 2h, the σ_y value for the

building with the RTS is 23% larger than that obtained with the flat-roof building, indicating a wider plume for the building with the RTS. However, at x = 5h, σ_y value increased by only 7%, as shown Figure 4.8b. This is further evidence that for $\theta = 0°$ the effect of RTS on plume is less significant at samplers located far (x > 5h) from the stack.

Results obtained by Wilson et al. (1998) for a flat-roofed building at x = 5h, M = 1 and h_s = 3 m (0.75h) are also included in Figure 4.8b. Note that the Wilson et al. (1998) data are generally similar to the present study results. However, c_{max} was greater than that obtained for the present study due to the lower M value used in Wilson's study. The low M value produced minimal plume rise, which resulted in higher concentrations.

Figure 4.9 shows the lateral C_N profiles for the low-rise building measured at x = 2h and x =5h for $\theta = 45°$. The σ_y values are also presented. With the RTS, c_{max} occurred at an offset of approximately y = -5 m. Therefore, in order to obtain a better fit for this case, y_c = -5 m for the building with the RTS.

The lateral shift in c_{maxy} for $\theta = 45°$ can be explained by the flow fields measured around buildings for oblique winds from Snyder (2005). Figure 4.10 shows the flow fields around buildings with W/H = 1 and W/H = 4 for normal and oblique wind directions. The complexity of the flow downwind of the buildings is clearly visible for both wind directions. The flow downwind of the building for the normal and oblique winds is symmetrical for the building with W/H= 1, as shown in Figures 4.10a and 4.10b. However, the flow field downwind of the wider building (W/H = 4) for an oblique wind is unsymmetrical, as shown in Figure 4.10d. In the present study, the flow around an RTS for an oblique wind could be even more complex due to building effects, causing a lateral

shift in c_{max}. Since the flow field downwind of the RTS for an oblique wind is not symmetrical along the approaching wind direction, the mean plume trajectory does not coincide with the approaching wind direction. Consequently, the lateral C_N profiles are unsymmetrical about the approaching wind direction.

Notice that for $\theta = 45°$, the σ_y value obtained at both locations x = 2h and x = 5h (Figures 4.9a and 4.9b) for the flat-roof case were about 10–20% smaller than those for $\theta = 0°$. This indicates that for the flat-roofed building, the plume is narrower for the oblique wind than that for the normal wind, further evidence that for $\theta = 45°$, the plume is less affected by the building generated turbulence than that for $\theta = 0°$. For the normal wind direction the turbulence generated due to the separation bubble formed at the building leading edge could significantly affect the plume. However, for an oblique wind, delta wing vortices are formed. Consequently, the maximum C_N value at both locations x = 2h and x = 5h is greater for $\theta = 0°$ and the concentration values are more spread out in the crosswind direction compared to $\theta = 45°$.

Similar to the normal wind case, the σ_y values obtained for $\theta = 45°$ were greater for the building with the RTS compared to the flat-roof case, indicating a wider plume with an RTS compared to the flat-roof case. At x = 2h, the plume spread for the building with the RTS nearly doubled compared to the flat-roof case (see figure 4.9a). A wider plume spread indicates that the downwash effect of the RTS on the plume is greater for $\theta = 45°$ than that for $\theta = 0°$.

The crosswind profiles for $\theta = 45°$ at x = 5h are shown in Figure 4.9b. As the plume travels farther from the stack it will spread in the crosswind and vertical directions.

Consequently, the σ_y value for the flat-roofed building at x = 5h increased by about 24% compared to the σ_y value obtained at x = 2h. However, it is interesting to see that there is only a marginal increase of nearly 5% in the σ_y value for the building with the RTS. This indicates that the effect of the RTS on the plume is still very strong at x = 5h. For $\theta = 45°$ the lowest D_N values were nearly similar at x = 2h and x = 5h for the building with the RTS. This further confirms the results presented previously in section 4.3.2.1, which showed the downwash effect of RTS on a downwind stack for $\theta = 45°$ (see Figure 4.7b).

4.3.3.3 Effect of RTS on vertical dilution profiles

Vertical dilution profiles were obtained for the low-rise building with and without RTS. The objective of the vertical profile concentration measurements is to demonstrate the effect of RTS on plume height (h_p). The plume height was estimated from the vertical dilution profiles obtained in the present study for the low-rise building and corresponds to the height at which minimum D_N value occurs.

The vertical dilution profiles obtained at x = 2h and x = 5h for $\theta = 0°$ are shown in Figures 4.11a and 4.11b, respectively. Results are shown for M = 2 and $h_s = 0.75h$. The decrease in measured value of h_p at both measured locations x = 2h and x = 5h for the building with an RTS is quite evident. At x = 2h, values of h_p for the flat-roof building and the building with RTS were 1.2h and 0.9h, respectively. At x = 5h, values of h_p for both the flat-roof case and the building with RTS were similar to those obtained at x = 2h. Thus, for this stack location, the presence of the RTS reduces h_p by 30%.

The vertical dilution profiles obtained at x = 2h and x = 5h for $\theta = 45°$ are shown in Figures 4.12a and 4.12b, respectively. For $\theta = 45°$, $h_p = 0.68h$ with the RTS, which is a reduction of 40% compared to the flat-roof case. A greater reduction in h_p for $\theta = 45°$ indicates a stronger downwash than that for $\theta = 0°$. This further supports the finding that the downwash effect of an RTS is stronger for oblique winds.

Note that in Figures 4.11 and 4.12, the vertical D_N profiles for the flat-roofed building are relatively symmetrical about the height at which the minimum D_N value was obtained. In addition, the profiles for $\theta = 45°$ are more symmetrical compared to that obtained for $\theta = 0°$, indicating that the effect of building on the plume for an oblique wind is less than that for the normal wind. This also supports the observation made previously that D_N values on the roof surface of the flat-roofed building are significantly higher for $\theta = 45°$ that those for $\theta = 0°$.

For the building with the RTS, the D_N profiles are relatively unsymmetrical. This happens because of the plume reflection [Turner (1994)]. Due to the downwash effect of the RTS, the plume makes contact with the roof and gets reflected upwards. Because of the reflection of the plume at the roof surface, the samplers located close to the RTS get double concentration, as also indicated by the classical Gaussian model.

The magnitude of the reduction in h_p varied significantly with h_s. Figure 4.13 shows h_p values estimated from the vertical D_N profiles and ASHRAE (2003, 2007) plume rise equations (Briggs (1984) simplified plume rise model) for the low-rise building with and without the RTS for M = 2 and $\theta = 0°$. Results are presented in the form of non-dimensionalized plume height (h_p/h) for h_s values ranging from 0.25h to

1.25h. The estimated h_p values obtained from Briggs (1984) extended plume rise equations (discussed later in Chapter 5) are also shown. It is important to note that the ASHRAE plume rise equations do not take into consideration the downwash effect of an RTS. Therefore, h_p values estimated with ASHRAE plume rise equations represent only for the building with no RTS.

As shown in Figure 4.13a, the plume rise values estimated from vertical D_N profiles are about 25% smaller compared to the ASHRAE (2003, 2007) estimated values. The difference is nearly same with the increase in stack height indicating that the plume rise is nearly independent of the release height. The differences between wind tunnel and ASHRAE estimated h_p for the flat-roof case is possibly due to the way plume height is estimated by ASHRAE (discussed later in Chapter 5). In brief, the plume rise equation adopted by ASHRAE (2003, 2007) is a simplified version of Briggs (1984) plume rise model, which does not take into consideration the effects of upstream terrain (roughness). Note that the h_p values estimated from measured data are similar to the values obtained with the Briggs (1984) extended plume rise equations.

Figure 4.13b shows the h_p values estimated from wind tunnel results and the ASHRAE equation for the building with the RTS for $\theta = 0°$ and $\theta = 45°$. The h_p values estimated from the vertical profiles for the building with no RTS are also shown for comparison. Note that, contrary to the flat-roofed building, the plume rise for the building with RTS is not independent of the release height. For a stack height increase from 0.25h to 0.75h, the change in plume rise for the both wind directions $\theta = 0°$ and $\theta = 45°$ was minimal, about $\pm$ 10%. For $\theta = 45°$, the plume height reduced with increase in stack

height indicating a stronger effect of RTS for $\theta = 45°$ compared to $\theta = 0°$. This further justifies that the plume was significantly entrained within the RTS downwind cavity, which limited the plume rise for a stack lower than RTS height (h = 4 m). With a further increase in stack height from 0.75h to 1.25h, the plume height increased by about 30%. This shows that for stacks taller than the RTS, more of the plume managed to escape the downwash effect of RTS.

The results presented above are limited for M = 2, x_s = 0.5h and limited stack heights. The subsequent sections will discuss in detail the effect of different h_s and M values on D_N values for the low-rise building with and without an RTS.

4.4 Effect of various parameters on normalized dilutions (D_N)

The present section will discuss the effect of different experimental parameters like h_s, M, θ and x_s on the along-wind D_N profiles (D_N vs. x/h) obtained on the roof of the low-rise building. Sampling locations are shown in Figure 3.5. For $\theta = 0°$, the measurement locations coincide with the plume centerline. However, for $\theta = 45°$, this may not be the case due to complexity of the flow for the oblique wind direction, as discussed previously in section 4.3.2.2. Nevertheless, the data for $\theta = 45°$ can still be used to investigate the influence of the parameters mentioned above.

4.4.1 Effect of stack height (h_s)

For the building with no RTS, an increase in h_s increased D_N values at all sampling locations for both normal and oblique wind directions. Results were similar for all M values tested (M = 1, 2, 3, and 5). The D_N profiles for the flat-roofed building for h_s

ranging from 1 m to 7 m for $\theta = 0°$ are shown in Figure 4.14. Results are shown for M = 2 and M = 5, respectively. Note that the effect of an increase in h_s is most significant close to the stack. For both M values, an increase in h_s by a factor of 7 increased D_N values by approximately 1000 times at the sampler located closest to the stack and nearly 10 times at the farthest sampler.

Similar D_N trends for the building with RTS (w/h = 7.5) are shown in Figure 4.15. For $\theta = 0°$, the effect of h_s on D_N was similar to that for the flat-roof case. However, the effect of h_s on D_N was more significant for $h_s > h$ for both M = 2 and M = 5. For $h_s < h$, the stack is engulfed within the RTS downwind cavity. Therefore, the plume is significantly affected by the RTS downwash effect. For $h_s = 1.75h$, the plume height is much greater than the height of the RTS recirculation zone and consequently, the downwash effects of the RTS are reduced. Therefore, for both M values, the maximum increase in D_N values occurred when the stack height was increased to 1.75h.

The D_N profiles for the flat-roofed building for h_s ranging from 1 m to 7 m for $\theta = 45°$ are shown in Figure 4.16. The results obtained for $\theta = 45°$ were similar to those obtained for $\theta = 0°$. Increasing the stack height increased the D_N values at all sampling locations. Note that for the low M value (M = 2), the D_N values increased significantly with increase in stack height. As shown in Figure 4.16a, for M = 2, the D_N values increased by a factor of 1000 with an increase in h_s from 1 m to 7. However for M = 5, the effect of an increase in stack height was about 10 times for the same increase in stack height (see Figure 4.16b). This indicates that the effect of stack height is more crucial for low M values where a small change in stack height could allow the plume to escape the

building effect on plume. At greater M values, the plume rise is higher compared to a low M value. Once the plume is outside the building turbulence region, the effect of stack height on D_N values is smaller, as shown in Figure 4.16b for M = 5.

Similar D_N trends for the building with an RTS (w/h = 7.5) for $\theta = 45°$ are shown in Figure 4.17. The effect of stack height is similar to the flat-roof case. However, increasing h_s was not that significant for the low M case, (M = 2). For an oblique wind, a stack height of 1.75h is required to significantly increase the D_N values when M is low due to severity of downwash. For M = 2 and h_s = 0.75h, the plume height is 6 m, which is nearly the same as the height recirculation zone formed on the top of the RTS measured from the building roof. Consequently the plume is entrained within the RTS downwind wake and dilutions are relatively similar for $h_s \leq 0.75h$. With an increase in stack height, a significant portion of plume escaped the effect of the RTS thus producing significantly higher D_N values for h_s = 1.75h.

4.4.2 Effect of exhaust momentum ratio (M)

Increasing M increases the plume rise and eventually the final plume height and thus has a similar effect as h_s on D_N profiles. In addition, an increase in M also produces increased entrainment of ambient air into the plume which creates additional dilution [Wilson and Lamb (1994)]. Consequently, a higher M value will produce an increase in D_N values at all locations.

Figures 4.18a and 4.18b show the effect of M on D_N values for the flat-roofed building for h_s = 1 m and 5 m, respectively. Results are presented for $\theta = 0°$ and for M

values 1, 2, 3, and 5. The effect of M was more significant closer to the stack. The D_N values increase as x decreases except for h_s = 1 and M = 1. As shown in Figure 4.18, increasing M from 1 to 5 increased D_N by a factor of 60 for h_s = 1 m and about 30 for h_s = 5 m. Note that the effect of M on D_N values is not as drastic as was observed with increase in h_s.

Figure 4.19 shows the effect of M on D_N values for the building with the RTS for h_s = 0.25h (1 m) and 1.25h (5 m) for θ = 0°. For the shorter stack, the plume is significantly affected by the downwash effect of the RTS, primarily for samplers located close to the stack (see Figure 4.19a). Compared to the flat roof results, the D_N values did not vary much with x even for the tall stack. Even an M value of 5 is not enough to discharge the plume outside the RTS recirculation zone. Consequently, increasing the M value to 5 produces only a moderate increase of about 10 times in D_N values near the stack compared to M = 1.

For the taller stack (h_s = 1.25h), the effect of increase in M was more apparent near the stack (see Figure 4.19b). Note that for M > 1 the D_N values increased near the stack indicating a portion of plume managed to escape the effect of the RTS. A five-fold increase in M value from 1 to 5 increased D_N values by a factor of nearly 10 close to the stack compared to an increase of nearly 30 times in D_N values for the flat-roof case.

Figures 4.20a and 4.20b show the effect of M on D_N values for θ = 45° for h_s = 1 m and 5 m, respectively. Similar to the normal wind case, D_N values at all sampling locations increased with increase in M values. The effect of M was significantly higher for h_s = 1 m compared to h_s = 5 m. With a five-fold increase in M, the D_N value increased

by up to 200 times for h_s = 1 and by a factor of 10 for h_s = 5 m. The reason being the same as highlighted earlier while demonstrating the effect of h_s on D_N for the oblique wind case. For a low stack height, a small increment in M value could allow the plume to escape the building turbulence zones. However, once the plume is outside the building turbulence region, such as for the tall stack height, the effect of M will be smaller, as shown in Figure 4.20b.

Similar D_N trends showing the effect of M on D_N for $\theta = 45°$ for the building with the RTS are shown in Figure 4.21. Results are shown for h_s = 0.25h and 1.25h. In general, increasing M from 1 to 5 increased the D_N values by a factor of 10 for both the stack heights. The along-wind length of the RTS downwind cavity for an oblique wind is greater than that for the normal wind case. Thus, the D_N profiles for all M values are relatively independent of x.

In general, increase in plume rise is the key factor for the plume to escape the influence of building recirculation zones. For oblique winds, the separation bubble is not produced at roof edges, and instead delta wing vortices are formed due to the absence of the separation bubble (see Figure 2.3b). Plume rise is also higher for an oblique wind. Therefore, for the low-rise building case, an increase in M or h_s increased D_N values at all sampling locations. However, the effect of M and h_s on D_N was more prominent closer to the stack.

4.4.3 Effect of stack location

Stack location is one of the most important parameters in the initial stack design process. This section demonstrates the importance of stack location with respect to an

RTS. The stack locations tested are shown in Figure 3.5 and x-y coordinates are provided in Table 3.1. Stacks S1 to S3 were located on the roof centerline at distances of x_s = 0.5h to 1.5h, each with a spacing of 0.5h between them. Stack A1 was located off the building centerline at x_s = 0.5h and y_s = 2.5h.

Along-wind D_N profiles obtained with stacks S1, S2, S3 and A1 for the low-rise building for $\theta = 0°$ are shown in Figure 4.22a. Results are shown for the building with and without RTS for h_s = 0.75h and M = 2. Moving the stack from S1 to S3 for the building with no RTS increased D_N values by nearly 10% and could be due to repeatability error, which was around 20% in the present study. However, moving the stack laterally from S1 to A1 had negligible effect on D_N values. The effect of stack location on D_N values was more significant for the building with an RTS. Moving the stack downstream of the RTS significantly increased D_N. With the RTS present, moving the stack from S1 to S3 increased the D_N values by approximately four times, primarily at sampling locations close to the stack ($x < 2.5h$). However, D_N values with stack A1 were similar to those obtained with stack S1, which indicate that the RTS downwind cavity extends for the entire RTS crosswind width.

Results obtained for $\theta = 45°$ are shown in Figure 4.22b. For the building with no RTS, the D_N values were similar for stacks S1 to S3 and stack A1. However, for the building with the RTS, moving the stack from S1 to S3 increased the D_N values by approximately 10 times within 2.5h of the stack. D_N values obtained within 2.5h of the stack A1 were about 50% lower than the dilutions obtained with S1 when an RTS was located upwind.

The primary reason for such differences between stack location effects for $\theta = 0°$ and $\theta = 45°$ when the RTS is present is due to the unsymmetrical nature of flow around RTS for an oblique wind. The general flow patterns around an RTS are similar to the flow patterns around a building. Snyder (2005) showed that, for an oblique wind, a recirculation area is formed near the upwind edge of the building (see Figure 4.10d). A similar recirculation zone formed around the RTS could produce lower dilutions from a stack located off the building centerline, as shown in Figure 4.10b.

Another reason for the difference in results for $\theta = 0°$ and $\theta = 45°$ could be that the minimum D_N value for $\theta = 45°$ was not measured due to insufficient sampling grid (i.e. sampling error). As mentioned previously, the along-wind D_N profiles represent the concentration measurements obtained at the sampling locations aligned with the wind direction approaching the building leading edge - the direction along which the plume is assumed to travel. However, this may not be the case for an oblique wind. As shown earlier in section 4.3.2.2, for $\theta = 45°$, the lowest D_N value did not occur along a path coinciding with the wind direction. Given this, such differences between stack location effects for $\theta = 0°$ and $\theta = 45°$ are plausible.

The above section demonstrated the effect of stack/RTS separation distance for one stack/exhaust scenario ($h_s = 0.75h$ and $M = 2$). Additional measurements obtained for different h_s and w/h showed similar trends as discussed above and are provided in Appendix E.

4.4.4 Required design stack height (h_{req})

The previous sections demonstrated that the downwash effect of an RTS is reduced by:

i) increasing x_s, h_s, M; and

ii) reducing RTS cross wind width.

Various researchers have provided different design aids or rules of thumb to estimate the required stack height in order to avoid the downwash effect of a building on a downwind stack. A few rules were mentioned in section 2.4.4.1, such as the ones proposed by Lucas (1972) and Snyder and Lawson (1976). Lucas suggested that the stack must be 2.5 times the height of the nearest tall building. Snyder and Lawson (1976) showed that Lucas' rule is justified for wide buildings (W/H > 2.5). However, for slender structures (W/H < 2.5), Lucas' rule could be relaxed to (H+1.5*l*). Petersen et al. (1999) provided a stack height reduction factor (SHR) to estimate required stack height for rooftop stacks surrounded with architectural screen walls. SHR is defined as the ratio of stack height without screen divided by stack height with screen.

The present study also aims at providing a simple method to estimate the required stack height for isolated stacks affected by the downwash effect of an RTS. The required design stack height (h_{req}) to avoid RTS downwash was determined for stack locations S1 to S5. By definition h_{req} is the stack height that gives similar D_N values with and without RTS. Values of h_{req} were obtained for two different RTS crosswind widths for $\theta = 0°$ and 45°. The smaller RTS was 10 m wide (w/h = 2.5) and the wider RTS was 30 m wide (w/h = 7.5).

Figure 4.23a shows the variation of h_{req} with h_r for stacks S1 to S5 for $\theta = 0°$. Values of h_r correspond to the different M values used in the present study (M = 1, 2, 3, and 5), and were calculated using Briggs (1984) plume rise formula. The h_r and h_{req} values shown are non-dimensionalized with the RTS height, h. The results indicate that the dependence of h_{req} on h_r was similar for all stack locations or stack-RTS separation distances (x_s). The required stack height decreased with an increase in h_r and x_s, due to reduction in plume capture. For stack S1 ($x_s = 0.5h$) and $h_r = 0.5h$ (M = 1), the h_{req} values are 2.5h and 3h for the smaller and larger RTS, respectively. The results also indicate that the effect of RTS is greatly reduced for $x_s > 1.5h$. Similarly, for all other h_r values, the required design stack height for the wider RTS is larger in comparison to that obtained for the smaller RTS.

Figure 4.23b shows similar plots for $\theta = 45°$. The trends were similar to the normal wind case. However, for $\theta = 45°$, h_{req} values were generally smaller than those obtained for $\theta = 0°$. For an oblique wind, the RTS downwind cavity is larger that that for the normal wind and increases with RTS crosswind width. However, the height of the cavity is not significantly affected with an increase in RTS crosswind width. On the other hand, for the normal wind, both the height and along-wind length of the RTS downwind cavity increase significantly with an increase in RTS width – see Table 4.3. Consequently, for $\theta = 45°$, the stack will be outside the RTS recirculation zone for lower values of h_{req} than that for $\theta = 0°$. In general, the stack height required to avoid the downwash effect of an RTS could vary from 2h to 3h depending upon the RTS width, wind direction, stack location, and plume rise.

4.5 Summary

The observations made from the wind tunnel results can be summarized as follows:

i) The presence of an RTS upwind of a stack always decreased the roof level dilutions for both normal and oblique winds.

ii) The downwash effect of the RTS was stronger for the oblique wind in comparison to the normal wind.

The downwash effect of the RTS decreased with increase in separation distance between the RTS and stack, stack height and exhaust momentum for both normal and oblique wind direction.

iv) In general, the downwash effect of the RTS was most visible for stacks located within a distance of 2h downwind of the stack.

v) For a normal wind, increasing the RTS width decreased the roof-level dilutions up to w/h = 7.5. For w/h > 7.5, dilution did not vary significantly. For an oblique wind, the presence of RTS decreased the roof level dilutions. However, dilution did not vary significantly with increase in RTS width.

vi) Depending on the stack height, RTS width, stack location, and wind direction, the plume height could be up to 40% smaller for the building with the RTS, compared to the building with no RTS.

vii) The stack height required to avoid downwash effects of RTS varied from 2h to 3h depending on the stack location, RTS width, wind direction, and plume rise.

Table 4.1 Experimental parameters used for the present and previous studies.

Experimental Parameters	Present study	Schulman and Scire (1991)	Lowery and Jacko (1996)	Wilson et al. (1998)	Peterson et al. (1999)
Model scale	1: 200	1: 100	1:120	1: 240	1:50
Boundary layer height (m)	185	**	**	88	50
Reference wind speed $U(Z_g)$ (m/s)	12.5	**	**	0.3	**
Wind speed at building height U_H (m/s)	5.4	1.37	3.40	0.17	3 to 9
Upstream terrain	urban	suburban	suburban	suburban	suburban
Power law exponent (α)	0.32	0.20	0.23	0.26	0.19
Upstream roughness z_o (m)	1.1	0.3	**	0.38	0.28
Upstream turbulence at building height (%)	27	**	**	18	22
Stack diameter d_e (m)	0.60	0.75	0.75	0.61	0.36–0.87
Wind direction (θ)	0°, 45°	0°, 45°	0°	0°	0°
Stack height h_s (m)	1–7	0–7.5	1.5, 6	2–6	0.3–6.2
Exhaust momentum M	1–5	0.75–5	2	1–8	1–5
Building length L (m)	50	75	90	72	30
Building width W (m)	50	75	90	60	15
Building height H (m)	15	15	7	12	15

** Not reported

Table 4.2 Plume rise estimates for the present and previous studies for M = 2.

Study	M	d_e (m)	h_r (m)
Present study	2.0	0.6	3.0
Schulman and Scire (1991)	1.5	0.8	2.3
Lowery and Jacko (1996)	2.0	0.8	3.8
Wilson et al. (1998)	2.0	0.6	3.1
Petersen et al. (1999)	1.4	0.9	2.2
ASHRAE (2003) model	2.0	0.6	3.0

Table 4.3 Estimated characteristic lengths for the RTS, based on Wilson (1979).

l (m)	w (m)	h (m)	R (m)	x_c (m)	h_c (m)	l_c (m)	l_r (m)
8.0	10	4.0	5.4	2.7	1.2	4.9	5.4
	20		6.8	3.4	1.5	6.1	6.8
	30		7.8	3.9	1.7	7.0	7.8
	40		8.6	4.3	1.9	7.7	8.6
	50		9.2	4.6	2.0	8.3	9.2

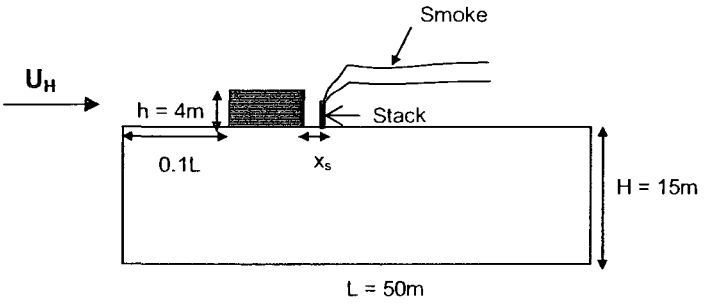

a) Side elevation

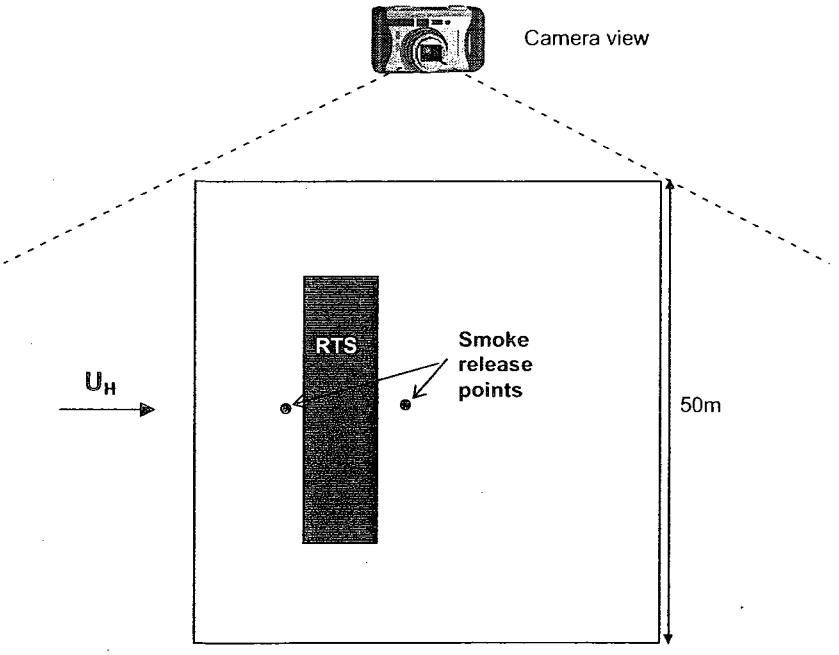

b) Plan view

Figure 4.1 Flow visualization set-up for the low-rise building.

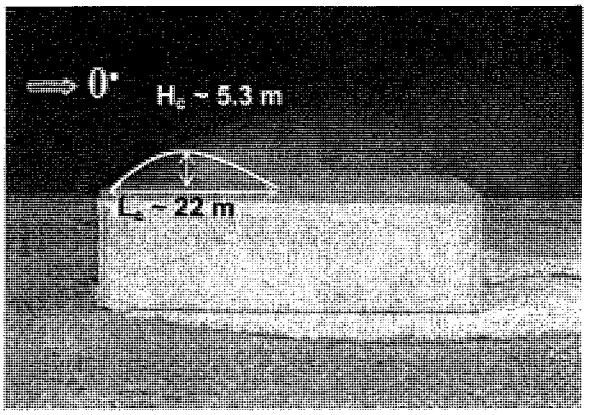

a) Flat-roof: measured

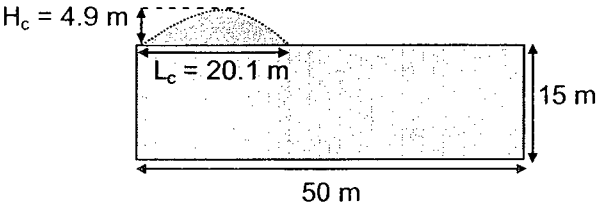

b) Flat-roof: estimated

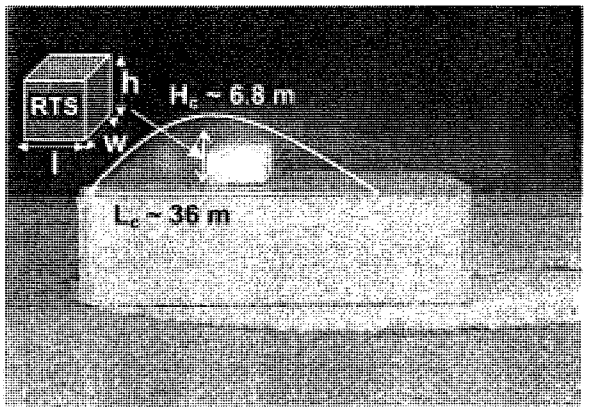

c) With RTS: measured

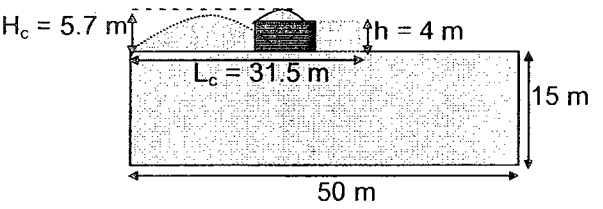

d) With RTS: estimated

Figure 4.2 Flow visualization for the low-rise building with and without an RTS for w/h = 7.5, and $\theta = 0°$. The estimated dimensions of the recirculation zones are from Wilson (1979).

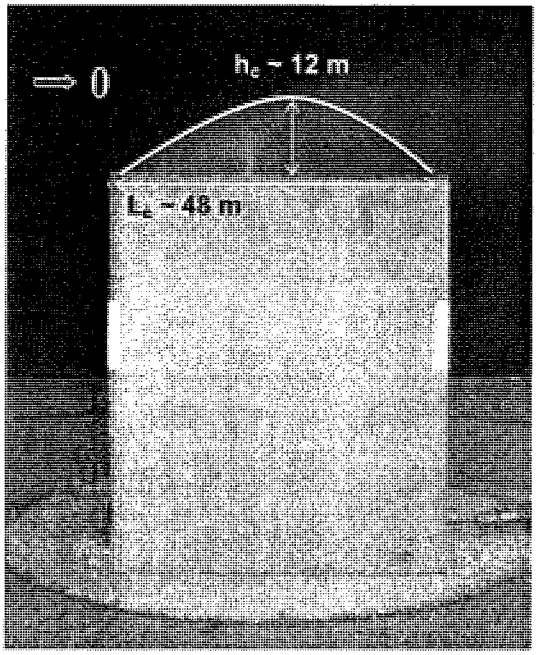

a) Flat-roof: estimated using flow viz. snaps

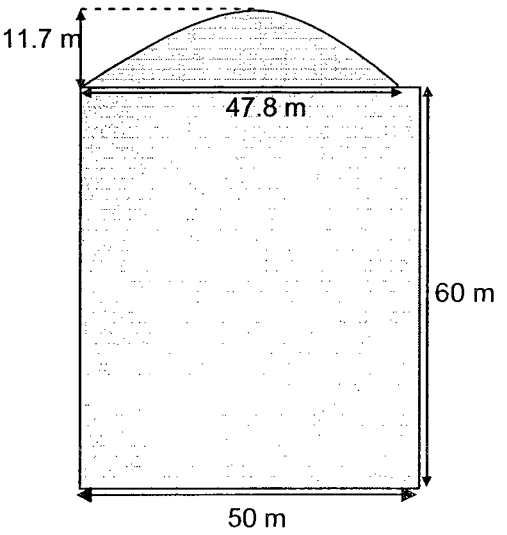

b) Flat-roof: estimated using Wilson (1997)

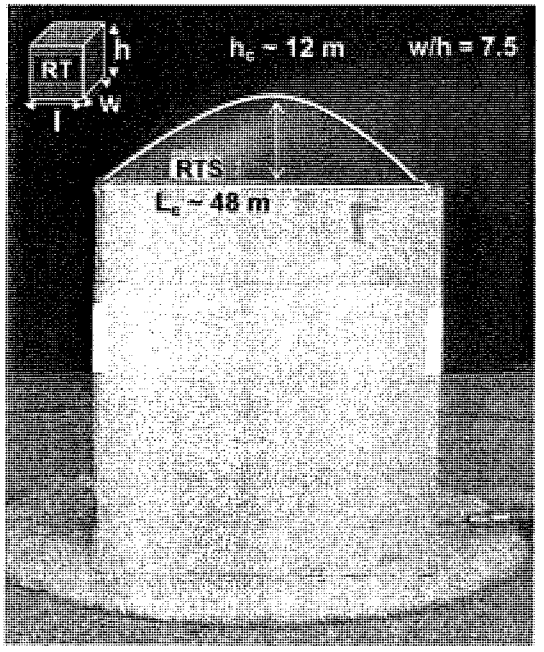

c) With RTS: estimated flow viz. snaps

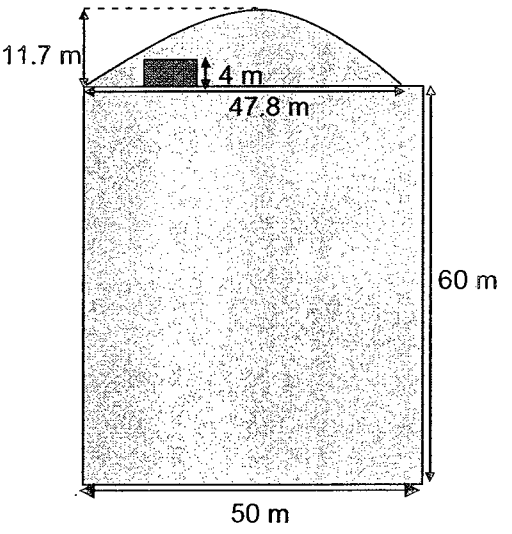

d) With RTS: estimated using Wilson (1997)

Figure 4.3 Flow visualization for the high-rise building with and without an RTS for w/h = 7.5, and θ = 0°. The estimated dimensions of the recirculation zones are from Wilson (1979).

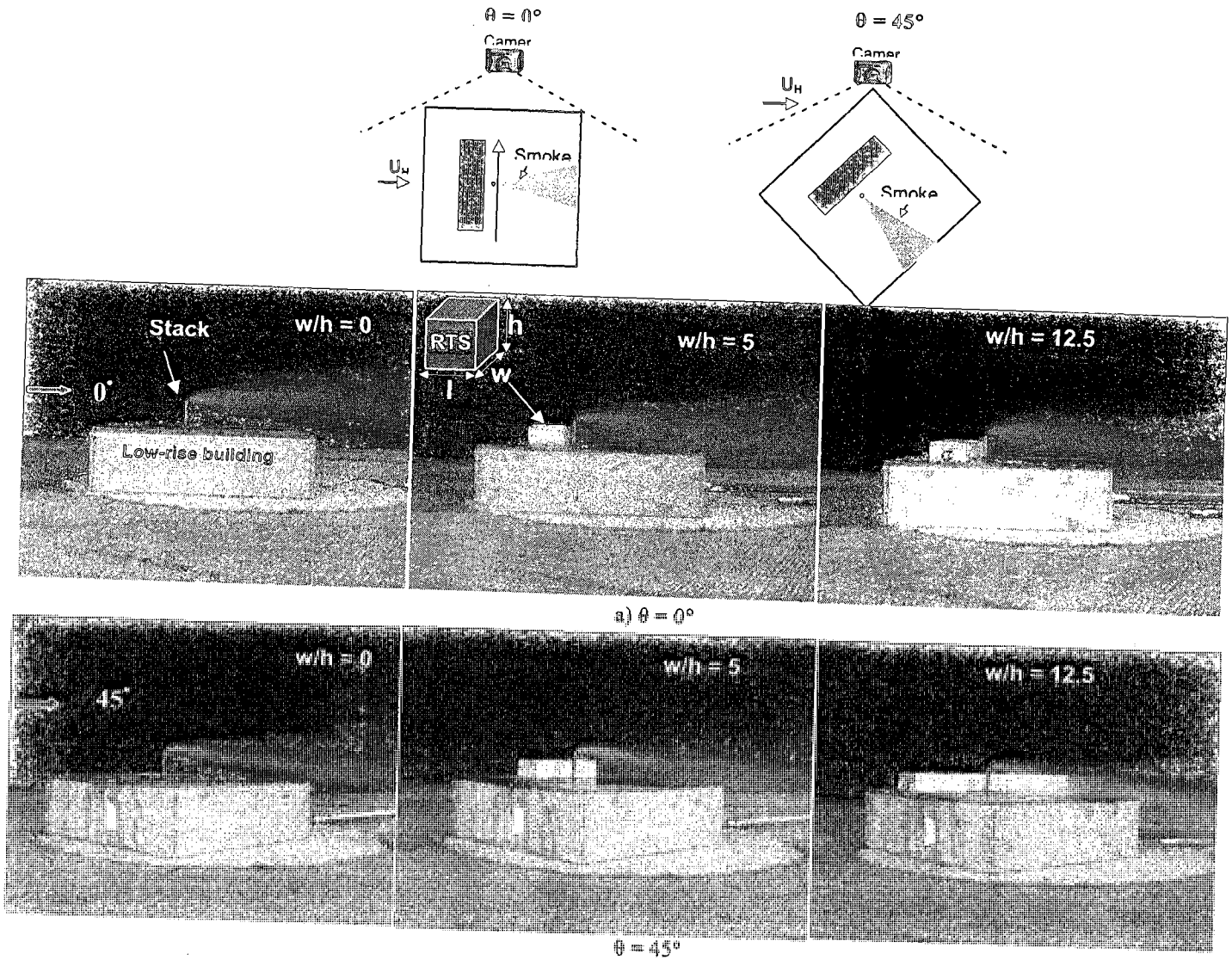

Figure 4.4 Flow visualizations for the low-rise building showing the downwash effect of the RTS with w/h = 0, 5, 12.5, h_s = 1.25h, and h = 4 m: a) θ = 0°; and b) θ = 45°.

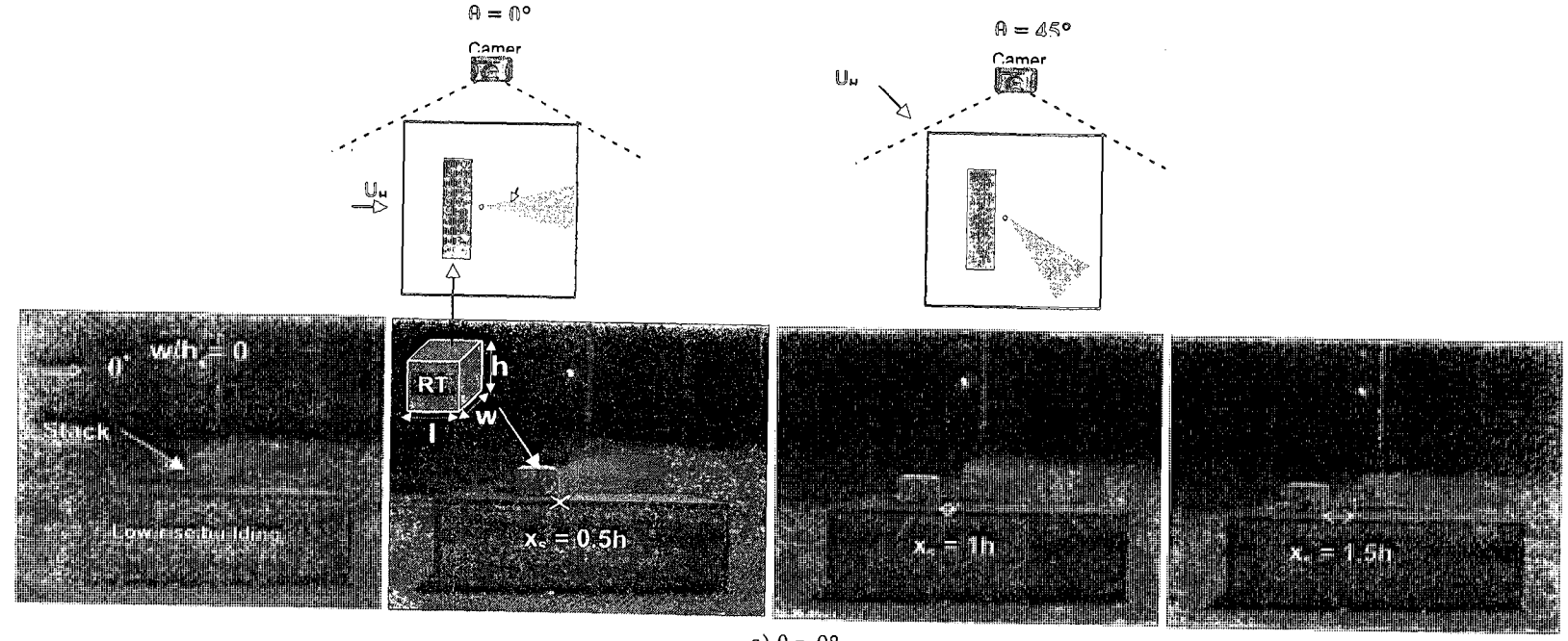

a) θ = 0°

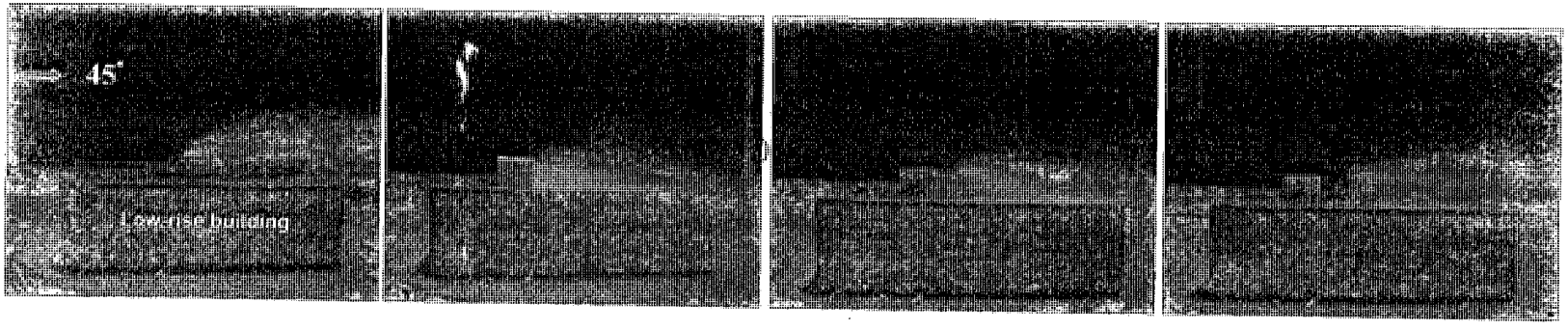

b) θ = 45°

Figure 4.5 Flow visualization for the low-rise building showing the effect of stack location (x_s) with respect to an RTS with w/h = 7.5 and for h_s = 4 m: a) θ = 0°; and b) θ = 45°.

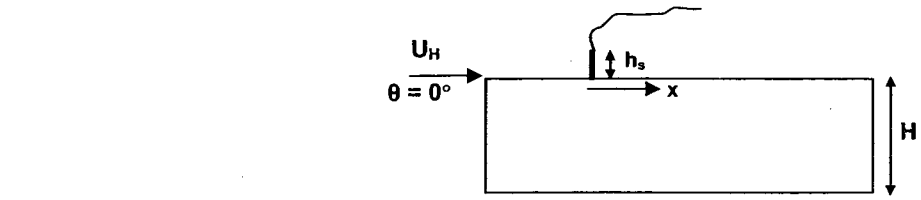

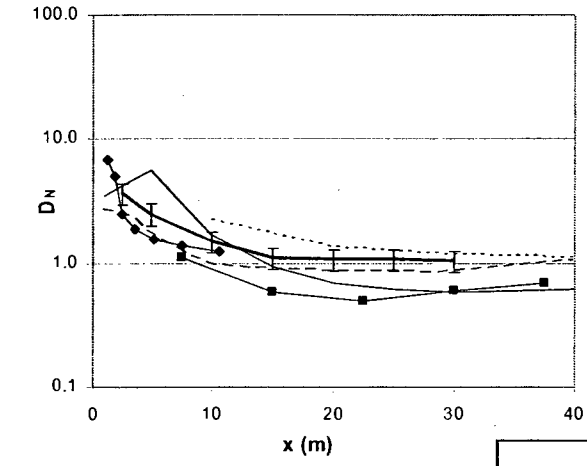

a) $h_s \sim 2$ m

study	a) h_s (m)	b) h_s (m)	M	
Present study	2.0	7.0	2.0	
Schulman and Scire (1991)	1.5	7.5	1.5	
Lowrey and Jacko (1996)	1.5		2.0	
Wilson et al (1998)	2.1	6.1	2.0	
Petersen et al (1999)	2.2		1.4	
ASHRAE (2003)	2.0	7.0	2.0	

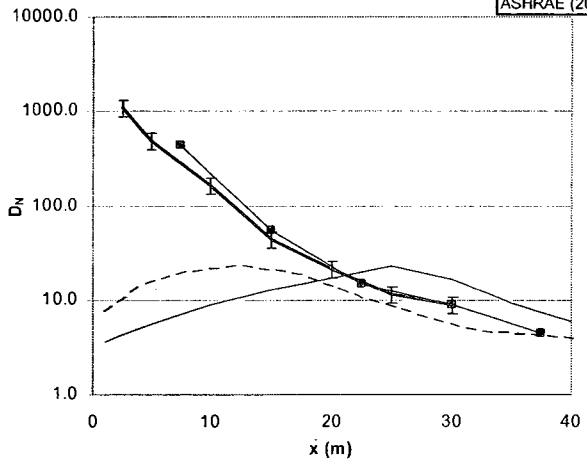

b) $h_s \sim 7$ m

Figure 4.6 Comparison between along-wind D_N profiles obtained with previous studies and present study for a typical low-rise building for $\theta = 0°$ and $M \sim 2$: a) $h_s \sim 2$ m; and b) $h_s \sim 7$ m.

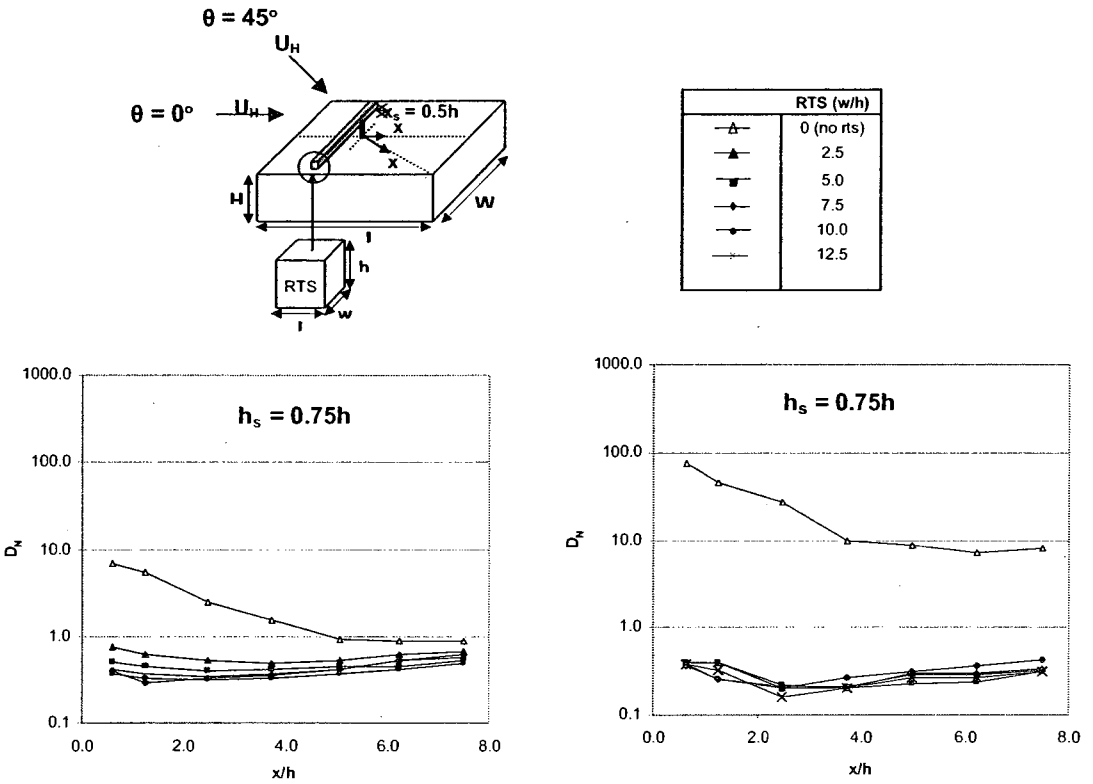

a) θ = 0°

b) θ = 45°

Figure 4.7 Effect of RTS crosswind width on along-wind D_N values for the low- rise building for h_s = 0.75h, M = 2 and h = 4 m. a) θ = 0°; and b) θ = 45°

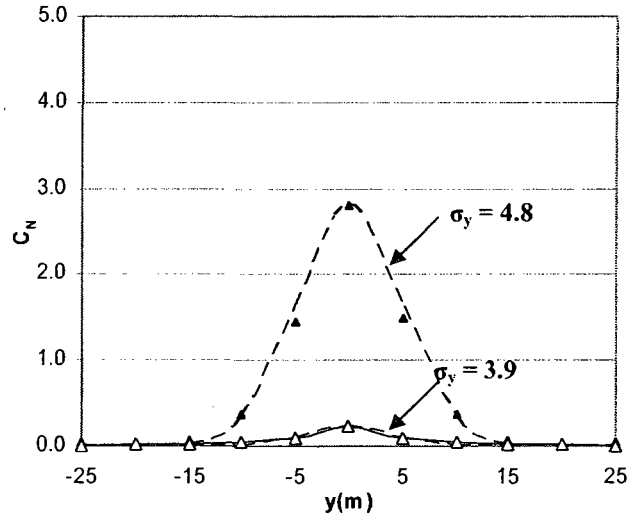

a) x = 2h

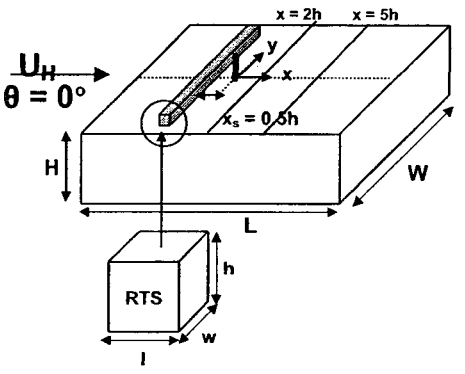

symbol	w/h
▲	7.5
Δ	0 (flat-roof)
– – ·	Gaussian fit

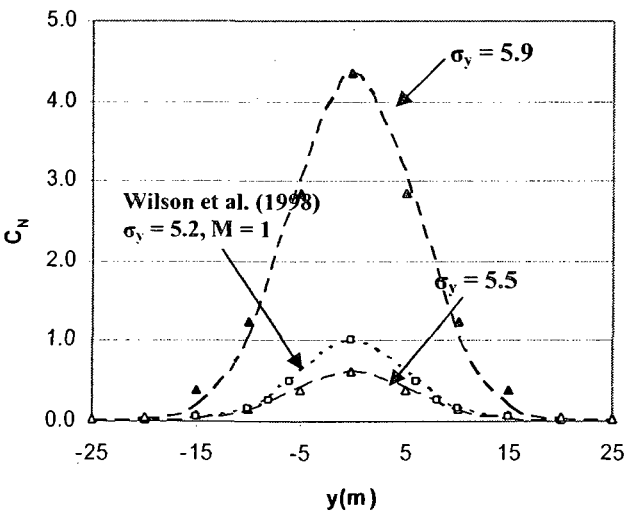

b) x = 5h

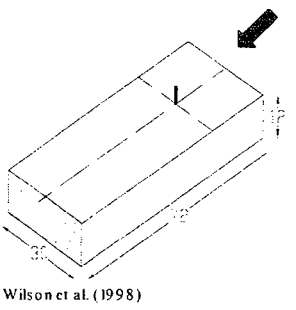

Figure 4.8 Crosswind profiles of normalized concentrations (C_N) for the low-rise building with and without an RTS for θ = 0°, h_s = 0.75h and M = 2: a) x = 2h; and b) x = 5h.

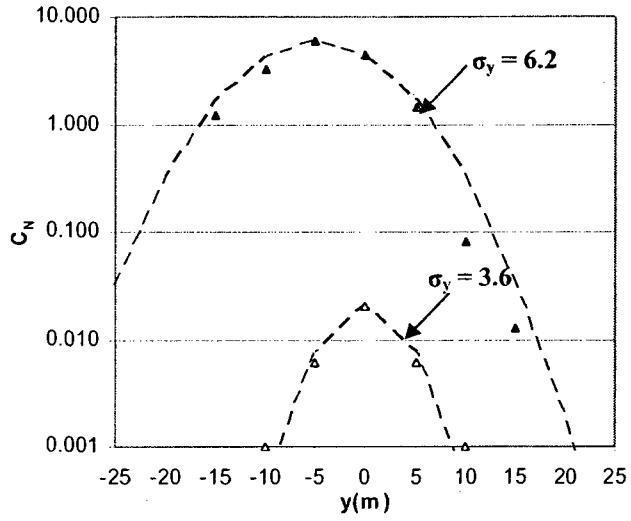

symbol	w/h
▲	7.5
Δ	0 (flat-roof)
– – –	Gaussian fit

a) x = 2h

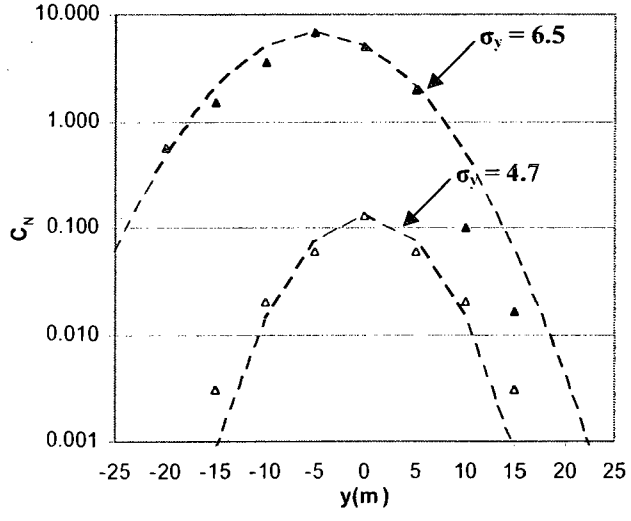

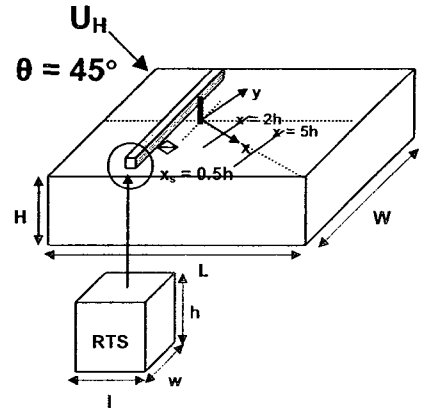

b) x = 5h

Figure 4.9 Crosswind profiles of normalized concentrations (C_N) for the low-rise building with and without an RTS for $\theta = 45°$, $h_s = 0.75h$ and M = 2: a: x = 2h; and b) x = 5h.

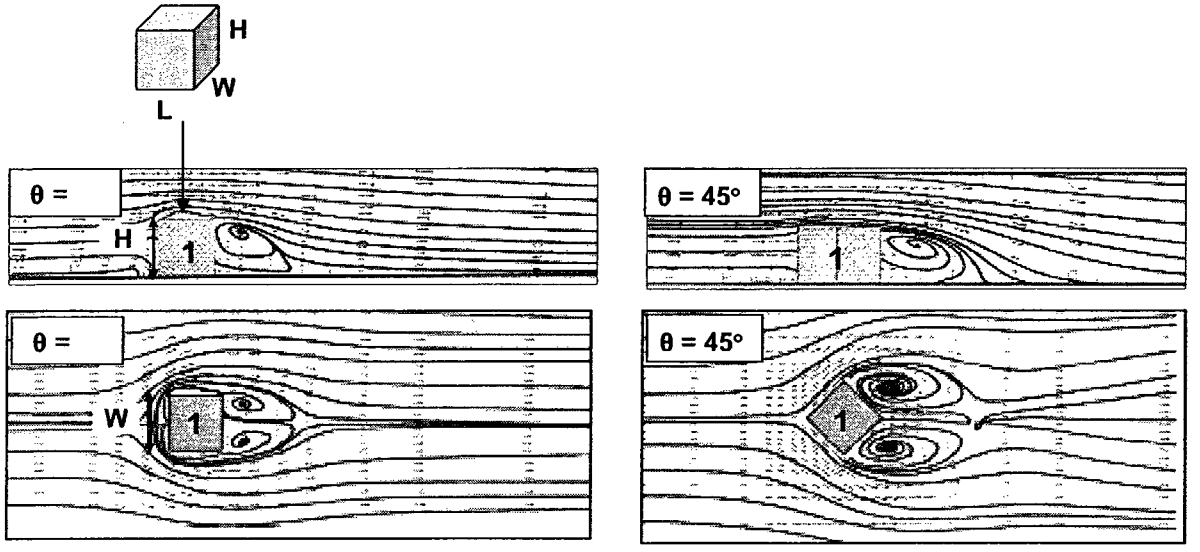

a) Vertical and ground plane streamlines for θ = 0°

b) Vertical and ground plane streamlines for θ = 45°

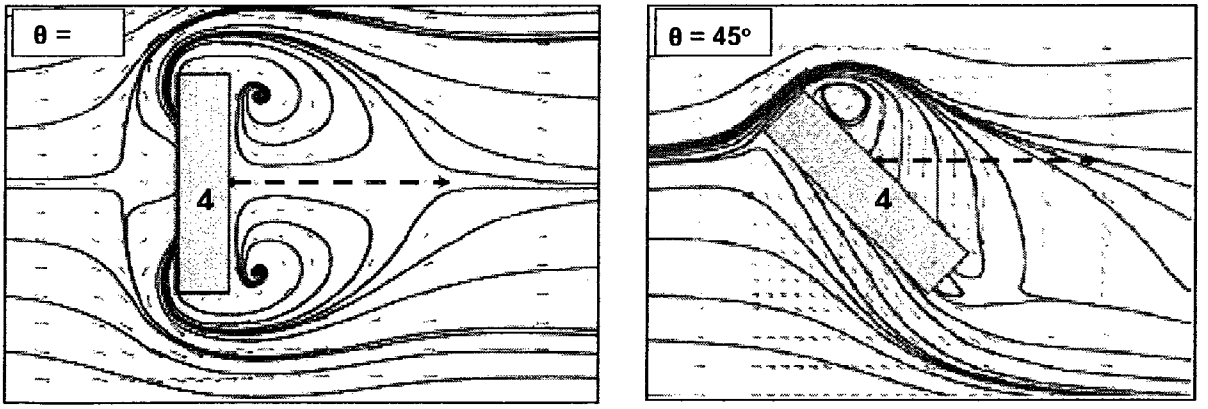

c) Ground plane streamlines for θ = 0°

d) Ground plane streamlines for θ = 45°

Figure 4.10 Vertical and ground plane streamlines around building for normal and oblique wind, from Snyder (2005). The number on the building represents the ratio of building width (W) to building height (H): a) θ = 0° for W/H = 1; b) θ = 45° for W/H = 1; c) θ = 0° for W/H = 4; d) θ = 45° for W/H = 4.

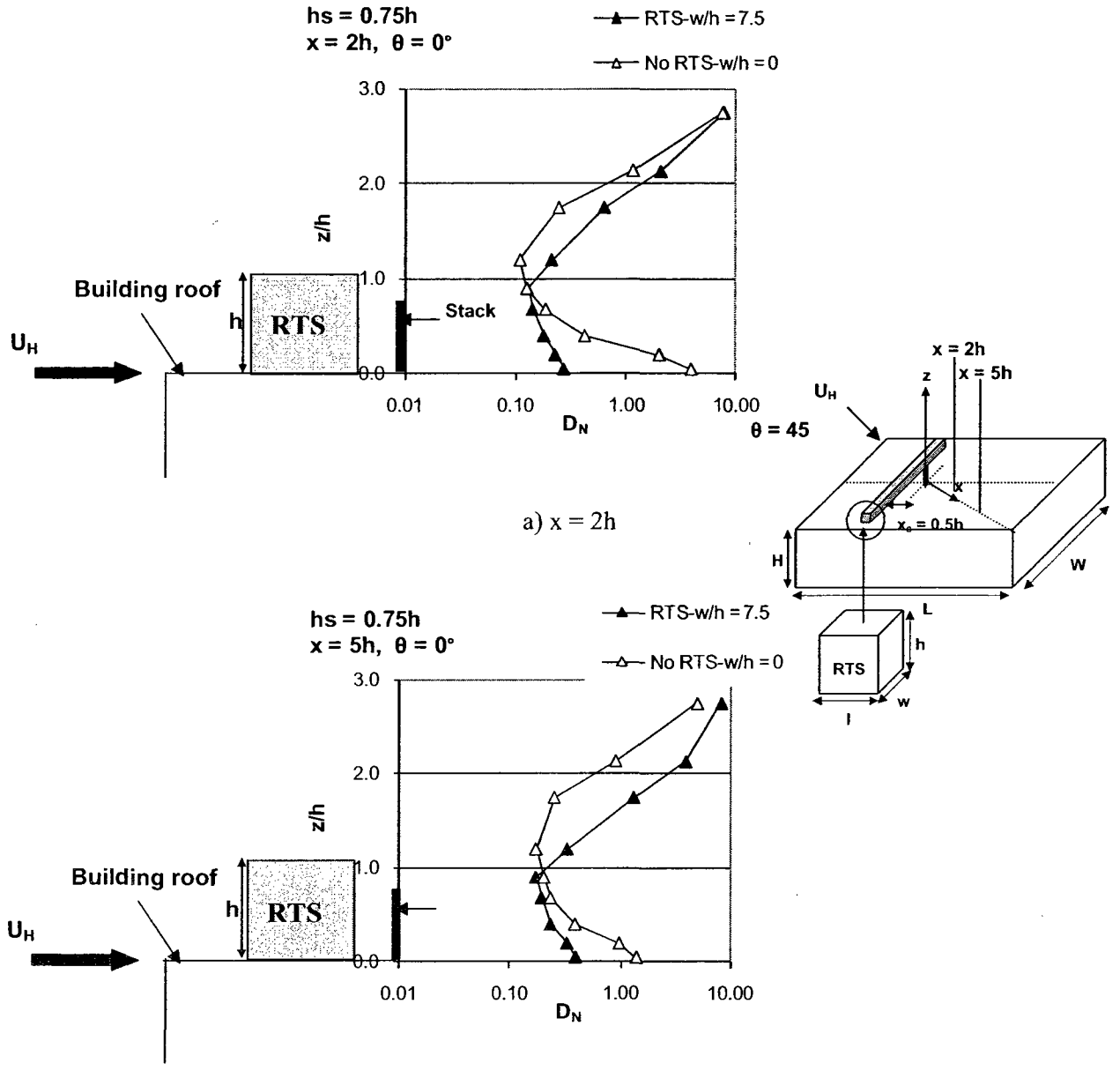

Figure 4.11 Vertical profiles of normalized dilutions for the low-rise building with and without an RTS for $\theta = 0°$, $h_s = 0.75h$ and $M = 2$: a: $x = 2h$ and b) $x = 5h$.

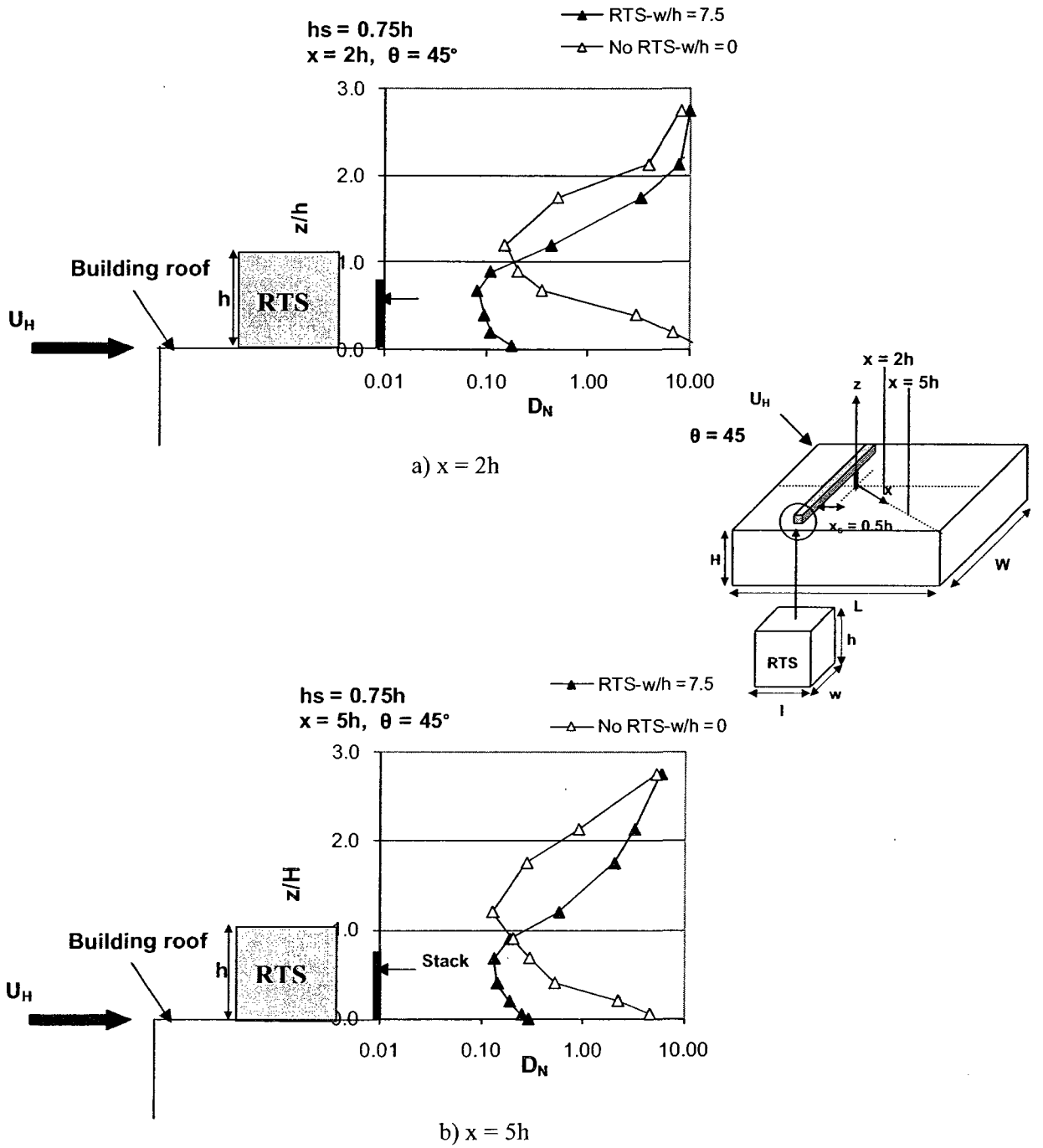

a) x = 2h

b) x = 5h

Figure 4.12 Vertical profiles of normalized dilutions for the low-rise building with and without an RTS for $\theta = 45°$, $h_s = 0.75h$ and M = 2: a) x = 2h and b) x = 5h.

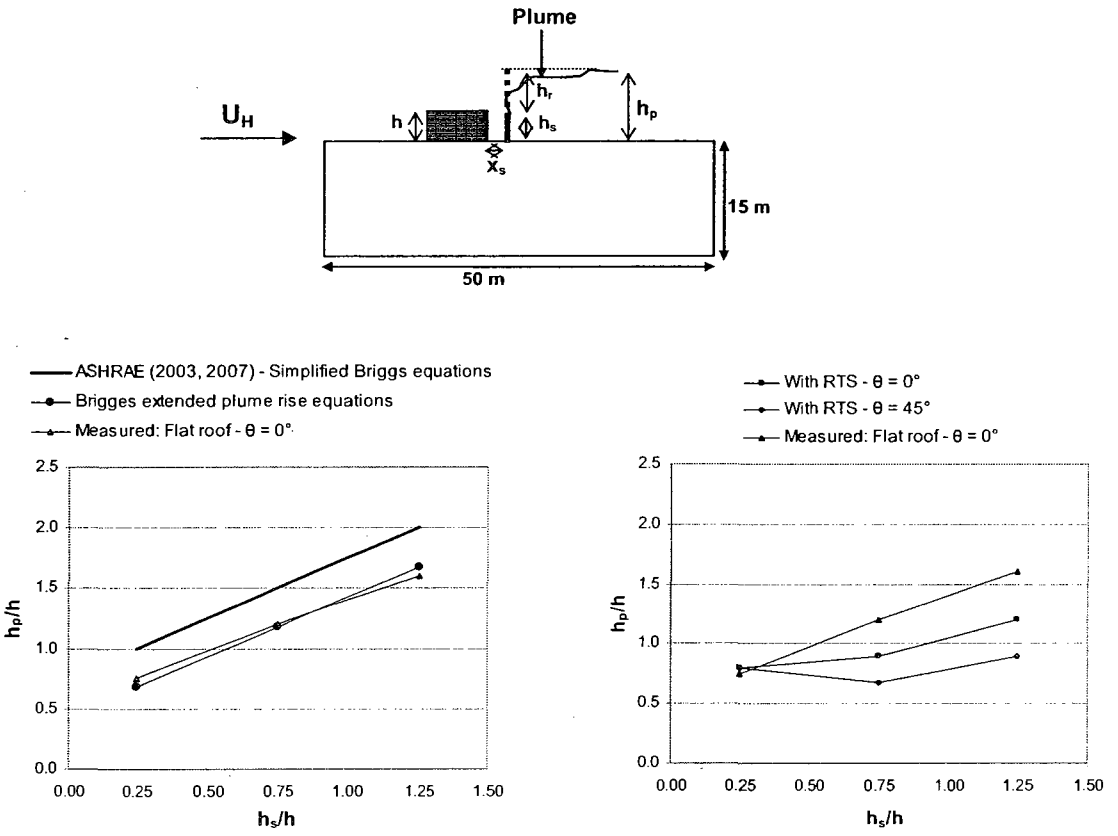

a) Building without RTS: θ = 0°

b) Building with the RTS: θ = 0° and 45°

Figure 4.13 Comparison between estimated and measured effective plume height for the low-rise building for M = 2 and h = 4 m: a) building without RTS: θ = 0°; and b) building with the RTS: θ = 0° and 45°.

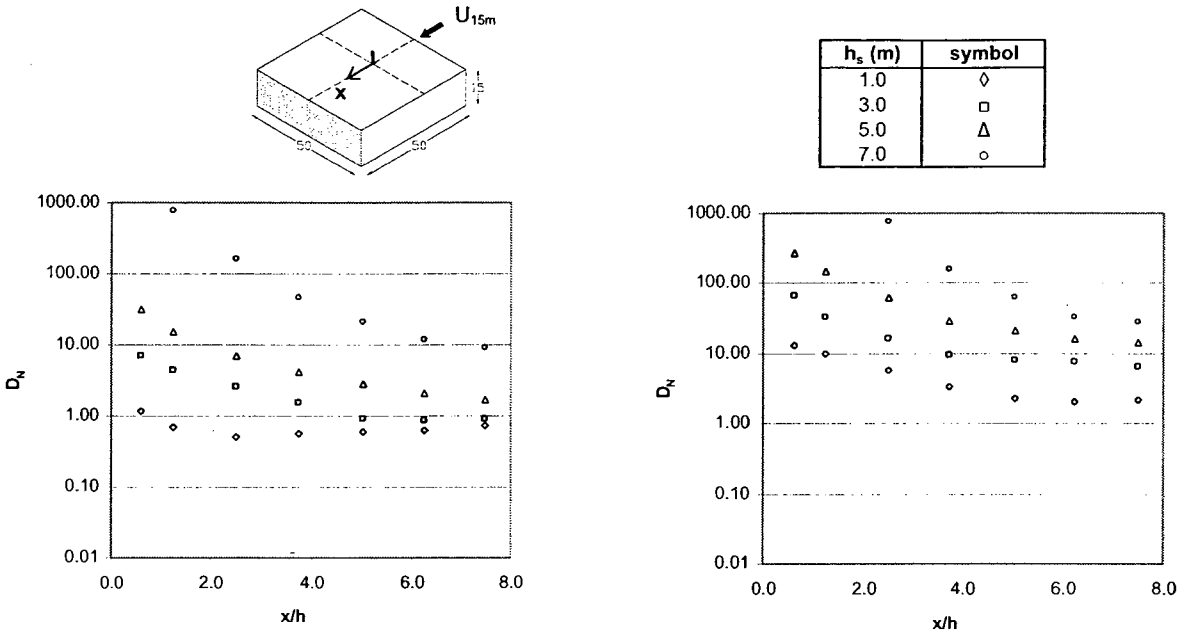

a) M = 2 b) M = 5

Figure 4.14 Effect of h_s on along-wind D_N profiles for the low-rise flat-roofed building for $\theta = 0°$: a) M = 1; and b) M = 5.

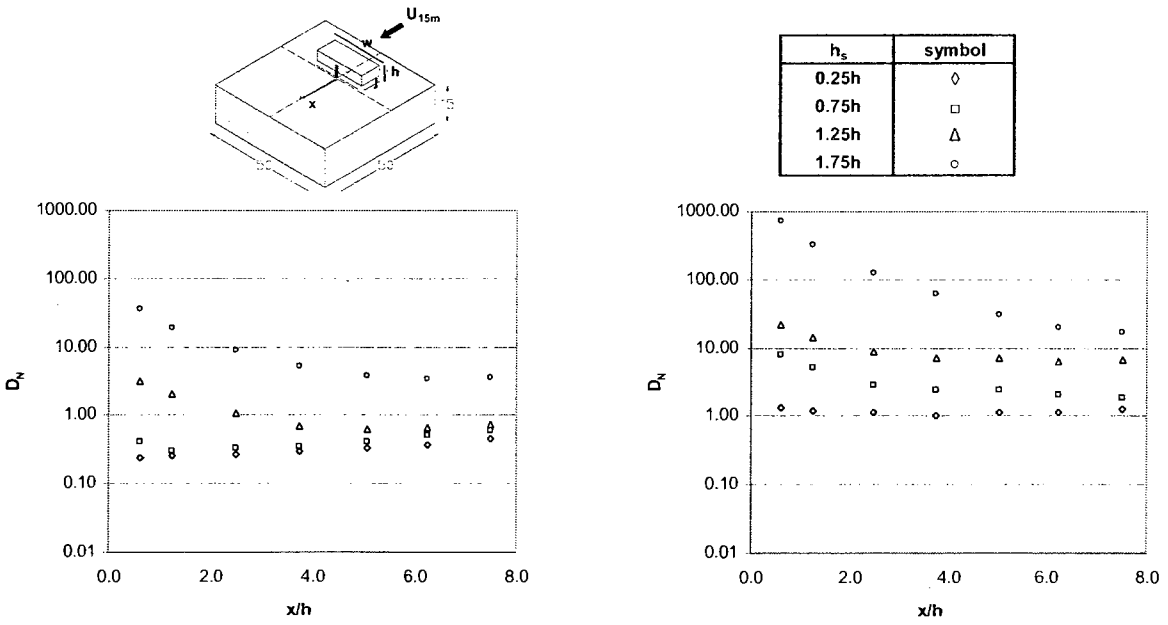

a) M = 2 b) M = 5

Figure 4.15 Effect of h_s on along-wind D_N profiles for the low-rise building with an RTS for $\theta = 0°$: a) M = 1; and b) M = 5.

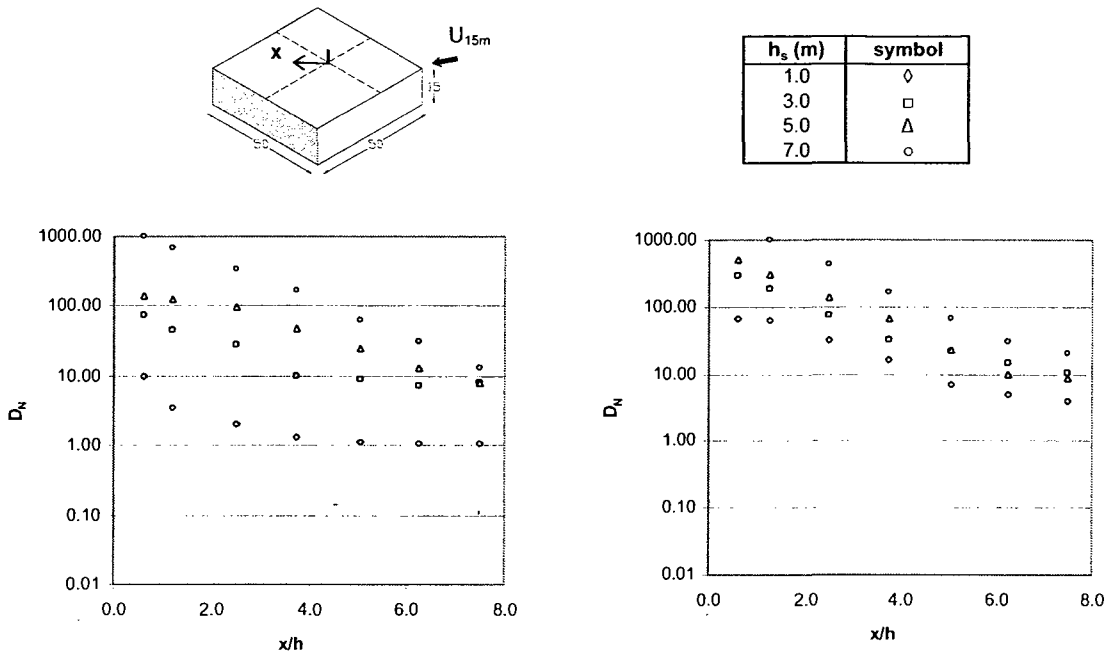

a) M = 2 b) M = 5

`Figure 4.16 Effect of h_s on along-wind D_N profiles for the low-rise flat-roofed building for θ = 45°: a) M = 1; and b) M = 5.

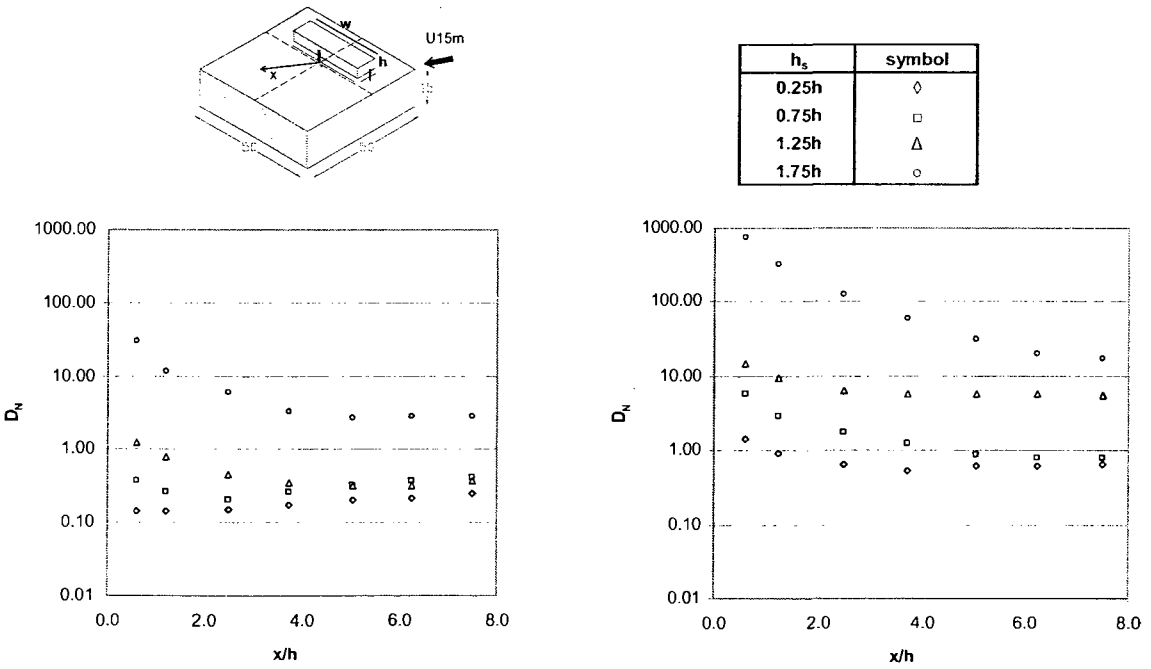

a) M = 2 b) M = 5

Figure 4.17 Effect of h_s on along-wind D_N profiles for the low-rise building with an RTS for θ = 45° and h = 4 m: a) M = 1; and b) M = 5.

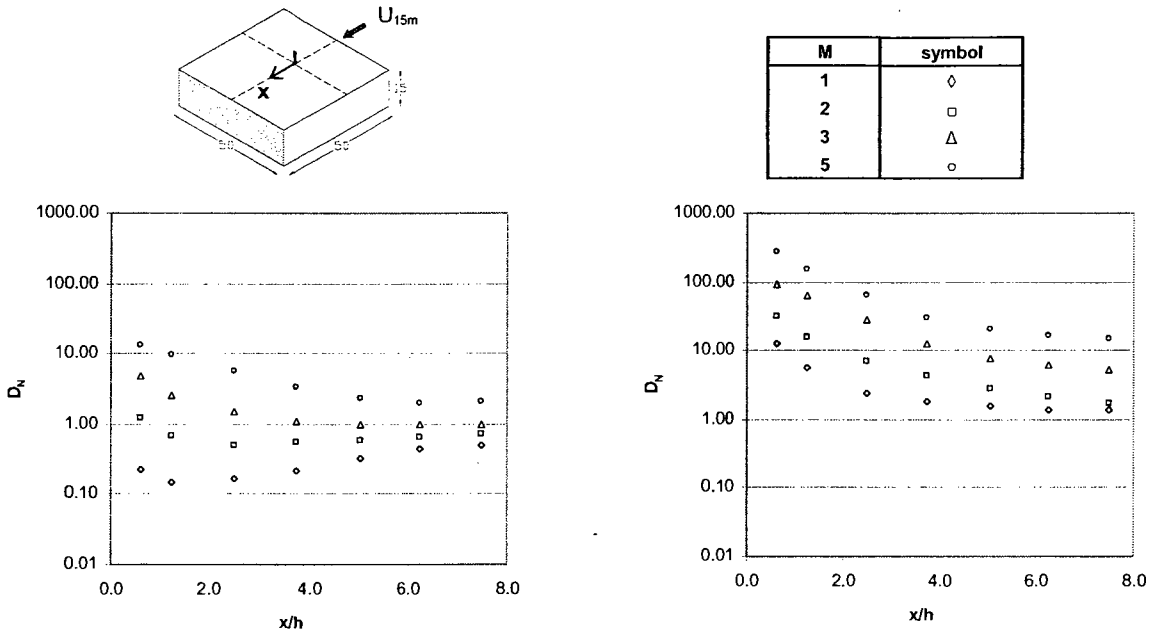

a) $h_s = 1$ m b) $h_s = 5$ m

Figure 4.18 Effect of M on along-wind D_N profiles for the low-rise flat-roofed building for $\theta = 0°$: a) $h_s = 1$ m; and b) $h_s = 5$ m.

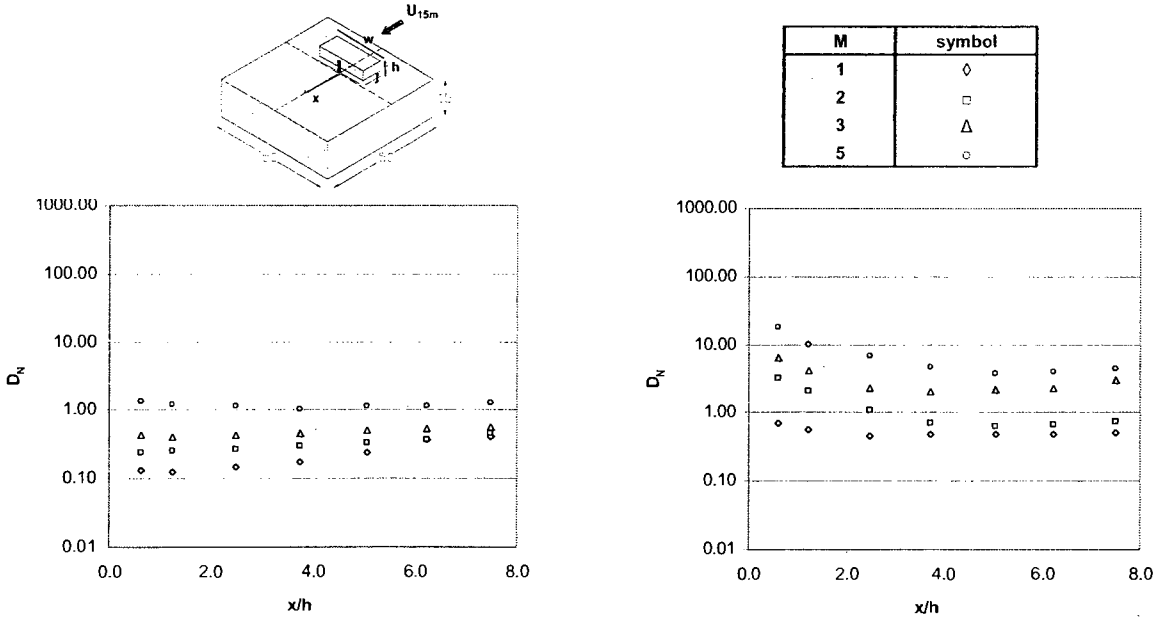

a) $h_s = 1$ m b) $h_s = 5$ m

Figure 4.19 Effect of M on along-wind D_N profiles for the low-rise flat building with an RTS for $\theta = 0°$ and h = 4 m: a) $h_s = 1$ m; and b) $h_s = 5$ m.

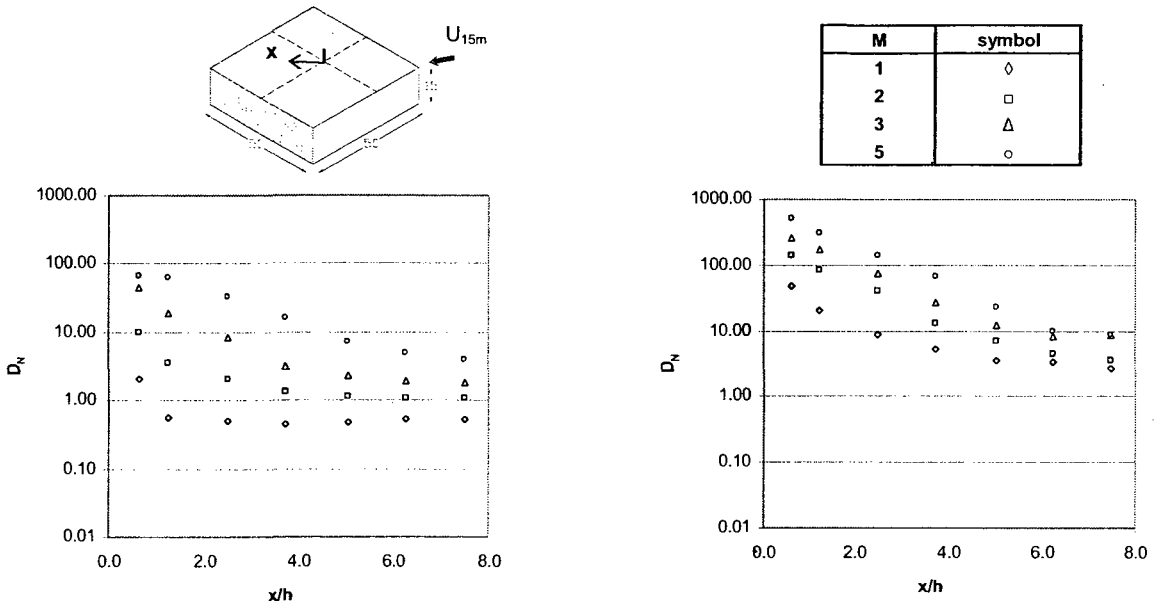

a) $h_s = 1$ m b) $h_s = 5$ m

Figure 4.20 Effect of M on along-wind D_N profiles for the low-rise flat-roofed building for θ = 45°: a) $h_s = 1$ m; and b) $h_s = 5$ m.

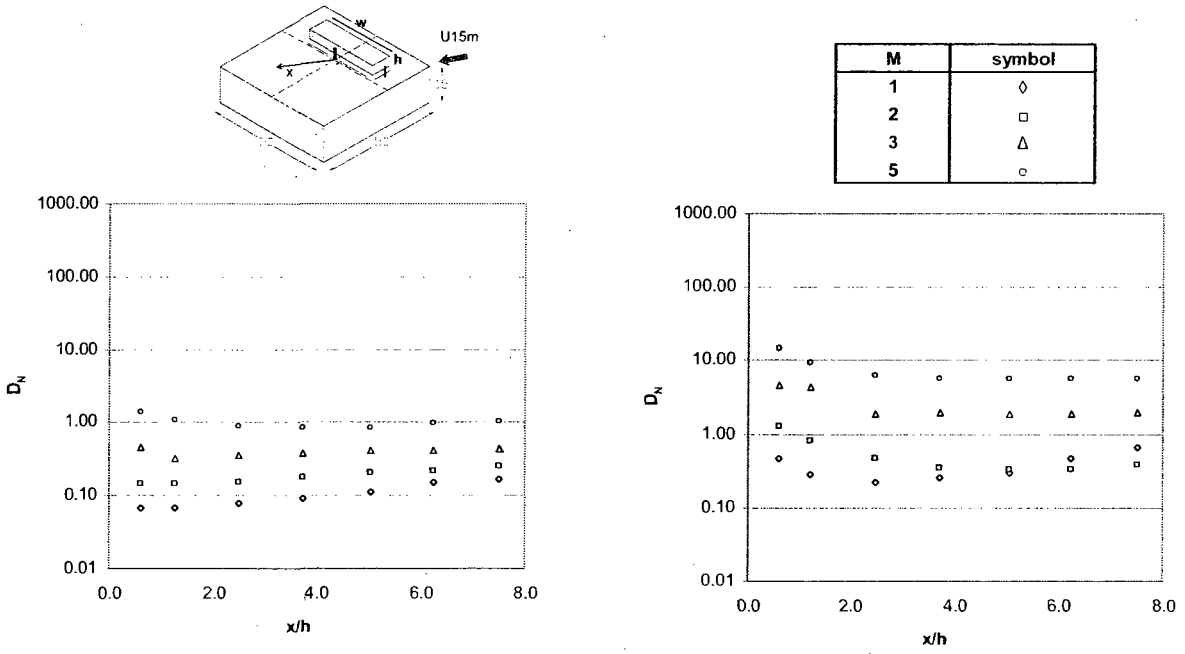

a) $h_s = 1$ m b) $h_s = 5$ m

Figure 4.21 Effect of M on along-wind D_N profiles for the low-rise flat building with an RTS for θ = 45° and h = 4 m: a) $h_s = 1$ m; and b) $h_s = 5$ m.

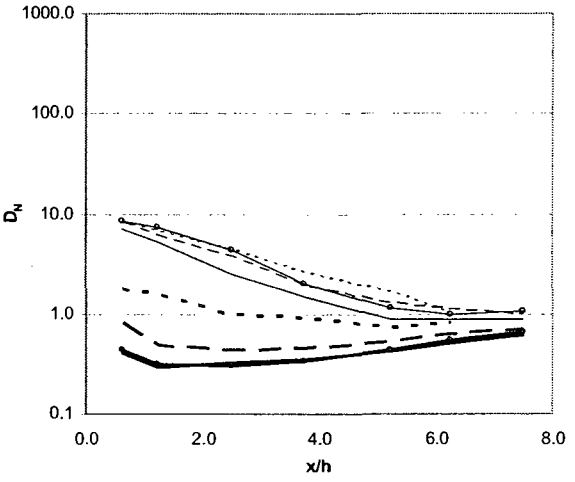

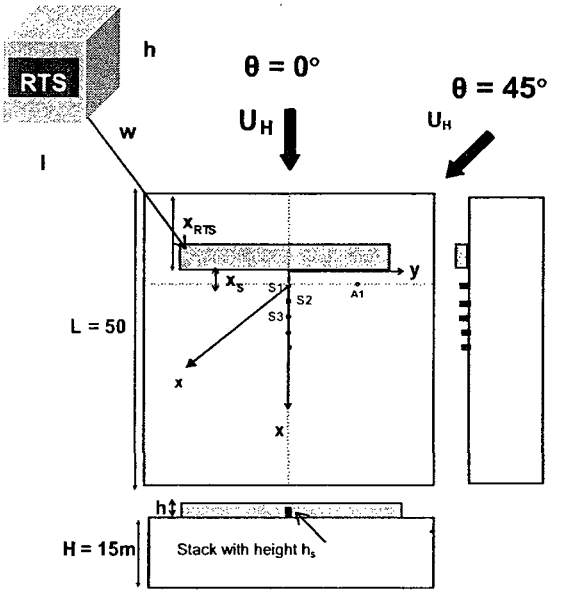

a) θ = 0°

Stack location			x_s
S1	——	No RTS	0.5h
S2	- - - -		h
S3	.....		1.5h
A1	—o—		0.5h
S1	——	RTS w/h = 7.5	0.5h
S2	– –		h
S3	.....		1.5h
A1	—●		0.5h

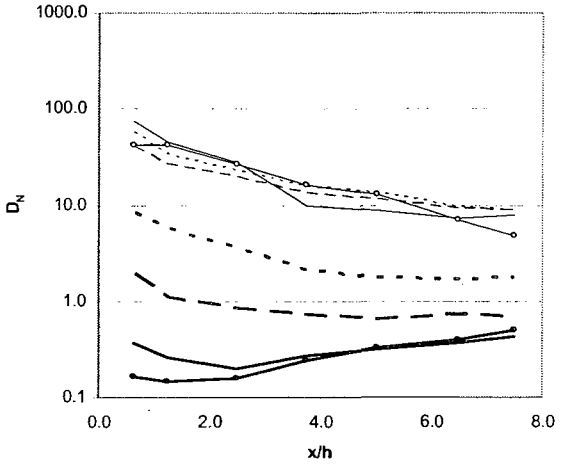

b) θ = 45°

Figure 4.22 Effect of separation distance between stack and RTS on along-wind D_N profiles for the low-rise building for h_s = 0.75h and M = 2: a) θ = 0°; and b) θ = 45°.

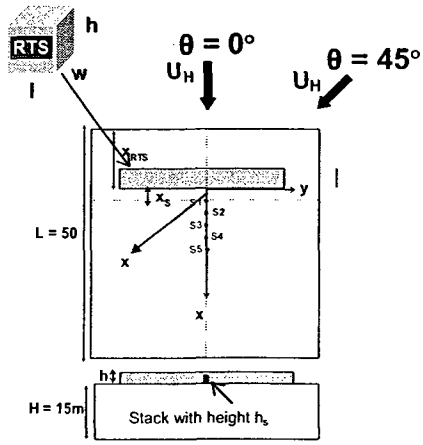

Stack	x_s/h	
S1	0.5	———
S2	1.0	——
S3	1.5	- - - -
S4	2.0	.....
S5	2.5	- - -

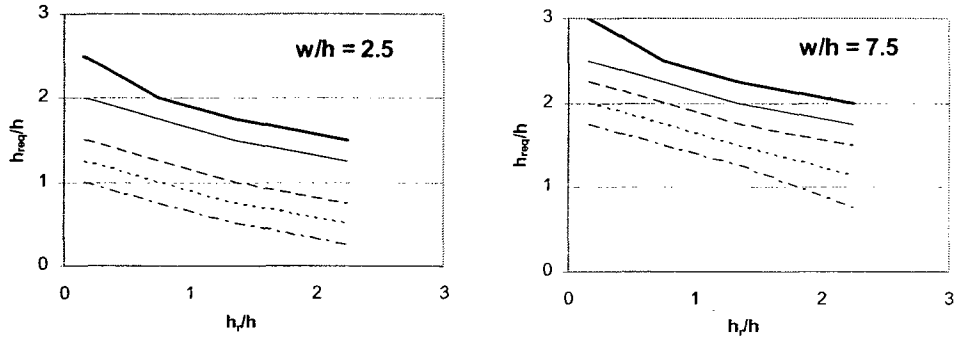

a) θ = 0°

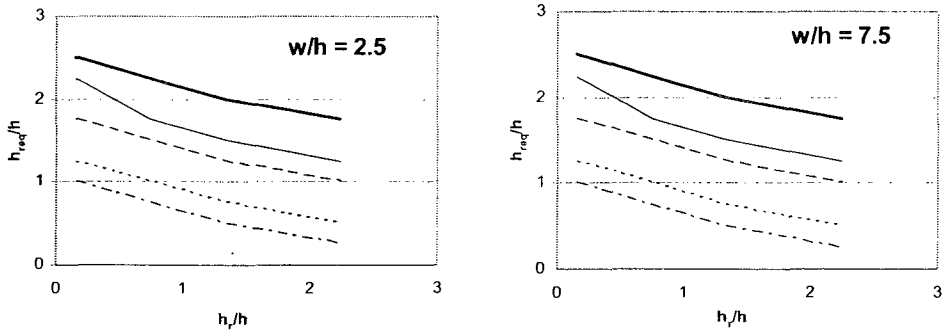

b) θ = 45°

Figure 4.23 Required stack height (h_{req}) to escape downwash effect of an RTS for the low-rise building with an RTS: a) θ = 0°; and b) θ = 45°.

Chapter 5

COMPARISON OF EXPERIMENTAL RESULTS WITH ASHRAE DISPERSION MODELS

5.1 Introduction

Several empirical and analytical models are available for predicting plume dispersion, but only a few models deal with near-field dispersion in the vicinity of buildings. As discussed in Chapter 2, the most widely used models for estimating dispersion of building roof exhausts are the ASHRAE (2003) and ASHRAE (2007) minimum dilution models.

In addition to the minimum dilution models, ASHRAE also provides a simple graphical way to estimate the stack height required to avoid re-entrainment for building-roof exhausts. The ASHRAE Geometric Stack Design Method (AGM) developed by Wilson (1979), was discussed in Chapter 2.

The present chapter evaluates the accuracy of the ASHRAE minimum dilution models and the AGM, and recommends enhancement to the models that take into account the downwash effect of an RTS.

5.2 ASHRAE dispersion models

The ASHRAE (2003) and ASHRAE (2007) dispersion models are applicable when the exhausts and intakes are located on the same building roof. Before discussing the assessment of these models, the methodology for using them will be presented

followed by a sample calculation for estimating dilution for an exhaust stack located on the roof of a low-rise building.

5.2.1 Using ASHRAE (2003) minimum dilution models

The ASHRAE (2003) recommends two minimum dilution models - the D_r model and the D_s model, as outlined in section 2.4.5.2. The D_r model is applicable for vertical uncapped stacks located on the building roof. The D_s model is applicable for exhausts discharging horizontally from building side walls or from exhausts discharged from capped stacks with negligible plume rise. The D_s model is also applicable for vertical uncapped stacks located within the separation bubble and plume height (h_p) is shorter than the height of the bubble. The D_r model provides some dilution due to plume height if the stack is tall enough. In order to use the D_r model, the plume height must be specified. In contrast, the D_s model does not take into account the effect of stack height or plume rise.

In the D_r model, the plume height is calculated as $h_p = h_s + h_r - h_d$ (Eq 2.6). According to ASHRAE (2003), proper stack design requires that h_p should be high enough to avoid the building roof, assuming a 5:1 slope of the plume (see Figure 2.11). This smallest height is referred to as h_{small}.

ASHRAE (2003) specifies that:

"*If the plume height is less than h_{small} but higher than any rooftop obstacle or highest re-circulation zone (h_{top} in Figure 2.11), then only the physical height above h_{top} should be used to compute plume height rather than the full physical stack height*".

If the plume height does not reach h_{top}, ASHRAE (2003) recommends the use of the D_s model, which provides more conservative estimates since it does not consider plume rise. In a design situation, the value of h_{small} depends upon the location of the critical receptor. It also depends on the exhaust velocity and the design wind speed, since these parameters determine the plume rise. In the present study, the value of h_{small} was determined for each combination of M and h_s for the particular case of an intake located at building leeward edge (the worst-case scenario). The criteria for using the D_r and D_s models are summarized in Table 5.1.

In the present study, the dilution values are expressed in the form of normalized dilution D_N. For comparison with wind tunnel data, the D_r and D_s model estimates have been normalized using the following equations:

$$D_N = D_r Q/(U_H H^2) \qquad \text{[Eq 5.1]}$$

$$D_N = D_s Q/(U_H H^2) \qquad \text{[Eq 5.2]}$$

where, D_r and D_s are the minimum dilutions obtained from ASHRAE (2003) dispersion models.

Sample calculation using the ASHRAE (2003) D_r model

An example that demonstrates the use of the ASHRAE D_r model for a typical low-rise building is presented. For this case, the stack is located on the roof of a 15 m tall building at a distance of 20 m from the leading edge of the building. A sample calculation is presented for a stack with h_s = 3 m and M = 2 for a normal wind ($\theta = 0°$). The building/stack/intake configuration is shown in Figure 5.1a and the experimental

parameters used to estimate dilutions are presented in Table 5.2. The D_N value is calculated at an intake located 30 m downwind of the stack.

Step 1: Estimate dimensions of building recirculation zones

From the AGM (Eq 2.19–2.23) the building characteristic length scales are:

$R = B_s^{0.67} B_L^{0.33} = 22.3$ m

$H_c = 0.22R = 4.9$ m

$X_c = 0.5R = 11.2$ m

$L_c = 0.9R = 20.1$ m

$L_r = 1.0R = 22.3$ m

The estimated recirculation zones for the building are shown in Figure 5.1b.

Step 2: Calculate h_{top} and h_p for the given exhaust parameters

$h_{top} = H_c = 4.9$ m (see Figure 5.2).

From Eq 2.6, $h_p = 6$ m

Step 3: Estimate h_{small}

Figure 5.2 shows the minimum height of a capped stack, h_{small}, for the plume to avoid a rooftop intake located 30 m downwind of the stack near the leeward edge of the building. It is worth noting that for a capped stack there is no contribution from plume rise. Assuming the plume expands vertically with a slope of 1:5, $h_{small} = 6$ m, then $h_{small} = h_p = 6$ m.

Since $h_{small} = h_p$, the D_r model is applicable, as indicated from the criteria shown in Table 5.1.

Step 4: Estimate of initial, lateral and vertical plume spreads

From Eq 2.11, the normalized initial plume spread $\frac{\sigma_o}{d_e} = 2.04$

From Eq 2.9, the normalized lateral plume spread $\frac{\sigma_y}{d_e} = 6.86$

Likewise from Eq 2.10, the normalized vertical plume spread $\frac{\sigma_z}{d_e} = 5.59$

Step 5: Estimate of dilution D_r at x = 30 m from the stack

From Eq 2.5, $D_r (x = 30\ m) = 381$

From Eq 5.1, $D_N = D_r Q/U_H H^2 = (381)\ (3.1)/(5.4)/(15)^2 = 0.97$

Likewise, D_N can be calculated at any distance 'x' from the stack.

5.2.2 Using the ASHRAE (2007) dispersion model

A description of the ASHRAE (2007) D_r model was presented in Chapter 2. The basic difference between the 2007 and 2003 D_r models lies in the way plume height is treated. The ASHRAE (2007) model eliminated h_{small} and replaced h_p with vertical separation factor (ξ). The vertical separation factor depends on h_p and h_{top}. The 2007 D_s model is same as the 2003 version. The criteria for using the ASHRAE (2007) D_r and D_s models are summarized in Table 5.3.

Sample calculation using the ASHRAE (2007) D_r model

The procedure for the ASHRAE (2007) D_r model is similar to that for the 2003 model procedure except for Step 3, where the vertical separation factor is calculated. As shown in Step 2 of Section 5.2.1.1, $h_{top} = 4.9$ and $h_p = 6$ m. Since $h_p > h_{top}$, the D_r model is applicable (see Table 5.3). Therefore, from Eq. 2.13 the vertical separation factor is:

$$\xi = h_p - h_{top} = 1.1 \text{ m}$$

Using the results obtained from Step 4 of the previous Section. D_r is calculated using step 5.

Step 5: Estimate of dilution D_r at distance x = 30 m from the stack

From Eq 2.12, $D_r (x = 30 \text{ m}) = 81$ and $D_N = 0.20$

Note that the ASHRAE (2007) D_N estimate is nearly one fifth of the D_N value estimated by ASHRAE (2003) for the same building/stack configuration. This indicates that the 2007 model could provide conservative estimates of minimum dilution than the 2003 model. Results for different building/stack/RTS configurations are presented in the following section.

5.3 Evaluating ASHRAE (2003, 2007) models with wind-tunnel results

ASHRAE (2003, 2007) D_r and D_s models were evaluated for all combinations of M (1, 2, 3, and 5) and h_s (1, 3, 5, and 7 m) for wind directions $\theta = 0°$ and $\theta = 45°$. In this section, a few critical cases have been selected for comparison with wind tunnel results for the low-rise and the high-rise building.

It was shown in Chapter 4 that for buildings with no RTS (low-rise and high-rise), lowest dilutions occur for $\theta = 0°$. However, for buildings with an RTS, $\theta = 45°$ generated the lowest dilutions. From a design point of view, only worst-case dilutions are important for comparison. Therefore, to represent the worst-case scenario, results for buildings with no RTS are presented for $\theta = 0°$ and results obtained with an RTS are presented for $\theta = 45°$.

5.3.1 Low-rise building with no RTS

Along-wind D_N profiles obtained with the ASHRAE (2003) and ASHRAE (2007) models for the low-rise building with no RTS are shown in Figures 5.3a and 5.3b, respectively. Also shown are the wind tunnel data for $\theta = 0°$. Results are shown for stack S1 ($x_s = 0.5h$), $h_s = 0.75h$ and M values ranging from 1 to 5. Estimated D_N values were obtained using the ASHRAE (2003) and ASHRAE (2007) D_r and D_s models. Based on the exhaust parameters and plume height requirements as per Tables 5.1 and 5.3, the D_r model is applicable for $M \geq 2$ and the D_s model for $M = 1$. Even though the results are presented for the building with no RTS, to be consistent, the data are plotted with respect to the non-dimensionalized distance from the stack, x/h, where h = 4 m is the height of the RTS.

As shown in Figure 5.3a, the measured D_N values for each M value decreased consistently with x/h. The ASHRAE (2003) D_r model predicted dilutions for M = 2, 3 and 5 increased with distance until $x < 2.5h$ and decreased for $x > 2.5h$. In contrast, the maximum measured D_N values always occurred near the stack for each M value. The

ASHRAE D_r model compared well with measurements for M = 5, and was unconservative for $M \leq 3$.

The ASHRAE (2007) D_r model estimates (Figure 5.3b) are overly conservative for all M values and at all sampling locations. Contrary to the measured D_N values, the estimated D_N values did not vary much with the distance from the stack. Note that the D_N trends obtained with the ASHRAE (2007) model are significantly different from those obtained with the 2003 version. The large difference between measured and predicted dilutions for both 2003 and 2007 D_r models is attributed to the way plume height is calculated in each version.

The D_r model limits the contribution of plume height near the stack. According to ASHRAE, close to the stack, the ratio $h_p^2/2\sigma_z^2$ in the 2003 D_r model and $\xi^2/2\sigma_z^2$ in the 2007 D_r model become very large, causing the exponential term in Eq 2.5 and Eq 2.12 to over-predict roof-level dilutions. Therefore, the ratios $h_p^2/2\sigma_z^2$ and $\xi^2/2\sigma_z^2$ are not allowed to exceed values of 5 and 7, respectively. Consequently, h_p and ξ are limited to values of $3.16\sigma_z$ and $3.74\sigma_z$ for the 2003 and 2007 D_r models, respectively. Hence, the 2003 model predicts lower D_N values close to the stack. Increasing the ξ value in ASHRAE (2007) D_r model from $3.16\sigma_z$ to $3.74\sigma_z$, improved the dilution estimations close to the stack. However, based on the value of h_{top}, the 2007 model applies a penalty to h_p, which further causes a significant reduction in dilution estimation. As a result, the 2007 D_r model predictions were conservative.

The D_s model profiles for M = 1 were significantly below the measured data for ASHRAE (2003 and 2007). Note that the D_s model trend is opposite to the trend shown

for the measured values. In the 2003 D_s model, $h_p = 0$ and in the 2007 version and $\xi = 0$. Consequently, the D_s model assumes that the plume is released at the building roof level with virtually no plume rise. Thus, the model produces extremely conservative D_N values.

5.3.2 Low-rise building with an RTS

Along-wind D_N profiles obtained with the 2003 D_r model for the low-rise building with an RTS (w/h = 7.5) are shown in Figure 5.4a. Results are shown for θ = 45°, stack S1, $h_s = 0.75h$ and M values ranging from 1 to 5. Due to the downwash effect of the RTS, the measured D_N values in this case decreased significantly in comparison to the building with no RTS, $\theta = 0°$ case. However, the model estimates remained the same as those for the building with no RTS because the model does not incorporate the effect of an RTS on plume rise. Models assume same recirculation zone dimensions as for θ = 0°. As a result, the ASHRAE (2003) D_r model significantly overestimated the dilutions.

The ASHRAE (2007) D_r model estimates for the building with RTS are shown in Figure 5.4b. The level of conservatism for the building with the RTS was less than that for the building with no RTS and decreased with an increase in M values. As shown in Chapter 4, the plume height could reduce up to 40% due to the downwash effect of the RTS. Therefore, the penalty applied to h_p in the ASHRAE (2007) D_r model is reasonable in this case. However, the 2007 model was still quite conservative for the low-rise building with RTS.

The ASHRAE (2003, 2007) D_s model estimates with RTS are also shown in Figure 5.4 and correspond to M = 1. Similar to the flat-roof case, the results clearly indicate a significant level of conservatism in D_s model estimates at all sampling locations. As mentioned previously, the D_s model did not provide any benefit for plume height, which is partially compensated with the downwash effect of the RTS. Therefore, the level of conservatism decreased significantly at samplers located close to the stack for the building with the RTS compared to building with no RTS.

5.3.3 High-rise building

Figure 5.5 shows the measured and estimated D_N values for the flat-roofed high-rise building. Note that the data are plotted with respect to the normalized distance from the stack, x/h, where h = 4 m, is the height of the RTS.

In this case, the ASHRAE (2003, 2007) D_s model is applicable because the plume is entrained within the building recirculation zone for all M values. Results are shown for $h_s = 0.75h$, M = 1 to 5, and $\theta = 0°$. Since the D_s model assumes no contribution of plume rise, the D_s model underestimated the dilutions at nearly all sampling locations for all M values. In general, the estimated D_N values were about 10 to 100 times lower than the measured D_N values.

5.4 Generalizing ASHRAE models' performance

To generalize the performance of ASHRAE dispersion models for different values of h_s and M, a new parameter 'φ' is introduced, where φ is defined at the ratio of

the D_N value estimated by the ASHRAE model with the wind-tunnel measured value. Depending on the magnitude of φ, the results are categorized as follows manner:

i) For $\varphi > 1$, the ASHRAE model is unconservative;

ii) For $\varphi \sim 1$, the ASHRAE and wind-tunnel results are comparable;

iii) For $\varphi < 1$, the ASHRAE model is conservative.

Figures 5.6a through 5.6d show the variation of φ with x/h for the ASHRAE (2003) and ASHRAE (2007) models in the case of the low-rise building with and without RTS. Results are shown for $h_s = 0.75h$ and for M ranging from 1 to 5. A trend is also shown for the D_r model comparison. This curve (solid line) was obtained by averaging the results over all M values for which the D_r model was applied (M = 2, 3, and 5) and is indicated by φ_m.

It is worth noting that in Figure 5.6, φ values for the low-rise building generally followed a similar trend for all M values and generally vary within a factor of $\pm$ 2, with a few exceptions. Trends shown in Figure 5.6a indicate that for M > 1, the ASHRAE (2003) estimates for the building with no RTS were moderately unconservative. However, for M = 1 the ASHRAE predictions are significantly conservative at all sampling locations. The ASHRAE 2003 model performance for the building with the RTS is shown in Figure 5.6b. For this case, the 2003 model predictions were extremely unconservative. For the same building configuration, the 2007 model was extremely conservative for the building with no RTS and moderately conservative for the building with the RTS, as shown in Figures 5.6c and 5.6d, respectively.

Figure 5.7 shows similar trends for φ for the high-rise building base. The φ values represent both ASHRAE (2003) and ASHRAE (2007) D_s model performance for h_s = 1.75h. For this case, φ values generally followed a similar trend for M > 1. The results indicate that the model predictions for the high-rise building were conservative for all M values tested.

For all building configurations tested, similar trends for φ vs. x/h were found for other values of h_s (0.25h, 1.25h, and 1.75h). Therefore, to demonstrate the performance of ASHRAE minimum dilution models for different stack heights, φ_m was calculated for all stack heights. The results will be presented in the form of φ_r and φ_s, where subscripts 'r' and 's' represent the trends obtained with D_r and D_s models, respectively.

Figures 5.8a and 5.8b show mean values of φ_r for the ASHRAE (2003) model for the low-rise building with and without RTS, respectively. In general, for the building with no RTS the D_r model estimates were unconservative for h_s < 1.75h. The maximum difference between D_r model estimates and wind-tunnel results was found for the tallest stack (h_s = 1.75h), where φ_r values were overly conservative near the stack. This occurred because close to the stack, the ratios $h_p^2/2\sigma_z^2$ is cannot exceed of 5 in the ASHRAE (2003) model. Consequently, plume height is limited and the model predicts extremely conservative D_N values close to the stack ($\varphi \approx 0.01$ to 0.1). This clearly demonstrates the complexity of the nature of building exhaust dispersion and the difficulty involved in modeling dispersion for such cases.

With an RTS (Figure 5.8b), φ_r values for all h_s were always significantly greater than 1, except close to the stack for h_s = 1.75h. The results indicate that the 2003 D_r

model is unconservative for low-rise buildings with RTS, since this model did not take into account the downwash effect of an RTS.

Similar comparisons for the ASHRAE (2007) D_r model are shown in Figures 5.8c and 5.8d. The results indicate that the 2007 D_r model was overly-conservative for the building with no RTS for almost all h_s tested and for almost all sampling locations. For the building with RTS, the 2007 model estimates for $h_s > 0.25h$ were about 3 to 4 times lower than the measured values ($\varphi \approx 0.25$). However, for $h_s = 0.25h$, the 2007 model estimates were significantly more conservative compared to other stack heights.

The ASHRAE (2003, 2007) D_s model performances are presented in Figures 5.9 and 5.10. Figures 5.9a and 5.9b show the variation of φ_s with x/h for the low-rise building, with and without RTS, respectively. The results indicate that the D_s model predicted significantly conservative dilutions for all cases.

Similar trends for φ_s for the high-rise building are shown in Figure 5.10. The results indicate that the level of conservatism of the D_s model, which is very high for the high-rise building. Since the D_s model does not take into account the effect of plume height, the conservatism increases with the increase in stack height.

5.5 Modified ASHRAE dispersion model

The findings presented in Section 5.4 indicate that the ASHRAE models may lead to conservative or unconservative results. The ASHRAE (2003) D_r model was moderately unconservative for the low-rise building with no RTS and overly conservative for the building with the RTS. However, the ASHRAE (2007) D_r model

was conservative for all cases presented. The ASHRAE (2003, 2007) D_s model was conservative irrespective of building height and presence of RTS.

In order to make the ASHRAE models more accurate, a few modifications are proposed based on the wind tunnel results:

i) The detailed Briggs (1984) plume rise equations (discussed later) should be used instead of the simplified equation (Eq 2.7).

ii) For low-rise buildings with the stack downwind of an RTS with height h and for RTS-stack separation distance $x_s < 2.5h$:

a) For $h_s < 2.5h$: reduce h_p by 50% for $h_p \leq h_{top}$ and 30% for $h_p > h_{top}$

b) For $h_s \geq 2.5h$: neglect the effect of RTS.

iii) For high-rise buildings with stacks engulfed within the building separation bubble:

a) For $h_s < h_{top}$: reduce h_p by 50%

b) For $h_s > h_{top}$: neglect the effect of the separation bubble.

These modifications are applicable when the RTS, the stack, and the intake are located on the same level and same building roof. The reasoning behind these modifications is discussed in the following sub-sections.

5.5.1 Modification applied to the ASHRAE plume rise equation

The most widely used equations for predicting plume rise are from Briggs (1984). Briggs developed the following equation for neutrally buoyant plumes (i.e. exhaust and ambient density are nearly equal).

$$h_{r,m} = \min\left\{\left(\frac{3F_m x}{\beta_j{}^2 U_s}\right)^{\frac{1}{3}}, h_{f,m}\right\} \qquad \text{[Eq 5.3]}$$

where F_m is the momentum flux, β_j is the jet entrainment coefficient, x is the distance from the stack, and U_s is the wind speed at the tip of the stack. The subscript 'm' stands for momentum. F_m and β_j are given by the expressions:

$$F_m = \left(\frac{T_a}{T_s}\right) w_e{}^2 \left(\frac{d_e{}^2}{4}\right) \qquad \text{[Eq 5.4]}$$

$$\beta_j = \frac{1}{3} + \frac{U_s}{w_e} \qquad \text{[Eq 5.5]}$$

where w_e is the exhaust velocity, T_a and T_s are the ambient and stack exhaust temperatures, respectively, and d_e is the stack diameter.

The one-third power law term in Eq 5.3 is only used to determine the distance at which the final plume rise from Eq 5.6 occurs. The value of h_r increases with x until the final plume rise $h_{f,m}$, is reached. The final plume rise is given by the following expression:

$$h_{f,m} = \frac{0.9\left[F_m U_s / U^*\right]^{1/2}}{U_H \beta_j} \qquad \text{[Eq 5.6]}$$

where

$$\frac{U_s}{U^*} = 2.5 \ln\left(\frac{H}{z_o}\right) \qquad \text{[Eq 5.7]}$$

is the standard logarithmic law representing the boundary layer profile, where U* is the friction velocity related to the upstream roughness z_o.

Note that in the present study, the wind speed was always measured at the building roof height. Therefore, the wind speed obtained at the building roof height was used to calculate the plume rise instead of the wind speed at stack height. This approximation does not produce a significant error in plume rise calculations, since building stacks are relatively short.

The upstream terrain in the present study is assumed to be urban with a surface roughness of z_o = 1.1 m. For the low-rise building, H = 15 m, substituting these values into the Equations 5.7 gives:

$$\frac{U_H}{U^*} = 6.53$$

In the present study, for M = 1, (w_e = U_H = 5.4 m/s), the jet entrainment coefficient and momentum flux are:

β_j = 1.3 and F_m = 2.6 m^4/s^2

Substituting the above values in Eq 5.6, the final plume rise with extended Briggs equations for M = 1 is 0.5 m.

The ASHRAE (2003, 2007) D_r models currently use a simplified version of Briggs (1984) plume rise equations for momentum-dominated plumes at the point of final rise, which is estimated using the following expression:

$$h_r = 3\beta d_e (w_e/U_H) \qquad \text{[Eq 2.7]}$$

It should also be noted that Eq 2.7 is a simplified version of a more complicated equation developed by Briggs (Eq 5.6) and is based on the assumption that the jet entrainment coefficient β_j (discussed later) is 0.6 and $\frac{U_H}{U^*} = 15$.

Table 5.4 lists the plume rise estimates obtained with the Briggs (1984) extended equations and the simplified equation adopted by ASHRAE (2003, 2007). For M > 1, the plume rise values estimated by the ASHRAE formula are significantly greater than those obtained with the extended Briggs equations. Therefore, to obtain more accurate plume rise estimates, Briggs (1984) extended equations have been used.

Peterson et al. (2008) conducted a wind tunnel study to quantify the effect of ganging on rooftop stacks on plume dispersion. He recommended using Briggs extended plume rise formulations over the simplified equation.

5.5.2 Modification to consider the downwash effect of an RTS for a typical low-rise building

The Briggs (1984) plume rise formula is based on results obtained for an isolated stack that is not affected by building generated turbulence. The second proposed modification takes into account the influence of the building and RTS on plume rise and is based on the wind tunnel results obtained in the present study for the low-rise building. In Chapter 4, it was demonstrated that h_p could be reduced by up to 40% (see Figures 4.11 and 4.12) due to the downwash effect of an RTS. In addition, the downwash was significant for $h_s < 2.5h$ (se Figure 2.23).

The wind tunnel data obtained in the present study was compared with the modified ASHRAE model for different reduction factors applied to the plume height. The results from the analysis indicated a reasonable agreement between the measured and estimated values when the h_p value was reduced by 50% for $h_p \leq h_{top}$ and 30% for $h_p > h_{top}$, where h_{top}, is the height of the tallest recirculation zone formed on the building roof. Since the downwash effect of RTS was negligible for $h_s > 2.5h$, the reduction in plume height is limited for $h_s \leq 2.5h$. For $h_s > 2.5h$, no reduction is required for h_p.

5.5.3 Modification for a typical high-rise building

The third proposed modification is applied to take into consideration the effect of building height. For high-rise buildings and $\theta = 0°$, the separation bubble generally extends over the entire roof or covers at least most of the roof (70% or more). As a result, the rooftop stack is generally engulfed inside the recirculation zone.

Consequently, most of the exhaust plumes are entrained within the bubble. For this case, the along-wind D_N profiles obtained showed similar trends (see Appendix C). The effect of M and/or h_s on D_N values was not that significant. This indicates that for the same set of h_s and M values, the plume height for stacks on a taller building is smaller than that for the low-rise building. Plume height reductions values were applied. Results showed that reducing the plume height by 50% in the ASHRAE (2007) D_r model provide a reasonably better agreement between the measured and estimated data with the modified model than those predicted by the ASHRAE (2003, 2007) D_s model (demonstrated later in section 5.6).

The data obtained in the present study for the high-rise building is limited to stack heights lower than the height of the tallest building roof recirculation zone (h_{top}). Therefore, the suggested reduction in plume height is valid for $h_p \leq h_{top}$, which will be applicable to any practical stack design. Previous studies such as Thompson et al. (2002) have shown that the effect of bubble on the plume is not that significant for $h_s > h_{top}$. Thus, for $h_s \geq h_{top}$, no reduction is required for h_p.

5.6 Evaluation of modified ASHRAE dispersion model with present study results

To evaluate the modified ASHRAE model, the generalized performance of the modified ASHRAE minimum dilution model is presented in terms of φ_{mod}, where the subscript "mod" represents values obtained with the modified ASHRAE minimum dilution model. Similar to the φ_s and φ_m trends presented in Section 5.4, the φ_{mod} values

generally follow a similar trend for all M values. Therefore, for simplicity, mean values of φ_{mod} were calculated for all stack heights tested.

Figure 5.11 shows the variation of φ_{mod} with x/h for h_s ranging from 0.25h to 1.75h. Results are shown for the low-rise building with and without RTS, respectively. Results for the no RTS case are presented for $\theta = 0^\circ$. For the building with the RTS, data obtained with $\theta = 45^\circ$ are shown.

For the building with no RTS, the modified ASHRAE model performed reasonably well for $h_s \leq 1.25h$, as shown in Figure 5.11a. The φ_{mod} values were generally within a factor of 3, at most of the sampling locations. For $h_s = 1.75h$, the modified model was still significantly conservative near the stack ($x < 2.5h$). A significant drop in dilution estimates close to the stack for $h_s = 1.75h$ is due to limiting the ratio $h_p^2/2\sigma_z^2$ to a maximum value of 7 as specified by the ASHRAE (2007) D_r model. This clearly indicates the complexity in modeling dispersion for building roof exhausts for different exhaust conditions.

For the building with the RTS, the modified model provides reasonably conservative estimates (within a factor of 3) at most of the sampling locations and for all stack heights tested, as shown in Figure 5.11b. The accuracy of the estimate for both cases building with RTS and without RTS is significantly improved compared to the ASHRAE (2003, 2007) D_r model predictions (see Figure 5.8).

Figure 5.12 shows similar trends for the high-rise building. The dilution values for the high-rise building are still somewhat conservative, as indicated by $\varphi_{mod} < 1$ for all h_s values tested. However, the accuracy of the estimate is significantly improved

compared to the ASHRAE (2003, 2007) D_s model. The D_N values obtained with the ASHRAE models were lower than the measured values by a factor of 10–100 (see Figure 5.10). However, with the modified model, D_N values are about two to five times lower than the measured data. Another significant improvement in the modified model is the effect of h_s on dilution estimates for the high-rise building. Its also worth noting that with the ASHRAE D_s dispersion model, φ_s reduced with an increase in h_s (see Figure 5.10). However, the modified model predicts the effect of increase in h_s correctly for the high-rise building. The φ_{mod} values increase with increase in h_s, indicating that D_N estimates increase with h_s.

In general, the accuracy of the estimates with the modified ASHRAE D_r model is significantly improved in comparison to either the ASHRAE (2003) or ASHRAE (2007) dispersion models.

5.7 ASHRAE Geometric Stack Design Method (AGM)

The AGM, which was developed by Wilson (1979), allows designers to determine the minimum required stack height for building roof exhausts. The goal of the AGM is to generate a stack design that will keep the plume well above any recirculation zones formed between the stack and the intake. The details on AGM can be found in section 2.4.5.4.

Although the AGM does not provide quantitative dilution estimates, practitioners use it as a screening tool if wind tunnel modeling is not readily achievable. Before evaluating AGM, the methodology for using it will be presented, followed by a sample calculation for an exhaust stack located on the roof of a low-rise building.

5.7.1 Using AGM

The procedure for using AGM is the same for both ASHRAE (2003) and ASHRAE (2007). Determining the required design stack height by AGM involves four steps:

Step 1: Determine the dimensions of recirculation zones.

Step 2: Assuming the plume spreads vertically with a slope of 1:5, draw a line at a slope of 1:5 from the intake to the desired stack location avoiding the tallest recirculation zone.

Step 3: Determine the stack height required by a capped stack (h_{small}).

Step 4: Determine the required stack height (here after h_{AGM}), by applying the plume rise and stack downwash (h_d) correction to h_{small}, using the following formula:

$$h_{AGM} = h_{small} - h_r + h_d \qquad \text{[Eq. 5.8]}$$

5.7.2 Example showing AGM design procedure

The same example used to describe the D_r model in section 5.2.1 will be used for this case. The test building is shown in Figure 5.2 and exhaust parameters are presented in Table 5.2.

The capped stack height, h_{small}, is 6.0 m; therefore, from Eq 5.8:

$$h_{AGM} = h_{small} - h_r + h_d = 3.0 \text{ m}$$

Thus, a minimum stack height of 3 m is required for this building to avoid reingestion at any intake located on the building roof.

5.7.3 Evaluating AGM using wind-tunnel data

Theoretically, the design stack height, h_{AGM}, should prevent the plume from making any contact with the fresh air intake. Therefore, D_{min} measured at the intake should be very high. Although the AGM does not specify a minimum allowable dilution, for the purpose of model validation, a dilution criterion, D_C, must be specified. The AGM will be considered successful if h_{AGM} provides dilution values that exceed D_C at all rooftop locations. The design dilution criterion used in the present study is that proposed by Wong et al. (2002) for laboratory fume hood stacks, the most common type of exhausts used in laboratories, hospitals and other research facilities. According to Wong et al. (2002), a D_{min} of 3,000:1 for 1,000 cfm flow rate is acceptable for laboratory fume hood exhausts. The study also showed that this criterion would provide an acceptable air quality for 90% of the 370 chemicals commonly used in laboratories.

Problems with fume hood exhausts usually arise from an accidental release from a single fume hood. Typically, however, a number of fume hoods are connected in a manifolded system. Exhausts from other the fume hoods can be considered relatively clean and will provide added dilution internal to the building before reaching the stack. This internal dilution should be taken into account. As internal dilution increases, less atmospheric dilution is needed, and the dilution criterion can be adjusted accordingly. As indicated earlier, the D_C value of 3,000:1 is for a flow rate of 1,000 cfm (typical for a single fume hood). The dilution for other stack flows is determined by dividing D_C by

the number of 1,000 cfm units. For example, the required dilution for a flow rate of 4,000 cfm is:

D_C = (design dilution) (1,000)/ (actual flow rate) = 750

The D_C corresponding to the different flow rates (Q) used in the present study are listed in Table 5.5. The design dilution criteria varied from around 900 for the lowest flow rate (M = 1) to around 200 for the highest flow rate (M = 5).

The estimated h_{AGM} values for the high-rise building ranged between 15 m and 20 m, which are significantly higher than the maximum stack height used in the wind tunnel study. Moreover, such tall stack heights are not practical and not preferred in real life. Therefore, AGM was evaluated only for a typical low-rise building for which h_{AGM} values were within a reasonable range of 3 m to 10 m.

The D_{min} values measured at two locations on the low-rise building were used to evaluate AGM. Receptor A was located near to the stack [x = 2.5 m (0.6h)], and receptor B was located at the leeward edge of the roof [x = 30 m (7.5h)]. The stack was located at a distance of x_s = 0.5h downstream of the RTS and 20 m from the building leading edge. The locations of the intakes and stack are shown in Figure 5.13.

Note that AGM is applicable for a wind approaching normal to a building wall (θ = 0°). However, as shown previously in Chapter 4, low dilutions can also occur for θ = 45° if an RTS is present. Therefore, in this discussion, the wind tunnel D_{min} values are shown for the two worst-case scenarios:

i) low-rise building without RTS for θ = 0°;

ii) building with RTS for $\theta = 45°$.

The stack heights estimated for the low-rise building with AGM are listed in Table 5.6. Histograms shown in Figure 5.14 show the measured D_{min} values obtained at receptors A and B for different M values for AGM estimated stack heights. The corresponding D_C values are also shown for comparison. As mentioned previously, for an acceptable h_{AGM} value, D_{min} should be greater than or equal to D_C.

As shown in Figure 5.14a, for intake A, $D_{min} > D_C$ for all M values. Therefore, h_{AGM} is acceptable for intake A. For intake B, the values of h_{AGM} were slightly unconservative for M = 2 and M = 3 because $D_{min} < D_C$. However, for M = 1 and M = 5, $D_{min} > D_C$. Thus, h_{AGM} values are acceptable for these cases. Figure 5.14b shows a similar comparison for the building with an RTS (w/h = 7.5) located upstream of the stack for $\theta = 45°$. The D_{min} values obtained at intakes A and B were approximately 50% lower than the required D_C for some M values, indicating that h_{AGM} is not acceptable for this building/RTS configuration.

As per AGM, if $h_s = h_{AGM}$, the plume should not make any contact with the intake. Consequently, D_{min} values at the intakes should be extremely high and the stack height should acceptable. However, the results in Figure 5.14 show that for all M values tested, the measured D_{min} values for the low-rise building without the RTS were either similar or lower in magnitude than the D_C.

On the other hand, for the building with the RTS, D_{min} values at the intakes were less than D_C for all M values. Thus, for this case, the AGM significantly underestimated the stack heights required to minimize reingestion. This suggests that the common belief

that AGM estimates are overly conservative is not true for at least some buildings, especially for typical low-rise buildings with stacks located downwind of an RTS.

5.8 Modified AGM (MAGM)

In this section, a modified AGM (hereafter MAGM) is proposed that will provide more accurate h_{AGM} values. In the modified procedure, the following changes have been made to AGM:

i) The detailed Briggs (1984) plume rise equations have been used instead of the simplified equation used in ASHRAE (2003, 2007).

ii) The reference roof level has been raised to the height of the tallest upstream rooftop structure located laterally within two RTS widths and longitudinally within three RTS heights of the stack, the area within which the effect of RTS is expected to be dominant. For stack located outside the specified area, the effect of the RTS is considered to be negligible.

These modifications are applicable when the RTS, the stack, and the intake are located on the same level and on the same building roof. The benefits of using detailed Briggs (1984) plume rise equations were discussed earlier in Section 5.5.1. The effect of increasing the roof height to RTS height is discussed in this section.

In the present study, the height of the low-rise building was H = 15 m and RTS height h = 4 m. Therefore, the new building height used for MAGM after raising the roof level to the RTS height level is:

$H + h = 19$ m.

The effect of proposed modifications on h_{small} for the building with RTS is shown in Figure 5.15. The h_{small} value for the building with the RTS estimated with AGM is shown in Figure 5.15a. Note that the h_{small} value for the building with the RTS is still the same as for the building with no RTS (see Figure 5.2).

With the proposed modification for the building with the RTS, the plume slope of 1:5 is now plotted to avoid the intake as it was located on a building with roof height of 19 m, as indicated in Figure 5.15b. For this case, the h_{small} value increased from 6 m for the building with no RTS to 10 m with the RTS. As noted previously, with AGM, the h_{AGM} values for the RTS case and building with the RTS were the same.

The stack heights using the MAGM (represented as h_{MAGM}) were estimated for different M values and are listed in Table 5.7. For the h_{MAGM} values listed, the D_{min} values were measured in the wind tunnel for the building with no RTS at 0° and the building with RTS at 45°. The results are presented in Figure 5.16, which shows the comparison between the measured D_{min} values at intakes A and B for the estimated h_{MAGM}. Also shown are the D_C values for each M value tested (M = 1 through 5). The D_{min} values for h_{MAGM} are greater than D_C values at intakes A and B for all cases, indicating that h_{MAGM} values are acceptable.

The MAGM validations presented for the low-rise building with and without an RTS are limited to the results obtained in the present study. Additional validations for the proposed MAGM with results from previous studies are required to test the proposed modifications suggested to AGM for a wide range of building/RTS/stack configurations.

Table 5.1 Design criteria from ASHRAE (2003) dispersion models.

Case	Criteria	Applicable stack height (h_s) for dispersion model	Applicable ASHRAE (2003) model
1	$h_p \geq h_{small}$	h_s	D_r
2	$h_p < h_{small}$ $h_s > h_{top}$	$h_s - h_{top}$	D_r
3	$h_p < h_{small}$ $h_s < h_{top}$	0	D_s

Table 5.2 Experimental parameters for the sample ASHRAE (2003, 2007) dilution estimation.

Stack diameter d_e (m)	Wind speed U_H (m/s)	Exit velocity w_e (m/s)	Flow rate Q (m^3/s)	Stack height h_s (m)	Exhaust momentum M
0.6	5.4	10.8	3.1	3	2

Table 5.3 Design criteria from ASHRAE (2007) dispersion models.

Case	Criteria	Vertical separation factor (ξ)	Applicable ASHRAE (2007) model
1	$h_p \geq h_{top}$	$h_p - h_{top}$	D_r
2	$h_p < h_{top}$	0	D_s

Table 5.4 Plume rise values estimated with Briggs (1984) simplified plume rise and expanded plume rise equation.

M	h_r (m) (from Briggs (1984) expanded plume rise equation)	h_r (m) (from ASHRAE (2003 and 2007) or Briggs (1984) simplified plume rise equation)
1	0.5	0.6
2	1.7	3.0
3	3.1	5.4
5	6.5	9.0

Table 5.5 Design criteria dilutions for different exhaust flow rates used in the present study.

M	Stack diameter (m)	Exit velocity (m/s)	Exit velocity (fpm)	Q (m^3/s)	Q (cfm)	D_c [Wong et al. (2002)]
1	0.6	5.4	1,063	1.5	3,235	930
2	0.6	10.8	2,126	3.0	6,470	460
3	0.6	16.2	3,189	4.6	9,706	310
5	0.6	27.0	5,315	7.6	16,176	190

Table 5.6 Stack heights estimated with AGM for the low-rise building: stack S1 and M values 1 through 5.

M	h_{AGM} (m)	
	No RTS	With RTS
1	5	5
2	3	3
3	1	1
5	1	1

Table 5.7 Stack heights estimated with MAGM for the low-rise building: stack S1 and M values 1 through 5.

M	h_{MAGM} (m)	
	No RTS	With RTS
1	5	10
2	5	8
3	3	7
5	1	3

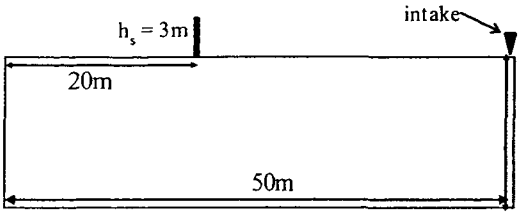

a) Building/stack configuration

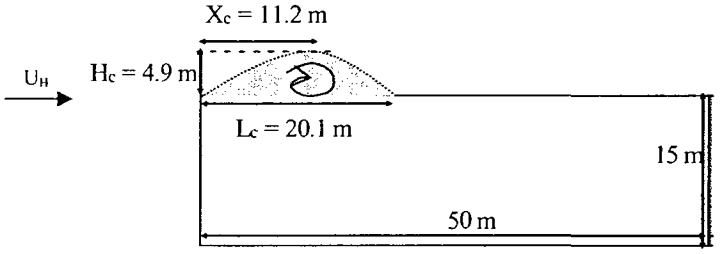

b) Separation bubble

Figure 5.1 Schematic view of a low-rise building: a) building/stack configuration; and b) estimated separation bubble from Wilson (1979).

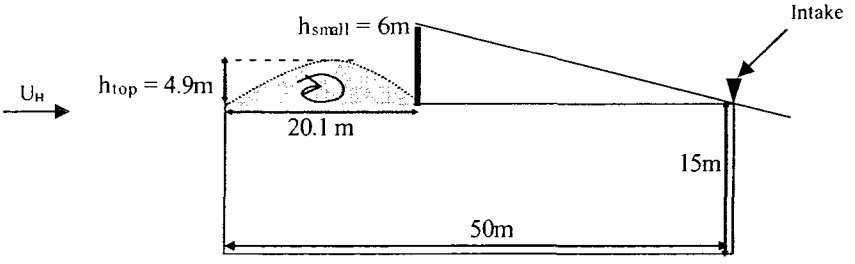

Figure 5.2 Required h_{small} estimated with AGM to avoid plume contact at the intake.

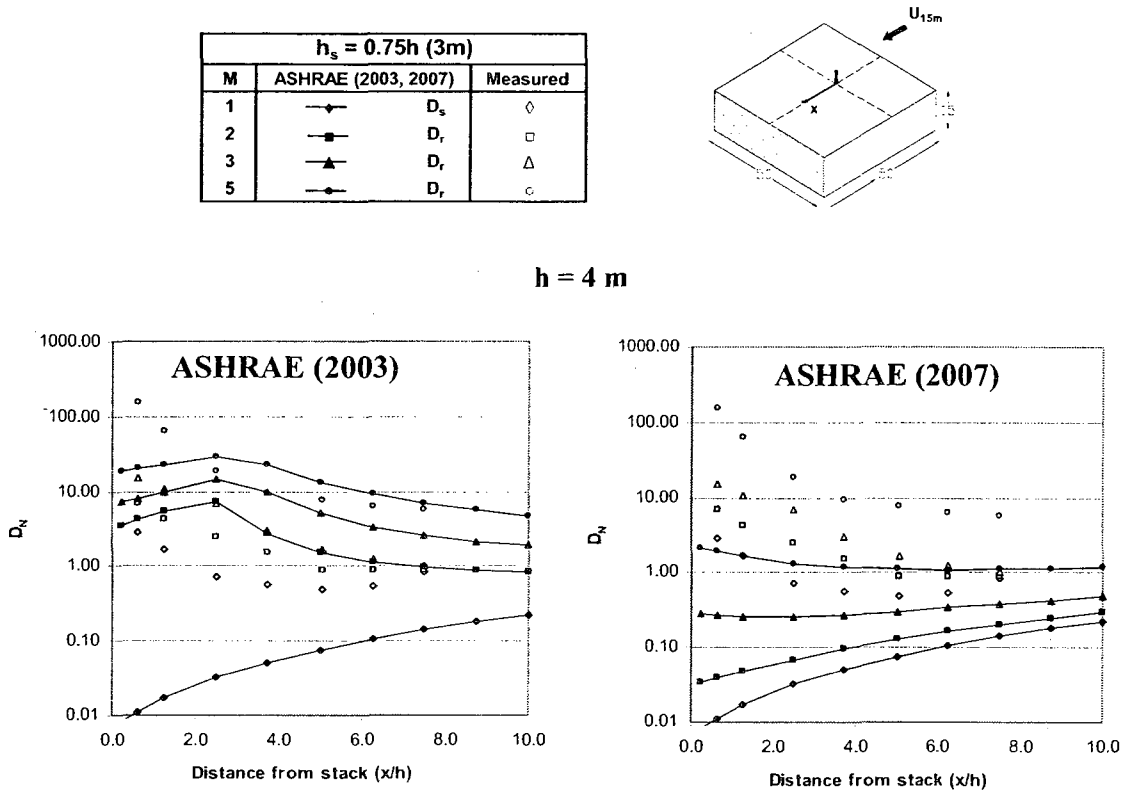

a) ASHRAE 2003 model

b) ASHRAE 2007 model

Figure 5.3 ASHRAE (2003, 2007) estimated vs. measured D_N values for the flat-roofed low-rise building for h_s = 0.75h, M = 1 to 5 and h = 4 m for $\theta = 0°$: a) ASHRAE (2003) model; and b) ASHRAE (2007) model.

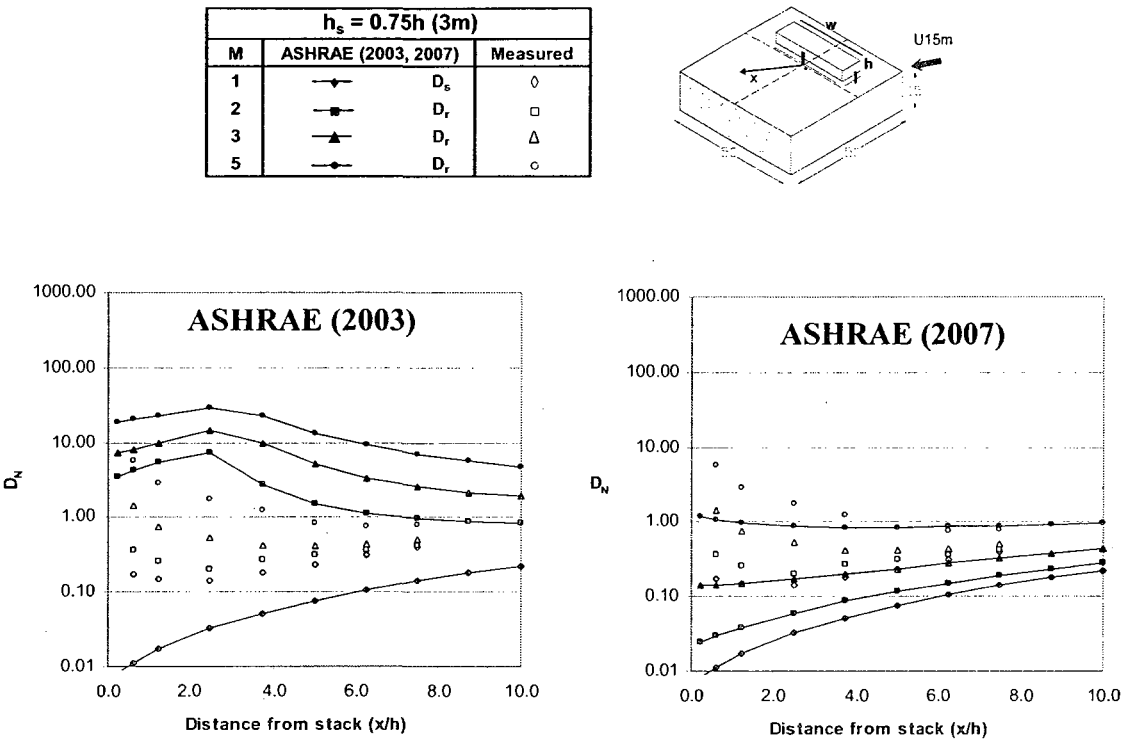

a) ASHRAE 2003 model

b) ASHRAE 2007 model

Figure 5.4 ASHRAE (2003, 2007) estimated vs. measured D_N values for the low-rise building with RTS for h_s = 0.75h, M = 1 to 5 with θ = 45°:a) ASHRAE (2003) model; and b) ASHRAE (2007) model.

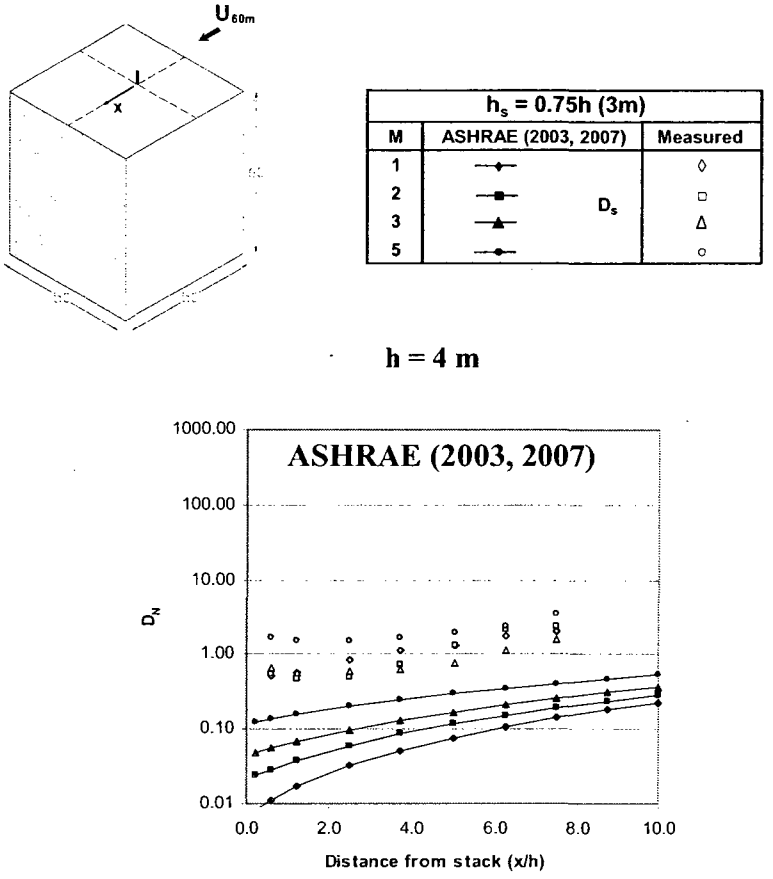

Figure 5.5 ASHRAE (2003, 2007) estimated vs. measured D_N values for the high-rise building for $h_s = 0.75h$: M = 1 to 5, $\theta = 0°$.

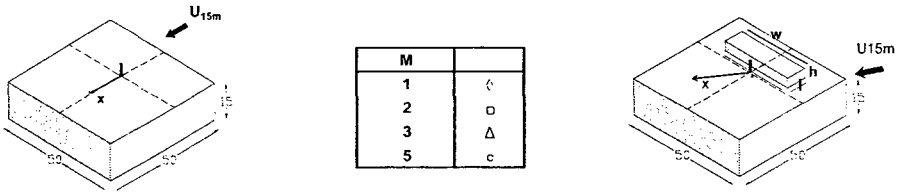

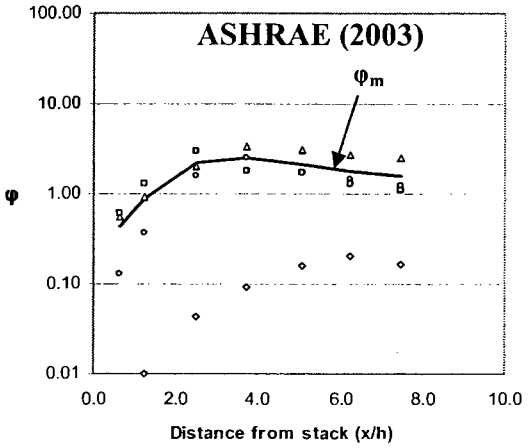

a) Flat-roof, θ = 0°, w/h = 0

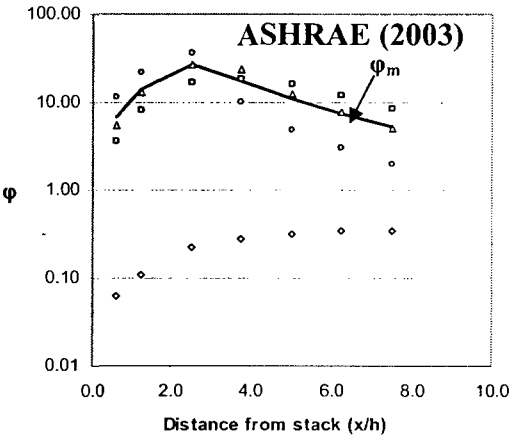

b) With RTS, θ = 45°, w/h = 7.5

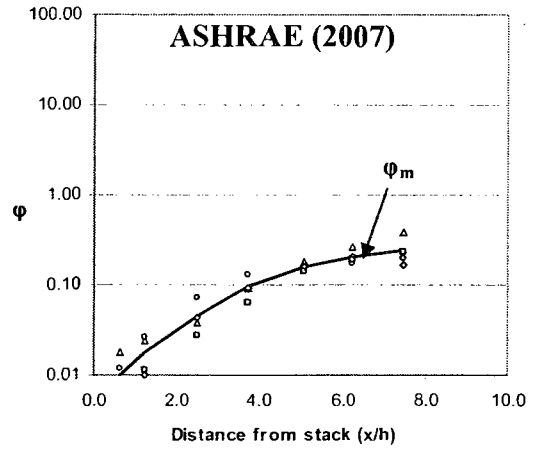

c) Flat-roof, θ = 0°, w/h = 0

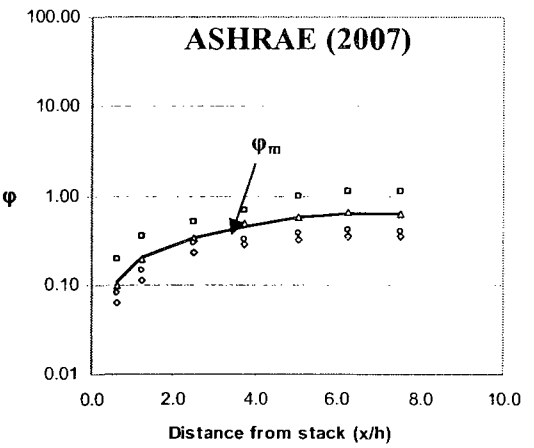

d) With RTS, θ = 45°, w/h =7.5

Figure 5.6 φ vs. x/h for the low-rise building for h_s = 0.75h (3 m): a) ASHRAE (2003) flat-roof; b) ASHRAE (2003) building with RTS; c) ASHRAE (2007) flat-roof; and d) ASHRAE (2007) building with RTS.

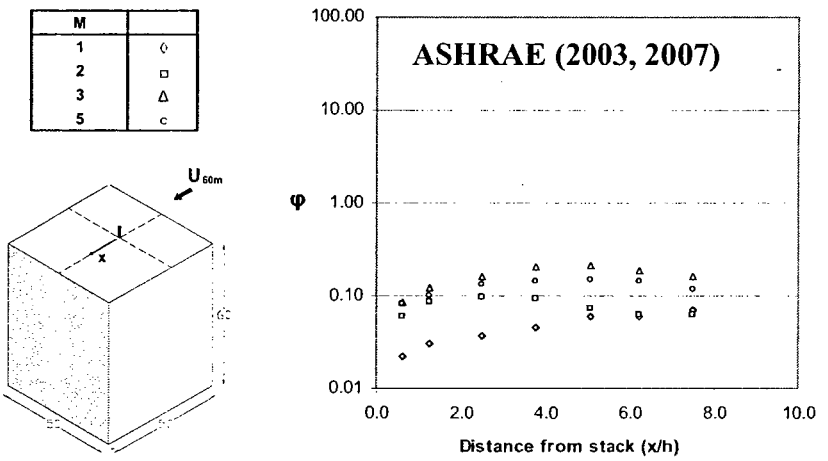

Figure 5.7 φ vs. x/h for the flat-roofed high-rise building for $h_s = 0.75h$ (3 m) and $\theta = 0°$.

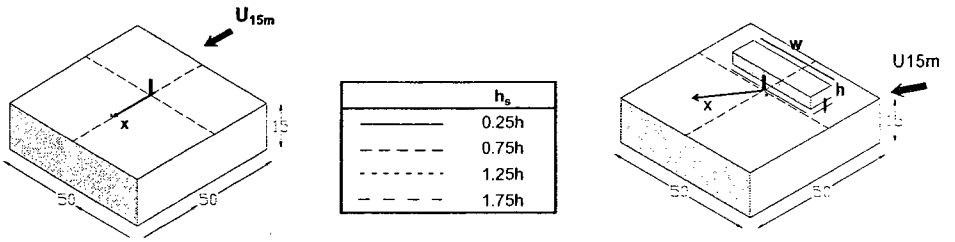

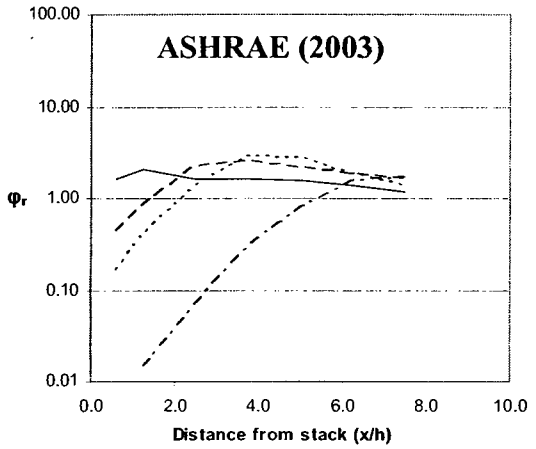

a) Flat-roof: θ = 0°

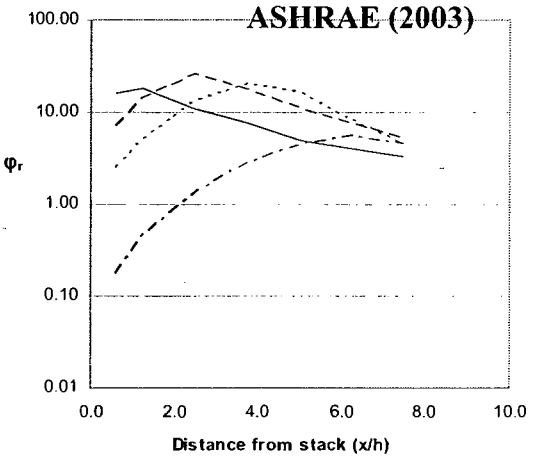

b) With RTS (w/h = 7.5): θ = 45°

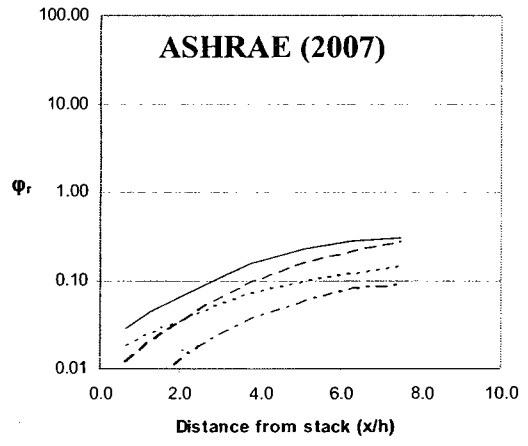

c) Flat-roof: θ = 0°

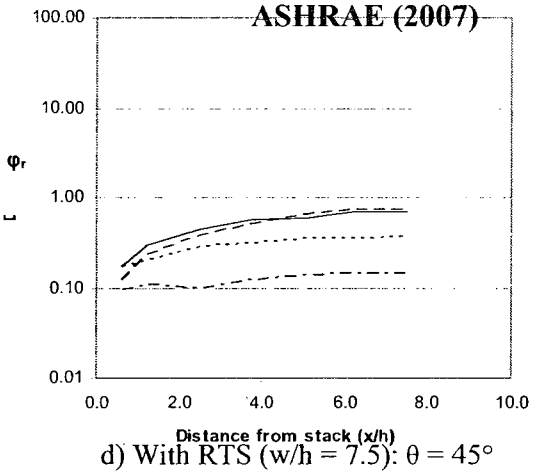

d) With RTS (w/h = 7.5): θ = 45°

Figure 5.8 Performance of ASHRAE (2003) and ASHRAE (2007) D_r minimum dilution models for the low-rise building: a) ASHRAE (2003) flat-roof; b) ASHRAE (2003) building with RTS; c) ASHRAE (2007) flat-roof; and d) ASHRAE (2007) building with RTS.

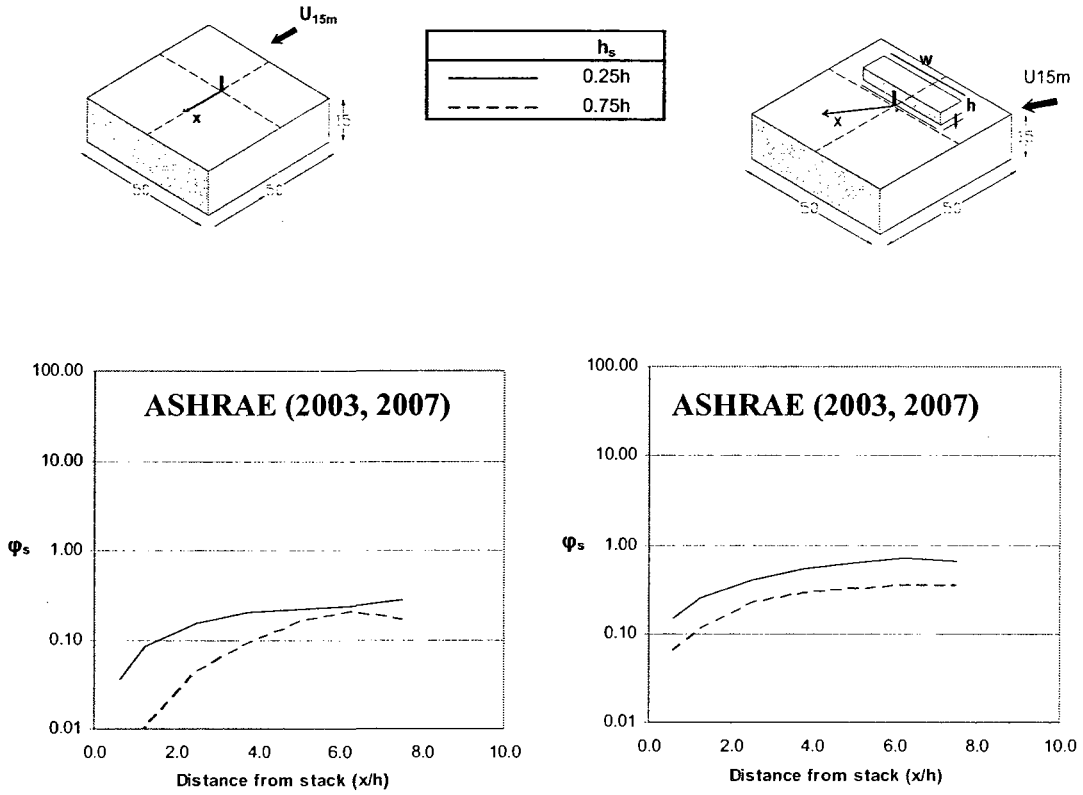

a) Flat-roof: $\theta = 0°$

b) With RTS (w/h = 7.5): $\theta = 45°$

Figure 5.9 Performance of ASHRAE (2003, 2007) D_s minimum dilution model: a) flat-roofed low-rise building; and b) building with RTS.

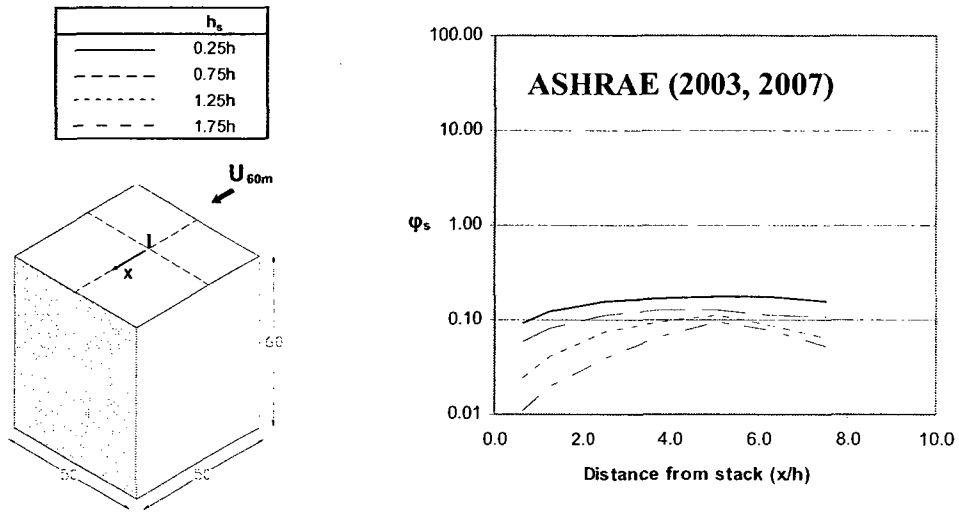

Figure 5.10 Performance of ASHRAE (2003, 2007) D_s minimum dilution model for the high-rise building with or without RTS with h = 4 m for $\theta = 0^{\circ}$.

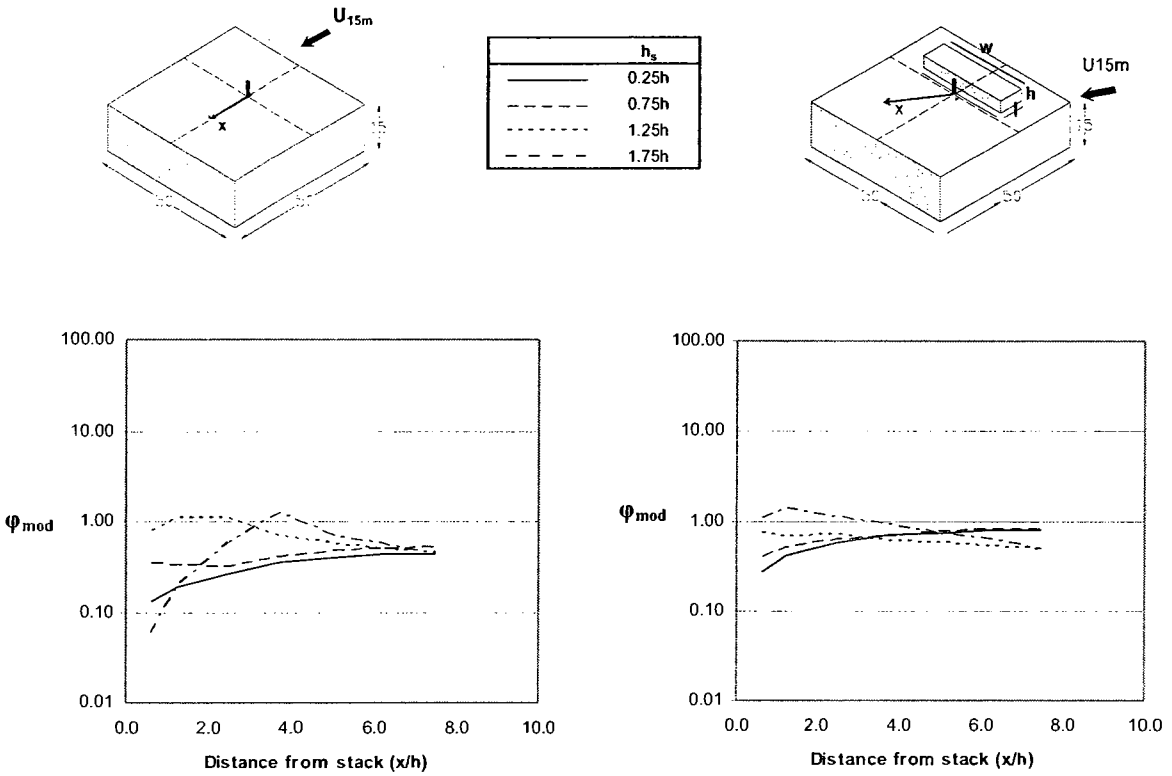

a) Flat-roof: $\theta = 0°$

b) With RTS w/h = 7.5): $\theta = 45°$

Figure 5.11 Performance of modified ASHRAE minimum dilution model for the low-rise building: a) flat-roofed building; and b) building with RTS.

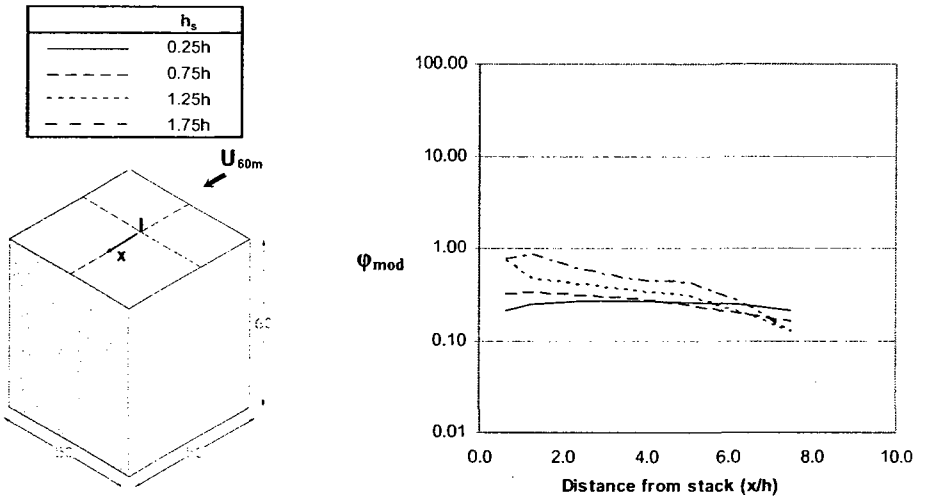

Figure 5.12 Performance of modified ASHRAE minimum dilution model for the high-rise building with or without RTS with h = 4 m and for $\theta = 0^{\circ}$.

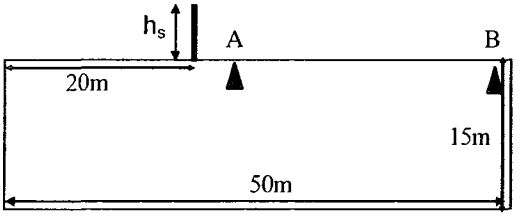

Figure 5.13 Low-rise building showing the location of intakes A and B used to evaluate AGM.

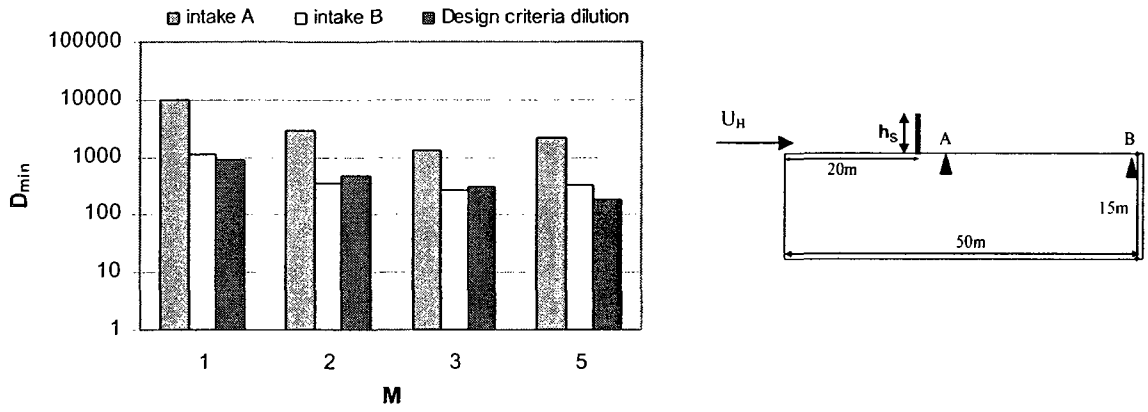

a) Flat-roof

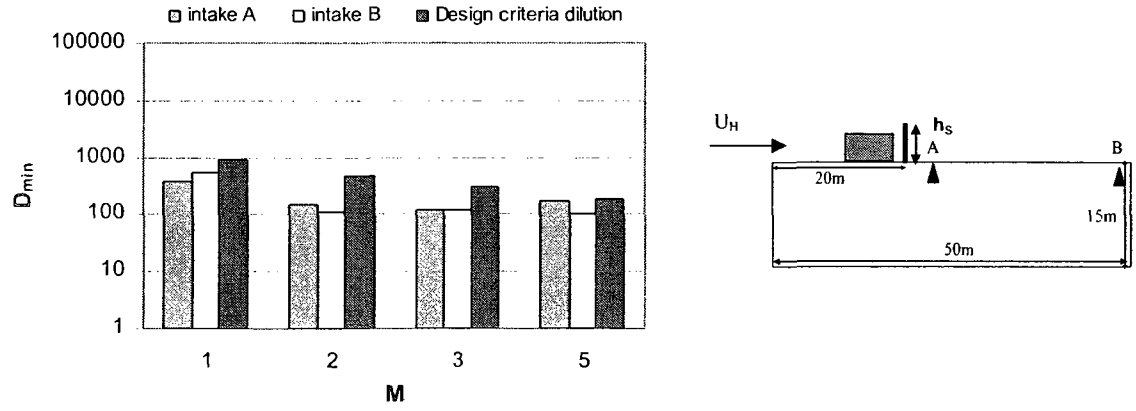

b) With RTS, w/h = 7.5

Figure 5.14 Measured dilutions for the low-rise building for AGM-estimated stack heights at intakes A and B: a) building with no RTS; and b) building with RTS.

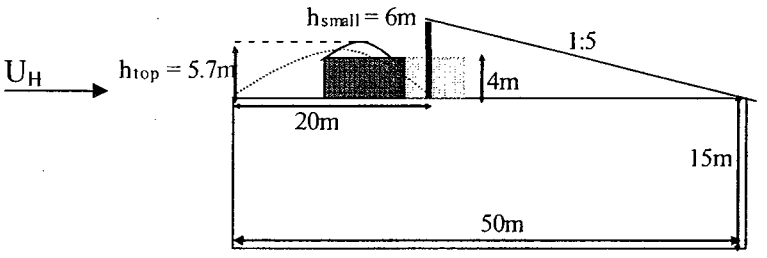

a) AGM

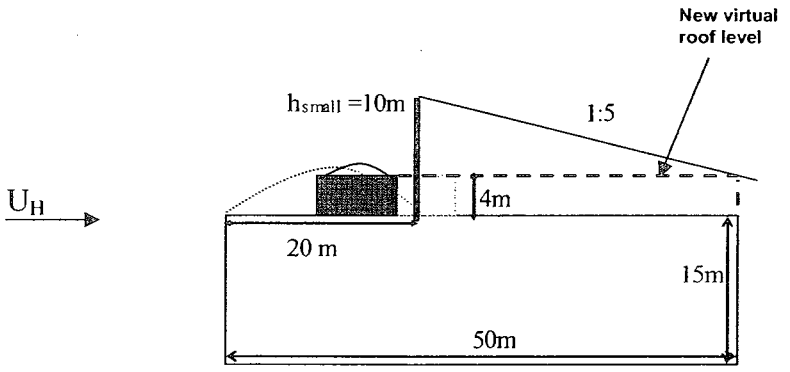

b) Modified AGM

Figure 5.15 Estimated h_{small} for the low-rise building with the RTS: a) with AGM; and b) with modified AGM.

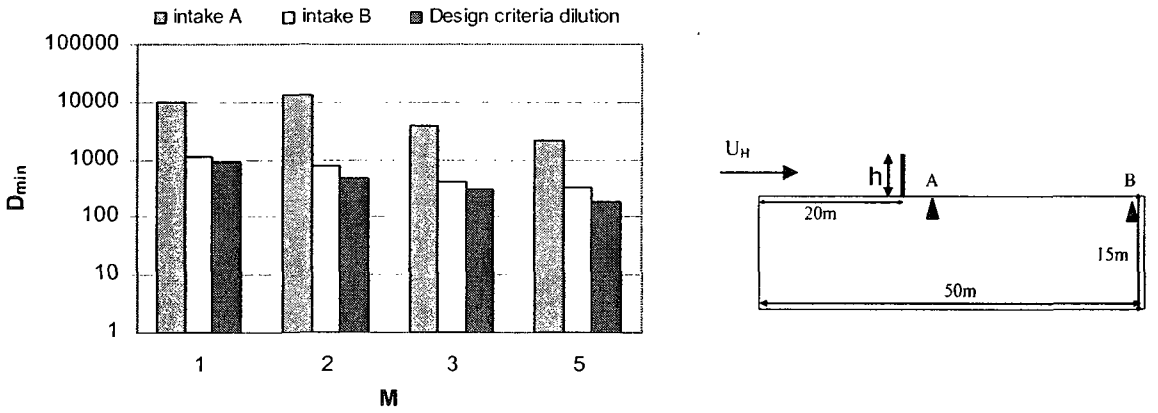

a) flat-roof

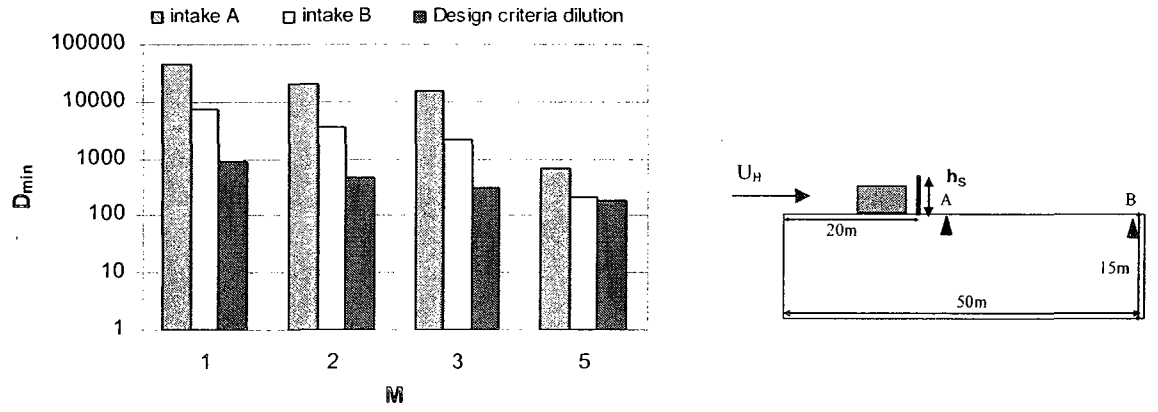

b) With RTS, w/h = 7.5

Figure 5.16 Measured dilutions for the low-rise building with modified AGM-estimated stack heights at intakes A and B: a) building with no RTS; and b) building with RTS.

Chapter 6

PROPOSED MICRO-SCALE DISPERSION MODEL: DEVELOPMENT AND EVALUATION

6.1 Introduction

Chapter 5 demonstrated the performance of ASHRAE (2003) and ASHRAE (2007) dispersion models for different building/RTS configurations. In general, for the low-rise buildings with and without RTS, the ASHRAE (2003) D_r model was unconservative and the ASHRAE (2007) D_r model was overly conservative for all cases evaluated. The ASHRAE (2003, 2007) D_s model was always excessively conservative, irrespective of whether or not an RTS was present. A few modifications to the ASHRAE dispersion models suggested in Chapter 5 improved dilution estimations in all cases. However, even with the proposed modifications, the ASHRAE models are not that accurate and require a good level of understanding of the flow around buildings in order to use them properly.

The objective of this chapter is to propose an empirical plume dispersion model that requires minimum experience to apply and provide more accurate dilution estimations than the ASHRAE minimum dilution models. The proposed model is applicable for exhaust sources on flat-roofed buildings and also takes into consideration the downwash effect of an RTS. As with previous minimum dilution models, it is a micro-scale model applicable at distances within 100 m from the stack. The assumptions,

methodology, and validation of the proposed dispersion model are presented in this chapter.

6.2 Model development

The proposed dispersion model is a modified form of the Wilson and Lamb (1994) minimum dilution model, hereafter referred to as the WL model. The WL model was chosen for its simplicity and ease of use, and was the basis of the earlier ASHRAE (1999) minimum dilution model. Details of this model have been discussed in Chapter 2.

Although the WL model was developed for flush stacks ($h_s = 0$) and for flat-roofed buildings, the new model takes into account the effect of building height, stack height, and the downwash effect of an RTS, but does not take into consideration the effect of wind direction. However, it does predict dilutions for the worst-case scenarios: normal wind direction for flat-roofed buildings and oblique wind for buildings with RTS.

6.2.1 The proposed dispersion model

To incorporate the effect of stack height and the downwash effect of an RTS, a plume height factor D_h, is introduced in the WL minimum dilution model. The expression for D_h is derived from the classical Gaussian plume dispersion model presented earlier in Chapters 2 and 3. The following discussion will show how D_h is derived.

Using the Gaussian model for a stack of height hs, the minimum dilution at the roof level along the plume centerline is:

$$D_{min} = \frac{U_H \pi \sigma_y \sigma_z}{Q} \left\{ \exp\left[\frac{(h_s + \Delta h)^2}{2\sigma_z^2} \right] \right\} \qquad \text{[Eq 6.1]}$$

where U_H is the wind speed at the building height, Q is the exhaust flow rate, and σ_y and σ_z are the plume spreads in the horizontal and vertical directions. The parameter Δh is the effective plume rise ($h_r - h_d$), where h_r is the momentum plume rise given by Eq 2.7 and h_d is the stack downwash given by Eq 2.8. From Eq 2.6, the plume height h_p is defined as, $h_p = h_s + \Delta h$

Replacing $h_s + \Delta h$ with h_p in Eq 6.1 gives:

$$D_{min} = \frac{U_H \pi \sigma_y \sigma_z}{Q} \left\{ \exp\left[\frac{(h_p)^2}{2\sigma_z^2} \right] \right\} \qquad \text{[Eq 6.2]}$$

Dilutions obtained with Eq 6.3 can be compared to the baseline values for a flush stack ($h_s = 0$) given by:

$$D(h_s = 0) = \frac{U_H \pi \sigma_y \sigma_z}{Q} \left\{ \exp\left[\frac{(\Delta h)^2}{2\sigma_z^2} \right] \right\} \qquad \text{[Eq 6.3]}$$

Dividing equation 6.1 with equation 6.3 gives:

$$D_{min} = D(h_s = 0) \left\{ \exp\left[\frac{(h_p{}^2 - \Delta h^2)}{2\sigma_z^2} \right] \right\} \qquad \text{[Eq 6.4]}$$

It is reasoned that the effect of the plume height can be included by multiplying the dilution for flush stacks by a factor that takes into account h_s and the potential downwash effect of RTS.

Theoretically, the expression $\left\{\exp\left[\frac{\left(h_p{}^2 - \Delta h^2\right)}{2\sigma_z^2}\right]\right\}$ in Eq 6.4 takes into account the enhanced dilution due to a non-zero stack height and plume rise for an isolated stack. However, the rooftop recirculation zone and the presence of an RTS may significantly change the plume rise and plume spread values. These changes to the plume are not considered in the classical Gaussian model. Therefore, for the proposed model, a modified form of the expression $\left\{\exp\left[\frac{\left(h_p{}^2 - \Delta h^2\right)}{2\sigma_z^2}\right]\right\}$ is assumed as the plume height factor D_h, and is given by the following expression.

$$D_h = \left\{\exp\left[\omega\frac{\left(h_p{}^2\right)}{2\sigma_z^2}\right]\right\} \qquad \text{[Eq 6.5]}$$

A new parameter 'ω' is introduced which is named as the 'adjustment factor'. This parameter accounts for the effect of the building and downwash effect of an RTS on plume height. With this new parameter, the proposed model is given by the following expression:

$$D_{min} = (D_{min})_{WL} * D_h \qquad \text{[Eq 6.6]}$$

where,

$$(D_{min})_{WL} = (D_o^{0.5} + D_d^{0.5})^2 \qquad \text{Eq 2.15]}$$

The parameters D_o and D_d are the initial dilution and distance dilution and M is the exhaust momentum ratio. The initial dilution factor D_o is proportional to M and is given by,

$$D_o = 1 + 13\beta M \qquad \text{[Eq 2.16]}$$

The parameter, β, is the stack-capping factor and is set equal to 1.0 for uncapped stacks and 0 for capped stacks.

The distance dilution factor D_d is associated with atmospheric and building turbulence and is given by:

$$D_d = B_1 S^2 / MA_e \qquad \text{[Eq 2.17]}$$

where B_1 is the distance dilution parameter.

Based on the dilution data obtained in a field study [Wilson and Lamb (1994)] and a wind tunnel study [Wilson and Chui (1987)], it was shown that B1 was strongly affected by the level of atmospheric turbulence in the approaching flow. To incorporate the effect of upstream turbulence, B1 was defined in ASHRAE (1999) as:

$$B_1 = 0.027 + 0.0021\sigma_\theta \qquad \text{[Eq 2.18]}$$

where σ_θ is the standard deviation of wind direction fluctuations in degrees. The model assumes that distance dilution has two components: the dilution due to building-generated turbulence and that due to atmospheric turbulence. For an urban environment, ASHRAE (1999) recommends a typical value of σ_θ =15°, which yields B1 = 0.027 + 0.032 = 0.059. Thus, more than 50% of D_d is assumed to be due to upstream turbulence.

ASHRAE (1999) also assumes that for buildings where the effect of atmospheric turbulence is low, building surface concentrations could be 5 to 10 times higher than that obtained with high atmospheric turbulence. For such cases, atmospheric turbulence B1 should be reduced to 0.027. This is generally the case for high-rise buildings where the rooftop stack is engulfed in the building roof recirculation zone and for low-rise buildings with stacks influenced by the downwash effect of an RTS. Therefore, in the proposed model, B1 = 0.059 for the flat-roofed low-rise building. However, for the high-rise building and the low-rise building with the RTS, B1 = 0.027.

The proposed minimum dilution model is obtained by substituting Eq 6.5 in Eq 6.6 and is given by the following expression:

$$D_{min} = (D_o^{0.5} + D_d^{0.5})^2 \left\{ \exp\left[\omega \frac{\left(h_p^2\right)}{2\sigma_z^2} \right] \right\} \qquad \text{[Eq 6.7]}$$

The expression for D_{min} can be rewritten in the form of normalized minimum dilution, D_N as,

$$D_N = (D_o^{0.5} + D_d^{0.5})^2 \frac{Q}{U_H H^2} \left\{ \exp\left[\omega \frac{\left(h_p^2\right)}{2\sigma_z^2} \right] \right\} \qquad \text{[Eq 6.8]}$$

The vertical plume spread σ_z in the classical Gaussian model is a function of atmospheric stability as discussed in Section 3.4.3. The curves developed by Pasquill and Gifford (PG) give σ_z values as a function of downwind distance, x, for six classes of stability from very unstable (A) to moderately stable (F). The PG curves are applicable

for x > 100 m and therefore cannot be used for building-scale dispersion. Furthermore, atmospheric stability is not a crucial factor for rooftop stacks since the worst-case scenario is generally associated with moderate to strong winds (i.e. neutral conditions).

Wilson et al. (1998) provided a modified equation to estimate σ_z, for exhausts released from building roofs. A simplified form of the Wilson et al. (1998) vertical plume spread equation (Eq 2.10) was adopted by ASHRAE (2003) and ASHRAE (2007) minimum dilution models and is used in the proposed model.

$$\frac{\sigma_z}{d_e} = 0.071\frac{x}{d_e} + \frac{\sigma_o}{d_e} \qquad \text{[Eq 2.10]}$$

where σ_o is the initial source size that accounts for stack diameter d_e and for dilution due to jet entrainment during plume rise.

$$\frac{\sigma_o}{d_e} = \left[0.125\beta\frac{w_e}{U_H} + 0.911\beta\left(\frac{w_e}{U_H}\right)^2 + 0.250\right]^{.5} \qquad \text{[Eq 2.11]}$$

Another important modification in the proposed model deals with the way plume rise is estimated. The proposed model uses the extended Briggs (1984) plume rise equations (Eq 5.3) in lieu of the simplified Briggs equation (Eq 2.7). This modification adds some level of complexity to the proposed model compared to the current ASHRAE models. However, as shown previously in Chapter 5, the plume rise estimated with the extended Briggs (1984) equations is more accurate than that estimated with the simplified version of Briggs (1984) equation. Therefore, for better accuracy, the extended equations were adopted for the proposed model.

6.2.2 Determining adjustment factor (ω)

The parameter ω in the proposed model is defined as an adjustment factor applied to the plume height based on the building/stack/RTS configuration. By definition, ω can vary between 0 and 1. When ω is zero, $h_p = 0$. On the other hand, when ω is 1, the plume reaches maximum plume height, as estimated by the Briggs (1984) empirical formulations. In the present study, the ω values are determined by minimizing the root-mean-square error (RMSE) between the predicted and measured D_N values for the different building/RTS configurations and combinations of M and h_s. The predicted D_N values from the proposed model were obtained using Eq 6.8. Microsoft Excel solver was used to determine the value of ω that minimizes RMSE.

Figures 6.1a and 6.1b show examples of the curve fitting process for the low-rise building with and without the RTS. Results are shown for $h_s = 0.75h$ (h = 4 m) and M = 2 and are presented for the worst-case scenarios. For the flat-roofed building, $\theta = 0^\circ$ produces lowest dilutions and for the building with an RTS, the worst-case occurs for $\theta = 45^\circ$. For the flat roofed building, the adjustment factor (ω) is set equal to 0.78 to fit the measured data. For the building with an RTS, ω = 0.23. The lower ω value for the building with the RTS indicates that the plume height was significantly smaller compared to the flat-roofed building. Further details are presented in later sections.

Note that in the proposed model, estimated D_N values vary exponentially with plume height. Therefore, depending on stack height and exhaust momentum ratio values, a small change in ω could produce significant variation in the predicted dilutions. Thus,

it's important to understand the sensitivity of estimated D_N values for a range of ω values and plume height.

Figure 6.2 demonstrates the effect of ω values on D_N for different stack heights for a typical flat-roofed low-rise building. The trends are shown for three stack heights, h_s values 1 m, 3 m, and 5 m with M = 2 and ω ranging from 0 to 1 using Eq 6.8. The results clearly indicate that the effect of ω on D_N values vary significantly with stack height, especially for x < 15 m. As shown in Figure 6.2a, for the short stack (h_s = 1 m), increasing ω from 0 to 1 causes D_N to increase by a factor of about 10 close to the stack. However for h_s = 3 m, an increase from 0 to 1 in ω increased D_N values by a factor of 100 at some locations (see Figure 6.2b). For short stacks, the plume height is smaller than that for tall stacks. Consequently, for short stacks, the estimated D_N values are not that dependent on the exponential component in the proposed model. With further increase in stack height, the effect of ω on D_N values increased significantly close to the stack. As shown in Figure 6.2c, for a tall stack (h_s = 5 m) increasing ω from 0 to 1 causes D_N to increase by several orders of magnitude close to the stack. This occurs because the exponent $\exp(\omega h_p^2/2\sigma_z^2)$ in Eq 6.8 becomes very large at samplers located close to the stack, especially for the tall stack.

It is also important that the proposed model corresponds to the worst-case exhaust design scenarios. For practical stack design, only moderate to strong winds are critical since these will produce minimum dilution values at the building roof level. Although the experiments were conducted for M values ranging from M = 1 to M = 5, design M values will generally range between 1 and 3, which corresponds to strong wind conditions for which plume rise is relatively small.

It is also worth noting that the American Industrial Hygiene Association (AIHA)/American National Standards Institute (AIHA) Z9.5 (2002) standard recommends that building rooftop stacks should extend at least 3 m above the local roof (or above any nearby obstructions) to prevent rooftop workers from being directly exposed to the plumes discharged from the stack. In general, the minimum preferred design stack height is 3 m.

The proposed model is intended for stack design purposes. Therefore, it was developed using measured data obtained for the recommended design M and h_s values: M $\leq$ 3 and $h_s \geq$ 3 m (0.75h).

The ω values were determined for the low-rise building (H = 15 m) with and without an RTS and the high-rise building (H = 60 m) for all combinations of M (1, 2, and 3) and h_s (3 m, 5 m, and 7 m). To model the worst-case scenario for the building with the RTS, dilution data obtained with the minimum stack-RTS separation distance, x_s = 0.5h, were used to obtain ω values. Further details are provided in the following subsections.

6.2.2.1 Low-rise building with no RTS

The results presented in Chapter 4 demonstrated that for the flat-roofed building with the stack located outside the separation bubble whose dimensions were estimated by AGM, the lowest D_N values occur for winds approaching normal to a building face (θ = 0°). For oblique winds (θ = 45°), the D_N values were on an average 3–10 times higher than those obtained for θ = 0°. For the purpose of stack design, only the worst-case

results are important. Therefore, for the flat-roofed building, ω was determined only for $\theta = 0°$.

For tall stacks ($h_s \geq 5$ m) and low M value (M = 1), the proposed model predicts extremely high D_N values close to the stack, as shown in Figure 6.2c. This occurs because near the stack ($x < 2.5h$), vertical plume spread is small and plume height is large, which causes the exponential term $\exp(\omega h_p^2/2\sigma_z^2)$ in Eq 6.8 to predict extremely high D_N values near the stack. ASHRAE (2007) faces a similar limitation with the D_r model, especially for tall stacks. As a result, ASHRAE (2007) recommends limiting the contribution of plume height near the stack by limiting the ratio $\xi^2/2\sigma_z^2$ to a maximum value of 7, as discussed previously in Chapter 5. The same concept is applied for the proposed model. Figure 6.3 shows the predicted and measured D_N values for the flat-roofed building for M = 1 and h_s = 7 m (1.75h) for $\omega = 0.7$. The predicted D_N trends are shown with and without limiting $\omega h_p^2/2\sigma_z^2$ to a maximum value of 7. Note that with actual values for $\omega h_p^2/2\sigma_z^2$, the predicted D_N values for $x < 2.5h$ are extremely high compared to the measured D_N values. However, with $\omega h_p^2/2\sigma_z^2$ limited to a maximum value of 7, the accuracy of the proposed model improved significantly. Therefore, in the proposed model the ratio $\omega h_p^2/2\sigma_z^2$ is not allowed to have a value greater than 7.

Figure 6.4 shows the variation of ω with M for different h_s. In general, the ω values varied between 0.65 and 0.80. To determine a value of ω that could represent most of the data set, the measured and predicted D_N values were compared for different values of ω. Figure 6.5 shows the scatter plots of measured versus predicted D_N values for h_s = 0.75h to 1.75h and for ω values ranging from 0.65 to 0.9. To see the extent of scatter,

trends representing five ratios - 0.25, 0.5, 1, 2, and 4 - of measured to estimated D_N values are also presented. The data for each stack height corresponds to M values of 1, 2 and 3. To judge the accuracy of the proposed model with respect to the measured values, the normalized RMSE (N-RMSE) values are also presented for all ω values. The N-RMSE values were obtained with the following expression:

$$\text{N-RMSE} = \frac{\sqrt{\sum_{i}^{n}(1-\frac{P_i}{ME_i})^2}}{n} \qquad \text{[Eq 6.9]}$$

where P_i and ME_i are the predicted and measured D_N value, respectively. The subscript i represents the sample number and n represents the total number of sampling points.

In Figure 6.5, the predicted data generally show good agreement with the measured data for $\omega < 0.75$. For these ω values, more than 80% of the predicted values are within a factor of two of the measured values with majority of data points within a reasonably conservative range. However, the N-RMSE value is the lowest for $\omega = 0.70$ (see Figure 6.5b). Thus, for simplicity, better accuracy, and to have reasonable level of conservatism (within a factor of 2) in the proposed model, ω is assumed to have a constant value of 0.70 for the low-rise building with no RTS.

6.2.2.2 Low-rise building with RTS

The results presented in Chapter 4 demonstrated that for the low-rise building with an RTS upwind of the stack, the minimum D_N values obtained for $\theta = 45°$ were lower than those obtained for $\theta = 0°$. The D_N values also varied with the cross-wind width

of the RTS and separation distance between the RTS and the stack. As a representative worst-case scenario, ω is estimated for $\theta = 45°$, w/h = 7.5, and $x_s = 0.5h$.

Figure 6.6 shows the variation of ω with M for different h_s values for the low-rise building with an RTS. In general, the ω values increased with increase in M values. The effect of increase in h_s on ω values was not that significant. The minimum and maximum values of ω varied from 0.18 to 0.42, which are significantly lower than the ω values found for the flat-roofed low rise building. A lower value of ω indicates a higher reduction applied to plume height as would be expected for the stacks affected by the downwash effect of the RTS.

Similar to the flat-roof configuration, to determine a value of ω that could represent most of the data set for the building with the RTS, the measured and predicted D_N values were compared for a range of ω values. Figure 6.7 shows the scatter plots of measured versus predicted D_N values for $h_s = 0.75h$ to 1.75h and for $\omega = 0.15$, 0.2, 0.25, 0.30 and 0.35. To see the extent of scatter, trends representing five ratios - 0.25, 0.5, 1, 2, and 4 - of predicted to estimated D_N values are also presented.

The results indicate that a single ω value may not represent the entire data. For example, for $\omega = 0.20$, the accuracy of predicted values which correspond to $h_s \leq 1.25h$ is relatively higher than those for $h_s = 1.75h$ - see Figure 6.7b. On the other hand, for $\omega >$ 0.30, the accuracy of the model increases for $h_s = 1.75h$, whereas the accuracy decreases for $h_s \leq 1.25h$, see Figures 6.7d and 6.7e. Thus, ω values were determined for $h_s \leq 1.25h$ and $h_s = 1.75h$.

Figure 6.8 shows similar scatter plots with data limited to h_s = 0.75h and 1.25h. The N-RMSE values are also shown. Since the N-RMSE value is lowest for ω = 0.20 (see Figure 6.8b), ω is assumed to have a constant value of 0.20 for the low-rise building with an RTS for $h_s \leq 1.25h$.

Figure 6.9 shows the scatter plots of measured versus predicted D_N values for h_s = 1.75h and for ω = 0.2, 0.25, 0.30, 0.35 and 0.4. Note that the correlation between the predicted and measured D_N values for h_s = 1.75h improved significantly for ω = 0.30. However, the majority of estimated values are on the conservative side - within a factor of four of the measured values. A higher ω value for the taller stack indicates that the downwash effect of the RTS on the plume was less than that for the shorter stacks. Since the N-RMSE value is lowest for ω = 0.30 (see Figure 6.9c), ω is assumed to have a constant value of 0.30 for the low-rise building an RTS for $h_s > 1.5h$.

It was demonstrated in Chapter 4 that the downwash effect of an RTS nearly vanished for very tall stacks ($h_s > 2.5h$) and large stack-RTS separation distance ($x_s > 2h$). Therefore, for $h_s > 2.5h$ and $x_s > 2h$, the effect of RTS is assumed to be negligible and the flat-roofed low-rise building case (ω = 0.7) is applicable. Note that the present study data is limited to one building height. However, the findings are also expected to be similar for other low-rise buildings where an RTS will see the flow over the building roof. As indicated previously in section 3.4.1, the results are expected to be generally applicable for majority buildings with height less than 30 m and W/H > 1.

In summary, for a typical low- to medium-rise building (H < 30 m and W/H > 1) with an RTS with height h, ω values are defined as:

(i) $\omega = 0.20$ for $h_s \leq 1.5h$

(ii) $\omega = 0.30$ for $1.5h < h_s \leq 2.5h$

(iii) $\omega = 0.70$ for $h_s > 2.5h$

Note that in the proposed model, there is a large discontinuity in the ω value for $h_s > 2.5h$. This can be explained on the basis of the re-circulation bubble formed by winds flowing over the building roof. Figure 6.10 shows the formation of the separation bubble and its effect on exhaust plumes from stacks discharging inside and outside the bubble. A plume released inside the bubble becomes trapped and undergoes limited dispersion resulting in a lower plume rise and greater re-entrainment at the rooftop intakes. On the other hand, when the stack tip is above the bubble, plume rise is relatively unaffected. Therefore, the plume will disperse more effectively in the atmosphere, away from the building roof. Note that a plume released further downwind of the RTS will escape the building/RTS effects.

6.2.2.3 High-rise building

The minimum D_N values obtained for the high-rise building generally occurred for $\theta = 0°$ irrespective of whether or not the RTS was present. Therefore, for the high-rise building, ω values are estimated for $\theta = 0°$.

Figure 6.11 shows the variation of ω with M for different h_s values for the high-rise building. For this case a 13 m high separation bubble is formed on the roof of the building. Thus, even for the maximum M and h_s values (M = 3 and $h_s = 1.75h$), the plume

is entrained in the building roof recirculation zone. As a result, the ω values depend only slightly on h_s and M. The minimum and maximum values of ω varied from 0.15 to 0.30.

As with previous building configurations, the value of ω was optimized using scatter plots of measured and predicted D_N values. Figure 6.12 shows the scatter plots of measured versus predicted D_N values for ω = 0.10, 0.15, 0.20, 0.25, and 0.3. To see the extent of scatter, trends representing five ratios - 0.25, 0.5, 1, 2, and 4 - of predicted to estimated D_N values are also presented. The N-RMSE values are also shown. Although, the N-RMSE value of 0.70 is lowest for ω = 0.15 (see Figure 6.8b), it was found that proposed model could predict more accurate dilutions with ω = 0.20 (see Figure 6.8c) with the exception of one data point (highlighted). The N-RMSE value for ω = 0.20 was 0.63, if this point is not considered.

Note that for high-rise buildings, the large rooftop separation bubble may cause the plume to undergo significant mixing. This causes limited plume rise and large lateral plume spread. Reduced plume height will decrease the D_N values at the building roof surface. However, a wide plume will produce higher D_N values than a narrow plume. The ω value in the proposed model takes into consideration only the reduction in plume rise. The lateral plume spread is not modeled. Plume spread increases with distance from the stack. Consequently, for some cases, D_N values are towards the conservative side, especially at distances farther from the stack. However, the level of conservatism is significantly lower than the ASHRAE (2007) D_s model, which totally ignores plume rise and does not consider the effect of separation bubble on the lateral plume spread. Consequently, D_N values estimated by ASHRAE D_s model can be about 10 - 50 times lower than the measured values (see Figure 5.10).

For simplicity and to have a reasonable level of conservatism in the proposed model, ω is assumed to have a constant value of 0.20 for the high-rise buildings. Note that in all the tests with the high-rise building, $h_s < h_{top}$, where h_{top} is defined as the height of the tallest obstruction or the separation bubble formed on the building roof. Given this, the ω value of 0.20 is valid for $h_s < h_{top}$.

Note that there is a large discontinuity in ω value for $h_s \geq h_{top}$. Thompson et al. (2002) showed that for high-rise buildings with stacks taller than the separation bubble, the effect of the bubble on the plume is negligible. Consequently, for $h_s > h_{top}$, the exhaust plume is emitted above the bubble and will see greater plume rise compared to a plume discharged within the bubble. Thus, significantly higher dilutions are expected to occur for $h_s > h_{top}$. For this case, a ω value of 0.7 is recommended. The above findings are assumed to be applicable for majority of tall buildings with $H > 30$ m and $W/H < 1$.

6.2.2.4 Summary

The variation of N-RMSE values with ω values for different building/RTS configurations discussed in the previous section are shown in Figure 6.13. The ω values that give minimum N-RMSE values for different configurations building with and without RTS are also highlighted. Note that the ω values for the low-rise building with RTS (h_s = 0.75h and 1.25h) and the high-rise building are relatively similar. Therefore, for different building/RTS configurations, ω values are classified as:

1) For a typical low- to medium-rise flat-roofed building and stack located outside the separation bubble (estimated by AGM), $\omega = 0.7$

2) For a typical low-rise building with an RTS with height h and $x_s < 2.5h$:

$\omega = 0.20$ for $h_s \leq 1.5h$

$\omega = 0.30$ for $1.5h < h_s \leq 2.5h$

$\omega = 0.70$ for $h_s > 2.5h$ and all x_s

3) For a typical high-rise building - irrespective of RTS or stack location on the roof:

$\omega = 0.20$ for $h_s \leq h_{top}$

$\omega = 0.70$ for $h_s > h_{top}$

The above proposed recommendations are summarized in Table 6.1.

Results obtained with the proposed dispersion model are compared with the present study wind tunnel results in Figure 6.14. The results are shown for the low-rise building, with and without an RTS and the high-rise building for M = 2 and $h_s = 0.75h$ to 1.75h. As expected, the model predictions are generally conservative compared to the measured data. For the high-rise building, Figure 6.14c, the model estimates are significantly conservative. As mentioned previously, the proposed model does not take into consideration the enhanced lateral plume spread caused by the separation bubble. Consequently, for the high-rise building case, the predicted D_N values were significantly conservative especially at receptors located far from the stack ($x > 4h$).

6.3 Model validation

The proposed model was validated using data obtained in previous studies. These include wind tunnel, water flume and field studies conducted on low-rise and high-rise buildings. The validations will be presented for the recommended stack design M and h_s values, $M \leq 3$ and $h_s \geq 0.75h$ for which the model is developed.

Even though the proposed model is developed to estimate dilutions for recommended M and h_s values: $M \leq 3$ and $h_s \geq 0.75h$, the proposed model still predicts reasonably conservative estimates for M and h_s values other than the recommended design values. This would be expected because the proposed model has some built-in conservatism and is developed considering worst-case design conditions. In addition, the model also takes into consideration the effect of building height, M and h_s. Proposed model validations with data from previous studies for seventeen different cases with $M > 3$ and $h_s < 0.75h$ are presented in Appendix F.

6.3.1 Model validation for buildings with no RTS

The proposed model predictions for the flat-roofed low-rise buildings were evaluated using dispersion data sets obtained by Schulman and Scire (1991), Wilson et al. (1998), and Stathopoulos et al. (2003). The following subsections will demonstrate the model performance for these studies.

6.3.1.1 Model evaluation with dispersion data from Schulman and Scire (1991)

Schulman and Scire (1991) conducted wind tunnel experiments to investigate the effect of stack height and exhaust momentum on dispersion of exhausts from a rooftop

stack. Tracer gas was released from a stack located at the center of the roof of a 15 m tall building for normal ($\theta = 0°$) and oblique ($\theta = 45°$) wind directions. The building had a square plan, with side dimension of 75 m. Plume centerline concentrations were obtained on the building roof, leeward wall and ground level for h_s varying from 0 to 7.5 m and for M values ranging from 0.75 to 5.

Schulman and Scire (1991) presented the results in the form of normalized concentration (k*), defined as:

$$k^* = C\, U_H/Q \qquad \text{[Eq 6.10]}$$

$$\text{and } C = c/C_e \qquad \text{[Eq 6.11]}$$

where c is the concentration measured at the receptor with the exhaust concentration C_e, and U_H is the mean wind speed at the building height, H. To evaluate the proposed model, k values obtained from Schulman and Scire (1991) are converted to normalized dilution (D_N), as shown below.

$$D_N = D_{min}Q/(U_H H^2) \qquad \text{[Eq 3.9]}$$

where $D_{min} = C_e/c = 1/C$

Substituting Q from Eq 6.10 in the Eq 3.9 gives,

$$D_N = D_{min}(CU_H/\,k)/(U_H H^2) = 1/(H^2 k) \qquad \text{[Eq 6.12]}$$

The proposed model is evaluated with the roof level D_N values for two stack heights (h_s = 4.5 m and 7.5 m) and two M values (M = 1.5 and 3) for $\theta = 0°$. The experimental parameters for Schulman and Scire (1991) are presented in Table 6.2. The

estimated height and length of the separation bubble formed at the building leading edge are 5.6 m and 23 m, respectively. The stack was located at the center of the roof, about 37.5 m from the building leading edge. Therefore, the stack tip was located outside the separation bubble. Therefore, the value of ω was set at 0.7 (see Table 6.1) corresponding to the test case - low-rise flat-roofed building with stack located outside the separation bubble.

Figures 6.15, and 6.16 show the comparison between the D_N values obtained from Schulman and Scire (1991) and the proposed model estimates for h_s = 4.5 m and 7.5 m. For each stack height, results are presented for M = 1.5 and 3. ASHRAE (2007) D_r model predictions are also shown. Note that the D_N trends predicted by the proposed model for all cases are similar to the measured values. This indicates the effectiveness of the proposed model to predict dilutions for different h_s and M values. In general, the proposed model appears to be reasonably conservative. D_N values are generally within a factor of 2 to 3 of the measured values. The results also indicate that the ASHRAE (2007) D_r model predictions were overly conservative for all cases examined. In general, D_N values are about 10-100 times lower compared to the measured data. Validations for other combinations of h_s and M are presented in Appendix F.

The main reason for such a large difference between the measured values and ASHRAE predicted dilutions is the penalty applied to the plume height when calculating the vertical separation factor (ξ). Based on the height of the tallest recirculation zone ($h_{top,}$) the ASHRAE (2007) model applies a reduction to the plume height (h_p), which causes a significant drop in the dilution values. This is more apparent for low M values, which generate low plume height. Figure 6.15a represents D_N values for M = 1.5 and h_s =

4.5 m. In this case, the h_{top} and h_p values are estimated using Equations 2.19 to 2.24. The estimated value of h_{top} = 5.6 m and h_p = 7.9 m. Therefore, for this case, vertical separation factor ξ (h_p - h_{top}) is 2.3 m. Note that the plume height used by the D_r model is by about 3.5 times smaller than the estimated value. Consequently, the D_r model predicts significantly lower D_N values than the measured data. Note that for M = 3, the ξ values will be greater than that for M = 1.5. However, the penalty applied to the plume height still causes the ASHRAE model to limit the plume height contribution, which produces D_N values lower than the measured data even for greater M and/or h_s values.

6.3.1.2 Model evaluation with dispersion data from Wilson et al. (1998)

Wilson et al. (1998) conducted extensive measurements in a water flume to evaluate the dispersion of exhaust from a stack located on the roof of a low-rise flat-roofed building. The dilutions were measured on the roof of a 12 m high building located in a suburban exposure. The experiments were conducted for h_s = 2.1 m, 3 m, and 6 m and M values ranging from 1 to 8. All measurements were obtained for the flow normal to the upwind face of the test building. A fluorescent dye was used to simulate the exhaust, which was illuminated by thin laser light sheets. Digital video images were used to measure dilution distributions for different building configurations.

The proposed model is evaluated with the roof level D_N values for two stack heights (h_s = 3 m, and 6 m) for θ = 0°. For each stack height, validation was conducted for two M values (M = 1.5 and 3). The experimental parameters for the tests used to evaluate the proposed model are presented in Table 6.3. These tests were selected because they were conducted with an isolated building with stack outside the separation

bubble. Note that an ω value of 0.7 is applicable (see Table 6.1) for the cases examined, since the stack is located on the roof of a flat-roofed low-rise building outside the separation bubble.

Figures 6.17 and 6.18 show the comparison between the estimated and measured D_N values for stack heights 3 m and 6 m. For h_s = 3 m, the stack was located at a distance of 0.6L from the building leading edge and for h_s = 6 m the stack was located at 0.2L from the leading edge. Results are presented for M = 1 and M = 3. ASHRAE (2007) D_r model estimates are also presented. Note that for stack height 3 m, the D_N profiles obtained from the proposed model are similar to the measured data. The predicted values are within a factor of 2 except at samplers located close to the stack. For h_s = 6 m, (see Figure 6.18), the model overestimated the measured dilutions close to the stack. The predicted values were at least 10 times higher than the measured values for x < 10 m. These discrepancies may be due to the experimental setup used by Wilson et al. (1998). For a tall stack, the dilution should increase as x approaches to zero. However, the Wilson data show the opposite trend, the reason for which is unclear. Results obtained by other researchers [e.g. Schulman and Scire (1991)] indicate that for tall stacks, the dilutions decrease as x decreases (see Figures 6.15 and 6.16). Concentrations were obtained by quantifying the brightness of the video images of the dispersion of dye in a water flume while most often researchers have used tracer gas measurements to evaluate plume dispersion. The data obtained by Wilson et al. (1998) suggest that video analysis technique may produce errors near the stack. Validations for other combinations of h_s and M are presented in Appendix F.

Dilution estimates obtained with the ASHRAE (2007) D_r model were significantly below the measured data. Similar to the previous cases presented, the level for conservatism decreased with increase in M and/or h_s values.

6.3.1.3 Model evaluation with dispersion data from Stathopoulos et al. (2003)

Stathopoulos et al. (2003) conducted 21 field tests to quantify the effect of h_s, wind direction, M, and stack location on dispersion of exhaust from a stack located on the roof of a low-rise building. Each test was carried out for 50 minutes. Thirteen tests were carried out for an open fetch with a suburban profile. However, the remaining field tests were carried out with the emitting building downwind of a tall building and are therefore not suitable for model validation. The stack and intake locations used for model validation are shown in Figure 6.19.

Although the building had a few RTS, the stack was not located downwind of the structures. Therefore, the RTS did not produce significant downwash for the wind directions tested. Majority of the field tests were carried out with h_s = 1 m. One open fetch field test datasets with h_s = 3 m listed in Table 6.4 was used to validate the proposed model. This test was considered suitable for model validation because the wind direction was nearly perpendicular to the building leading edge. Other tests carried out with h_s = 3 m used similar parameters to the one used for validation. Validations for other combinations of h_s and M are presented in Appendix F.

It is worth noting that many samplers in the field tests were located away from the plume centerline. Therefore, the proposed minimum dilution model should produce a lower bound on the data obtained in the field test.

During the 50-minute field test the exhaust gas (SF_6) was released from the stack. Ten 5-minute samples were collected at 15 different locations on the building roof. The wind direction and wind speed data were recorded using a sonic or cup anemometer located on the test building roof (see Figure 6.19a). The wind direction and wind speed varied during each field test. Therefore, for the validation, only field data with relatively similar wind speed and wind direction were used. Note that the concentration data obtained from the field test were converted to D_N using Eq 3.9.

Figure 6.20 shows results obtained with a 3 m tall stack and M = 3 at the 15 rooftop samplers. The x value represents the shortest distance between the stack and receptor. Model D_N values were obtained with ω set at 0.7 (see Table 6.1). Since the stack is upwind of the RTS, the plume is not significantly affected by the downwash effect of the RTS. The dilutions estimated with the proposed model were reasonably conservative (within a factor of 2 of the field data). The model estimates are conservative at larger distances because some of the rooftop samples were not on the plume centerline.

Similar to other comparisons presented in the previous sections, the ASHRAE (2007) D_r model underestimated the dilutions by a factor of at least 10 for the different cases presented in Figures 6.15 and 6.18. The primary reason for the large discrepancy between the measured values and D_r model estimates is the penalty applied to the plume height.

6.3.2 Model validation for buildings with RTS

Model performance for RTS configurations was evaluated using field data obtained by Wilson and Lamb (1994) and Saathoff et al. (2002). Both studies were

conducted on University laboratory buildings and therefore represent realistic building exhaust dispersion scenarios. For both studies, the stack was located downwind of the RTS, making them ideal to evaluate the performance of the proposed model.

6.3.2.1 Model evaluation with dispersion data from Wilson and Lamb (1994)

Wilson and Lamb (1994) used field study data of Lamb and Cronn (1986) to develop the WL minimum dilution model that was later adopted by ASHRAE (1997). The field tests were carried out on a long rectangular building on the campus of Washington State University. The building shown in Figure 6.21a had several RTS. The surrounding buildings were of similar height with the exception of a 60 m building located on the south side of the test building. For the tested wind directions the tall adjacent building is assumed to have negligible impact on the results. The tracer gas (SF_6) was emitted from various stacks located on the roof of the test building. In most of the cases, four 1-hour samples were collected at various locations on the building roof and at ground level. Wind data were obtained at a height of 8 m above the penthouse on the east side of the building. Locations of the rooftop samplers are shown in Figure 6.21b.

For validation purpose, an averaging-time correction as suggested by ASHRAE (1997) has been applied to convert measured dilution from 1-hour mean values to 15-minute means. The effect of averaging time can be estimated by the 0.2 power law and is given by the following equation:

$$D_{min,1}/D_{min,2} = (t_{a1}/t_{a2})^{0.2} \qquad \text{[Eq 6.13]}$$

where dilutions $D_{min,1}$ and $D_{min,2}$ correspond to an averaging time of t_{a1} and t_{a2}, respectively. The above equation is valid for converting dilutions with averaging time ranging from 3 minutes up to 3 hours [ASHRAE (1997)].

Data obtained from Field Tests 1, 2, and 3 were used to validate the proposed model. For these tests, a 3.6 m tall stack was located adjacent to a 3.7 m tall RTS on the east side of the building. The wind direction was east-southeast for all tests. For this wind direction, the stack was significantly affected by the downwash caused due to the RTS. The experimental parameters for the tests examined are presented in Table 6.5. Note that the M values varied significantly in each of the tests. Note that the stack used to carry out Tests 6A and 7A (see Figure 6.21b) are also affected by the upstream RTS. However, due to lack of rooftop samplers downwind of the stack, the concentration data from these tests were not considered for model validation.

The receptors shown within the region highlighted in Figure 6.21b are located close to the RTS and therefore potentially most affected by the RTS downwash effect. Note that the data presented in Wilson and Lamb (1994) are not differentiated with respect to roof or ground level receptors. Therefore, to isolate data points affected by the RTS, data from samplers located more than 30 m from the stack have not been used for model validation. The stack was located within the downwind cavity of the RTS and was shorter than the height of the RTS. Thus, a ω value of 0.20 is applicable (see Table 6.1).

Figure 6.22 shows the comparisons between the field data and predicted values obtained with the proposed model and the ASHRAE (2007) D_r model. Wilson and Lamb (1994) reported the results in the form of minimum dilutions (D_{min}). Therefore, for model

validation the dilution values have been converted to D_N using Eq 3.9. The results are shown for M varying from 3 to 7.1. To capture the worst-case scenario, the lowest M value reported for each field test has been used to estimate dilution values with the proposed and ASHRAE (2007) models. In general, for the two cases presented, the proposed model estimates compare well with the lowest D_N values. However, for $x > 20$ m, the predicted values are significantly conservative, which is likely due to mixed ground- and roof-level data points.

The ASHRAE (2007) D_r model predictions are reasonably conservative compared to the worst-case scenario D_N values, primarily for $x < 20$ m. Even though the ASHRAE estimates are towards the conservative side for the building with the RTS, the level of conservatism is significantly lower than those for the flat-roofed building presented in previous sections.

Note that due to the downwash effect of the RTS, the D_N values are much lower than those for flat-roofed buildings. As shown in Chapter 4, the plume height could reduce up to 40% due to the downwash effect of the RTS. Therefore, the penalty applied to h_p in the ASHRAE (2007) D_r model is reasonable in this case. Consequently, the D_r model is reasonably conservative (by a factor of at least 2) for this case. For $x > 20$ m, the D_r model is overly conservative (by a factor of at least 5). However, this is likely due to mixed ground- and roof-level data points.

6.3.2.2 Model evaluation with dispersion data from Saathoff et al. (2002)

Saathoff et al. (2002) evaluated the downwash effect of an RTS on plume dispersion in a series of field experiments. Measurements were conducted on the roof of

the same building used by Stathopoulos et al. (2003) discussed previously in Section 6.2.1.3. Tracer gas (SF_6) was emitted from a 3.1 m tall stack with a diameter of 0.9 m. The stack was located approximately 1 m from an RTS that had a height of 2.2 m and crosswind width of 35 m (see Figure 6.23a). The samplers were placed on the building roof and penthouse roof as shown in Figure 6.23b. Three 150-minute tests were conducted when the stack was downwind of the RTS. During each field test, ten 15-minute samples were collected at each measurement location and the wind speed and wind direction were recorded with a sonic anemometer located 3 m above the RTS (see Figure 6.23b). Wind data varied significantly during each field test. Therefore, for each validation, the field data have been grouped into data sets with relatively similar wind speed and wind direction.

Saathoff et al. (2002) reported the results in the form of minimum dilution. In the present study, values of D_{min} have been converted to D_N using Eq 3.9. The dilution data obtained from two tests was used to validate the present model. The experimental parameters for Tests 1 and 2 are presented in Table 6.6. For these cases, $h_s < 1.5h$ and $x_s < 2.5h$, where $h = 2.2$ m. Therefore, $\omega = 0.2$ (see Table 6.1).

Figure 6.24 shows the variation of D_N with x for two field tests. Also shown are the predicted values obtained with the proposed model and the ASHRAE (2007) D_r model. In general, for the cases presented, the proposed model estimates compare well with the worst-case values.

The ASHRAE (2007) D_r model predictions were significantly conservative for M = 2 and M = 3 (see Figure 6.24). For M = 2, $\xi = 0$, since $h_p < h_{top}$. Consequently,

ASHRAE predicted D_N values are significantly lower than the measured data. As with the Wilson and Lamb (1994) results, the accuracy of ASHRAE (2007) D_r model improved with increase in M value. As discussed in the previous section, the improved performance of the ASHRAE model is due to the downwash effect of the RTS. In this case, the plume height penalty in ASHRAE is justified.

6.3.3 Model validation for a tall building: Stathopoulos et al. (1997)

Field data from Stathopoulos et al. (1997) have been used to validate the model for a moderately tall building. Stathopoulos et al. (1997) conducted four tests on the roof of a nearly cubical building 62 m tall located in an urban environment. The tests were conducted for a short stack (h_s = 0.5 m), located on the southwest side of the roof (see Figure 6.24). During each test, ten 15-minute samples were collected at 15 different sampling locations on the building roof. The wind direction and wind speed data were recorded using a cup anemometer located on the roof of the building.

Note that the effect of stack height on plume dispersion is not that significant for a stack engulfed inside the building roof recirculation zone. This is generally the case for a tall building such as the one considered for model validation. Therefore, even though the proposed model is developed for $h_s \geq 3$ m, the validation presented for h_s = 0.5 m is justified.

The results presented by Stathopoulos et al. (1997) are in the form of dilution values. The data have been converted to D_N using Eq 3.9. Note that only a few samplers were located on the plume centerline in the field tests. Therefore, the proposed minimum dilution model is expected to produce a lower bound to the data. The experimental

parameters for Test 1, Test3 and Test 4 are presented in Table 6.7. The proposed model is evaluated for M = 2.3.

Figure 6.25 shows the comparison between the D_N values obtained from Stathopoulos et al. (1997) and the proposed model. For this case, h_p is less than h_{top}. Thus, the stack is engulfed within the building roof re-circulation zone. Note that for his case the ASHRAE (2007) D_s model is applicable and for the proposed model, $\omega = 0.2$ is applicable (see Table 6.1). The proposed dilution model produced a lower bound on the data obtained in the field tests. A low ω value indicates that the plume height is limited, which is typical for high-rise buildings when the stack is engulfed within the building roof recirculation zone.

The ASHRAE (2007) D_s model predicted values that are close to the stack are more than 5 times lower than the measured data. However, the level of conservatism decreases for samplers located farther from the stack. As mentioned previously, emissions from short stacks are often completely entrained within the building roof recirculation zone. Consequently, the plume rise is small even if M is large. The ASHRAE D_s model does not include plume rise and therefore predicted overly conservative values. Validations for other tests for the high-rise building are presented in Appendix F.

6.4 Benefits of the proposed model over ASHRAE (2007) model

It was demonstrated that the dilutions estimated with the proposed model are significantly more accurate compared to the ASHRAE (2007) minimum dilution models. In particular, for the low-rise buildings with and without RTS, the ASHRAE (2007) D_r

and D_s models were overly conservative for most of the cases evaluated. Therefore, ASHRAE (2007) model will generate significantly taller stacks or high exhaust flow rates to meet air quality standards. Taller stacks are aesthetically non-pleasing and are expensive to install. On the other hand, high exhaust flow rates will require large energy consumption. The proposed model estimations are reasonably conservative for nearly all cases examined.

Table 6.1 Design criteria for the proposed minimum dilution model.

Building type	Presence of upstream RTS	Stack height (h_s)	Stack-RTS separation x_s	ω
Low-rise	No	h_s	N/A	0.70
Low-rise	Yes	$h_s \leq 1.5h$	$x_s < 2h$	0.20
		$1.5h < h_s \leq 2.5h$		0.30
		$h_s > 2.5h$	N/A	0.70
High-rise	N/A	$h_s \leq h_{top}$	N/A	0.20
		$h_s > h_{top}$		0.7

* 'h' is the height of the RTS

Table 6.2 Wind tunnel experimental parameters from Schulman and Scire (1991).

Stack location (x/L)	Building size (L x W x H)	Wind direction (θ)	Exhaust momentum (M)	Stack height (h_s)	Stack diameter (d_e)
0.5	75 m x 75 m x 15 m	0°	3, 5	4.5 m, 7.5 m	0.75 m

Table 6.3 Water flume experimental parameters from Wilson et al. (1998).

Stack location (x/L)	Building size (L x W x H)	Wind direction (θ)	Exhaust momentum (M)	Stack height (h_s)	Stack diameter (d_e)
0.3	72 m x 30 m x 12.2 m	0°	3, 5	6 m	0.67 m
0.6			3, 8	3 m	

Table 6.4 Field test details from Stathopoulos et al. (2003).

Stack location	Building size (L x B x H)	Wind direction (θ)	Exhaust momentum (M)	Stack height (h_s)	Stack diameter (d_e)
SL2	52.5 m x 51 m x 12.5 m	302°–309°	2.8–3.2	3 m	0.4 m

Table 6.5 Field test details from Wilson and Lamb (1994).

Field test	Building size (L x W x H)	Wind direction (θ)	Exhaust momentum (M)	Stack height (h_s)	Stack diameter (d_e)
1	60 m x 30 m x 18 m	114°–137°	2.9–4.6	3.6 m	0.2 m
2		92°–125°	3.9–7.5		

Table 6.6 Field test details from Saathoff et al. (2002).

Field test	Building size (L x W x H)	Wind direction (θ)	Exhaust momentum (M)	Stack height (h_s)	Stack diameter (d_e)
1	50 m x 50 m x 12.5m	260°–280°	1.7–2.5	3.1 m	0.9 m
2			2.6–3.2		

Table 6.7 Field test details from Stathopoulos et al. (1997).

Field test	Building size (L x W x H)	Wind direction (θ)	Exhaust momentum (M)	Stack height (h_s)	Stack diameter (d_e)
1	60 m x 60 m x 62 m	210°–220°	2.4–3.0	0.5 m	0.9 m
3		150°–170°	2.3–3.0		
4		210°–220°	2.6		

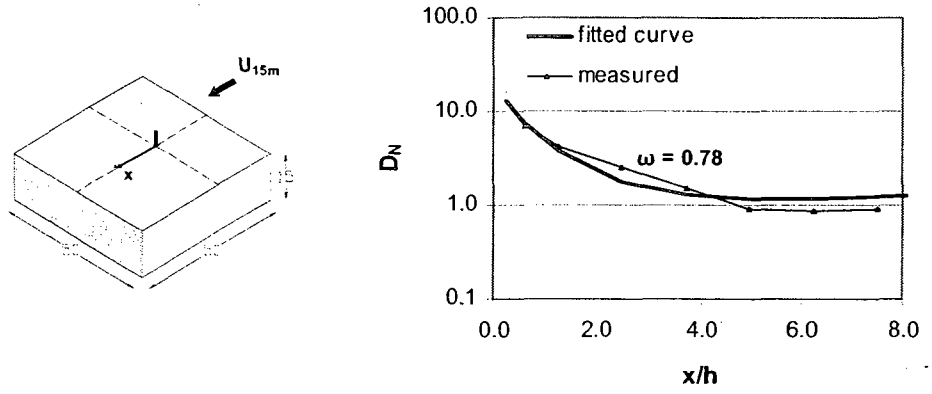

a) Worst-case for flat-roofed case: $\theta = 0^{\circ}$

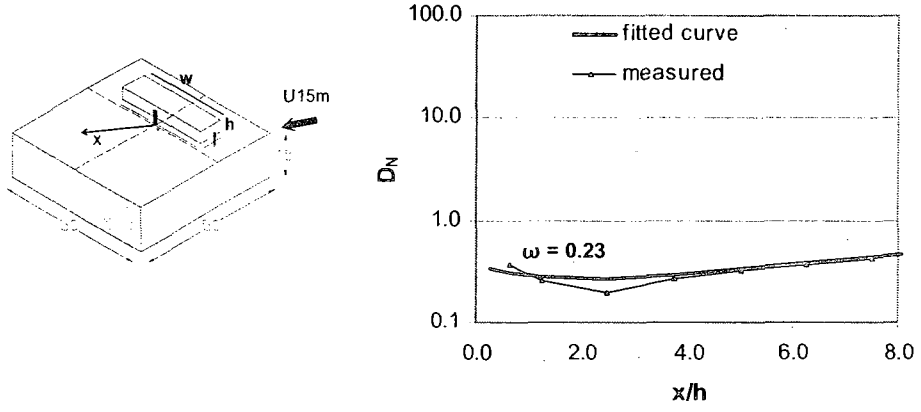

b) Worst-case scenario for building with RTS (w/h = 7.5): $\theta = 45^{\circ}$

Figure 6.1 Example of curve fitting used in the present study for the low-rise building for h_s = 3 m, M = 2 and h = 4: a) building with no RTS; b) building with RTS.

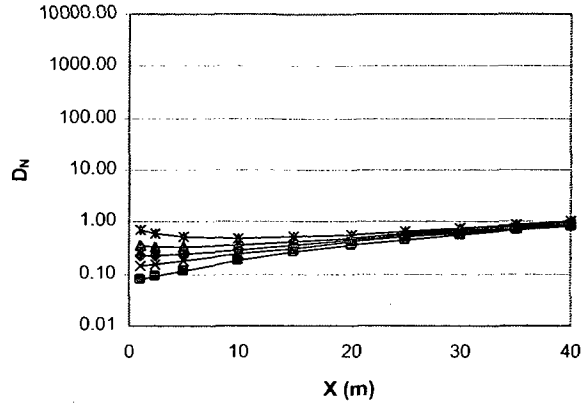

a) h_s = 1 m

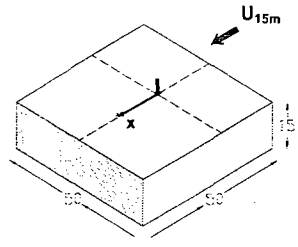

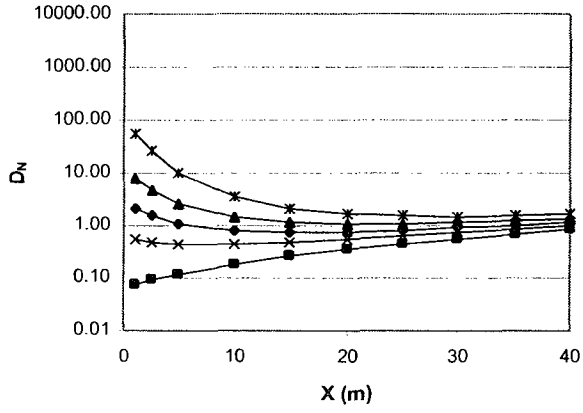

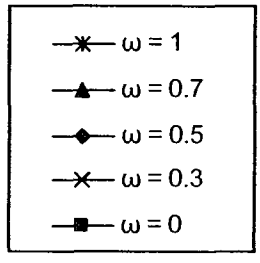

b) h_s = 3 m

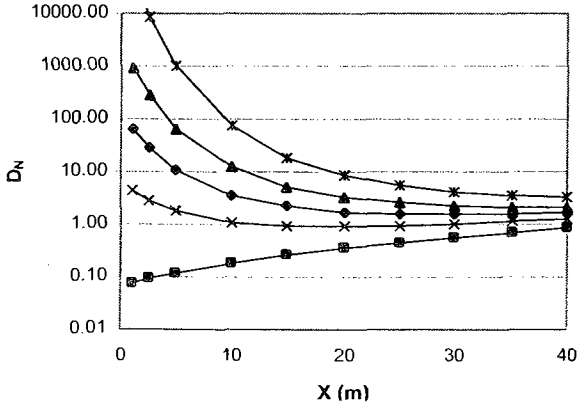

c) h_s = 5 m

Figure 6.2 Effect of ω values on D_N curves obtained from Eq 6.8 for M = 2: a) h_s = 1m, b) 3 m and, c) 5 m.

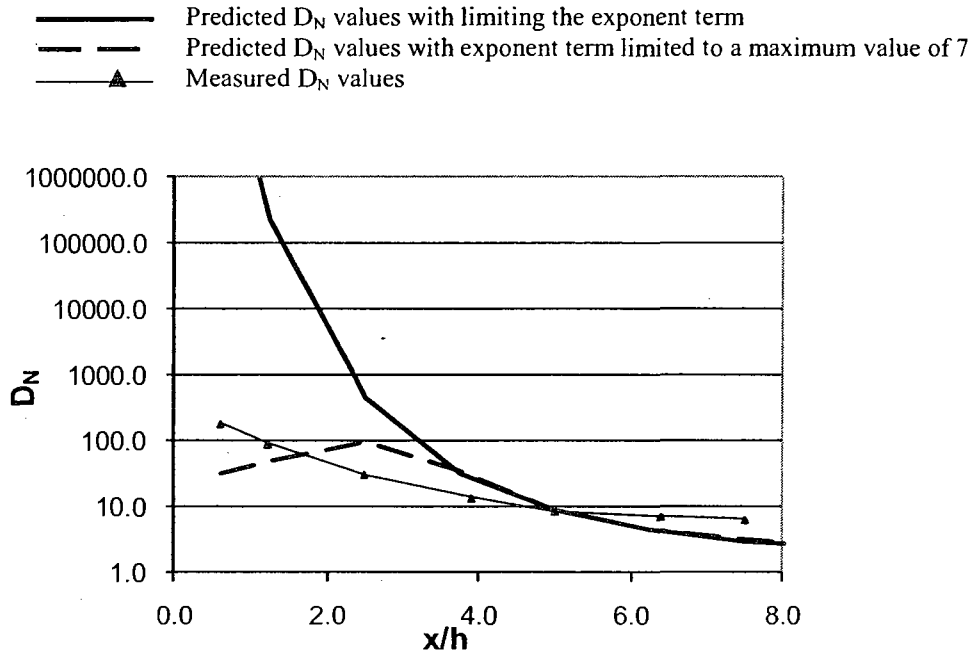

Figure 6.3 Effect of limiting the value of the exponent term on D_N values obtained from Eq 6.8 for M = 1 and h_s = 7 m. Results are shown for ω = 0.7.

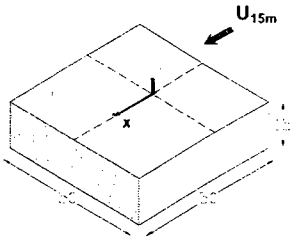

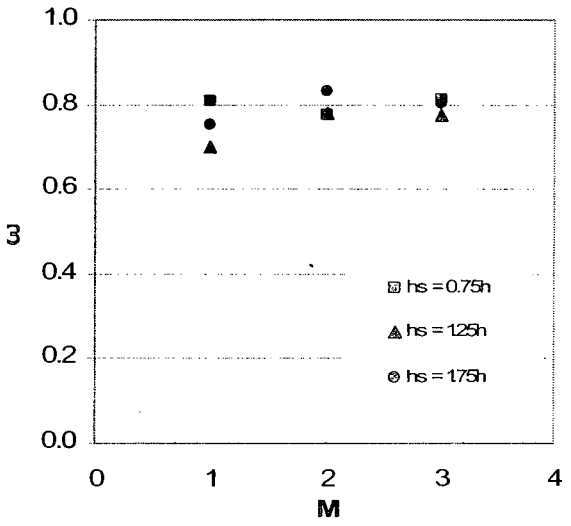

Figure 6.4 Variation of ω with M for the flat-roofed low rise building for h_s = 0.75h–1.75h (h = 4 m) and $\theta = 0^{\circ}$.

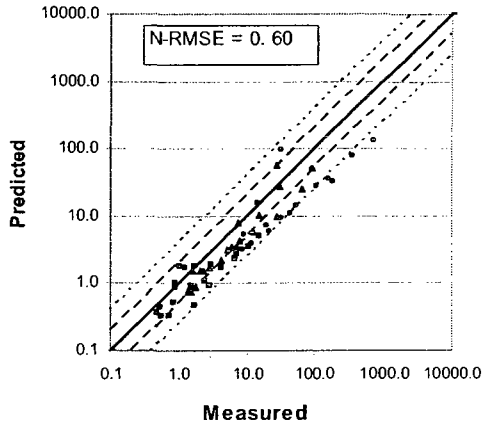

a) ω = 0.65

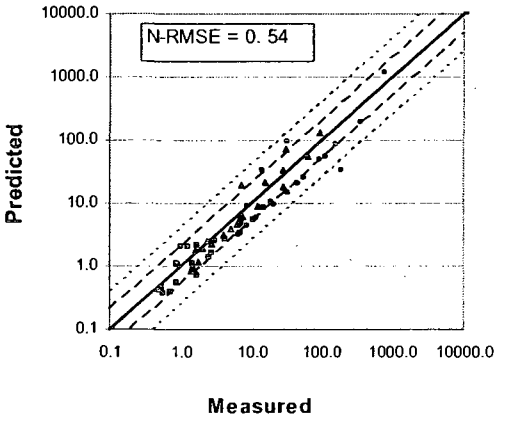

b) ω = 0.70

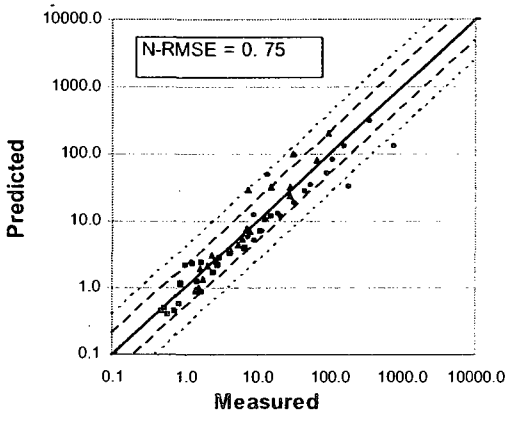

c) ω = 0.75

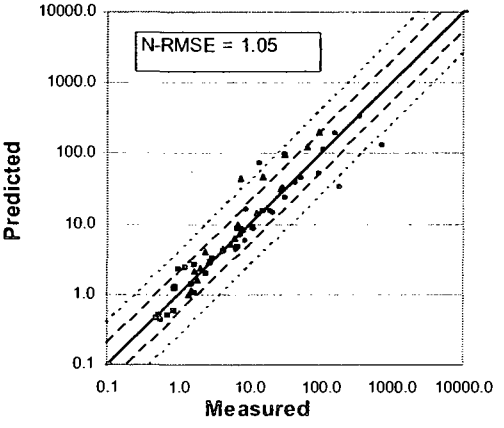

d) ω = 0.80

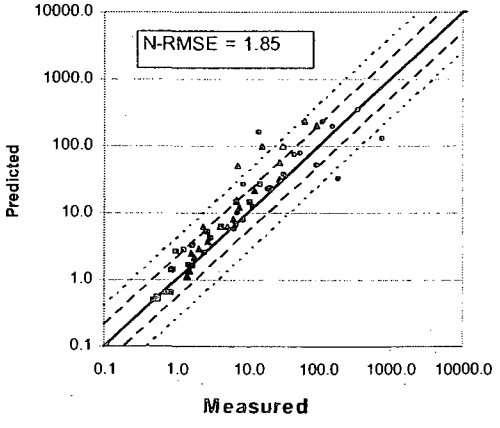

e) ω = 0.90

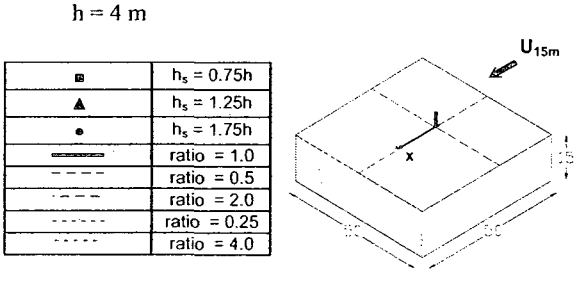

Figure 6.5 Scatter plots of measured and predicted D_N data for the flat-roofed low-rise building for h_s = 0.75h – 1.75h (h = 4m) and M = 1-3: a) ω = 0.65, b) ω = 0.7, c) ω = 0.75, d) ω = 0.80, and e) ω = 0.90.

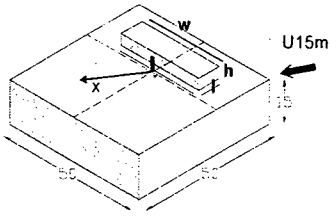

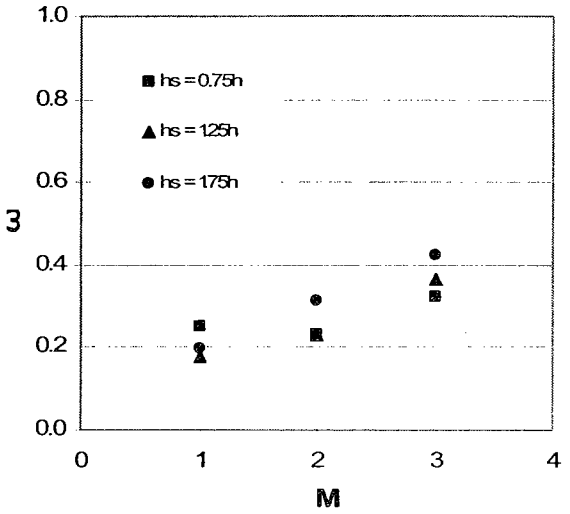

Figure 6.6 Variation of ω with M for the low rise building with RTS for h_s = 0.75h–1.75h (h = 4 m) and θ = 45°.

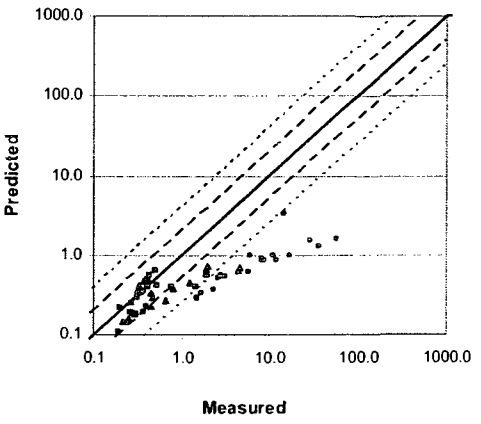

a) $\omega = 0.15$

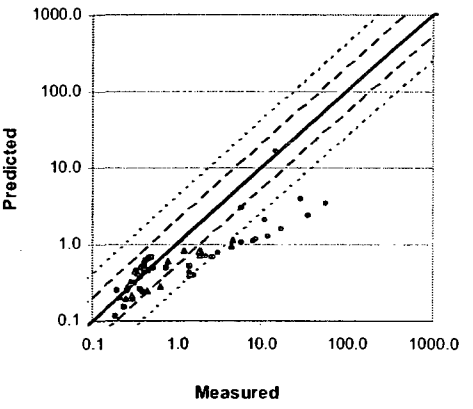

b) $\omega = 0.20$

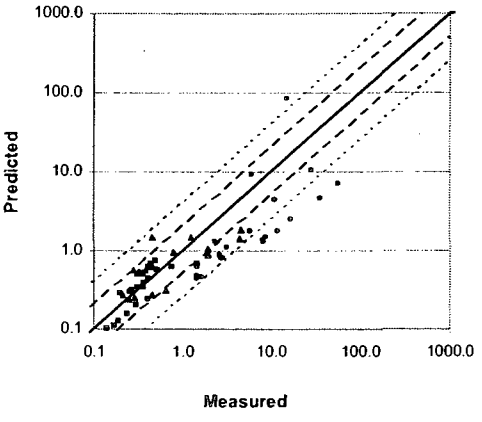

c) $\omega = 0.25$

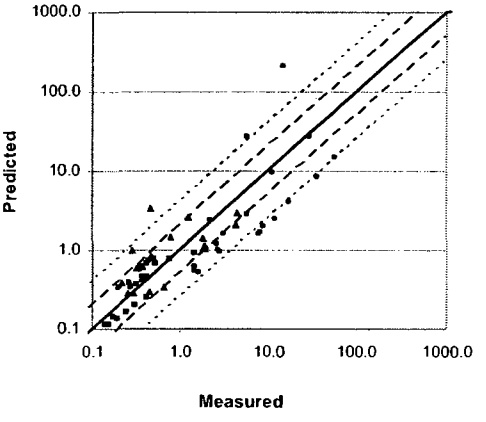

d) $\omega = 0.30$

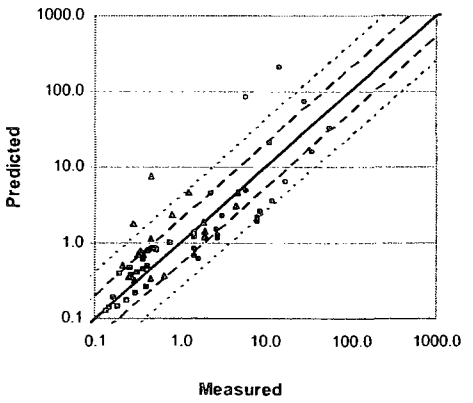

e) $\omega = 0.35$

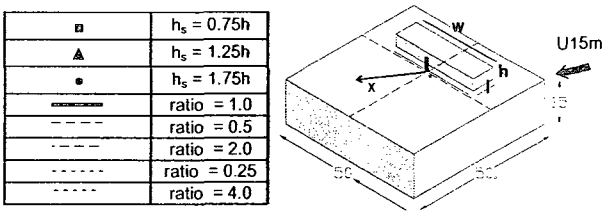

h = 4 m

Figure 6.7 Scatter plots of measured and predicted D_N data for the low-rise building with RTS for h_s = 0.75h - 1.75h (h = 4m) and M = 1-3: a) $\omega = 0.15$, b) $\omega = 0.20$, c) $\omega = 0.25$, d) $\omega = 0.30$, and e) $\omega = 0.35$.

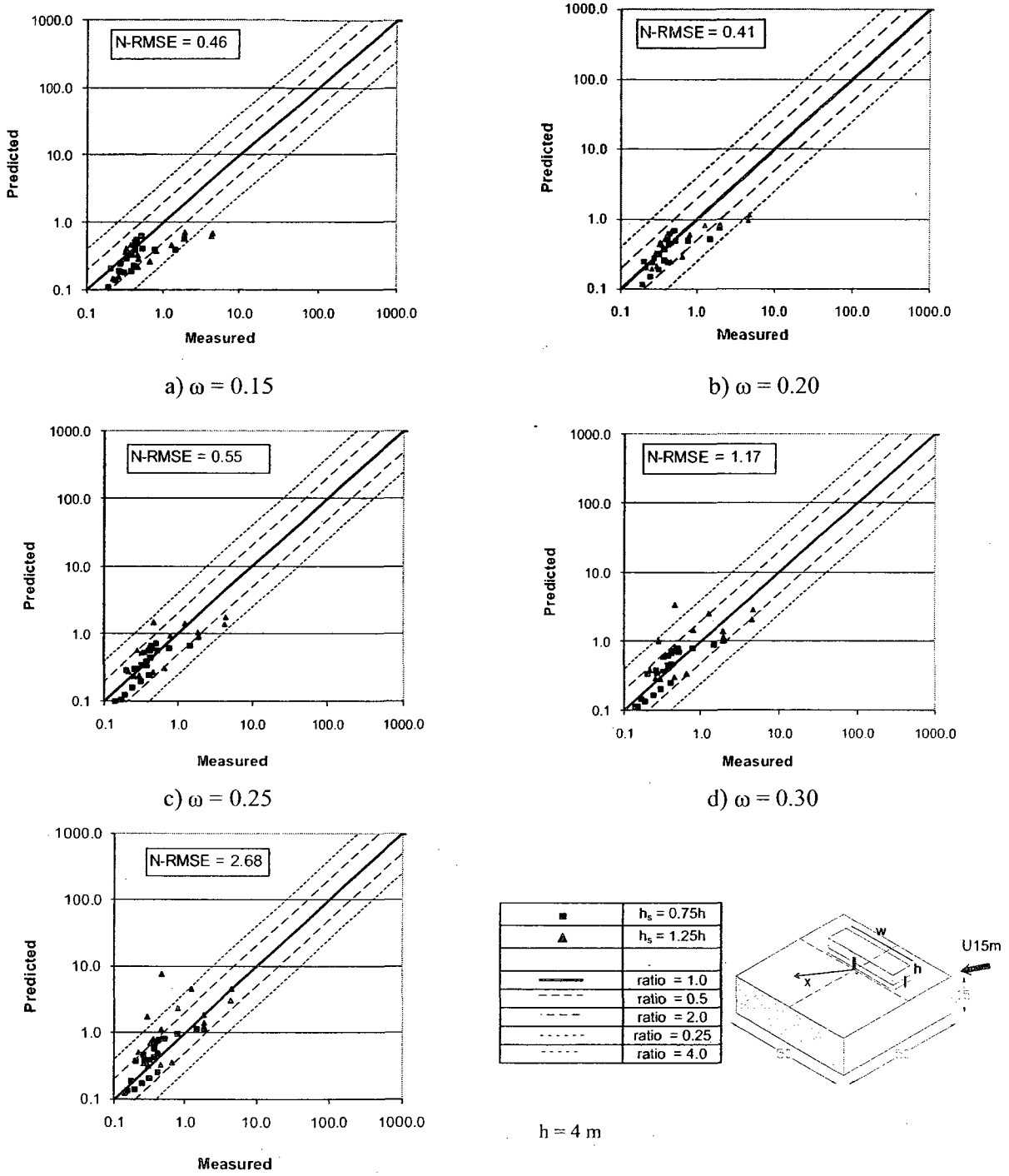

Figure 6.8 Scatter plots of measured and predicted D_N data for the low-rise building with RTS for h_s = 0.75h and 1.25h (h = 4m) and M = 1-3: a) ω = 0.15, b) ω = 0.20, c) ω = 0.25, d) ω = 0.30, and e) ω = 0.35.

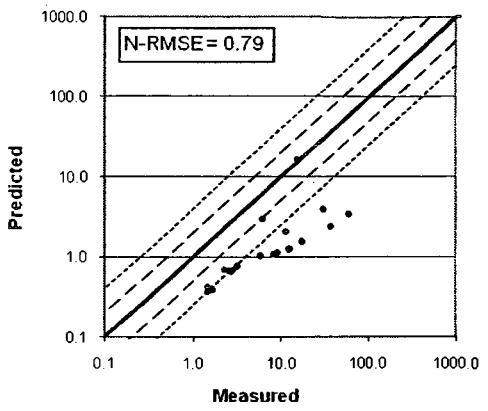

a) ω = 0.20

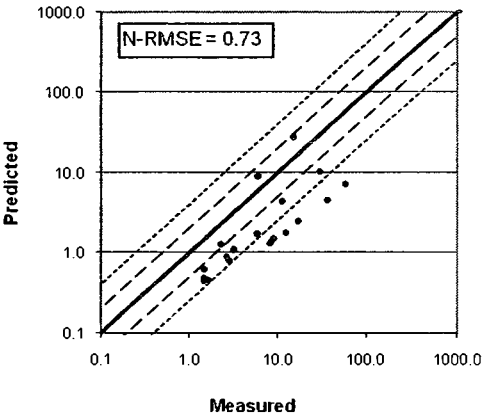

b) ω = 0.25

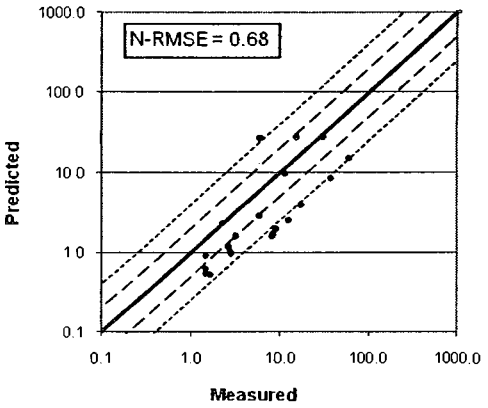

c) ω = 0.30

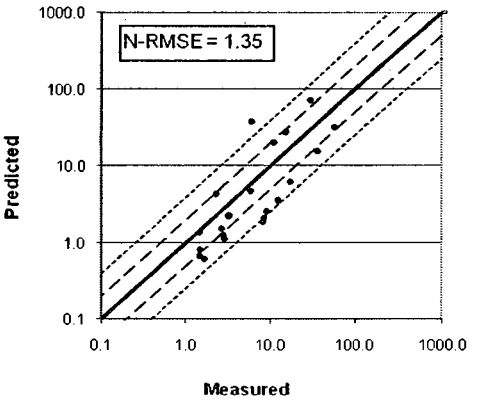

d) ω = 0.35

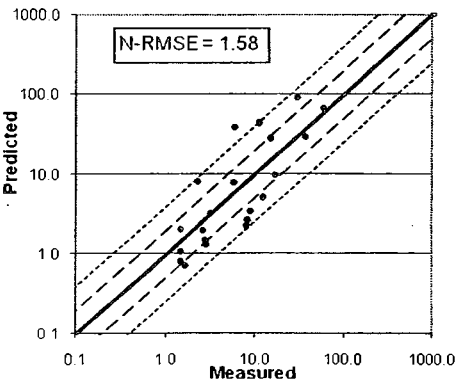

e) ω = 0.40

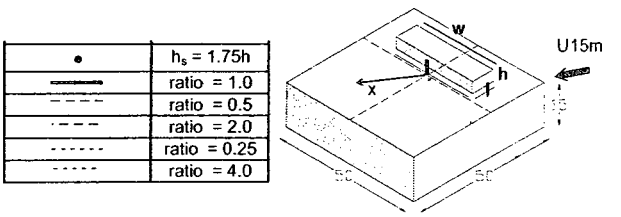

h = 4 m

Figure 6.9 Scatter plots of measured and predicted D_N data for the low-rise building with RTS for h_s = 1.75h (h = 4m) and M = 1-3: a) ω = 0.20, b) ω = 0.25, c) ω = 0.30, d) ω = 0.35 and, e) d) ω = 0.40.

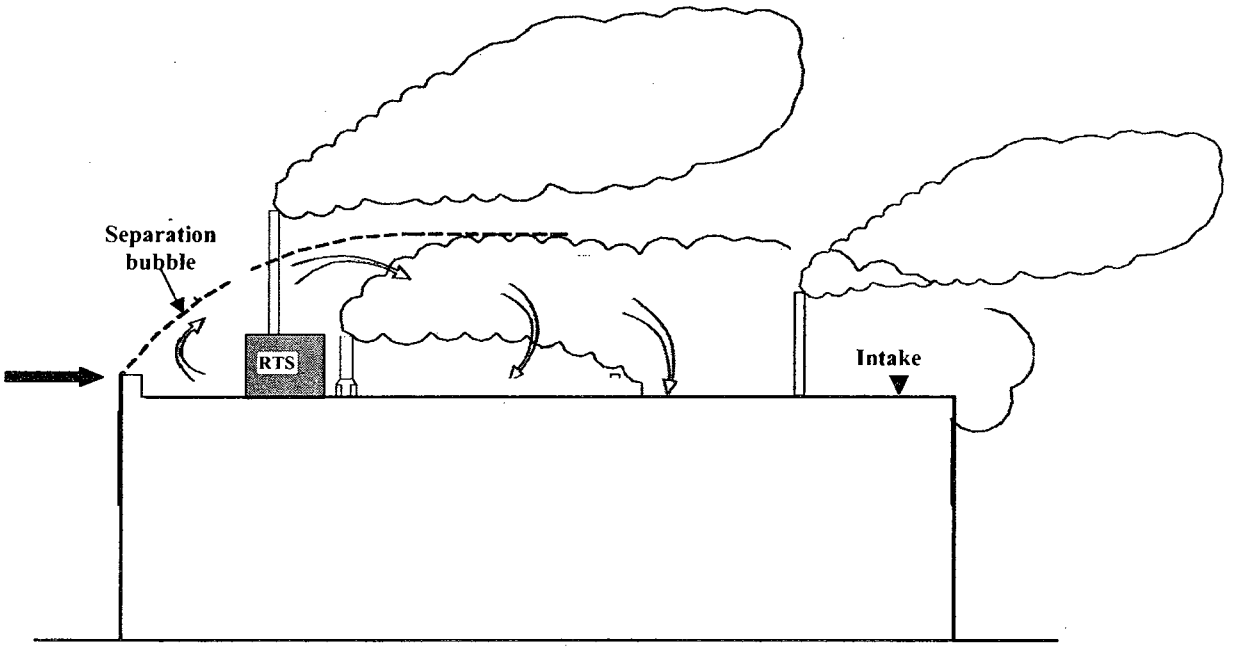

Figure 6.10 Formation of recirculation zones (separation bubble) on a building roof and its impact on exhausts released at different location on the building roof.

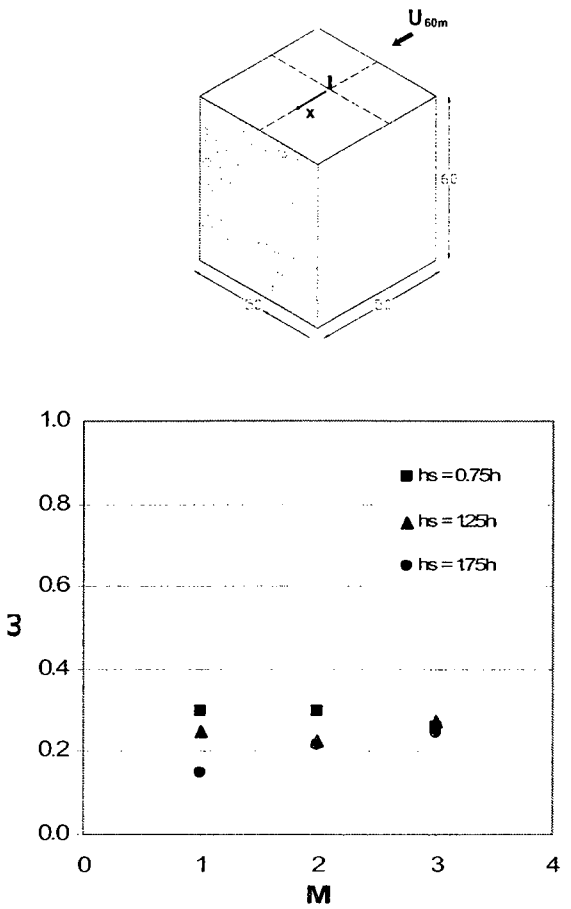

Figure 6.11 Variation of ω with M for the flat-roofed high-rise building for h_s = 0.25h – 1.75h (h = 4 m) and $\theta = 0^{\circ}$.

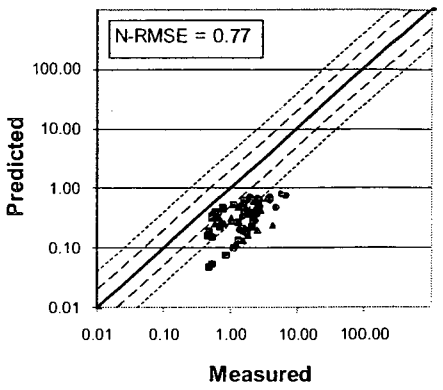

a) ω = 0.10

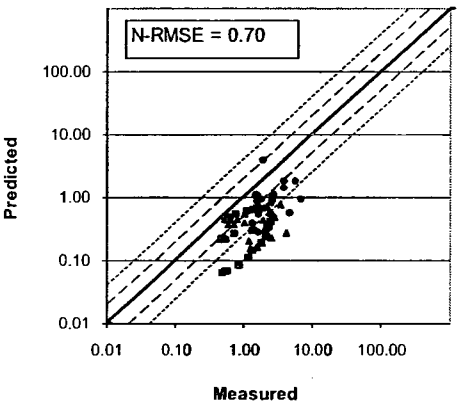

b) ω = 0.15

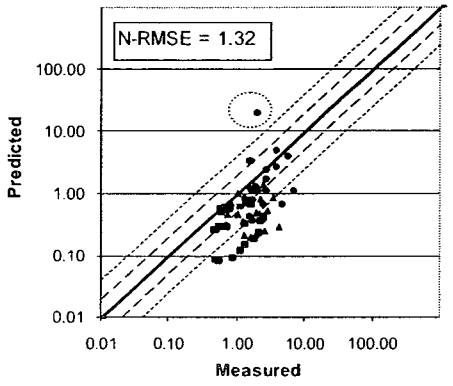

c) ω = 0.20

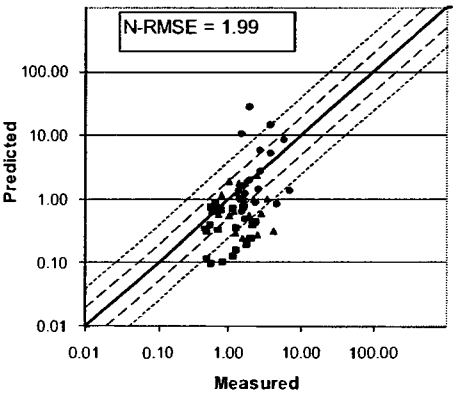

d) ω = 0.25

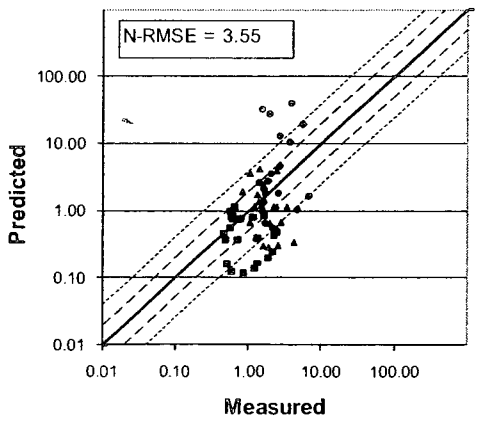

e) ω = 0.30

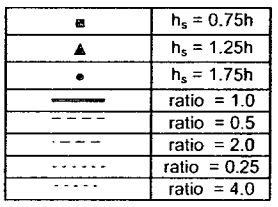

h = 4 m

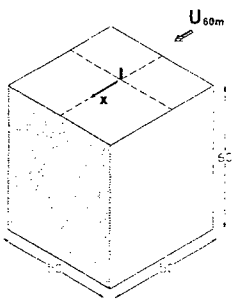

Figure 6.12 Scatter plots of measured and predicted D_N data for the High-rise building for h_s = 0.75h – 1.75h (h = 4m) and M = 1-3: a) ω = 0.10, b) ω = 0.15, c) ω = 0.20, d) ω = 0.25 and, e) d) ω = 0.30.

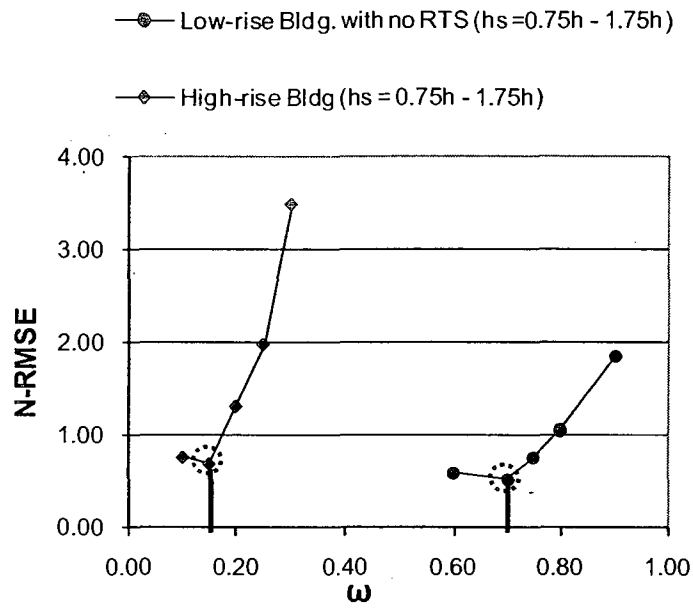

a) Low- and high-rise building with no RTS

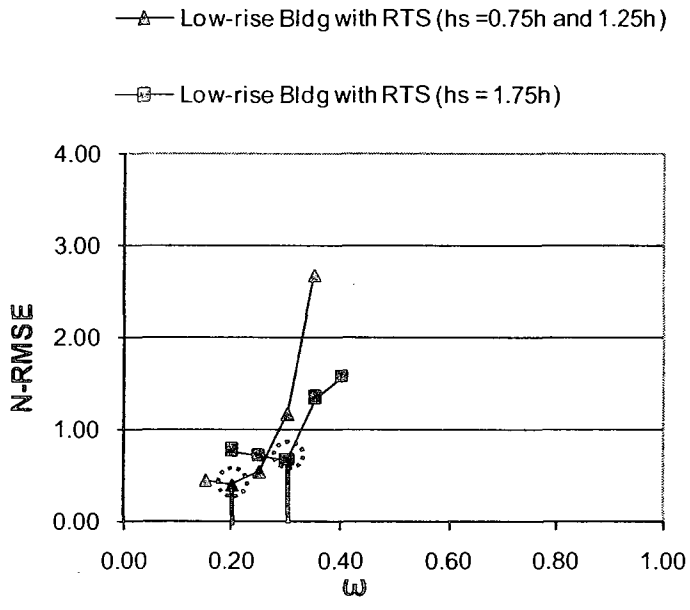

b) Low-rise building with RTS

Figure 6.13 Variation of N-RMSE with ω values for different building configurations tested.

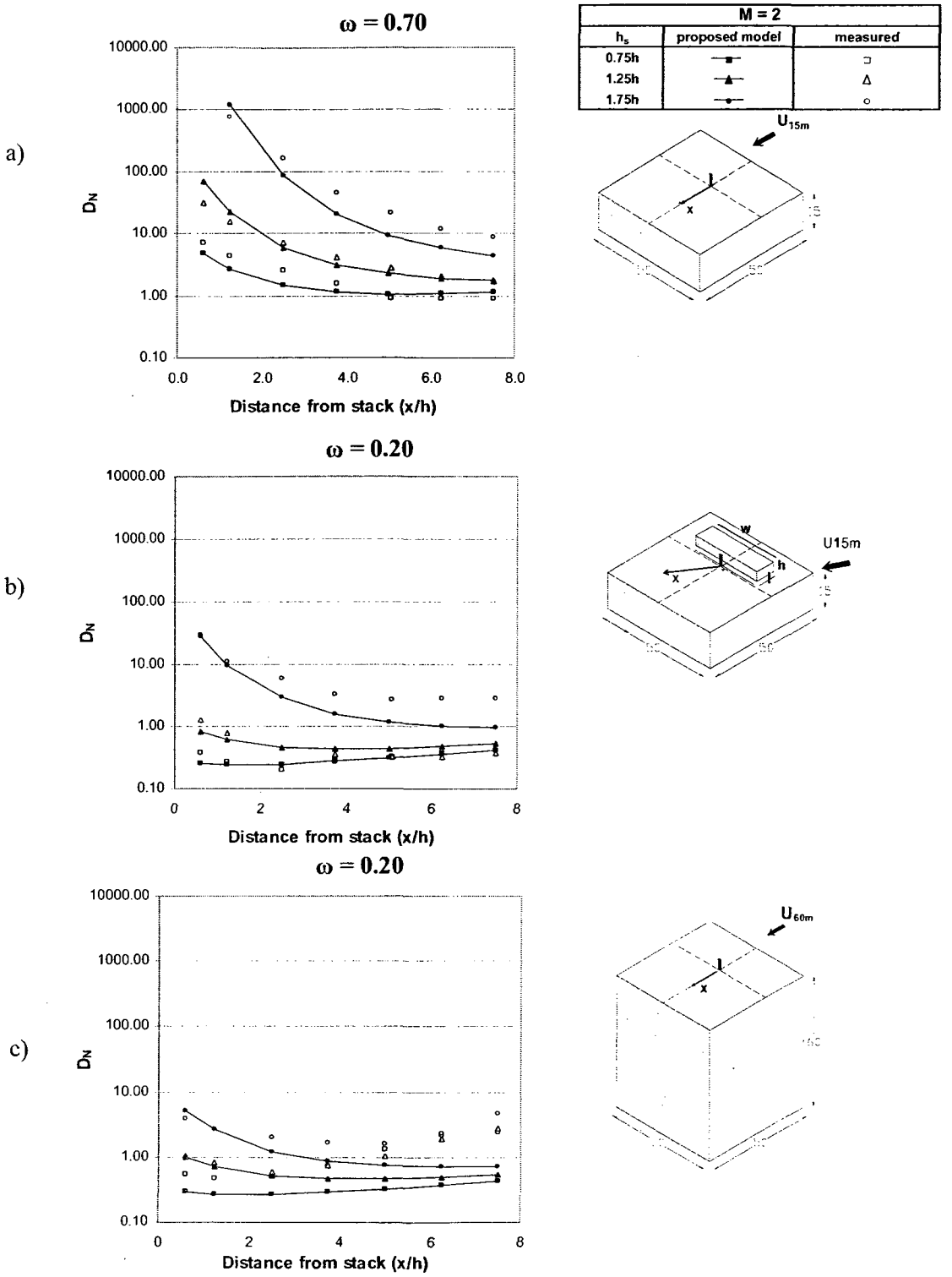

Figure 6.14 Model estimates vs. present data for M = 2 and h_s = 0.75h to 1.75: a) flat-roofed low-rise building; b) low-rise building with RTS; and c) flat-roofed high-rise building.

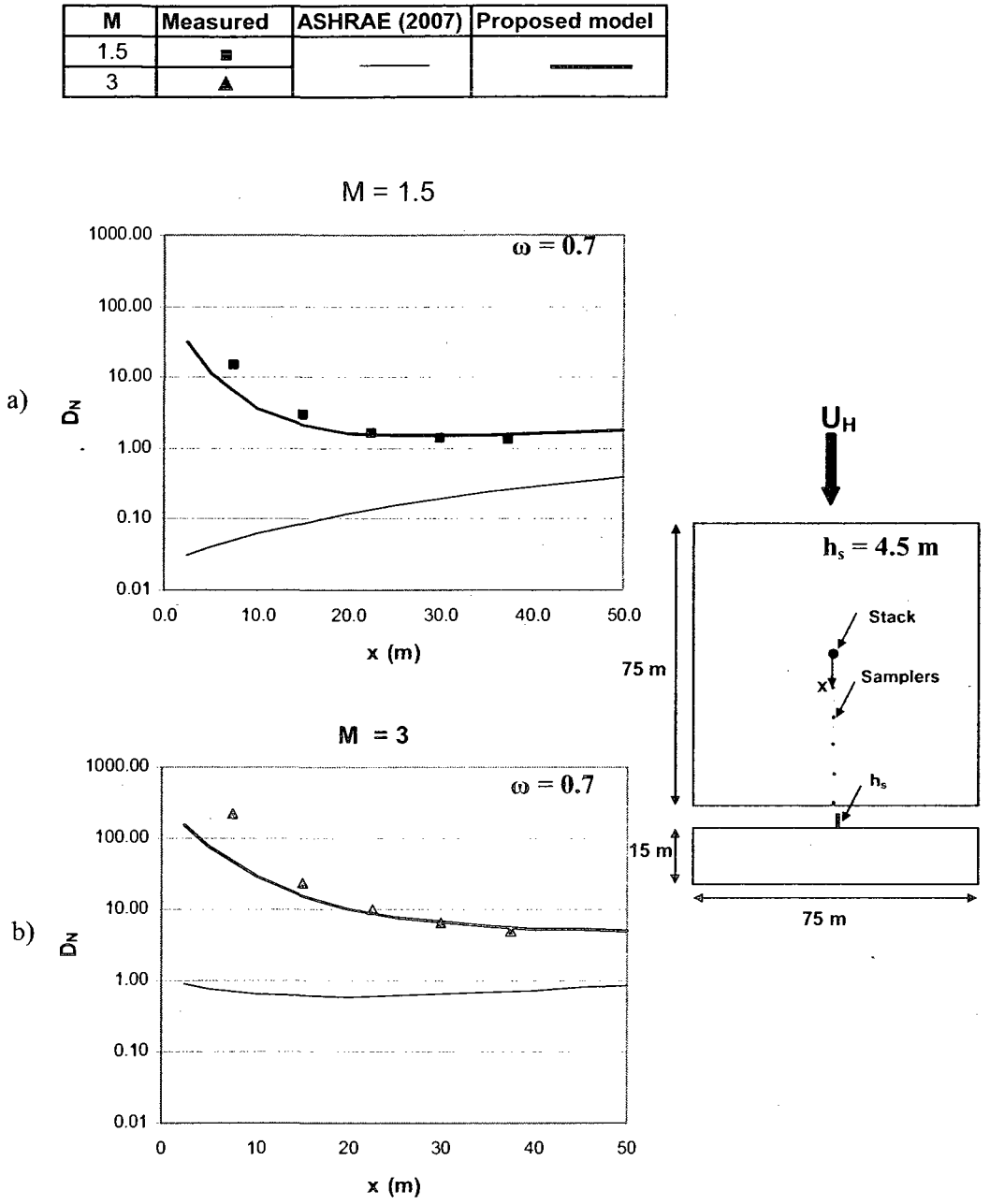

Figure 6.15 Model validations with Schulman and Scire (1991) wind-tunnel data for the flat-roofed low-rise building for h_s = 4.5 m: a) M = 1.5; and b) M = 3

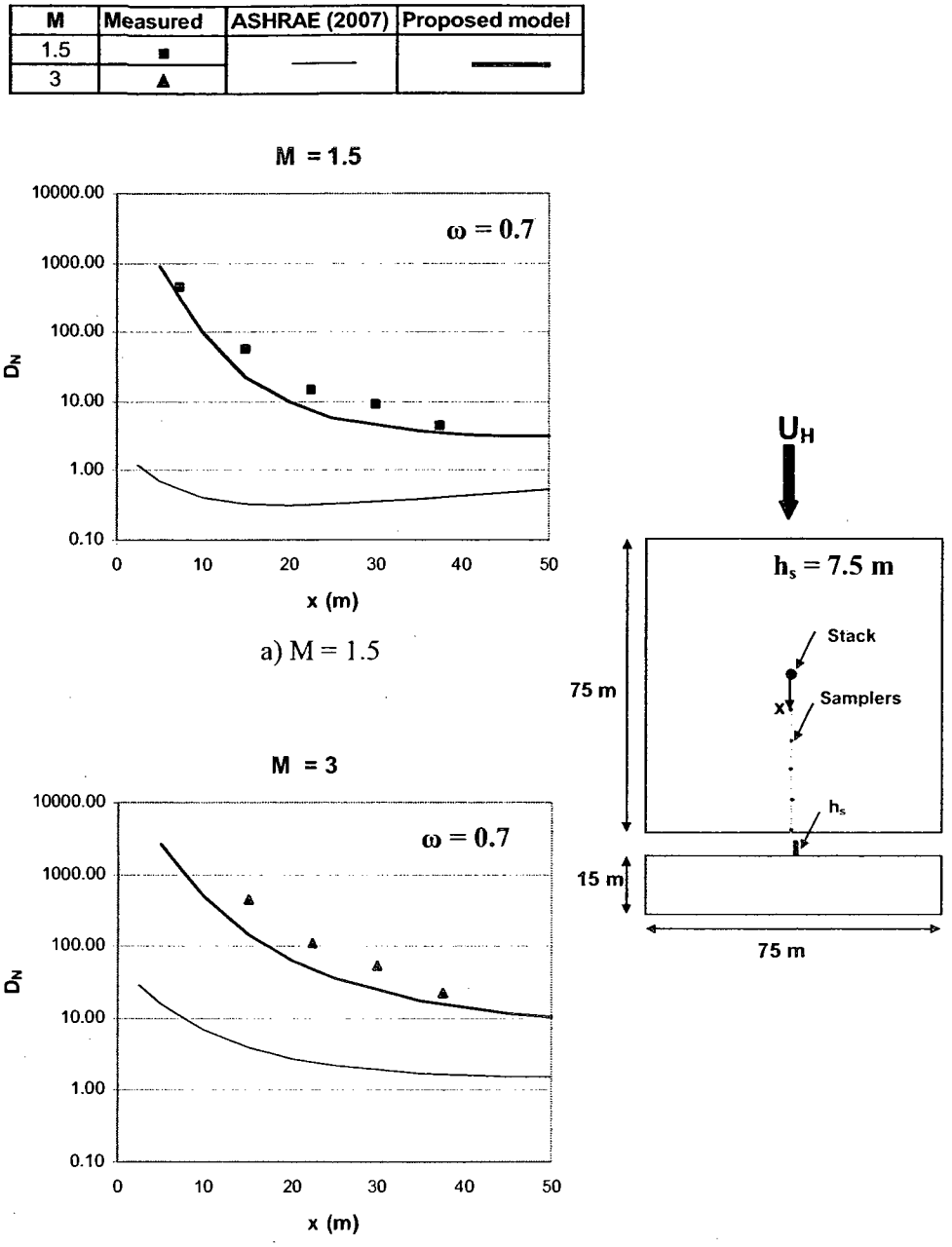

Figure 6.16 Model validations with Schulman and Scire (1991) wind-tunnel data for the flat-roofed low-rise building for h_s = 7.5 m: a) M = 1.5; and b) M = 3

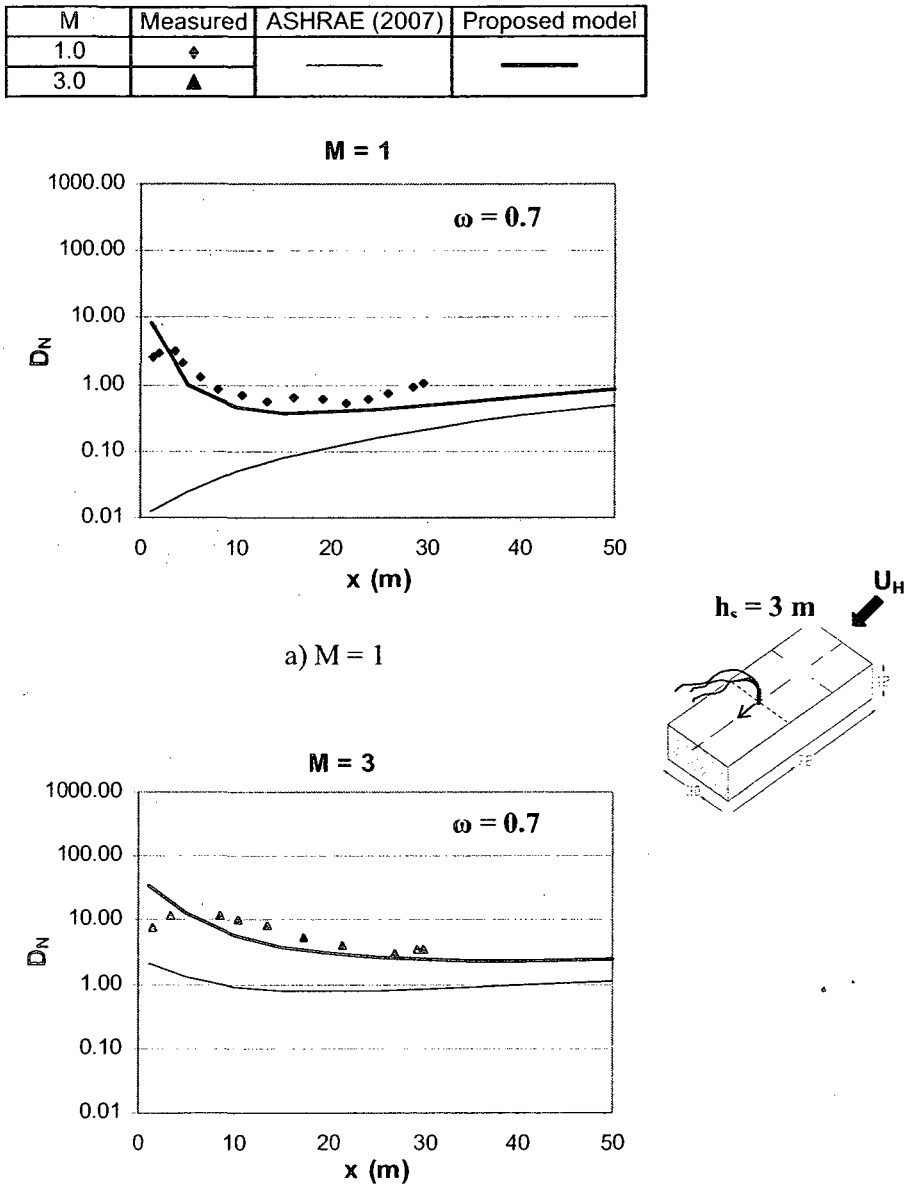

a) M = 1

b) M = 3

Figure 6.17 Model validations with Wilson et al. (1998) water flume data for the flat-roofed low-rise building for h_s = 3 m: a) M = 1; and b) M = 3

M	Measured	ASHRAE (2007)	Proposed model
1.0	♦	——	——
3.0	▲		

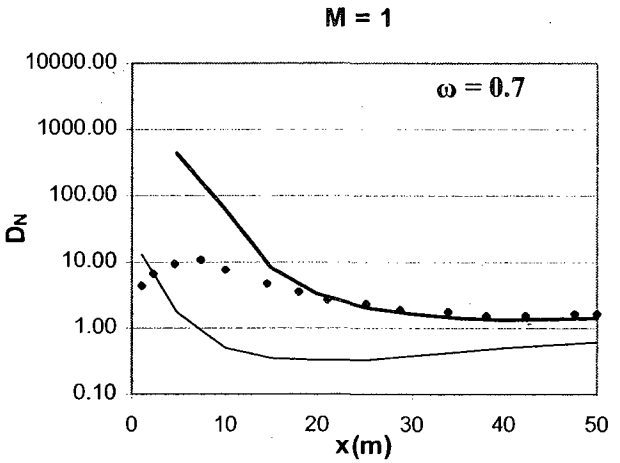

a) M = 1

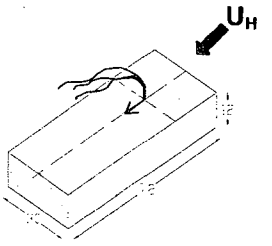

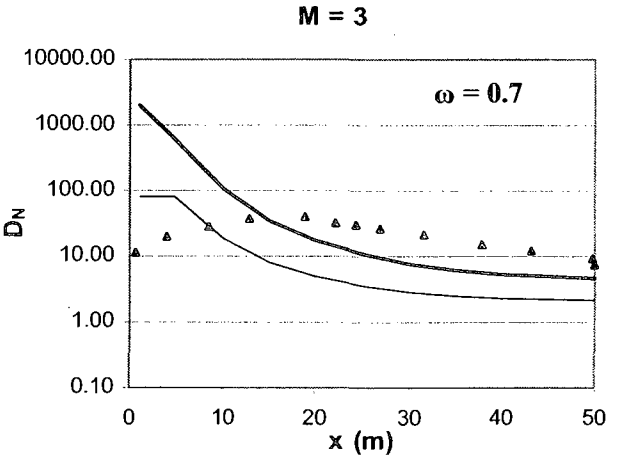

b) M = 3

Figure 6.18 Model validations with Wilson et al. (1998) water flume data for the flat-roofed low-rise building for h_s = 6 m: a) M = 1; and b) M = 3.

a)

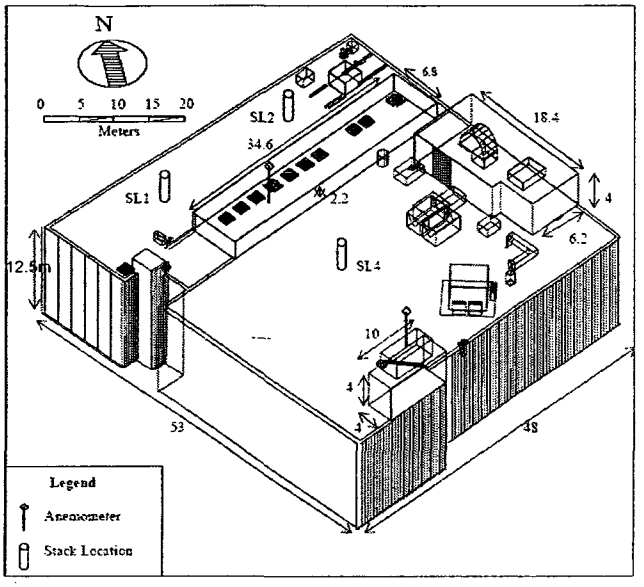

b)

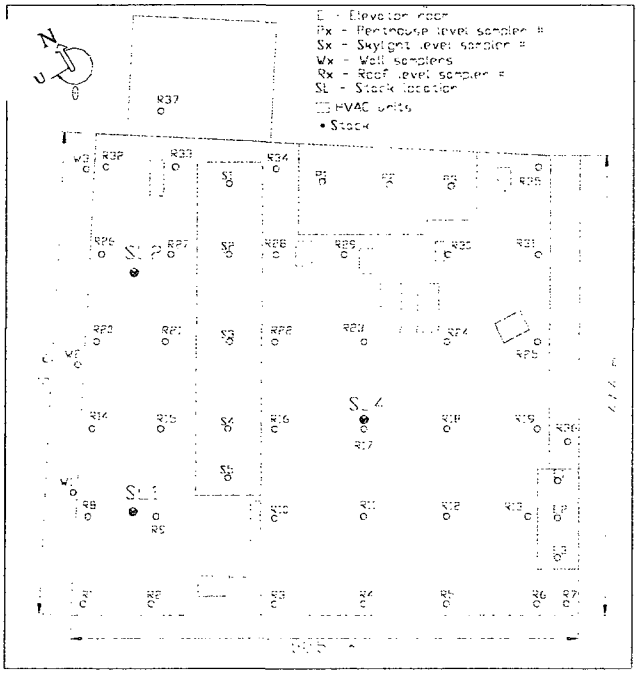

Figure 6.19 Test building set-up from Stathopoulos et al. (2003): a) schematic view of the test building showing location of stacks; b) location of samplers.

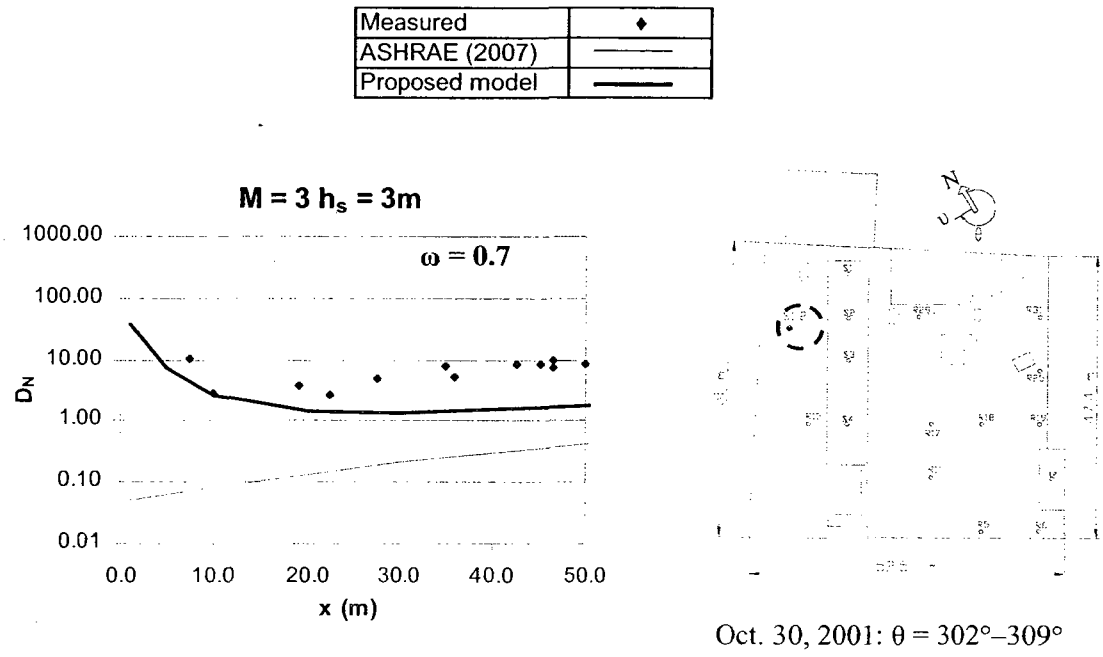

Figure 6.20 Model validations with Stathopoulos et al. (2003) for the low-rise building for h_s = 3 m and M = 3.

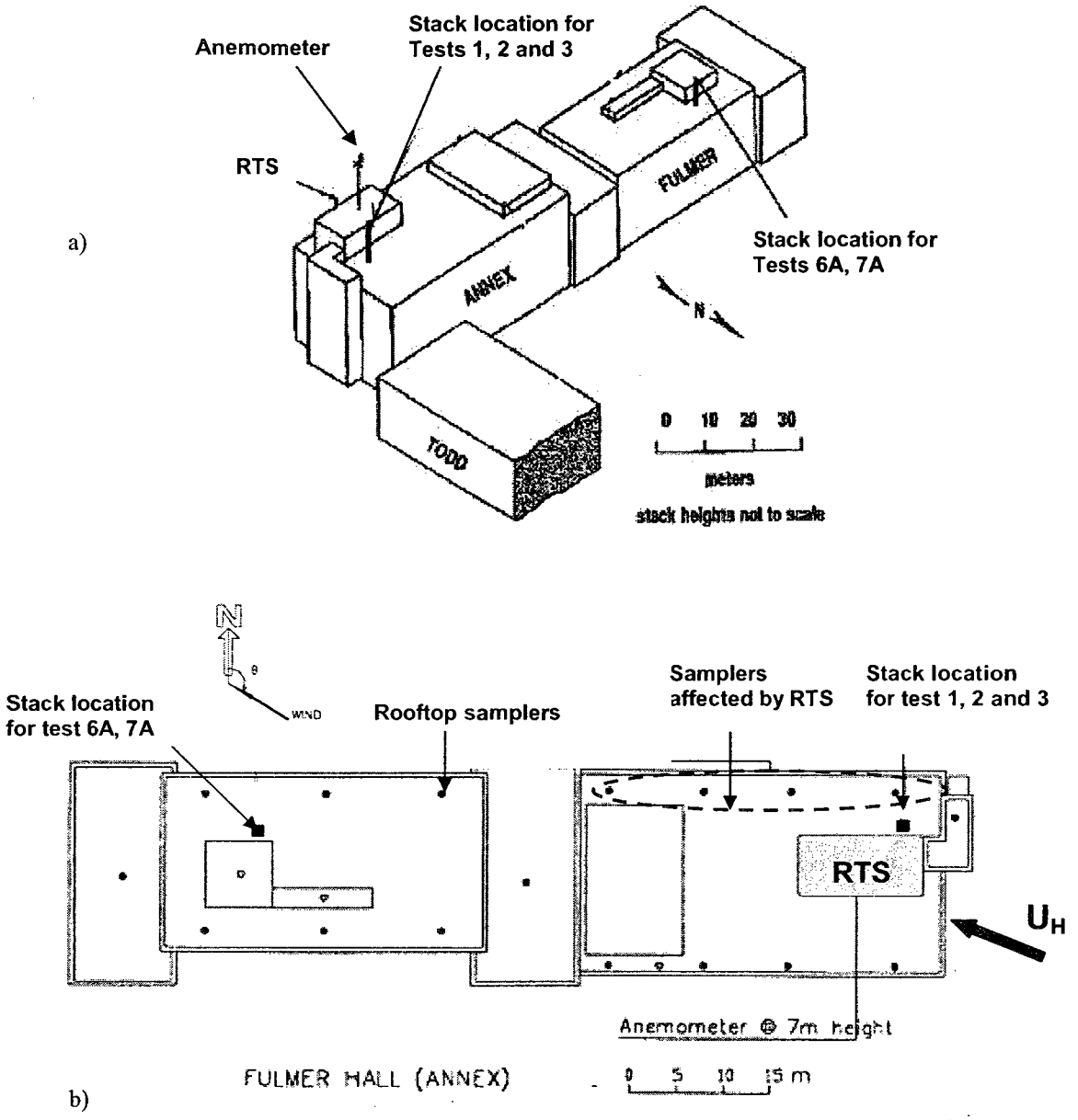

Figure 6.21 Test building set-up for Wilson and Lamb (1994): a) schematic view of the test building showing location of stacks; and b) plan view showing location of roof, with emphasis on samplers affected by potential downwash effect of the highlighted RTS.

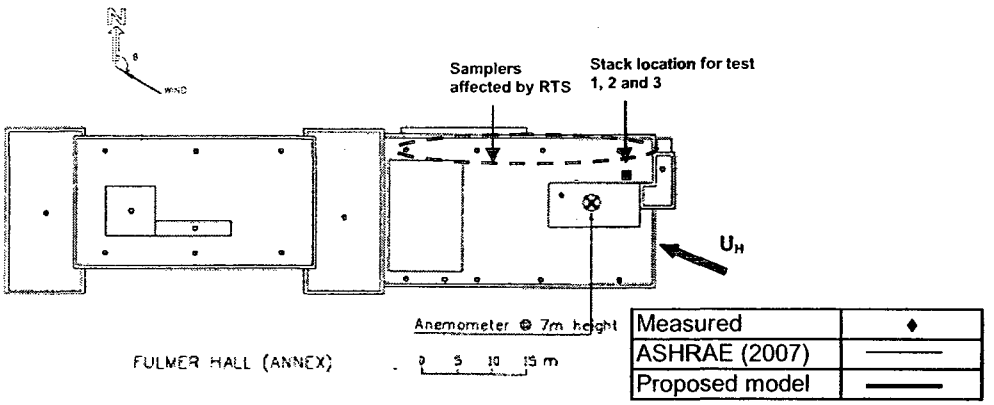

a) Test 1: θ = 114°–137°

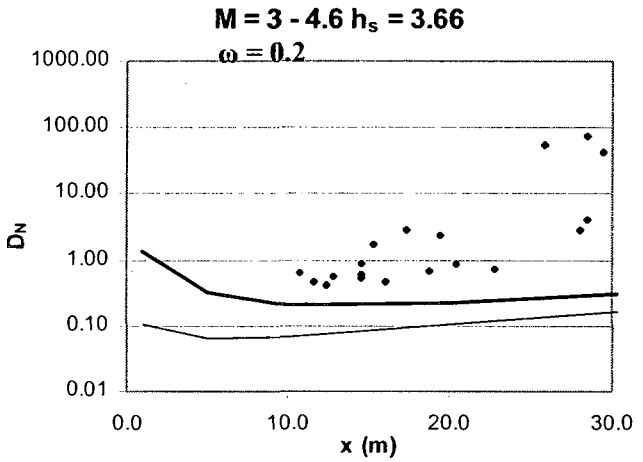

b) Test 2: θ = 92°–125°

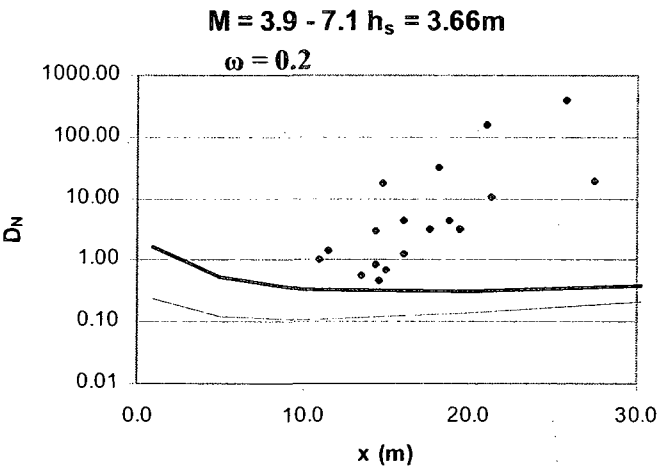

Figure 6.22 Model validations with Wilson and Lamb (1994) for a low-rise building with an RTS upwind of stack for h_s = 3.66 m: a) Test 1: M = 3–4.6; and b) Test 2: M = 3.9–7.1.

a)

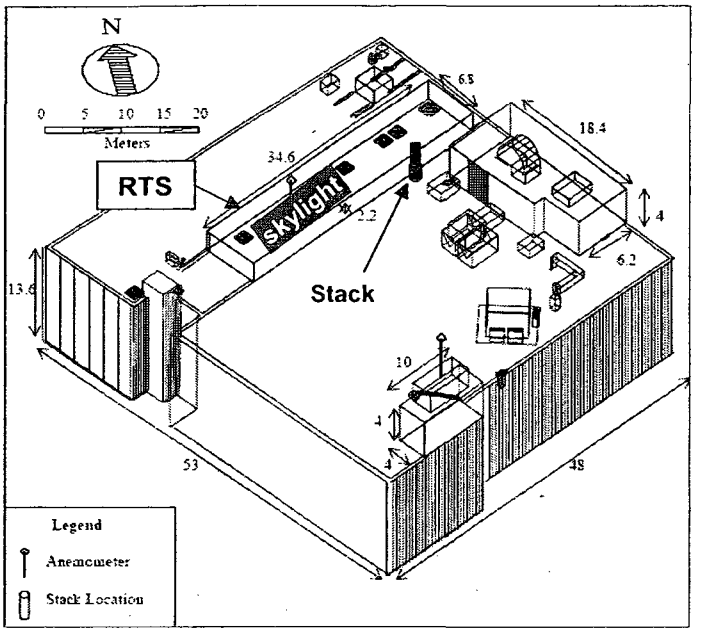

b)

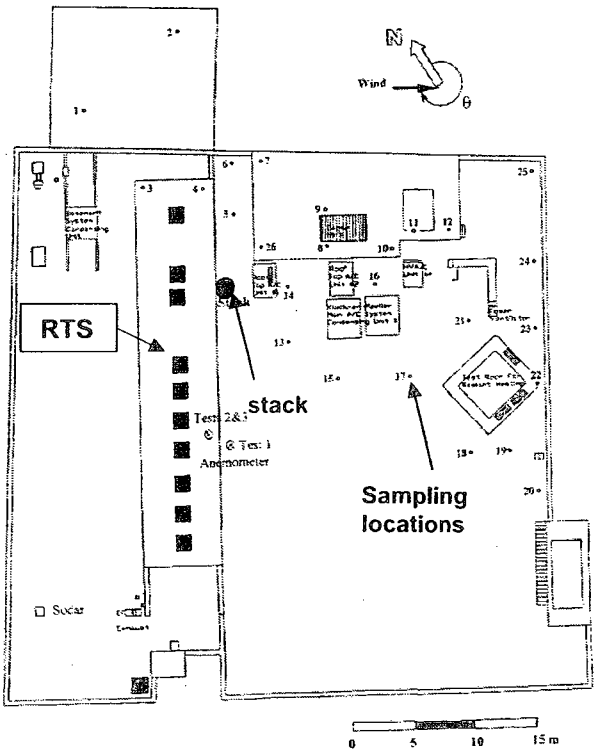

Figure 6.23 Test building set-up for Saathoff et al. (2002): a) schematic view of the test building showing location of stacks; and b) location of samplers.

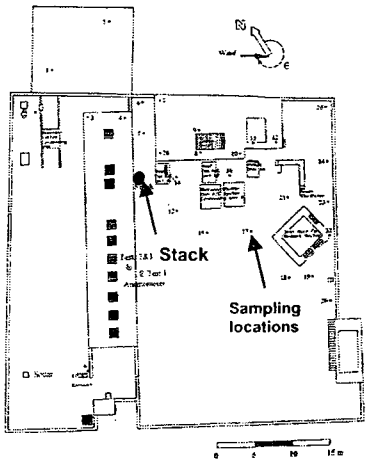

a) Test 1: θ = 260°–280°

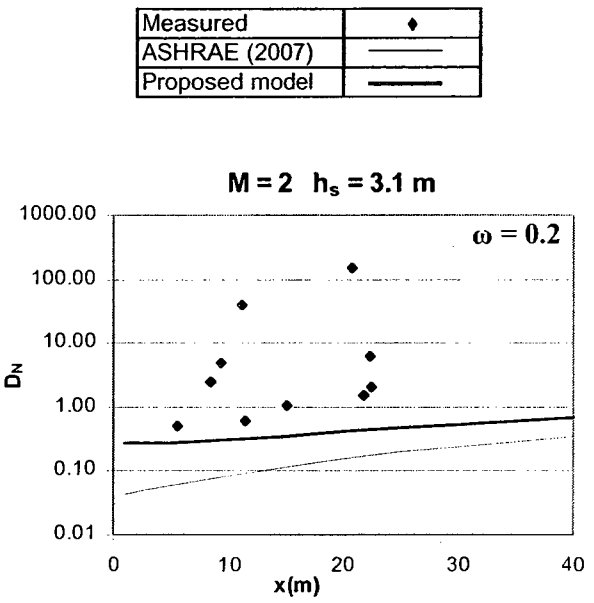

b) Test 2: θ = 260°–280°

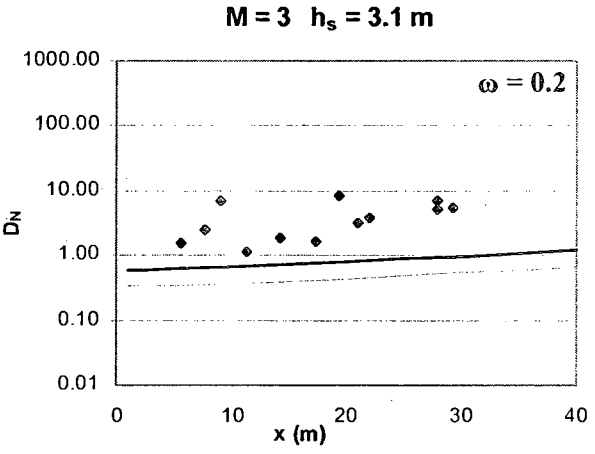

Figure 6.24 Model validations with field data from Saathoff et al. (2002): a) Test 1: M = 2; and b) Test2: M = 3.

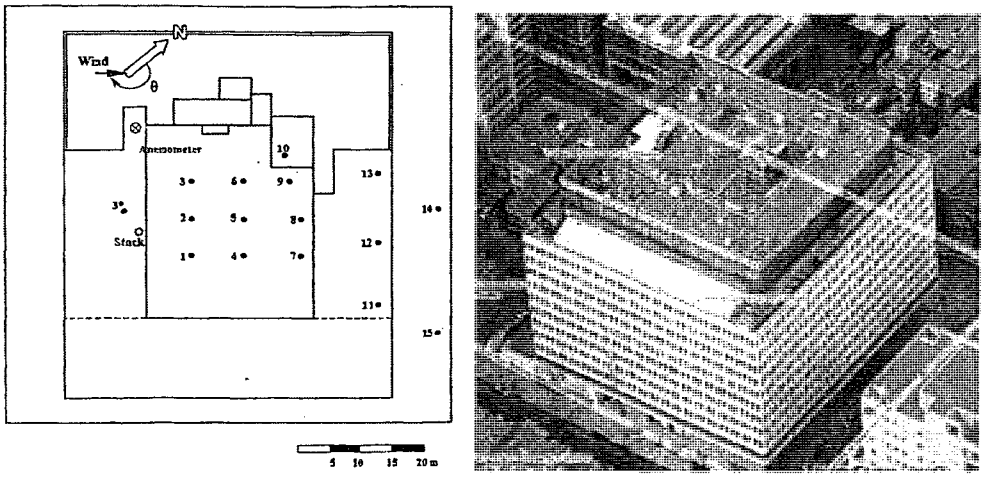

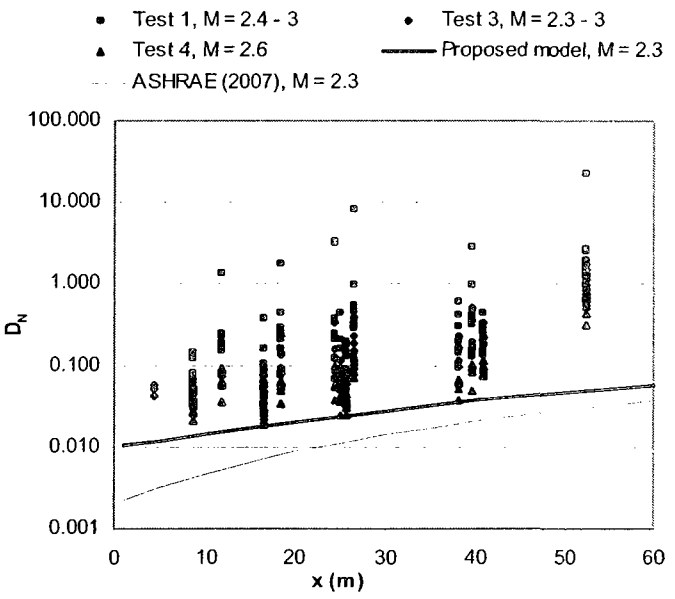

Figure 6.25 Model validations with Stathopoulos et al. (1997) for the high-rise building for h_s = 0.5 m, θ = 210°–220° and M ~ 2–3.

Chapter 7

NEW DEVELOPMENTS, CONCLUSIONS, LIMITATIONS, AND RECOMMENDATIONS

7.1 General

This thesis describes an experimental investigation of dispersion of exhaust from rooftop stacks. The main aim of the study was to extend the current research on flat-roofed buildings to buildings with rooftop structures (RTS). In particular, the downwash effect of RTS on building exhausts has been evaluated. This topic has received little attention in past.

The downwash effect of an RTS located upwind of a stack was investigated by means of flow visualization and tracer gas experiments in a boundary layer wind tunnel. The influence of various parameters on the downwash effect was evaluated. These included building height, RTS crosswind width, stack height, exhaust momentum ratio, stack location, and wind direction. Concentration measurements were obtained for both low-rise and high-rise buildings with and without an RTS. For each configuration, tracer gas concentration was measured on the plume centerline. Measurements were also obtained in the vertical and crosswind directions. The study focused on determining the minimum dilution at rooftop as a function of distance from the source.

Short-range dispersion models recommended by ASHRAE (2003) and ASHRAE (2007) were evaluated. Based on the comparisons between experimental and predicted

dilutions, modifications to the ASHRAE (2007) D_r dispersion model were proposed. In addition to the ASHRAE dispersion models, another qualitative method suggested by ASHRAE, the ASHRAE Geometric Method (AGM) was also evaluated. Modifications to AGM were proposed.

A new empirical model to predict D_{min} was developed that is capable of predicting roof-level dilutions from a stack located on a building roof. The model also incorporates the effect of building height and the downwash effect of an RTS on plume dispersion. The model was validated using results from previous experimental studies.

7.2 New developments in this thesis

- The downwash effect of an RTS was quantified for a wide range of experimental parameters: stack height, exhaust momentum ratio, wind directions, stack locations, building height, and RTS crosswind width.
- The effectiveness of ASHRAE (2003) and ASHRAE (2007) dispersion models in dealing with RTS downwash was evaluated. Several drawbacks were noted and highlighted.
- Modifications were proposed to the ASHRAE (2007) dispersion models to improve the minimum dilution predictions for buildings with and without RTS.
- A modified approach for using the AGM was proposed, which includes the downwash effect of an RTS.

- A new near-field empirical plume dispersion model that takes into account the downwash effect of RTS and building height is proposed and validated. The new model is capable of estimating minimum dilutions for buildings without RTS as well.

7.3 Conclusions

The major conclusions of the study are:

- The ASHRAE dispersion models tend to be either over-conservative or un-conservative depending upon the building/stack/RTS configuration. In general, for low-rise buildings with and without an RTS, the ASHRAE (2003) D_r model is generally un-conservative and the ASHRAE (2007) D_r model is generally overly conservative. The ASHRAE (2003, 2007) D_s model estimates were always overly conservative for all configurations tested.

- The AGM may generate un-conservative stack design for low-rise buildings with an RTS.

- The downwash effect of RTS is more significant if the RTS is exposed to the upstream flow, which is generally the case with low-rise buildings. However, the effect may be negligible if the RTS is engulfed inside the building recirculation zone, which is generally the case with high-rise buildings.

- For the low-rise building with an RTS upwind of the stack:

    - The plume height can decrease by up to 50% depending on the stack height, stack location, and exhaust momentum ratio.

- The roof level dilutions can decrease by a factor of 2 to 100 depending on RTS dimensions, stack location, and exhaust parameters.

- The downwash effect of an RTS is greater for oblique winds than for winds normal to the structure. In general, the roof-level dilution values can be up to half for oblique winds compared to winds approaching normal to a building face.

- The downwash effect of an RTS increases with the RTS crosswind width, reaching a maximum at w/h = 7.5, where w and h are the crosswind width and height of the RTS, respectively.

- The downwash effect of an RTS was significant for $x_s < 2.5h$ where x_s is the separation distance between stack and RTS. The effect was maximum for $x_s = 0.5h$. For $x_s < 2.5h$, the stack height required to escape RTS downwash varied from 1.5h to 3h, depending on the RTS width, plume rise, and stack location.

- Increasing stack height (h_s) or exhaust momentum ratio (M) reduces the downwash effect of RTS on plume.

7.4 Limitations of the present study

- Although from a practical point of view, a 4 m high RTS represents a typical height of penthouse found on building roofs, using a single height of the RTS can be considered as a limitation. Studying the effect of a 4 m tall RTS with varying crosswind widths rather than varying the height was an important simplification.

- The validity of extrapolating the findings of the present study for different RTS heights clearly depends on the extent to which the flow around the studied RTS differs from other RTS cases.

- The experiments were carried out with a single building in order to isolate the effect of RTS on plume dispersion. The presence of nearby upstream buildings could significantly change the flow around the emitting building.

- The experiments were carried for only urban exposure. The influence of upstream exposure on plume dispersion needs further investigation.

- The present study focused on worst-case dilution values at plume center line, which were obtained for the along-wind direction. The influence of RTS on plume in the vertical and crosswind directions needs further investigation.

- The RTS was always located upstream of the stack in order to obtain the worst-case scenario for rooftop receptors. This will not always be the case in real-life situations.

- The experimental work was carried out assuming neutral exhaust. The effect of plume buoyancy needs further investigation.

7.5 Recommendations for future research

There exists a significant scope for further research on building-scale dispersion. The limitations of the present study addressed in the previous section can form the basis for future research on the effect of RTS on building exhaust dispersion.

- The RTS parameters used in the present study can be expanded to include the effect of height and along-wind length of the RTS; as well as size variations. The effect of an RTS located downstream of a stack and the presence of additional RTS should also be considered in any generalized model for RTS effects.

- Additional wind-tunnel measurements would be required to quantify the effect of surrounding buildings for typical configurations, such as a tall building located upstream of a emitting building.

- CFD modeling of wind flow and dispersion around buildings can be used for predicting plume dispersion. However, the development of good CFD modeling would rely on experimental data sets similar to those provided in the present study.

REFERENCES

- ANSI/AIHA Z9.5 (2002) American National Standards Institute. American National Standards Institute, Inc./ American Industrial Hygiene Association NY.

- ASCE-7 (1999) Wind tunnel testing for buildings and other structures. *American Society of Civil Engineers:* Reston VA.

- ASCE (1999) Manual of practice for wind tunnel studies of buildings and structures. Number 67. *American Society of Civil Engineers.* Reston VA.

- ASHRAE (1997) Airflow around buildings (Chapter 15). ASHRAE Fundamentals Handbook. *American Society of Heating, Refrigerating and Air-Conditioning Engineers;* Atlanta, GA.

- ASHRAE (1999) Building Air Intake and Exhaust Design (Chapter 43). ASHRAE Applications Handbook. *American Society of Heating, Refrigerating and Air-Conditioning Engineers*; Atlanta, GA.

- ASHRAE (2003) Building Air Intake and Exhaust Design (Chapter 43). ASHRAE Applications Handbook. *American Society of Heating, Refrigerating and Air-Conditioning Engineers;* Atlanta, GA.

- ASHRAE (2007) Building Air Intake and Exhaust Design (Chapter 44). ASHRAE Applications Handbook *American Society of Heating, Refrigerating and Air-Conditioning Engineers;* Atlanta, GA.

- Bachlin W, Theurer W, and Plate EJ (1991) Wind field and dispersion in a built-up area: a comparison between field measurements and wind tunnel data. *Atmospheric Environment* 25A, No. 7: 1135-1142.

- Bahloul A, Stathopoulos T, Hajra B, and Gupta A (2008) A Comparative study of ADMS, ASHRAE and Wind Tunnel Simulation for Rooftop dispersion of airborne pollutants. Accepted at the *11th International Conference on Indoor Air Quality and Climate.* Technical University of Denmark, Denmark: August 17-22.

- Barrett CF, Hall DJ, and Simmonds AC (1978), Dispersion from Chimneys downwind of cubical buildings – a wind tunnel study, *Proc. NATO/CCMS 9th Int. Mtg. on Air Pollution Modelling and its Applications*: Toronto, Canada: August 28-31.

- Briggs GA (1984) Plume rise and buoyancy effects. In: (D Randerson, ed) *Atmospheric Science and Power Production.* U.S. Department of energy D.O.E./TIC-27601 DE 84005177. Washington, DC.

- Canepa E (2004) An overview about the study of downwash effects on dispersion of airborne pollutants. *Environmental Modelling and Software.* 19: 1077-1087.

- Carruthers DJ, Holroyd RJ, Hunt JCR, Weng WS, Robins AG, Apsley DD, Thompson DJ, and Smith FB (1994) UK-ADMS: A new approach to modelling dispersion in the earth's atmospheric boundary layer. *Journal of Wind Engineering and Industrial Aerodynamics;* 52: 139-153.

- Castro IP and Robins AG (1977) The flow around a surface-mounted cube in uniform and turbulent streams. *Journal of Fluid Mechanics;* 79: 307-335.

- Cermak JE (1995) Physical Modeling of Flow and Dispersion over Urban Areas. Wind Climate in Cities. Kluwer Academic Publishers; Amsterdam: 383-403.

- Cermak JE (1976) Nature of air flow around buildings. *ASHRAE Transactions;* 82: 1044-1060

- Chui EH and Wilson DJ (1988) Effects of varying wind direction on exhaust gas dilution. *Journal of Wind Engineering and Industrial Aerodynamics;* 31: 87-104.

- Counihan J (1969) An improved method of simulating an atmospheric boundary layer in a wind tunnel. *Atmospheric Environment;* 3: 197-214.

- Davenport AG (1963) The relationship of wind structure to wind loading. Presented at the *International Conference on The Wind Effects on Building and Structures.* Teddinton, Middlesex, England: June 26-28.

- EPA (1995) Compilation of Air Pollutant Emission Factors, Volume I: Stationary Point and Area Sources. AP-42, (5th Edition). Office of Air Quality Planning and Standards;

- Fackrell JE (1984a) Parameters characterizing dispersion in the near wake of buildings. *Journal of Wind Engineering and Industrial Aerodynamics;* 16: 97-118.

- Fackrell JE (1984b) An examination of simple models for building influenced dispersion. *Atmospheric Environment;* 18: 89-98.

- Georgakis K, Smith J, Goodfellow H and Pye J (1995) Review and evaluation of models estimating the minimum atmospheric dilution of gases exhausted near buildings. *Journal of the Air and Waste Management Association;* 45: 722-729.

- Gupta A, Saathoff P, and Stathopoulos T (2005a) Plume dispersion on the roof of a building: influence of rooftop structure geometry. *10th Americas Conference on Wind Engineering.* Louisiana: May 31-June 4.

- Gupta A, Saathoff P, and Stathopoulos T (2005b) Effect of building orientating on downwash effect of rooftop structures. *Proceedings of PHYSMOD.* London, ON: August 24-26

- Gupta A (2006) Considering the effect of rooftop structures in modeling exhaust dispersion. *Proceedings of Labs 21.* San Antonio, TX: October 17-19.

- Gupta A, Saathoff P, and Stathopoulos T (2007) Physical modeling of downwash due to rooftop structure. *Proceedings of PHYSMOD.* Orleans, France: August 24-26

- Halitsky J (1961) Vent to intake air circuit. *Air Conditioning, Heating and Ventilation.* pp.81.

- Halitsky J (1962) Diffusion of vented gas around buildings. *Journal of Air Pollution Control and Association;* 2: 74-80.

- Halitsky J (1963) Gas diffusion near buildings. *ASHRAE Transactions;* 69: 464-484.

- Halitsky J (1995). Concentration coefficients in atmospheric dispersion calculations. *ASHRAE Transactions;* 91: 1722-1736.

- Higson HL, Griffiths RF, Jones CD, and Hall DJ (1994) Concentration measurements around an isolated building: a comparison between wind tunnel and field data. *Atmospheric Environment* 28: 1827-1836.

- Higson HL, Griffiths RF, Jones CD, and Biltoft C (1995) Effect of atmospheric stability on concentration fluctuations and wake retention times for dispersion in the vicinity of an isolated building. *Environmetrics;* 6: 571-581.

- Holmes JD 2001. *Wind Loading of Structures*. Spon Press; London.

- Hosker RP (1984) Flow and diffusion near obstacles. In: (D. Randerson, ed) *Atmospheric science and power production* (Chapter 7). US Dept. of Energy, Office of Scientific and Technical Information, Technical Information Centre DOE/TIC-27601, ISBN 0-87079-126-5.

- Hosker RP (1985) Flow around isolated structures and building clusters: a review. *ASHRAE Transactions;* 91, 1672-1692

- Hoven V. (1957) Power spectrum of horizontal wind speeding the frequency range from 0.0007 to 900 cycles per hour. *Journal of Meteorology*; 14, 160-164.

- Huber AH and Snyder WH (1982) Wind tunnel investigation of the effects of a rectangular-shaped building on dispersion of effluents from short adjacent stacks. *Atmospheric Environment;* 16: 2837-2848.

- Huber AH (1988) Performance of a Gaussian model for centerline concentrations in the wake of buildings. *Atmospheric Environment;* 22: 1039–1050.

- Huber AH and Snyder WH (1989) The influence of building width and orientation on plume dispersion in wake of building. *Atmospheric Environment;* 16: 2837-2848.

- Huber AH (1991) Wind tunnel and Gaussian plume modeling of building wake dispersion. *Atmospheric Environment;* 7: 1199-1209.

- Hunt JCR, Abell CJ, Peterka JA, and Woo HCG (1978) Kinematical studies of flows around free or surface mounted obstacles; applying topology to flow visualisation. *Journal of Fluid Mechanics;* 86: 179-200.

- Isyumov N and Tanaka, H (1979) Wind tunnel modelling of stack gas dispersion - difficulties and approximations. *Proceedings of fifth international conference on wind engineering.* Fort Collins, Colorado, USA. July 9-14

- Lamb B and Cronn D (1986) Fume hood exhaust re-entry into a chemistry building. *Journal of the American Industrial Hygiene Association;* 47: 115-123.

- Li W and Meroney RN (1983) Gas dispersion near a cubical model building. *Journal of Wind Engineering and Industrial Aerodynamics;* 12: 15-23.

- Lowery KP and Jacko RB (1996) A wind tunnel study into the effects of raised intakes and parapets on fresh air intake contamination by a rooftop stack. *Journal of the Air and Waste Management Association; 46:* 847-852.

- Lucas DH (1972) Choosing chimney heights in presence of buildings. *Proceedings of International Clean Air Conference.* Melbourne; May 15-18: pp.47-52.

- Meroney RN (1982) Turbulent diffusion near buildings. In: (EJ Plate, ed) *Engineering Meteorology* (Chapter 10). Elsevier; Amsterdam: Ch 10, 481-525.

- Meroney RN (1990) Bluff body aerodynamics influence on transport and diffusion. *Journal of Wind Engineering and Industrial Aerodynamics;* 33: 21-33.

- Meroney R.N (1990) Perspectives on air pollution aerodynamics, Plenary Session Paper, *10th International Wind Engineering Conference*, Copenhagen, Denmark, June 21-25.

- Mirzai MH, Harvey JK, and Jones CD (1994) Wind tunnel investigation of dispersion of pollutants due to wind flow around a small building. *Atmospheric Environment;* 28: 1819–1826.

- Ogawa Y, Oikawa S, and Uehara K (1983) Field and wind-tunnel study of the flow and diffusion around a model cube-I flow measurements. *Atmospheric Environment;* 17: 1145-1159.

- Oikawa S and Meng Y (1997) A field study of diffusion around a model cube in a suburban area. *Boundary-Layer Meteorology;* 84: 399-410.

- Perera MD, Tull RG, White MK and Walker RR (1991) Assessing intake contamination from atmospheric dispersion of building exhaust. *12th AIVC Conference*. Ottawa, ON: 347-357.

- Peterka JA, Meroney RN, and Kothori KM (1985) Wind flow patterns about buildings. *Journal of Wind Engineering and Industrial Aerodynamics;* 21: 21-38.

- Petersen RL (1986) Wind tunnel investigation on the effect of platform-type structures on dispersion of effluents from short stacks. *Journal of the Air Pollution Control Association;* 36: 1347-1352.

- Petersen RL and Wilson DJ (1989) Analytical versus wind tunnel determined concentrations due to laboratory exhaust. *ASHRAE Transactions;* 95 (2): 729-736.

- Petersen RL and Ratcliff MA (1991) An objective approach to laboratory stack design. *ASHRAE Transactions;* 97 (2): 553-561.

- Petersen RL, Carter JJ, and Ratcliff M (1999) Influence of architectural screens on rooftop concentrations due to effluent from short stacks. *ASHRAE Transactions;* 105(1).

- Petersen RL (2002a) Assessing the Re-entry of Laboratory Pollutants Into the Indoor Environment–Analytical, Computational Fluid Dynamics or Wind-Tunnel Modeling? *Proceedings of Labs 21.* Washington DC: January 8-10.

- Petersen RL, Cochran C and LeCompte JW (2002b) Specifying exhaust systems that avoid fume re-entry and adverse health effects. *ASHRAE Transaction;* 108(1).

- Petersen RL, and LeCompte JW (2002c) Exhaust contamination of hidden versus visible intakes. ASHRAE *Research report 1168-TRP.*

- Petersen RL, and Reifschneider JD (2008) The effect of ganging on pollutant dispersion from building exhausts.. *ASHRAE Ttransactions;* 114: 458-470

- Ramsdell JV (1990) Diffusion in building wakes for ground-level releases. *Atmospheric Environment;* 24: 377–388.

- Ramsdell JV and Fosmire CJ (1998a) Estimating concentrations in plumes released in the vicinity of buildings: model development. *Atmospheric Environment;* 32: 1663–1677.

- Ramsdell JV and Fosmire CJ (1998b) Estimating concentrations in plumes released in the vicinity of buildings: model evaluation. *Atmospheric Environment;* 32: 1679–1689.

- Robins AG and Macdonald R (1999) A review of flow and dispersion in the vicinity of groups of buildings. ME-FD/99.93, University of Surrey; Guildford, UK.

- Saathoff P, Stathopoulos T, and Dobrescu M (1995) Effects of model scale in estimating pollutant dispersion near buildings. *Journal of Wind Engineering and Industrial Aerodynamics;* 54/55: 549-559.

- Saathoff P, Wu H, Stathopoulos T (1996) Dilution of exhausts from rooftop stacks – Comparison of wind tunnel data with full-scale measurements. *Proceeding of 9th Joint Conference on Applications of Air Pollution Meteorology; Atlanta*: 341-345.

- Saathoff T, Stathopoulos T, and Wu H (1998) The influence of free-stream turbulence on near field dilution of exhaust from building vents. *Journal of Wind Engineering and Industrial. Aerodynamics;* 77/78: 741-752.

- Saathoff P, Gupta A, Stathopoulos T, and Lazure L (2003a) Effect of roof top structures on the plume from a nearby stack. *Proceedings of 11th International Conference on Wind Engineering.* Lubbock, TX: June 2-5.

- Saathoff P, Gupta A, Stathopoulos T, and Lazure L (2003b) Dispersion of emissions from a low building located downwind a building. *Proceedings of International Workshop on Physical Modeling of Flow and Dispersion Phenomena.* Prato, Italy: September 3-5.

- Saathoff P, Gupta A, Stathopoulos T, and Lazure L (2008) Contamination of fresh air intakes due to downwash from a rooftop structure. *Journal of the Air and Waste Management Association*; In press.

- Schulman LL and Scire JS (1991) Effect of stack height, exhaust speed, and wind direction on concentrations from a rooftop stack. *ASHRAE transaction;* 573-585.

- Schulman LL, Strimaitis DG, and Scire JS (2000) Development and evaluation of the PRIME plume rise and building downwash model. *Journal of Air and Waste Management Association;* 50: 378–390.

- Schulze RH (1995) Balancing simplicity with accuracy in the use of dispersion modeling in the United States. *International Journal of Environmental Pollution;* 5: 521-529.

- Schuyler GD and Turner GG (1989) Comparison of wind tunnel test results with empirical exhaust dilution factors. *ASHRAE Transactions;* 952: 737-744.

- Singh S, Fulker MJ, and Marshall G (1994) A wind tunnel examination of the variation of sigma y and sigma z with selected parameters. *Atmospheric Environment;* 28 (11): 1837-1848.

- Snyder WH and Lawson RE (1976) Determination of a necessary height for a stack close to a building: a wind-tunnel study. *Atmospheric Environment;* 10: 683-691.

- Snyder WH (1981) Guidelines for fluid modeling of atmospheric diffusion. USEPA Report EPA-600/8-81-009. *EPA Office of Air Quality Planning and Standards.* Research Triangle Park, NC.

- Snyder WH (1994) Downwash of plumes in the vicinity of buildings: a wind tunnel study. *Recent Research Advances in the Fluid Mechanics of Turbulent Jets and Plumes.* Kluwer Academic Pub.; 343-356.

- Snyder WH and Lawson RE (1994) Wind-tunnel measurements of flow fields in the vicinity of buildings. *Proceedings of 8th AMS Conference on Applied Air Pollution Meteorology, with AWMA.* Nashville, TN: January 23-28.

- Snyder WH (2005) Streamline patterns around buildings deduced from wind-tunnel measurement. *Proceedings of Physmod.* London, ON: August 24-26

- Stathopoulos T (1984) Design and fabrication of wind tunnel for building aerodynamics. *Journal of Wind Engineering and Industrial Aerodynamics;* 54/55: 549-559.

- Stathopoulos T, Lazure L, Saathoff P, and Wei X (2002) Dilution of exhaust from a roof top stack on a cubical building in an urban environment. *Atmospheric Environment;* 36: 4577-4591.

- Stathopoulos T, Lazure L, Saathoff P, and Gupta A (2003) The effect of stack height, stack location and rooftop structures or air intake contamination: a laboratory and full scale study. Research report. *IRSST Institut de recherche Robert-Sauvé en santé et en sécurité du travail.* Montréal, QC.

- Stathopoulos T, Lazure L, Saathoff P, and Gupta A (2004) Wind-induced dispersion of exhaust in urban environment. *Proceedings of International Workshop on Wind Engineering and Wind Sciences.* New Delhi: October 29-30.

- Thompson K, Wong E, Slusarzik J (2002) Reducing stack height – Understanding the formation of rooftop recirculation zones. *Proceedings of Labs 21.* Durham, NC: October 7-9.

- Thompson R (1993) Building amplification factors for sources near buildings: a wind tunnel study. *Atmospheric Environment;* 27: 2313-2325.

- Turner D (1994) *Workbook of Atmospheric Dispersion Estimates.* (2nd Edition). CRC Press; London.

- Weiringa J (1992) Updating the Davenport terrain roughness classification. *Journal of Wind Engineering and Industrial Aerodynamics;* 41: 357-368.

- Wilson DJ (1976) Contamination of air intakes from roof exhaust vents. *ASHRAE Transactions;* 8: 1024-1038.

- Wilson DJ (1977) Dilution of exhaust gases from building surface vents. *ASHRAE Transactions;* 83: 168-176.

- Wilson DJ and Netterville DJ (1978) Interaction of a roof level plume with a downwind building. *Atmospheric Environment;* 12: 1051-1059.

- Wilson DJ (1979) Flow patterns over flat-roofed buildings and application to exhaust stack design. *ASHRAE Transactions;* 85: 284-295.

- Wilson DJ and Winkel G (1982) The effect of varying exhaust stack height on contaminant concentration at roof level. *ASHRAE Transactions;* 88: 513-533

- Wilson DJ and Britter RE (1982) Estimates of building surface concentrations from nearby point sources. *Atmospheric Environment;* 16: 2631-2646.

- Wilson DJ and Chui EH (1985) Influence of exhaust velocity and wind incidence angle on dilution from roof vents. *ASHRAE Transactions;* 91: 1693-1706.

- Wilson DJ and Chui EH (1987) Effect of turbulence from upwind buildings on dilution of exhaust gases. *ASHRAE Transactions;* 93: 2186-2197.

- Wilson DJ and Chui EH (1994) Influence of building size on rooftop dispersion of exhaust gas. *Atmospheric Environment;* 28: 2325-2334.

- Wilson DJ and Lamb BK (1994) Dispersion of exhaust gases from roof-level stacks and vents on a laboratory building. *Atmospheric Environment;* 28 (15): 3099-3111.

- Wilson DJ, Fabris I, Chen J, and Ackerman M (1998) Adjacent building effects on laboratory fume hood exhaust stack design. *ASHRAE Transaction; 104* : 1012-1027.

- Wong E, Ratcliff R (2002) Dilution criteria for laboratory fume hood exhausts. *Proceedings of Labs 21.* Washington DC: January 8-10.

APPENDIX A

List of experimental cases for the comprehensive study

Test cases with the low-rise building with cross-wind width 50 m (see Figure 3.3a)

Test Number	RTS-length	RTS-width	RTS-height	Building type	Stack location	Stack height (m)	Exhaust momentum	Wind speed (m/s)	Wind direction (degrees)	concentration profile
1	NA	NA	NA	LR-1	1	1	1	5.4	0	along-wind
2	NA	NA	NA	LR-1	1	1	2	5.4	0	along-wind
3	NA	NA	NA	LR-1	1	1	3	5.4	0	along-wind
4	NA	NA	NA	LR-1	1	1	5	5.4	0	along-wind
5	NA	NA	NA	LR-1	1	2	1	5.4	0	along-wind
6	NA	NA	NA	LR-1	1	2	2	5.4	0	along-wind
7	NA	NA	NA	LR-1	1	2	3	5.4	0	along-wind
8	NA	NA	NA	LR-1	1	2	5	5.4	0	along-wind
9	NA	NA	NA	LR-1	1	3	1	5.4	0	along-wind
10	NA	NA	NA	LR-1	1	3	2	5.4	0	along-wind
11	NA	NA	NA	LR-1	1	3	3	5.4	0	along-wind
12	NA	NA	NA	LR-1	1	3	5	5.4	0	along-wind
13	NA	NA	NA	LR-1	1	5	1	5.4	0	along-wind
14	NA	NA	NA	LR-1	1	5	2	5.4	0	along-wind
15	NA	NA	NA	LR-1	1	5	3	5.4	0	along-wind
16	NA	NA	NA	LR-1	1	5	5	5.4	0	along-wind
17	NA	NA	NA	LR-1	1	7	1	5.4	0	along-wind
18	NA	NA	NA	LR-1	1	7	2	5.4	0	along-wind
19	NA	NA	NA	LR-1	1	7	3	5.4	0	along-wind
20	NA	NA	NA	LR-1	1	7	5	5.4	0	along-wind
21	NA	NA	NA	LR-1	2	3	2	5.4	0	along-wind
22	NA	NA	NA	LR-1	2	5	5	5.4	0	along-wind
23	NA	NA	NA	LR-1	3	3	2	5.4	0	along-wind
24	NA	NA	NA	LR-1	3	5	5	5.4	0	along-wind
25	NA	NA	NA	LR-1	4	3	2	5.4	0	along-wind
26	NA	NA	NA	LR-1	4	5	2	5.4	0	along-wind
27	NA	NA	NA	LR-1	1	1	2	5.4	0	vertical
28	NA	NA	NA	LR-1	1	3	2	5.4	0	vertical
29	NA	NA	NA	LR-1	1	5	2	5.4	0	vertical
30	NA	NA	NA	LR-1	1	1	2	5.4	0	cross-wind
31	NA	NA	NA	LR-1	1	3	2	5.4	0	cross-wind
32	NA	NA	NA	LR-1	1	5	2	5.4	0	cross-wind
33	8	10	4	LR-1	1	1	1	5.4	0	along-wind
34	8	20	4	LR-1	1	1	1	5.4	0	along-wind
35	8	30	4	LR-1	1	1	1	5.4	0	along-wind
36	8	40	4	LR-1	1	1	1	5.4	0	along-wind
37	8	50	4	LR-1	1	1	1	5.4	0	along-wind
38	8	10	4	LR-1	1	1	2	5.4	0	along-wind
39	8	20	4	LR-1	1	1	2	5.4	0	along-wind
40	8	30	4	LR-1	1	1	2	5.4	0	along-wind
41	8	40	4	LR-1	1	1	2	5.4	0	along-wind
42	8	50	4	LR-1	1	1	2	5.4	0	along-wind
43	8	10	4	LR-1	1	1	3	5.4	0	along-wind
44	8	20	4	LR-1	1	1	3	5.4	0	along-wind
45	8	30	4	LR-1	1	1	3	5.4	0	along-wind
46	8	40	4	LR-1	1	1	3	5.4	0	along-wind
47	8	50	4	LR-1	1	1	3	5.4	0	along-wind
48	8	10	4	LR-1	1	1	5	5.4	0	along-wind
49	8	20	4	LR-1	1	1	5	5.4	0	along-wind
50	8	30	4	LR-1	1	1	5	5.4	0	along-wind
51	8	40	4	LR-1	1	1	5	5.4	0	along-wind
52	8	50	4	LR-1	1	1	5	5.4	0	along-wind

53	8	10	4	LR-1	1	3	1	5.4	0	along-wind
54	8	20	4	LR-1	1	3	1	5.4	0	along-wind
55	8	30	4	LR-1	1	3	1	5.4	0	along-wind
56	8	40	4	LR-1	1	3	1	5.4	0	along-wind
57	8	50	4	LR-1	1	3	1	5.4	0	along-wind
58	8	10	4	LR-1	1	3	2	5.4	0	along-wind
59	8	20	4	LR-1	1	3	2	5.4	0	along-wind
60	8	30	4	LR-1	1	3	2	5.4	0	along-wind
61	8	40	4	LR-1	1	3	2	5.4	0	along-wind
62	8	50	4	LR-1	1	3	2	5.4	0	along-wind
63	8	10	4	LR-1	1	3	3	5.4	0	along-wind
64	8	20	4	LR-1	1	3	3	5.4	0	along-wind
65	8	30	4	LR-1	1	3	3	5.4	0	along-wind
66	8	40	4	LR-1	1	3	3	5.4	0	along-wind
67	8	50	4	LR-1	1	3	3	5.4	0	along-wind
68	8	10	4	LR-1	1	3	5	5.4	0	along-wind
69	8	20	4	LR-1	1	3	5	5.4	0	along-wind
70	8	30	4	LR-1	1	3	5	5.4	0	along-wind
71	8	40	4	LR-1	1	3	5	5.4	0	along-wind
72	8	50	4	LR-1	1	3	5	5.4	0	along-wind
73	8	10	4	LR-1	1	5	1	5.4	0	along-wind
74	8	20	4	LR-1	1	5	1	5.4	0	along-wind
75	8	30	4	LR-1	1	5	1	5.4	0	along-wind
76	8	40	4	LR-1	1	5	1	5.4	0	along-wind
77	8	50	4	LR-1	1	5	1	5.4	0	along-wind
78	8	10	4	LR-1	1	5	2	5.4	0	along-wind
79	8	20	4	LR-1	1	5	2	5.4	0	along-wind
80	8	30	4	LR-1	1	5	2	5.4	0	along-wind
81	8	40	4	LR-1	1	5	2	5.4	0	along-wind
82	8	50	4	LR-1	1	5	2	5.4	0	along-wind
83	8	10	4	LR-1	1	5	3	5.4	0	along-wind
84	8	20	4	LR-1	1	5	3	5.4	0	along-wind
85	8	30	4	LR-1	1	5	3	5.4	0	along-wind
86	8	40	4	LR-1	1	5	3	5.4	0	along-wind
87	8	50	4	LR-1	1	5	3	5.4	0	along-wind
88	8	10	4	LR-1	1	5	5	5.4	0	along-wind
89	8	20	4	LR-1	1	5	5	5.4	0	along-wind
90	8	30	4	LR-1	1	5	5	5.4	0	along-wind
91	8	40	4	LR-1	1	5	5	5.4	0	along-wind
92	8	50	4	LR-1	1	5	5	5.4	0	along-wind
93	8	10	4	LR-1	1	7	1	5.4	0	along-wind
94	8	20	4	LR-1	1	7	1	5.4	0	along-wind
95	8	30	4	LR-1	1	7	1	5.4	0	along-wind
96	8	40	4	LR-1	1	7	1	5.4	0	along-wind
97	8	50	4	LR-1	1	7	1	5.4	0	along-wind
98	8	10	4	LR-1	1	7	2	5.4	0	along-wind
99	8	20	4	LR-1	1	7	2	5.4	0	along-wind
100	8	30	4	LR-1	1	7	2	5.4	0	along-wind
101	8	40	4	LR-1	1	7	2	5.4	0	along-wind
102	8	50	4	LR-1	1	7	2	5.4	0	along-wind
103	8	10	4	LR-1	1	7	3	5.4	0	along-wind
104	8	20	4	LR-1	1	7	3	5.4	0	along-wind
105	8	30	4	LR-1	1	7	3	5.4	0	along-wind
106	8	40	4	LR-1	1	7	3	5.4	0	along-wind
107	8	50	4	LR-1	1	7	3	5.4	0	along-wind
108	8	10	4	LR-1	1	7	5	5.4	0	along-wind
109	8	20	4	LR-1	1	7	5	5.4	0	along-wind

110	8	30	4	LR-1	1	7	5	5.4	0	along-wind
111	8	40	4	LR-1	1	7	5	5.4	0	along-wind
112	8	50	4	LR-1	1	7	5	5.4	0	along-wind
113	8	30	4	LR-1	2	3	2	5.4	0	along-wind
114	8	30	4	LR-1	3	3	2	5.4	0	along-wind
115	8	30	4	LR-1	4	3	2	5.4	0	along-wind
116	8	30	4	LR-1	2	5	2	5.4	0	along-wind
117	8	30	4	LR-1	3	5	2	5.4	0	along-wind
118	8	30	4	LR-1	4	5	2	5.4	0	along-wind
119	8	10	4	LR-1	1	1	2	5.4	0	vertical
120	8	10	4	LR-1	1	3	2	5.4	0	vertical
121	8	10	4	LR-1	1	5	2	5.4	0	vertical
122	8	10	4	LR-1	1	1	2	5.4	0	cross-wind
123	8	10	4	LR-1	1	3	2	5.4	0	cross-wind
124	8	10	4	LR-1	1	5	2	5.4	0	cross-wind
125	8	30	4	LR-1	1	1	2	5.4	0	vertical
126	8	30	4	LR-1	1	3	2	5.4	0	vertical
127	8	30	4	LR-1	1	5	2	5.4	0	vertical
128	8	30	4	LR-1	1	1	2	5.4	0	cross-wind
129	8	30	4	LR-1	1	3	2	5.4	0	cross-wind
130	8	30	4	LR-1	1	5	2	5.4	0	cross-wind
131	NA	NA	NA	LR-1	1	1	1	5.4	45	along-wind
132	NA	NA	NA	LR-1	1	1	2	5.4	45	along-wind
133	NA	NA	NA	LR-1	1	1	3	5.4	45	along-wind
134	NA	NA	NA	LR-1	1	1	5	5.4	45	along-wind
135	NA	NA	NA	LR-1	1	2	1	5.4	45	along-wind
136	NA	NA	NA	LR-1	1	2	2	5.4	45	along-wind
137	NA	NA	NA	LR-1	1	2	3	5.4	45	along-wind
138	NA	NA	NA	LR-1	1	2	5	5.4	45	along-wind
139	NA	NA	NA	LR-1	1	3	1	5.4	45	along-wind
140	NA	NA	NA	LR-1	1	3	2	5.4	45	along-wind
141	NA	NA	NA	LR-1	1	3	3	5.4	45	along-wind
142	NA	NA	NA	LR-1	1	3	5	5.4	45	along-wind
143	NA	NA	NA	LR-1	1	5	1	5.4	45	along-wind
144	NA	NA	NA	LR-1	1	5	2	5.4	45	along-wind
145	NA	NA	NA	LR-1	1	5	3	5.4	45	along-wind
146	NA	NA	NA	LR-1	1	5	5	5.4	45	along-wind
147	NA	NA	NA	LR-1	1	7	1	5.4	45	along-wind
148	NA	NA	NA	LR-1	1	7	2	5.4	45	along-wind
149	NA	NA	NA	LR-1	1	7	3	5.4	45	along-wind
150	NA	NA	NA	LR-1	1	7	5	5.4	45	along-wind
151	8	30	4	LR-1	1	1	1	5.4	45	along-wind
152	8	30	4	LR-1	1	1	2	5.4	45	along-wind
153	8	30	4	LR-1	1	1	3	5.4	45	along-wind
154	8	30	4	LR-1	1	1	5	5.4	45	along-wind
155	8	30	4	LR-1	1	2	1	5.4	45	along-wind
156	8	30	4	LR-1	1	2	2	5.4	45	along-wind
157	8	30	4	LR-1	1	2	3	5.4	45	along-wind
158	8	30	4	LR-1	1	2	5	5.4	45	along-wind
159	8	30	4	LR-1	1	3	1	5.4	45	along-wind
160	8	30	4	LR-1	1	3	2	5.4	45	along-wind
161	8	30	4	LR-1	1	3	3	5.4	45	along-wind
162	8	30	4	LR-1	1	3	5	5.4	45	along-wind
163	8	30	4	LR-1	1	5	1	5.4	45	along-wind
164	8	30	4	LR-1	1	5	2	5.4	45	along-wind
165	8	30	4	LR-1	1	5	3	5.4	45	along-wind
166	8	30	4	LR-1	1	5	5	5.4	45	along-wind

167	8	30	4	LR-1	1	7	1	5.4	45	along-wind
168	8	30	4	LR-1	1	7	2	5.4	45	along-wind
169	8	30	4	LR-1	1	7	3	5.4	45	along-wind
170	8	30	4	LR-1	1	7	5	5.4	45	along-wind
171	8	10	4	LR-1	1	3	2	5.4	45	along-wind
172	8	20	4	LR-1	1	3	2	5.4	45	along-wind
173	8	30	4	LR-1	1	3	2	5.4	45	along-wind
174	8	40	4	LR-1	1	3	2	5.4	45	along-wind
175	8	50	4	LR-1	1	3	2	5.4	45	along-wind
176	8	10	4	LR-1	1	5	2	5.4	45	along-wind
177	8	20	4	LR-1	1	5	2	5.4	45	along-wind
178	8	30	4	LR-1	1	5	2	5.4	45	along-wind
179	8	40	4	LR-1	1	5	2	5.4	45	along-wind
180	8	50	4	LR-1	1	5	2	5.4	45	along-wind
181	8	10	4	LR-1	1	3	5	5.4	45	along-wind
182	8	20	4	LR-1	1	3	5	5.4	45	along-wind
183	8	30	4	LR-1	1	3	5	5.4	45	along-wind
184	8	40	4	LR-1	1	3	5	5.4	45	along-wind
185	8	50	4	LR-1	1	3	5	5.4	45	along-wind
186	8	10	4	LR-1	1	5	5	5.4	45	along-wind
187	8	20	4	LR-1	1	5	5	5.4	45	along-wind
188	8	30	4	LR-1	1	5	5	5.4	45	along-wind
189	8	40	4	LR-1	1	5	5	5.4	45	along-wind
190	8	50	4	LR-1	1	5	5	5.4	45	along-wind
191	NA	NA	NA	LR-1	1	1	2	5.4	45	vertical
192	NA	NA	NA	LR-1	1	3	2	5.4	45	vertical
193	NA	NA	NA	LR-1	1	5	2	5.4	45	vertical
194	8	10	4	LR-1	1	1	2	5.4	45	vertical
195	8	10	4	LR-1	1	3	2	5.4	45	vertical
196	8	10	4	LR-1	1	5	2	5.4	45	vertical
197	8	30	4	LR-1	1	1	2	5.4	45	vertical
198	8	30	4	LR-1	1	3	2	5.4	45	vertical
199	8	30	4	LR-1	1	5	2	5.4	45	vertical
200	NA	NA	NA	LR-1	1	1	2	5.4	45	cross-wind
201	NA	NA	NA	LR-1	1	3	2	5.4	45	cross-wind
202	NA	NA	NA	LR-1	1	5	2	5.4	45	cross-wind
203	8	10	4	LR-1	1	1	2	5.4	45	cross-wind
204	8	10	4	LR-1	1	3	2	5.4	45	cross-wind
205	8	10	4	LR-1	1	5	2	5.4	45	cross-wind
206	8	30	4	LR-1	1	1	2	5.4	45	cross-wind
207	8	30	4	LR-1	1	3	2	5.4	45	cross-wind
208	8	30	4	LR-1	1	5	2	5.4	45	cross-wind
209	NA	NA	NA	LR-1	2	3	2	5.4	45	along-wind
210	NA	NA	NA	LR-1	2	5	5	5.4	45	along-wind
211	8	60	4	LR-1	2	3	2	5.4	45	along-wind
212	8	90	4	LR-1	2	5	2	5.4	45	along-wind
213	NA	NA	NA	LR-1	3	3	2	5.4	45	along-wind
214	NA	NA	NA	LR-1	3	5	5	5.4	45	along-wind
215	8	70	4	LR-1	3	3	2	5.4	45	along-wind
216	8	100	4	LR-1	3	5	2	5.4	45	along-wind
217	NA	NA	NA	LR-1	4	3	2	5.4	45	along-wind
218	NA	NA	NA	LR-1	4	5	2	5.4	45	along-wind
219	8	80	4	LR-1	4	3	2	5.4	45	along-wind
220	8	110	4	LR-1	4	5	2	5.4	45	along-wind
221	NA	NA	NA	HR	1	1	1	5.4	0	along-wind
222	NA	NA	NA	HR	1	1	2	5.4	0	along-wind
223	NA	NA	NA	HR	1	1	3	5.4	0	along-wind

224	NA	NA	NA	HR	1	1	5	5.4	0	along-wind
225	NA	NA	NA	HR	1	3	2	5.4	0	along-wind
226	NA	NA	NA	HR	1	3	3	5.4	0	along-wind
227	NA	NA	NA	HR	1	3	5	5.4	0	along-wind
228	NA	NA	NA	HR	1	5	1	5.4	0	along-wind
229	NA	NA	NA	HR	1	5	2	5.4	0	along-wind
230	NA	NA	NA	HR	1	5	3	5.4	0	along-wind
231	NA	NA	NA	HR	1	5	5	5.4	0	along-wind
232	NA	NA	NA	HR	1	7	1	5.4	0	along-wind
233	NA	NA	NA	HR	1	7	2	5.4	0	along-wind
234	NA	NA	NA	HR	1	7	3	5.4	0	along-wind
235	NA	NA	NA	HR	1	7	5	5.4	45	along-wind
236	NA	NA	NA	HR	1	1	1	5.4	45	along-wind
237	NA	NA	NA	HR	1	1	2	5.4	45	along-wind
238	NA	NA	NA	HR	1	1	5	5.4	45	along-wind
239	NA	NA	NA	HR	1	3	1	5.4	45	along-wind
240	NA	NA	NA	HR	1	3	2	5.4	45	along-wind
241	NA	NA	NA	HR	1	3	3	5.4	45	along-wind
242	NA	NA	NA	HR	1	3	5	5.4	45	along-wind
243	NA	NA	NA	HR	1	5	2	5.4	45	along-wind
244	NA	NA	NA	HR	1	5	5	5.4	45	along-wind
245	NA	NA	NA	HR	2	3	2	5.4	0	along-wind
246	NA	NA	NA	HR	3	3	2	5.4	0	along-wind
247	NA	NA	NA	HR	4	3	2	5.4	0	along-wind
248	NA	NA	NA	HR	2	5	2	5.4	0	along-wind
249	NA	NA	NA	HR	3	5	2	5.4	0	along-wind
250	NA	NA	NA	HR	4	5	2	5.4	0	along-wind
251	NA	NA	NA	HR	2	3	2	5.4	45	along-wind
252	NA	NA	NA	HR	3	3	2	5.4	45	along-wind
253	NA	NA	NA	HR	4	3	2	5.4	45	along-wind
254	NA	NA	NA	HR	2	5	2	5.4	45	along-wind
255	NA	NA	NA	HR	3	5	2	5.4	45	along-wind
256	NA	NA	NA	HR	4	5	2	5.4	45	along-wind
257	NA	NA	NA	HR	1	1	1	5.4	0	cross-wind
258	NA	NA	NA	HR	1	5	1	5.4	0	cross-wind
259	NA	NA	NA	HR	1	1	5	5.4	0	cross-wind
260	NA	NA	NA	HR	1	5	5	5.4	0	cross-wind
261	NA	NA	NA	HR	1	1	1	5.4	45	cross-wind
262	NA	NA	NA	HR	1	5	1	5.4	45	cross-wind
263	NA	NA	NA	HR	1	1	5	5.4	45	cross-wind
264	NA	NA	NA	HR	1	5	5	5.4	45	cross-wind
265	8	10	4	HR	1	1	1	5.4	0	along-wind
266	8	20	4	HR	1	1	1	5.4	0	along-wind
267	8	30	4	HR	1	1	1	5.4	0	along-wind
268	8	40	4	HR	1	1	1	5.4	0	along-wind
269	8	50	4	HR	1	1	1	5.4	0	along-wind
270	8	10	4	HR	1	1	2	5.4	0	along-wind
271	8	20	4	HR	1	1	2	5.4	0	along-wind
272	8	30	4	HR	1	1	2	5.4	0	along-wind
273	8	40	4	HR	1	1	2	5.4	0	along-wind
274	8	50	4	HR	1	1	2	5.4	0	along-wind
275	8	10	4	HR	1	1	3	5.4	0	along-wind
276	8	20	4	HR	1	1	3	5.4	0	along-wind
277	8	30	4	HR	1	1	3	5.4	0	along-wind
278	8	40	4	HR	1	1	3	5.4	0	along-wind
279	8	50	4	HR	1	1	3	5.4	0	along-wind
280	8	10	4	HR	1	1	5	5.4	0	along-wind

281	8	20	4	HR	1	1	5	5.4	0	along-wind
282	8	30	4	HR	1	1	5	5.4	0	along-wind
283	8	40	4	HR	1	1	5	5.4	0	along-wind
284	8	50	4	HR	1	1	5	5.4	0	along-wind
285	8	10	4	HR	1	3	1	5.4	0	along-wind
286	8	20	4	HR	1	3	1	5.4	0	along-wind
287	8	30	4	HR	1	3	1	5.4	0	along-wind
288	8	40	4	HR	1	3	1	5.4	0	along-wind
289	8	50	4	HR	1	3	1	5.4	0	along-wind
290	8	10	4	HR	1	3	2	5.4	0	along-wind
291	8	20	4	HR	1	3	2	5.4	0	along-wind
292	8	30	4	HR	1	3	2	5.4	0	along-wind
293	8	40	4	HR	1	3	2	5.4	0	along-wind
294	8	50	4	HR	1	3	2	5.4	0	along-wind
295	8	10	4	HR	1	3	3	5.4	0	along-wind
296	8	20	4	HR	1	3	3	5.4	0	along-wind
297	8	30	4	HR	1	3	3	5.4	0	along-wind
298	8	40	4	HR	1	3	3	5.4	0	along-wind
299	8	50	4	HR	1	3	3	5.4	0	along-wind
300	8	10	4	HR	1	3	5	5.4	0	along-wind
301	8	20	4	HR	1	3	5	5.4	0	along-wind
302	8	30	4	HR	1	3	5	5.4	0	along-wind
303	8	40	4	HR	1	3	5	5.4	0	along-wind
304	8	50	4	HR	1	3	5	5.4	0	along-wind
305	8	10	4	HR	1	5	1	5.4	0	along-wind
306	8	20	4	HR	1	5	1	5.4	0	along-wind
307	8	30	4	HR	1	5	1	5.4	0	along-wind
308	8	40	4	HR	1	5	1	5.4	0	along-wind
309	8	50	4	HR	1	5	1	5.4	0	along-wind
310	8	10	4	HR	1	5	2	5.4	0	along-wind
311	8	20	4	HR	1	5	2	5.4	0	along-wind
312	8	30	4	HR	1	5	2	5.4	0	along-wind
313	8	40	4	HR	1	5	2	5.4	0	along-wind
314	8	50	4	HR	1	5	2	5.4	0	along-wind
315	8	10	4	HR	1	5	3	5.4	0	along-wind
316	8	20	4	HR	1	5	3	5.4	0	along-wind
317	8	30	4	HR	1	5	3	5.4	0	along-wind
318	8	40	4	HR	1	5	3	5.4	0	along-wind
319	8	50	4	HR	1	5	3	5.4	0	along-wind
320	8	10	4	HR	1	5	5	5.4	0	along-wind
321	8	20	4	HR	1	5	5	5.4	0	along-wind
322	8	30	4	HR	1	5	5	5.4	0	along-wind
323	8	40	4	HR	1	5	5	5.4	0	along-wind
324	8	50	4	HR	1	5	5	5.4	0	along-wind
325	8	10	4	HR	1	7	1	5.4	0	along-wind
326	8	20	4	HR	1	7	1	5.4	0	along-wind
327	8	30	4	HR	1	7	1	5.4	0	along-wind
328	8	40	4	HR	1	7	1	5.4	0	along-wind
329	8	50	4	HR	1	7	1	5.4	0	along-wind
330	8	10	4	HR	1	7	2	5.4	0	along-wind
331	8	20	4	HR	1	7	2	5.4	0	along-wind
332	8	30	4	HR	1	7	2	5.4	0	along-wind
333	8	40	4	HR	1	7	2	5.4	0	along-wind
334	8	50	4	HR	1	7	2	5.4	0	along-wind
335	8	10	4	HR	1	7	3	5.4	0	along-wind
336	8	20	4	HR	1	7	3	5.4	0	along-wind
337	8	30	4	HR	1	7	3	5.4	0	along-wind

338	8	40	4	HR	1	7	3	5.4	0	along-wind
339	8	50	4	HR	1	7	3	5.4	0	along-wind
340	8	10	4	HR	1	7	5	5.4	0	along-wind
341	8	20	4	HR	1	7	5	5.4	0	along-wind
342	8	30	4	HR	1	7	5	5.4	0	along-wind
343	8	40	4	HR	1	7	5	5.4	0	along-wind
344	8	50	4	HR	1	7	5	5.4	0	along-wind
345	8	60	4	HR	2	3	2	5.4	0	along-wind
346	8	70	4	HR	3	3	2	5.4	0	along-wind
347	8	80	4	HR	4	3	2	5.4	0	along-wind
348	8	90	4	HR	2	5	2	5.4	0	along-wind
349	8	100	4	HR	3	5	2	5.4	0	along-wind
350	8	110	4	HR	4	5	2	5.4	0	along-wind
351	8	10	4	HR	1	3	2	5.4	45	along-wind
352	8	20	4	HR	1	3	2	5.4	45	along-wind
353	8	30	4	HR	1	3	2	5.4	45	along-wind
354	8	40	4	HR	1	3	2	5.4	45	along-wind
355	8	50	4	HR	1	3	2	5.4	45	along-wind
356	8	50	4	HR	1	3	5	5.4	45	along-wind
357	8	10	4	HR	1	5	2	5.4	45	along-wind
358	8	20	4	HR	1	5	2	5.4	45	along-wind
359	8	30	4	HR	1	5	2	5.4	45	along-wind
360	8	40	4	HR	1	5	2	5.4	45	along-wind
361	8	50	4	HR	1	5	2	5.4	45	along-wind
362	8	50	4	HR	1	5	5	5.4	45	along-wind
363	8	50	4	HR	2	3	2	5.4	45	along-wind
364	8	50	4	HR	3	3	2	5.4	45	along-wind
365	8	50	4	HR	4	3	2	5.4	45	along-wind
366	8	50	4	HR	2	5	2	5.4	45	along-wind
367	8	50	4	HR	3	5	2	5.4	45	along-wind
368	8	50	4	HR	4	5	2	5.4	45	along-wind
369	8	10	4	HR	1	3	2	5.4	15	along-wind
370	8	10	4	HR	1	3	2	5.4	30	along-wind
371	8	10	4	HR	1	3	2	5.4	60	along-wind
372	8	30	4	HR	1	3	2	5.4	15	along-wind
373	8	30	4	HR	1	3	2	5.4	30	along-wind
374	8	30	4	HR	1	3	2	5.4	60	along-wind
375	8	10	4	HR	1	1	2	5.4	0	cross-wind
376	8	10	4	HR	1	3	2	5.4	0	cross-wind
377	8	10	4	HR	1	5	2	5.4	0	cross-wind
378	8	10	4	HR	1	3	2	5.4	45	cross-wind
379	8	10	4	HR	1	5	2	5.4	45	cross-wind
380	8	30	4	HR	1	1	2	5.4	0	cross-wind
381	8	30	4	HR	1	3	2	5.4	0	cross-wind
382	8	30	4	HR	1	5	2	5.4	0	cross-wind
383	8	30	4	HR	1	3	2	5.4	45	cross-wind
384	8	30	4	HR	1	5	2	5.4	45	cross-wind

Test cases with the low-rise building with cross-wind width 30 m (see Figure 3.3a)

Test Number	RTS-length	RTS-width	RTS-height	Building type	Stack location	Stack height (m)	Exhaust momentum	Wind speed (m/s)	Wind direction (degrees)	concentration profile
385	NA	NA	NA	LR-2	1	1	1	5.4	0	along-wind
386	NA	NA	NA	LR-2	1	1	2	5.4	0	along-wind
387	NA	NA	NA	LR-2	1	1	3	5.4	0	along-wind
388	NA	NA	NA	LR-2	1	1	5	5.4	0	along-wind
389	NA	NA	NA	LR-2	1	2	1	5.4	0	along-wind
390	NA	NA	NA	LR-2	1	2	2	5.4	0	along-wind

391	NA	NA	NA	LR-2	1	2	3	5.4	0	along-wind
392	NA	NA	NA	LR-2	1	2	5	5.4	0	along-wind
393	NA	NA	NA	LR-2	1	3	1	5.4	0	along-wind
394	NA	NA	NA	LR-2	1	3	2	5.4	0	along-wind
395	NA	NA	NA	LR-2	1	3	3	5.4	0	along-wind
396	NA	NA	NA	LR-2	1	3	5	5.4	0	along-wind
397	NA	NA	NA	LR-2	1	5	1	5.4	0	along-wind
398	NA	NA	NA	LR-2	1	5	2	5.4	0	along-wind
399	8	10	4	LR-2	1	1	1	5.4	0	along-wind
400	8	10	4	LR-2	1	1	2	5.4	0	along-wind
401	8	10	4	LR-2	1	1	3	5.4	0	along-wind
402	8	10	4	LR-2	1	1	5	5.4	0	along-wind
403	8	10	4	LR-2	1	3	1	5.4	0	along-wind
404	8	10	4	LR-2	1	3	2	5.4	0	along-wind
405	8	10	4	LR-2	1	3	3	5.4	0	along-wind
406	8	10	4	LR-2	1	3	5	5.4	0	along-wind
407	8	10	4	LR-2	1	5	1	5.4	0	along-wind
408	8	10	4	LR-2	1	5	2	5.4	0	along-wind
409	8	10	4	LR-2	1	5	3	5.4	0	along-wind
410	8	10	4	LR-2	1	5	5	5.4	0	along-wind
411	8	10	4	LR-2	1	7	1	5.4	0	along-wind
412	8	10	4	LR-2	1	7	2	5.4	0	along-wind
413	8	20	4	LR-2	1	3	2	5.4	0	along-wind
414	8	20	4	LR-2	1	3	3	5.4	0	along-wind
415	8	20	4	LR-2	1	3	5	5.4	0	along-wind
416	8	20	4	LR-2	1	5	5	5.4	0	along-wind
417	NA	NA	NA	LR-2	1	1	2	5.4	0	lateral
418	NA	NA	NA	LR-2	1	2	2	5.4	0	lateral
419	NA	NA	NA	LR-2	1	3	2	5.4	0	lateral
420	NA	NA	NA	LR-2	1	5	2	5.4	0	lateral

Specific tests to determine h_{req}

Test Number	RTS-length	RTS-width	RTS-height	Building type	Stack location	Stack height (m)	Exhaust momentum	Wind speed (m/s)	Wind direction (degrees)	concentration profile
421	8	10	4	LR-1	1	8	1	5.4	0	N/A
422	8	10	4	LR-1	1	10	1	5.4	0	N/A
423	8	10	4	LR-1	1	11	1	5.4	0	N/A
424	8	10	4	LR-1	1	12	1	5.4	0	N/A
425	8	10	4	LR-1	1	8	2	5.4	0	N/A
426	8	10	4	LR-1	1	10	2	5.4	0	N/A
427	8	10	4	LR-1	1	11	2	5.4	0	N/A
428	8	10	4	LR-1	1	12	2	5.4	0	N/A
429	8	10	4	LR-1	1	8	3	5.4	0	N/A
430	8	10	4	LR-1	1	10	3	5.4	0	N/A
431	8	10	4	LR-1	1	11	3	5.4	0	N/A
432	8	10	4	LR-1	1	12	3	5.4	0	N/A
433	8	10	4	LR-1	1	8	5	5.4	0	N/A
434	8	10	4	LR-1	1	10	5	5.4	0	N/A
435	8	10	4	LR-1	1	11	5	5.4	0	N/A
436	8	10	4	LR-1	1	12	5	5.4	0	N/A
437	8	10	4	LR-1	2	8	1	5.4	0	N/A
438	8	10	4	LR-1	2	10	1	5.4	0	N/A
439	8	10	4	LR-1	2	8	2	5.4	0	N/A
440	8	10	4	LR-1	2	9	2	5.4	0	N/A
441	8	10	4	LR-1	2	8	3	5.4	0	N/A

442	8	10	4	LR-1	2	9	3	5.4	0	N/A
443	8	10	4	LR-1	2	7	5	5.4	0	N/A
444	8	10	4	LR-1	2	8	5	5.4	0	N/A
445	8	10	4	LR-1	3	9	1	5.4	0	N/A
446	8	10	4	LR-1	3	10	1	5.4	0	N/A
447	8	10	4	LR-1	3	8	2	5.4	0	N/A
448	8	10	4	LR-1	3	9	2	5.4	0	N/A
449	8	10	4	LR-1	3	5	3	5.4	0	N/A
450	8	10	4	LR-1	3	5	5	5.4	0	N/A
451	8	10	4	LR-1	3	6	5	5.4	0	N/A
452	8	10	4	LR-1	3	7	5	5.4	0	N/A
453	8	10	4	LR-1	4	5	1	5.4	0	N/A
454	8	10	4	LR-1	4	7	1	5.4	0	N/A
455	8	10	4	LR-1	4	8	1	5.4	0	N/A
456	8	10	4	LR-1	4	5	2	5.4	0	N/A
457	8	10	4	LR-1	4	7	2	5.4	0	N/A
458	8	10	4	LR-1	4	5	3	5.4	0	N/A
459	8	10	4	LR-1	4	6	3	5.4	0	N/A
460	8	10	4	LR-1	4	7	3	5.4	0	N/A
461	8	10	4	LR-1	4	3	5	5.4	0	N/A
462	8	10	4	LR-1	4	5	5	5.4	0	N/A
463	8	10	4	LR-1	5	5	1	5.4	0	N/A
464	8	10	4	LR-1	5	7	1	5.4	0	N/A
465	8	10	4	LR-1	5	5	2	5.4	0	N/A
466	8	10	4	LR-1	5	6	2	5.4	0	N/A
467	8	10	4	LR-1	5	7	2	5.4	0	N/A
468	8	10	4	LR-1	5	1	3	5.4	0	N/A
469	8	10	4	LR-1	5	3	3	5.4	0	N/A
470	8	10	4	LR-1	5	5	3	5.4	0	N/A
471	8	10	4	LR-1	5	1	5	5.4	0	N/A
472	8	10	4	LR-1	5	3	5	5.4	0	N/A
473	8	10	4	LR-1	5	11	5	5.4	0	N/A
474	8	10	4	LR-1	1	8	1	5.4	45	N/A
475	8	10	4	LR-1	1	10	1	5.4	45	N/A
476	8	10	4	LR-1	1	11	1	5.4	45	N/A
477	8	10	4	LR-1	1	12	1	5.4	45	N/A
478	8	10	4	LR-1	1	8	2	5.4	45	N/A
479	8	10	4	LR-1	1	10	2	5.4	45	N/A
480	8	10	4	LR-1	1	11	2	5.4	45	N/A
481	8	10	4	LR-1	1	12	2	5.4	45	N/A
482	8	10	4	LR-1	1	8	3	5.4	45	N/A
483	8	10	4	LR-1	1	10	3	5.4	45	N/A
484	8	10	4	LR-1	1	11	3	5.4	45	N/A
485	8	10	4	LR-1	1	12	3	5.4	45	N/A
486	8	10	4	LR-1	1	8	5	5.4	45	N/A
487	8	10	4	LR-1	1	10	5	5.4	45	N/A
488	8	10	4	LR-1	1	11	5	5.4	45	N/A
489	8	10	4	LR-1	1	12	5	5.4	45	N/A
490	8	10	4	LR-1	2	8	1	5.4	45	N/A
491	8	10	4	LR-1	2	10	1	5.4	45	N/A
492	8	10	4	LR-1	2	8	2	5.4	45	N/A
493	8	10	4	LR-1	2	9	2	5.4	45	N/A
494	8	10	4	LR-1	2	8	3	5.4	45	N/A
495	8	10	4	LR-1	2	9	3	5.4	45	N/A
496	8	10	4	LR-1	2	7	5	5.4	45	N/A
497	8	10	4	LR-1	2	8	5	5.4	45	N/A
498	8	10	4	LR-1	3	9	1	5.4	45	N/A

499	8	10	4	LR-1	3	10	1	5.4	45	N/A
500	8	10	4	LR-1	3	8	2	5.4	45	N/A
501	8	10	4	LR-1	3	9	2	5.4	45	N/A
502	8	10	4	LR-1	3	5	3	5.4	45	N/A
503	8	10	4	LR-1	3	5	5	5.4	45	N/A
504	8	10	4	LR-1	3	6	5	5.4	45	N/A
505	8	10	4	LR-1	3	7	5	5.4	45	N/A
506	8	10	4	LR-1	4	5	1	5.4	45	N/A
507	8	10	4	LR-1	4	7	1	5.4	45	N/A
508	8	10	4	LR-1	4	8	1	5.4	45	N/A
509	8	10	4	LR-1	4	5	2	5.4	45	N/A
510	8	10	4	LR-1	4	7	2	5.4	45	N/A
511	8	10	4	LR-1	4	5	3	5.4	45	N/A
512	8	10	4	LR-1	4	6	3	5.4	45	N/A
513	8	10	4	LR-1	4	7	3	5.4	45	N/A
514	8	10	4	LR-1	4	3	5	5.4	45	N/A
515	8	10	4	LR-1	4	5	5	5.4	45	N/A
516	8	10	4	LR-1	5	5	1	5.4	45	N/A
517	8	10	4	LR-1	5	7	1	5.4	45	N/A
518	8	10	4	LR-1	5	5	2	5.4	45	N/A
519	8	10	4	LR-1	5	6	2	5.4	45	N/A
520	8	10	4	LR-1	5	7	2	5.4	45	N/A
521	8	10	4	LR-1	5	1	3	5.4	45	N/A
522	8	10	4	LR-1	5	3	3	5.4	45	N/A
523	8	10	4	LR-1	5	5	3	5.4	45	N/A

Model scale variation 1: 350

Test Number	RTS-length	RTS-width	RTS-height	Building type	Stack location	Stack height (m)	Exhaust momentum	Wind speed (m/s)	Wind direction (degrees)	concentration profile
524	8	10	4	LR-1	5	1	5	5.4	45	N/A
525	8	10	4	LR-1	5	3	5	5.4	45	N/A
526	8	10	4	LR-1	5	11	5	5.4	45	N/A
527	8	40	4	LR-1	1	3	3	5.4	0	along-wind
528	8	40	4	LR-2	1	3	5	5.4	0	along-wind
529	8	40	4	LR-1	1	3	3	5.4	0	along-wind
530	8	40	4	LR-2	1	3	5	5.4	0	along-wind
531	8	40	4	HR	1	3	2	5.4	0	along-wind
532	8	40	4	HR	1	3	3	5.4	0	along-wind
533	8	40	4	HR	1	3	5	5.4	0	along-wind
534	0.2	20	4	LR-1	1	3	2	5.4	0	along-wind
535	4	20	4	LR-1	1	3	2	5.4	0	along-wind
536	8	20	4	LR-2	1	3	2	5.4	0	along-wind
537	0.2	20	4	LR-1	1	3	3	5.4	0	along-wind
538	4	20	4	LR-1	1	3	3	5.4	0	along-wind
539	8	20	4	LR-2	1	3	3	5.4	0	along-wind
540	0.2	20	4	LR-1	1	3	2	5.4	45	along-wind
541	8	20	4	LR-2	1	5	2	5.4	45	along-wind

APPENDIX B

Calibration curves for the Mass-flow meter and Gas Chromatograph

Mass Flow Meter Calibration

Company: Matheson

Model: 8270
Range: 0-10 LPM

$y = 0.998x - 0.2337$
$R^2 = 1$

y – Meter reading in LPM
x – Actual flow in LPM

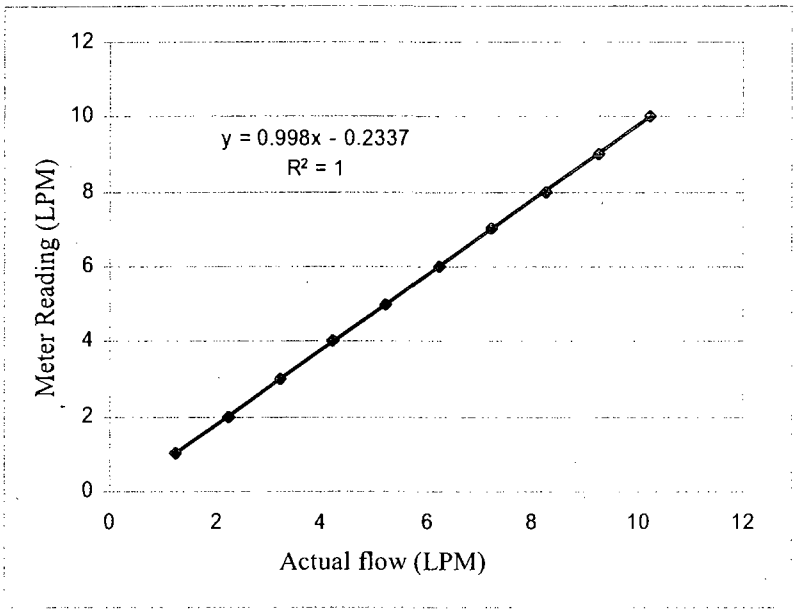

Figure B.1 Calibration curve of mass flow meter - Matheson 1-10 SLPM @ 20psi

GC Calibration

A VARIAN (Model 3400) gas chromatograph in the Building Aerodynamics Lab at Concordia University was used to measure SF_6 concentrations.

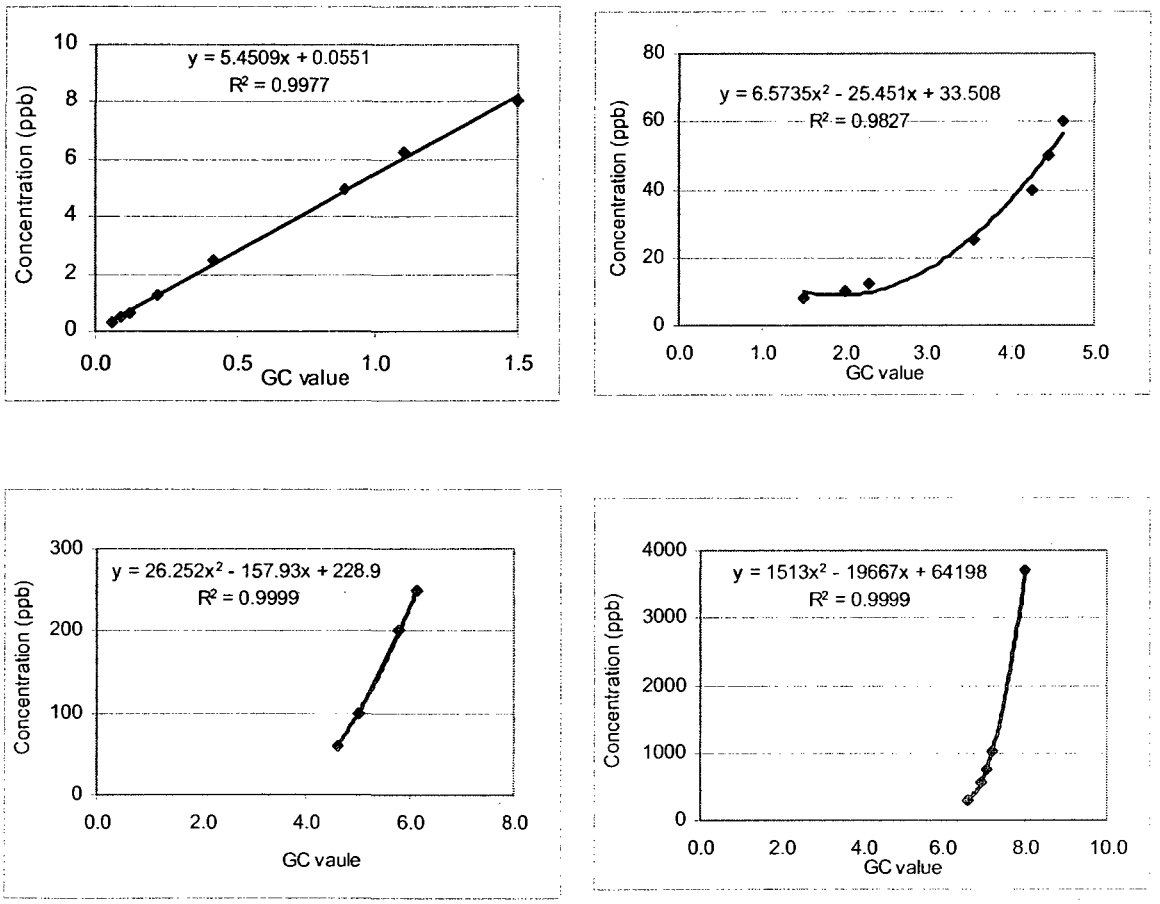

Figure B.2 Gas chromatograph calibration curve for different concentration ranges obtained in September 2003.

APPENDIX C

Along-wind D_N profiles for the high-rise building test cases

Figures C1 to C3 show along-wind D_N profiles for the high-rise building with and without the RTS for the normal wind direction ($\theta = 0°$). Results are shown for h_s ranging from 0.25h to 1.25h, M ranging from 1 to 5, and RTS cross-wind widths ranging from 2.5h to 12.5h. Note that for all cases the effect of RTS on D_N values is negligible.

Figure C4 shows the D_N profiles for the flat roofed building for $h_s = 1.75h$. Since RTS had no effect on D_N values for $h_s < 1.75h$, dilution measurements with an RTS were not obtained for the taller stack.

Figures C5 to C7 show along-wind D_N profiles for the high-rise building for the oblique wind direction, $\theta = 45°$. Results are shown for $h_s = 0.25h$ to 1.25h, M = 1 to 5, and RTS cross-wind width = 2.5h to 12.5h. Note that similar to the low-rise building results presented previously in Chapter 4, a significant influence of the RTS downwash effect on D_N values is quite evident. In addition, the D_N trends and results are very similar to the low-rise building results obtained for $\theta = 45°$.

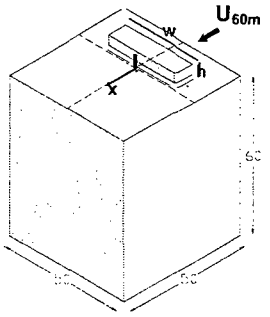

	RTS (w/h)
—△—	Flat roof
—▲—	2.5
—◆—	7.5
—x—	12.5

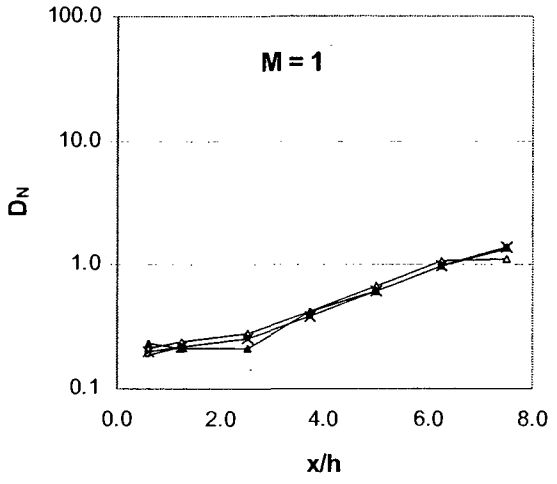

a) M = 1

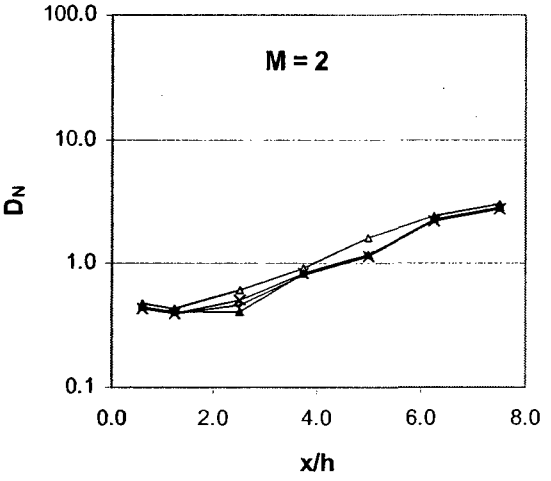

b) M = 2

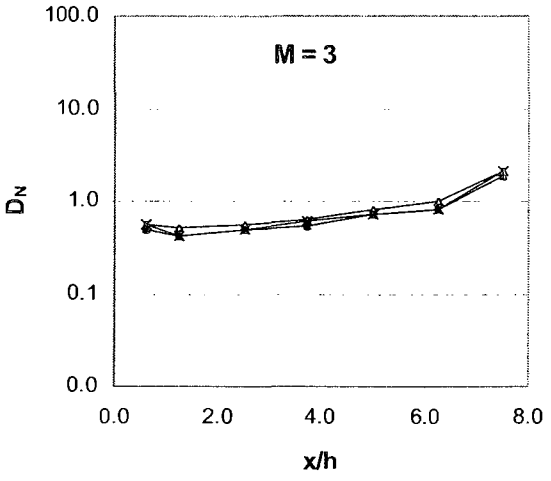

c) M = 3

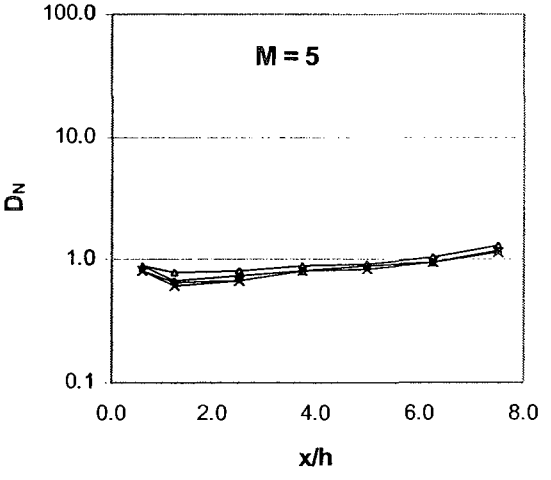

d) M = 5

Figure C1 Effect of RTS cross wind width on minimum dilutions for the high-rise building for $h_s = 0.25h$, $\theta = 0°$, h = 4 m, and M = 1, 2, 3 and 5.

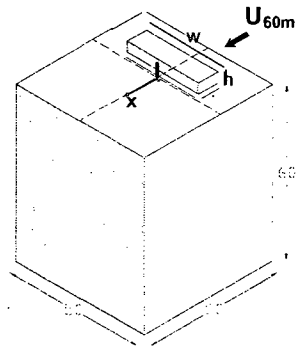

	RTS (w/h)
—△—	Flat roof
—▲—	2.5
—■—	5.0
—◆—	7.5
—×—	12.5

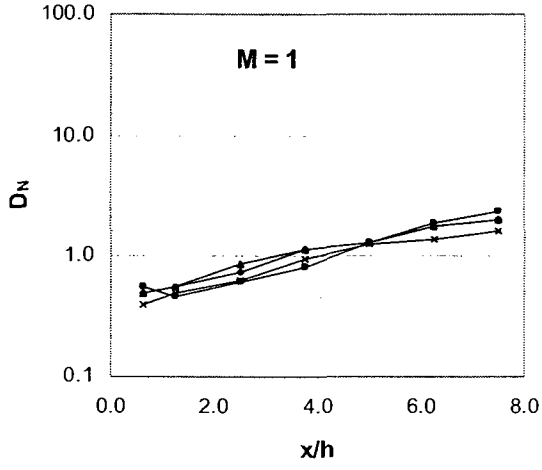

a) M = 1

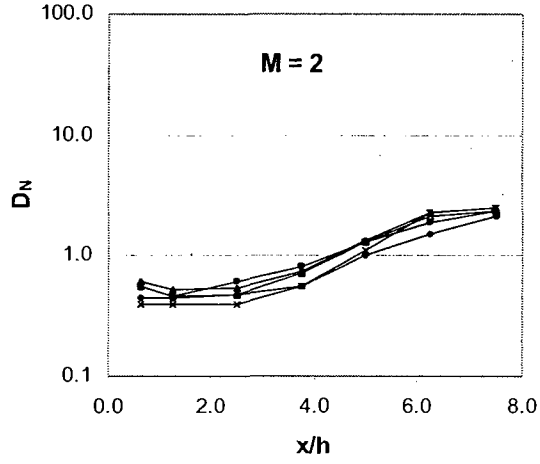

b) M = 2

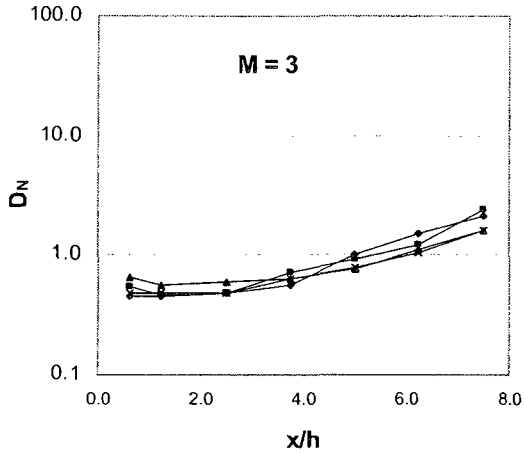

c) M = 3

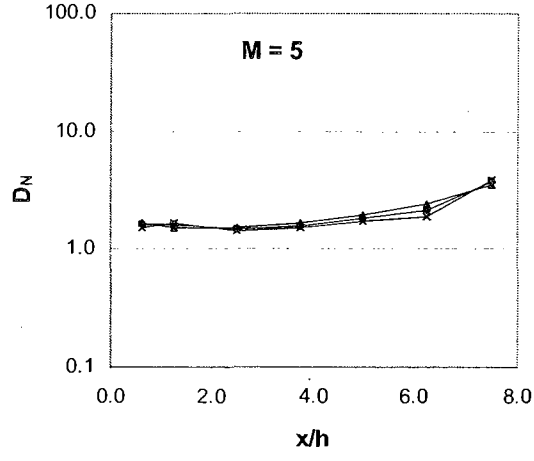

d) M = 5

Figure C2 Effect of RTS cross wind width on minimum dilutions for the high-rise building for $h_s = 0.75h$, $\theta = 0°$, h = 4 m, and M = 1, 2, 3 and 5.

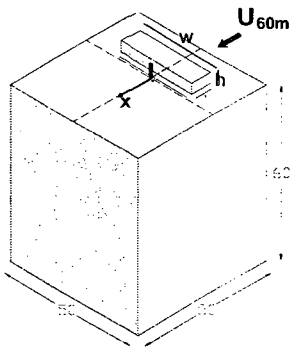

	RTS (w/h)
—△—	Flat roof
—▲—	2.5
—×—	12.5

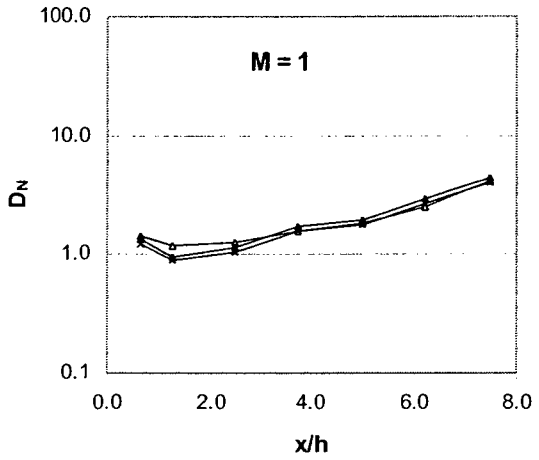

a) M = 1

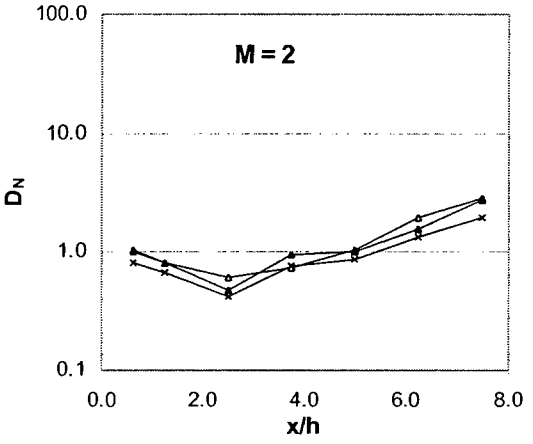

b) M = 2

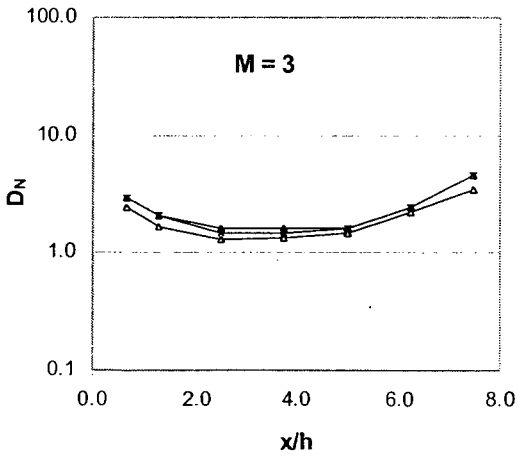

c) M = 3

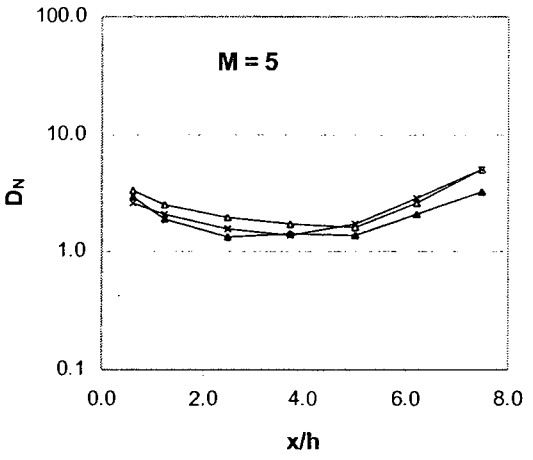

d) M = 5

Figure C3 Effect of RTS cross wind width on minimum dilutions for the high-rise building for h_s = 1.25h, θ = 0° h = 4 m, and M = 1, 2, 3 and 5.

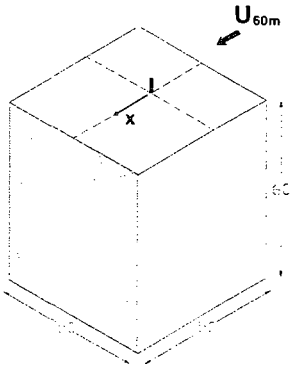

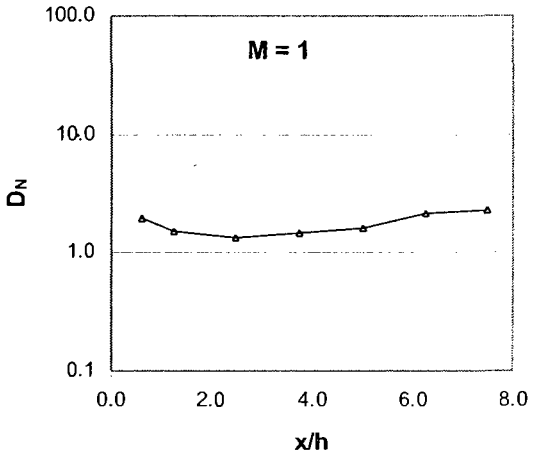

a) M = 1

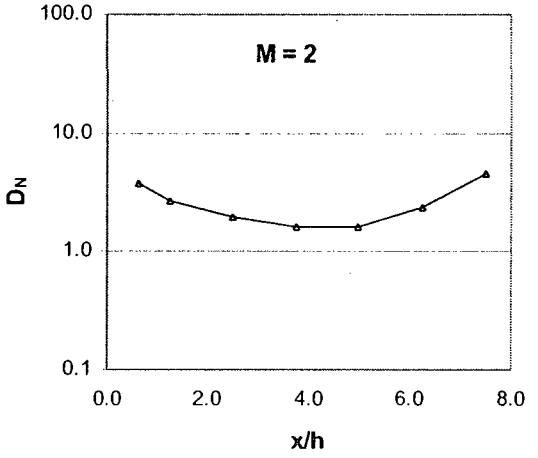

b) M = 2

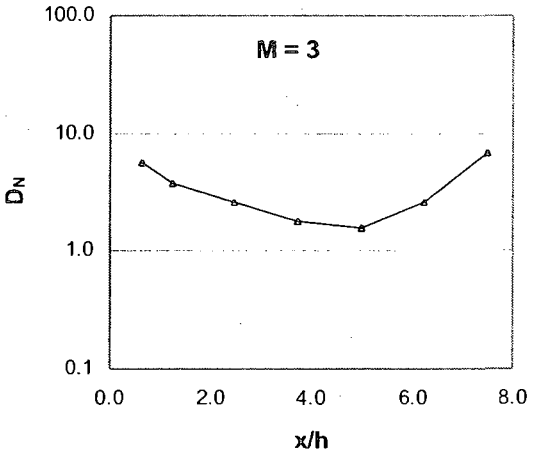

c) M = 3

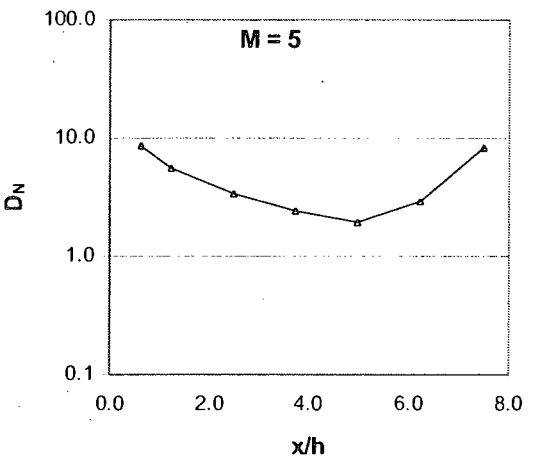

d) M = 5

Figure C4 Minimum dilutions for the flat-roofed high-rise building for $h_s = 1.75h$, $\theta = 0°$ h = 4 m, and M = 1, 2, 3 and 5.

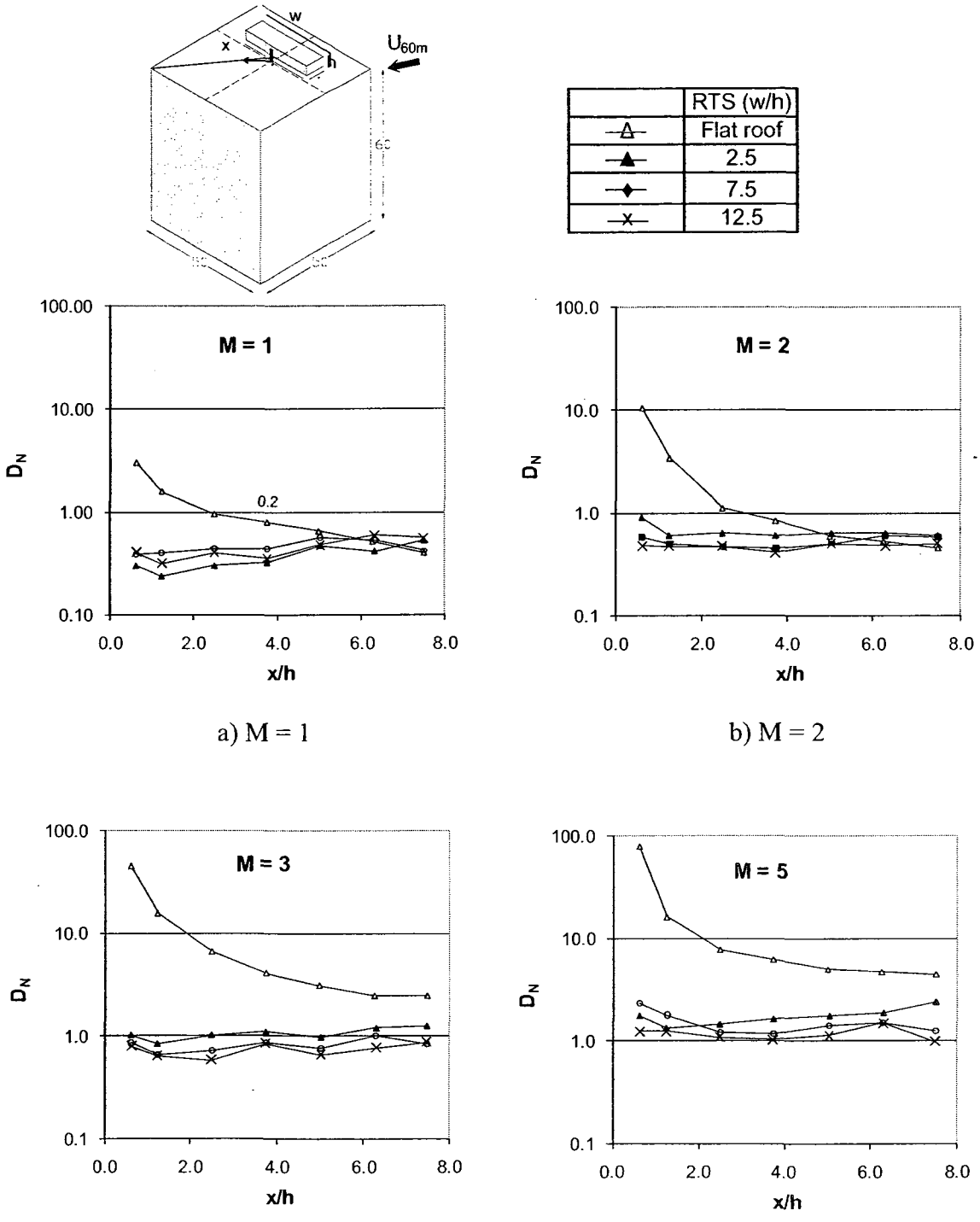

Figure C5 Effect of RTS cross wind width on minimum dilutions for the high-rise building for $h_s = 0.25h$, $\theta = 45°$ h = 4 m, and M = 1, 2, 3 and 5.

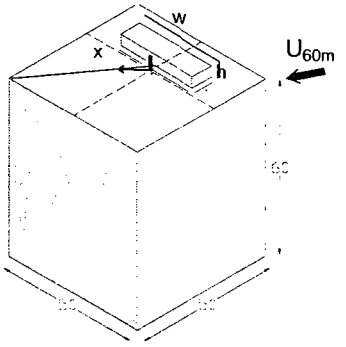

	RTS (w/h)
—△—	Flat roof
—▲—	2.5
—■—	5.0
—◆—	7.5
—×—	12.5

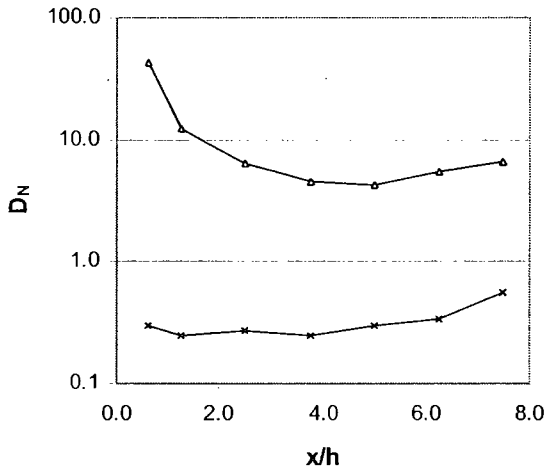

a) M = 1

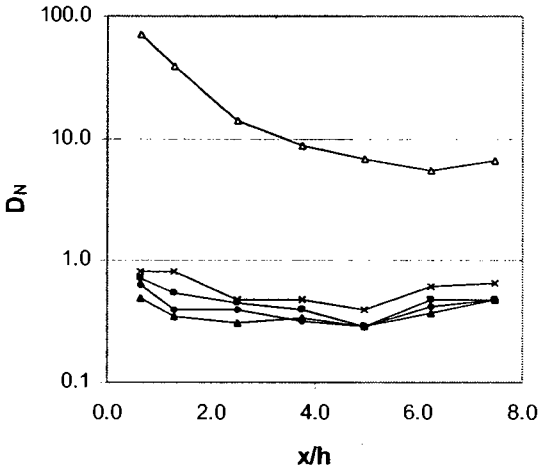

b) M = 2

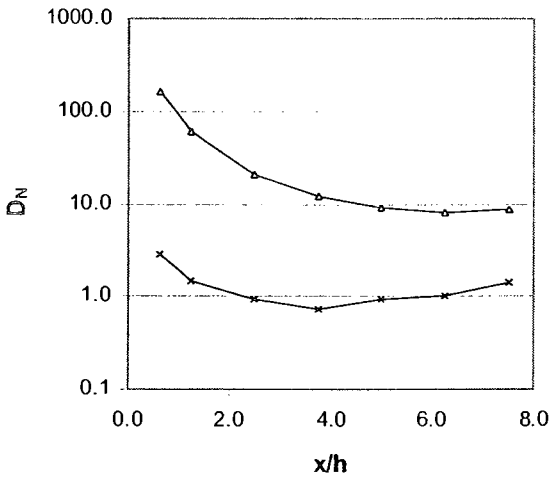

c) M = 3

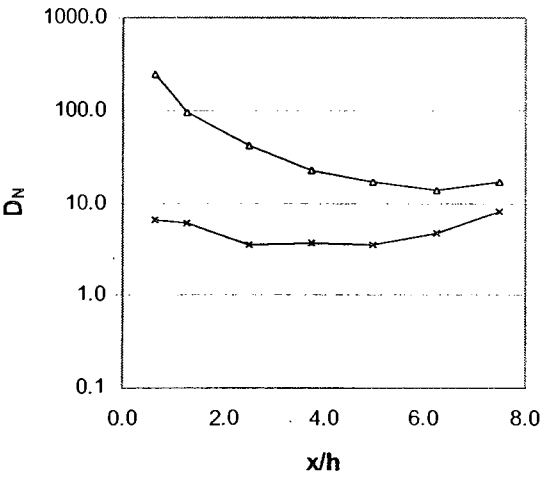

d) M = 5

Figure C6 Effect of RTS cross wind width on minimum dilutions for the high-rise building for $h_s = 0.75h$, $\theta = 45°$ h = 4 m, and M = 1, 2, 3 and 5.

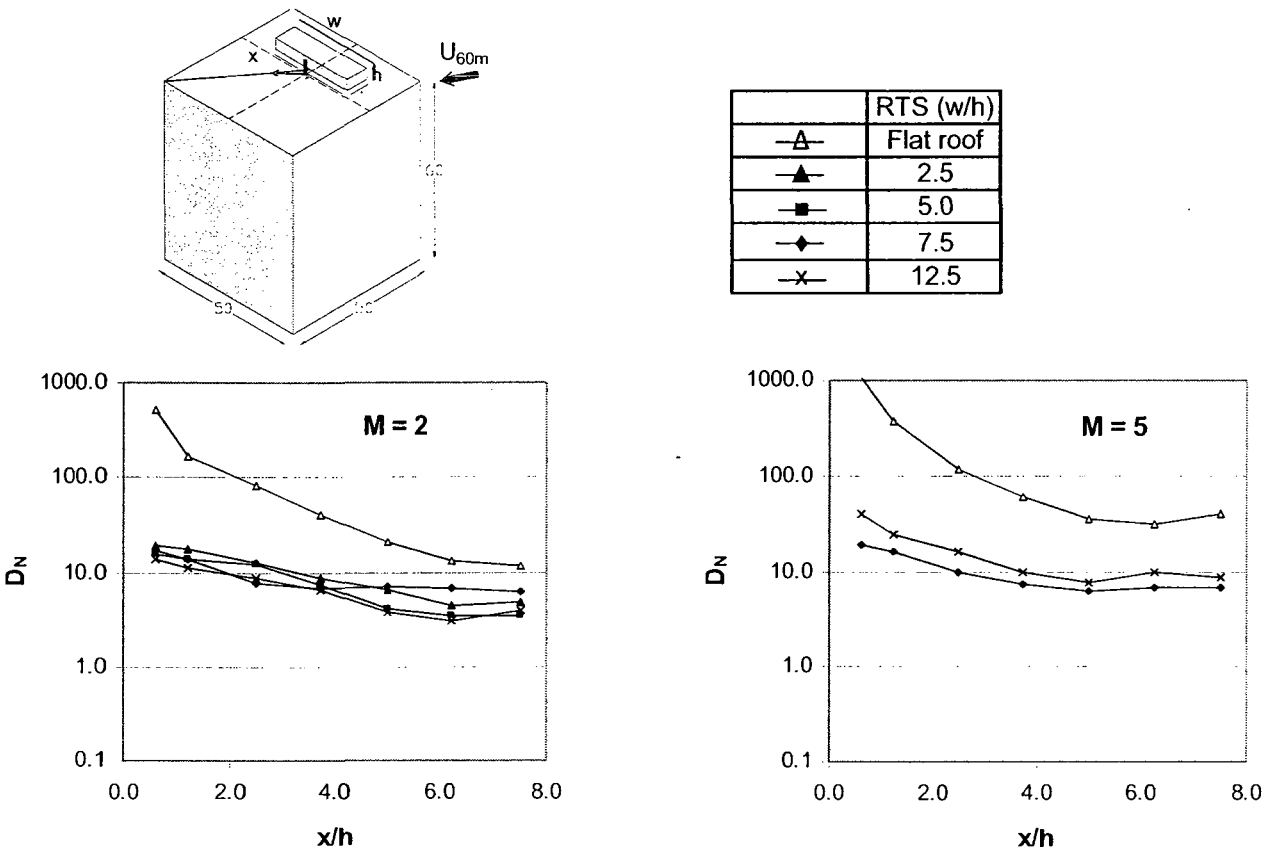

a) M = 3

(b) M = 5

Figure C7 Effect of RTS cross wind width on minimum dilutions for the high-rise building for h_s = 1.25h, θ = 45° h = 4 m, and M = 1, 2, 3 and 5.

APPENDIX D

Additional comparisons of the present study data (along-wind D_N profiles) for the low-rise building with results from previous studies

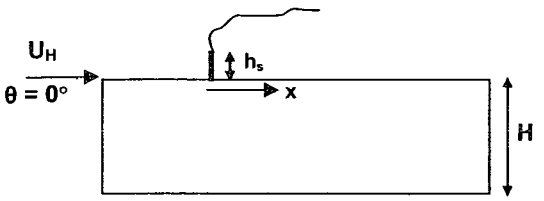

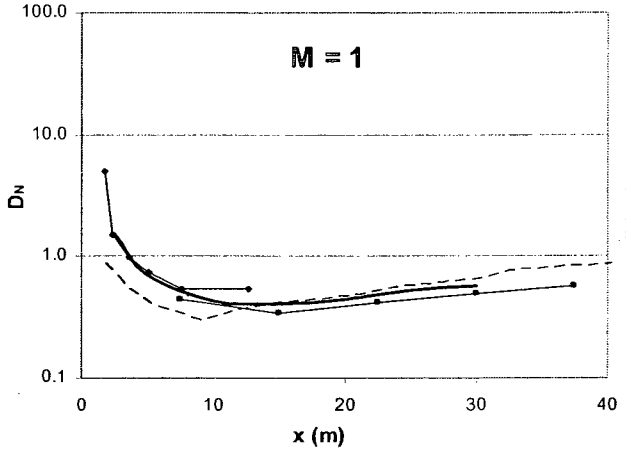

study	hs (m)	M	
Present study	2.0	1.00	
Schulman and Scire (1991)	1.5	0.75	
Wilson et al (1998)	2.1	1.00	
Petersen et al (1999)	2.2	1.00	

a) M ~ 1

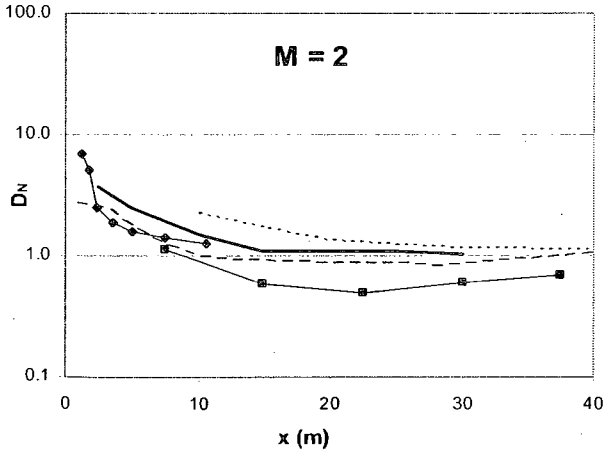

study	hs (m)	M	
Present study	2.0	2.0	
Schulman and Scire (1991)	1.5	1.5	
Lowrey and Jacko (1996)	1.5	2.0	
Wilson et al (1998)	2.1	2.0	
Petersen et al (1999)	2.2	1.4	

b) M ~ 2

Figure D1 Comparison between plume centerline D_N values obtained with previous and present studies for the low-rise building for $h_s \sim 2$ m and $\theta = 0°$.

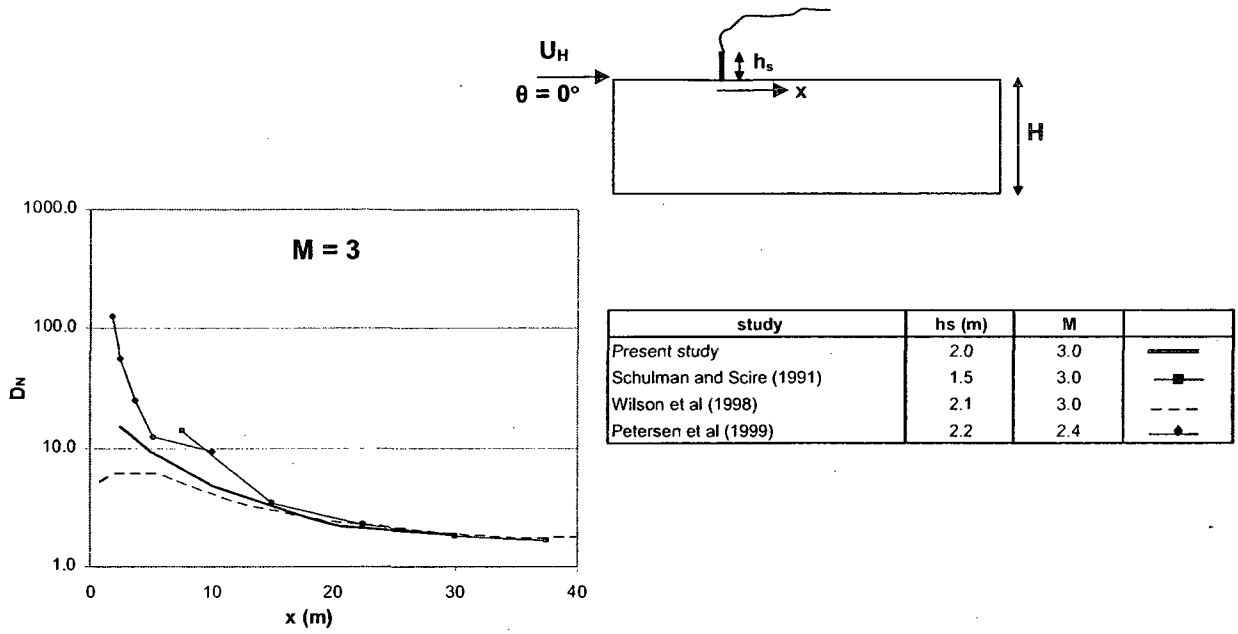

study	hs (m)	M
Present study	2.0	3.0
Schulman and Scire (1991)	1.5	3.0
Wilson et al (1998)	2.1	3.0
Petersen et al (1999)	2.2	2.4

a) M ~ 3

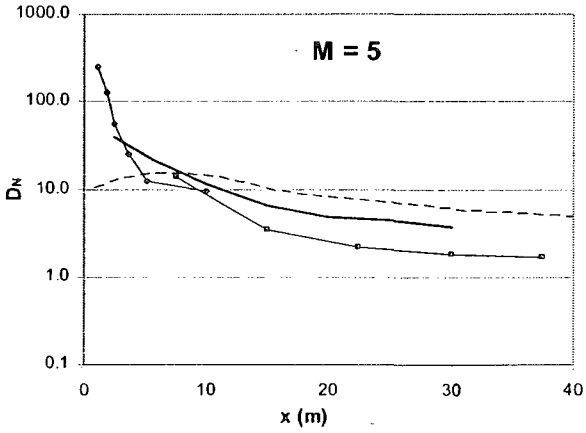

study	hs (m)	M
Present study	2.0	5.0
Schulman and Scire (1991)	1.5	3.0
Wilson et al (1998)	2.1	5.0
Petersen et al (1999)	3.0	2.4

b) M ~ 5

Figure D2 Comparison between plume centerline D_N values obtained with previous and present studies for the low-rise building for $h_s \sim 2$ m and $\theta = 0°$.

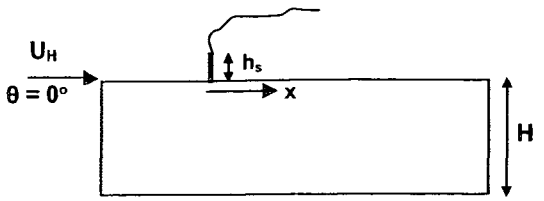

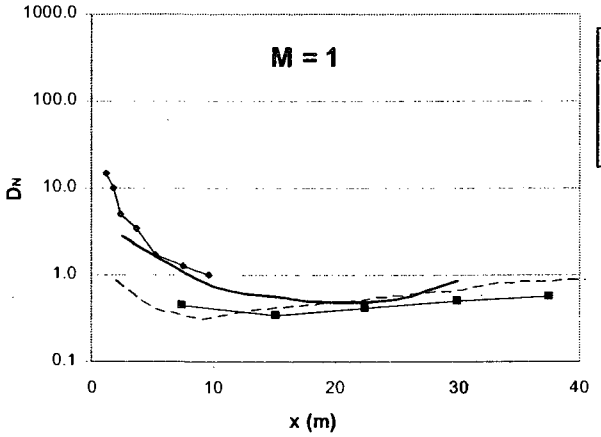

study	hs (m)	M	
Present study	3.0	1.00	
Schulman and Scire (1991)	1.5	0.8	
Wilson et al (1998)	3.0	1.00	
Petersen et al (1999)	3.0	1.00	

a) M ~ 1

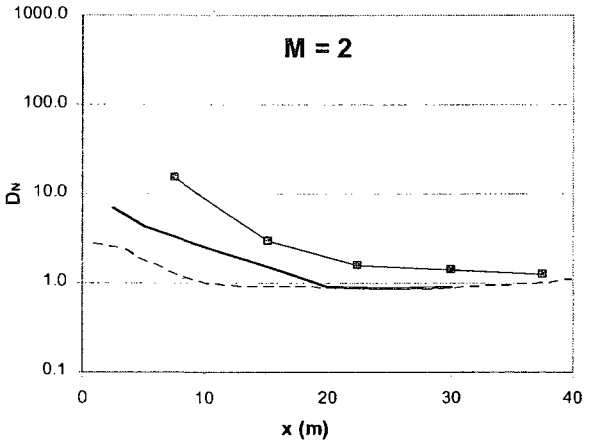

study	hs (m)	M	
Present study	3.0	2.0	
Schulman and Scire (1991)	4.5	1.5	
Wilson et al (1998)	3.0	2.0	

b) M ~ 2

Figure D3 Comparison between plume centerline D_N values obtained with previous and present studies for the low-rise building for $h_s \sim 3$ m and $\theta = 0°$.

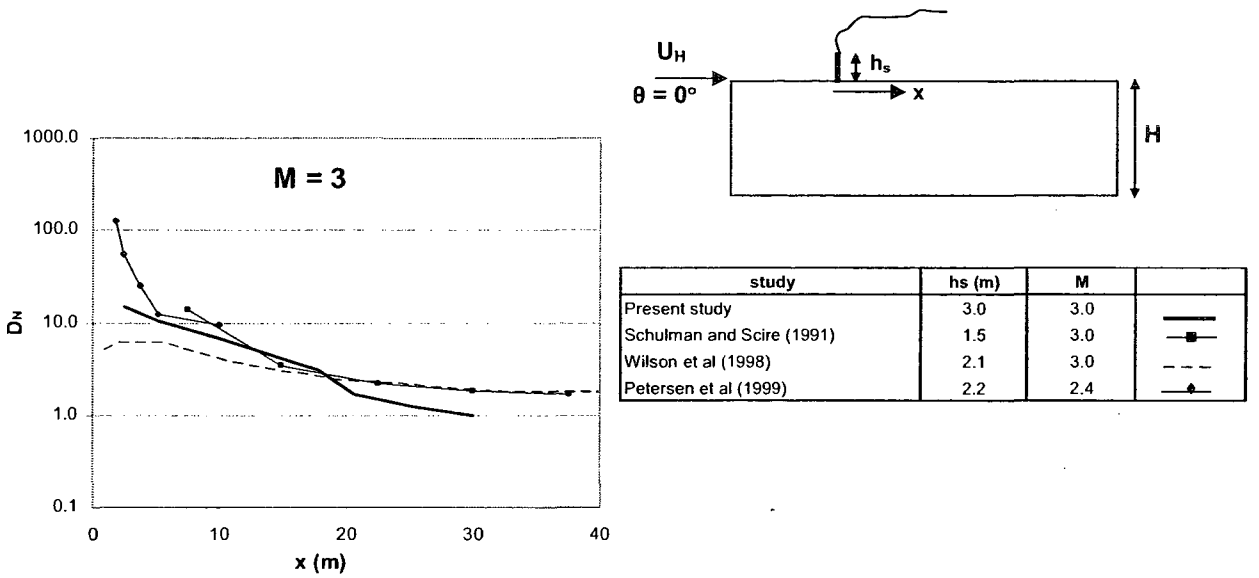

study	hs (m)	M
Present study	3.0	3.0
Schulman and Scire (1991)	1.5	3.0
Wilson et al (1998)	2.1	3.0
Petersen et al (1999)	2.2	2.4

a) M ~ 3

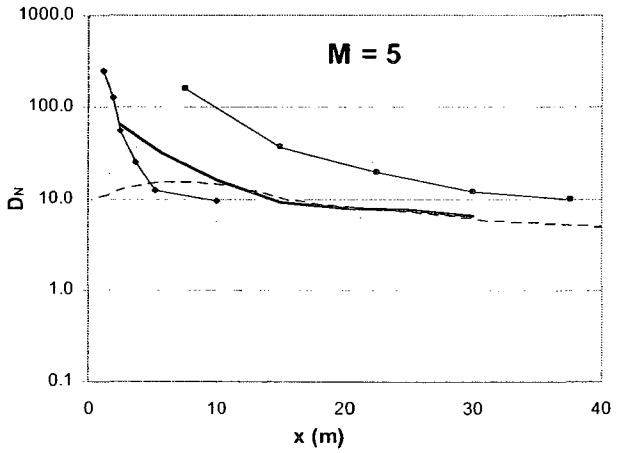

study	hs (m)	M
Present study	2.0	5.0
Schulman and Scire (1991)	1.5	5.0
Wilson et al (1998)	2.1	5.0
Petersen et al (1999)	3.0	2.4

b) M ~ 5

Figure D4 Comparison between plume centerline D_N values obtained with previous and present studies for the low-rise building for $h_s \sim 3$ m and $\theta = 0°$.

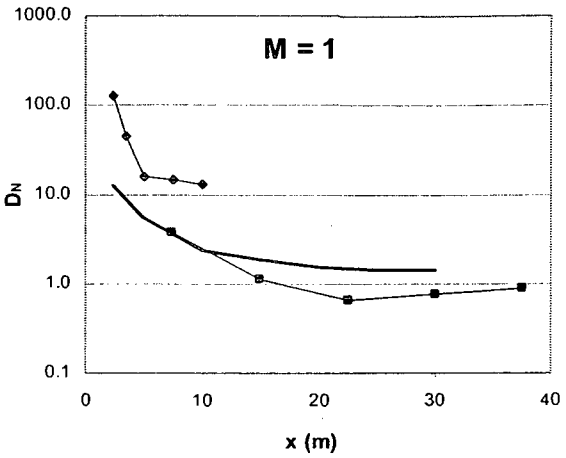

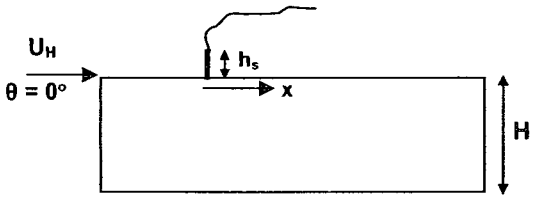

study	hs (m)	M	
Present study	5.0	1.0	
Schulman and Scire (1991)	4.5	0.8	
Petersen et al (1999)	4.5	1.4	

a) M ~ 1

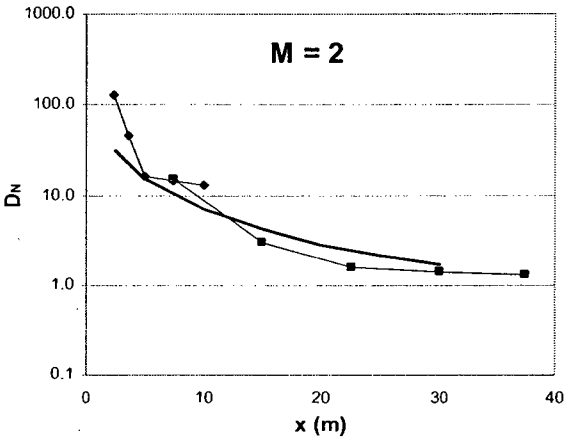

study	hs (m)	M	
Present study	5.0	2.0	
Schulman and Scire (1991)	4.5	1.5	
Petersen et al (1999)	4.5	2.4	

b) M ~ 2

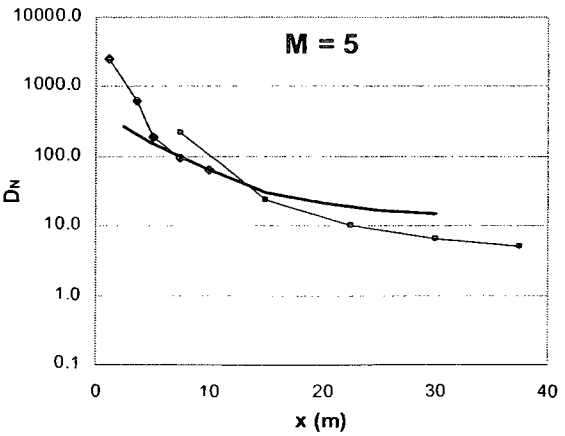

study	hs (m)	M	
Present study	5.0	5.0	
Schulman and Scire (1991)	4.5	3.0	
Petersen et al (1999)	6.0	4.3	

c) M ~ 5

Figure D5 Comparison between plume centerline D_N values obtained with previous and present studies for the low-rise building for h_s ~ 5 m and θ = 0°.

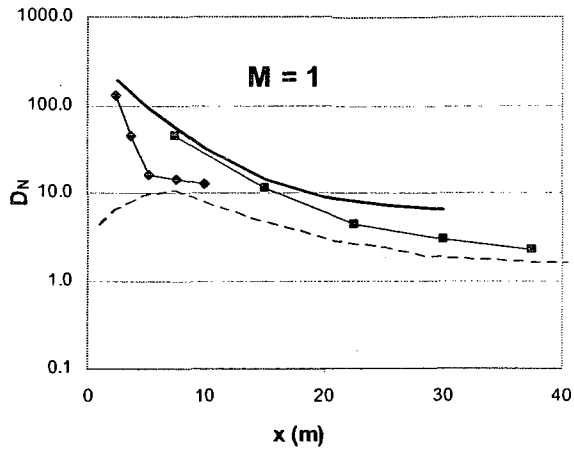

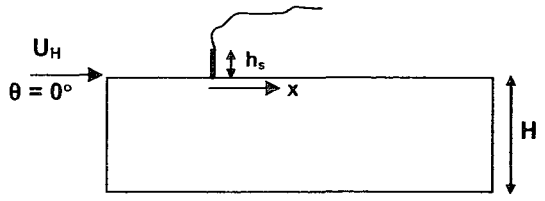

study	hs (m)	M
Present study	7.0	1.0
Schulman and Scire (1991)	7.5	0.8
Wilson et al (1998)	6.1	1.0
Petersen et al (1999)	4.6	1.0

a) M ~ 1

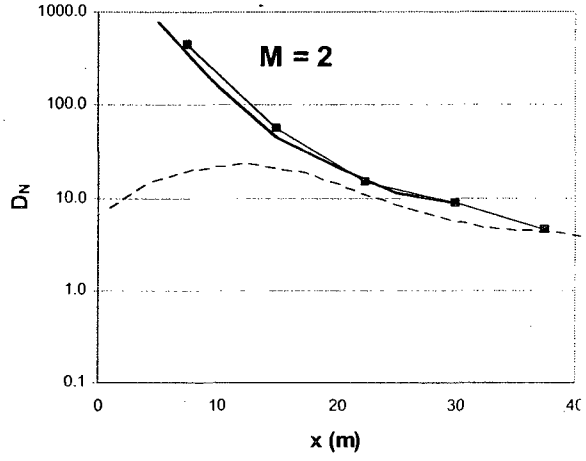

study	hs (m)	M
Present study	7.0	2.0
Schulman and Scire (1991)	7.5	1.5
Wilson et al (1998)	6.1	2.0

b) M ~ 2

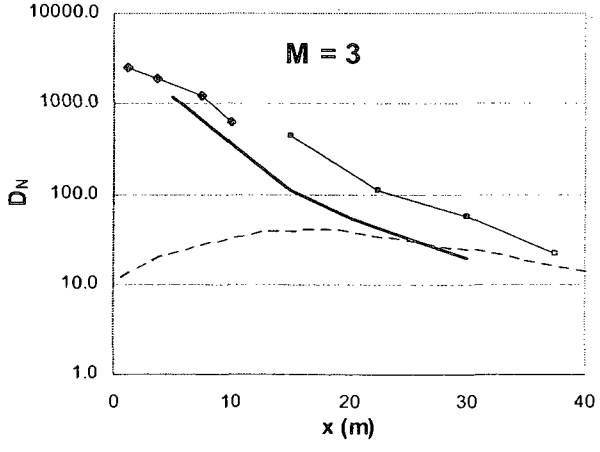

study	hs (m)	M
Present study	7.0	3.0
Schulman and Scire (1991)	7.5	3.0
Wilson et al (1998)	6.1	3.0
Petersen et al (1999)	6.0	2.4

c) M ~ 3

Figure D6 Comparison between plume centerline D_N values obtained with previous and present studies for the low-rise building for h_s ~ 7 m and $\theta = 0°$.

APPENDIX E

Complete set of along-wind D_N profiles for the low-rise building

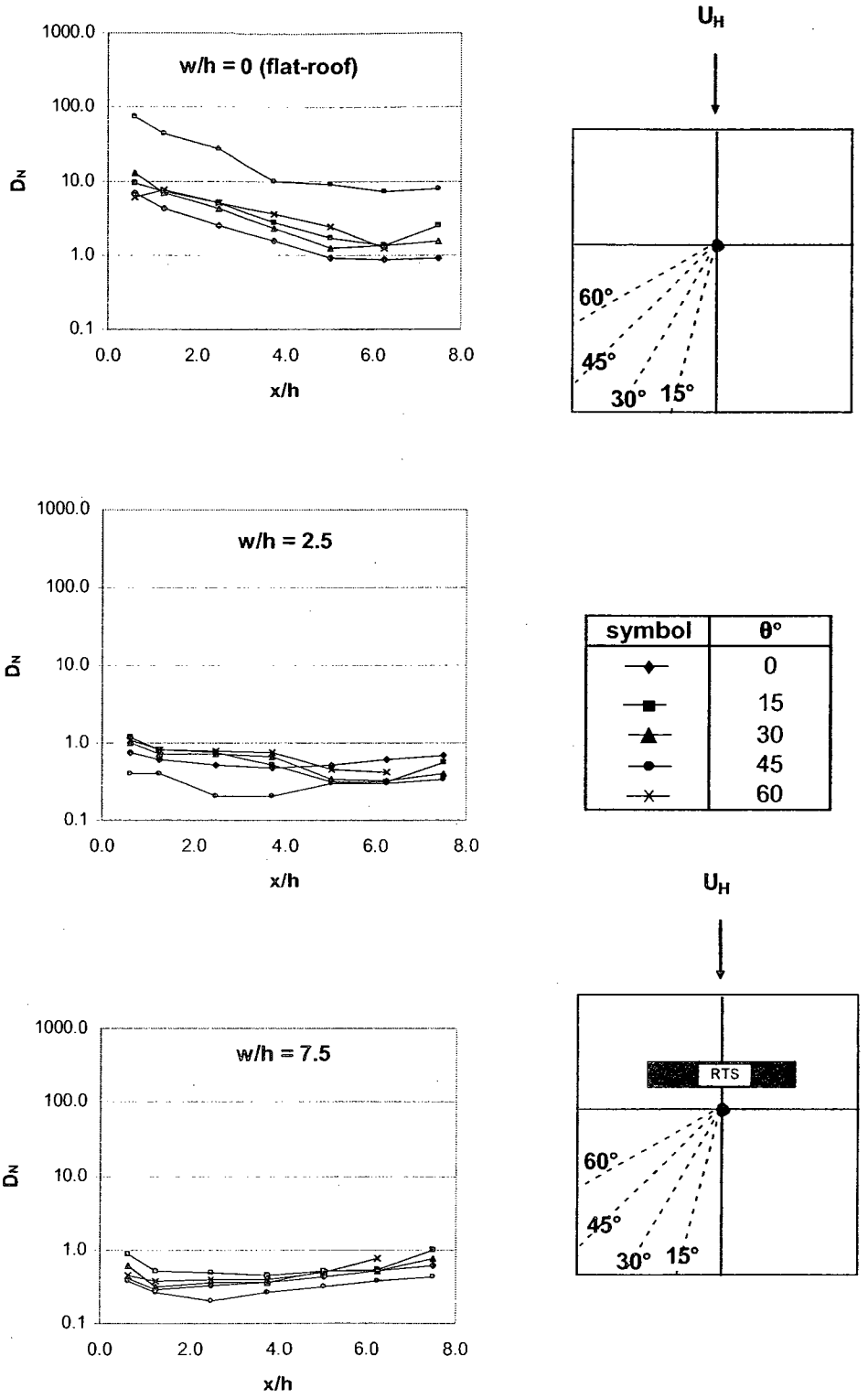

Figure E1 Effect of wind direction on minimum D_N values for the low-rise building with and without RTS for stack height for $h_s = 0.75h$, $\theta = 0°$ to $60°$, $h = 4$ m, and $M = 2$.

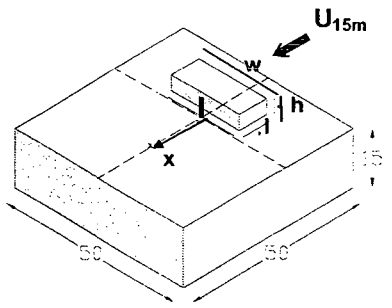

Symbol	RTS (w/h)
▲	2.5
■	5.0
◆	7.5
●	10.0
×	12.5
△	Flat roof

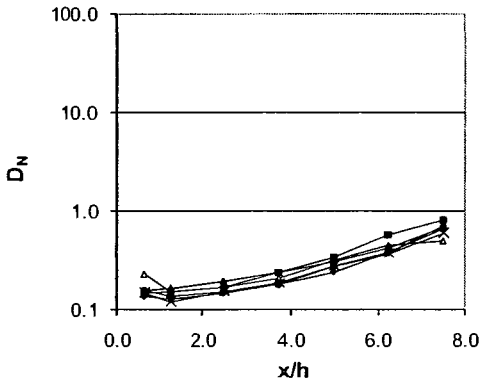

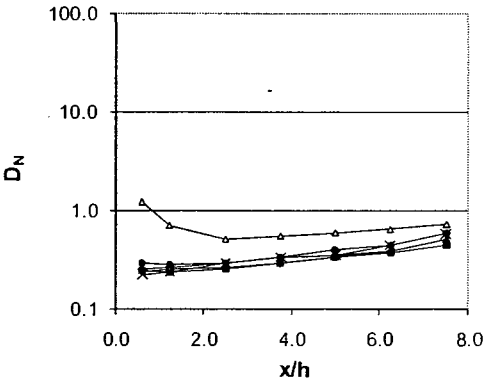

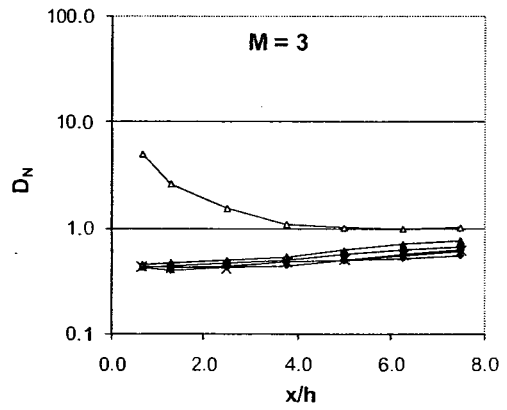

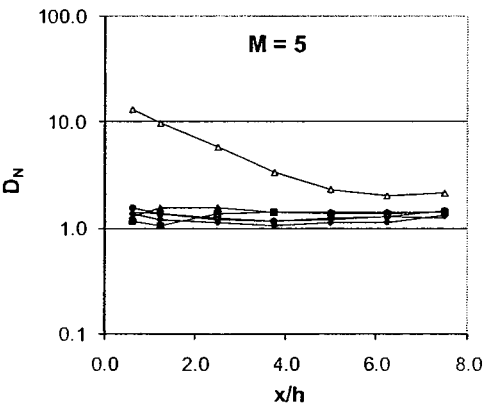

Figure E2 Effect of RTS cross-wind width on minimum dilution values for the low-rise building for stack height $h_s = 0.25h$, $\theta = 0°$, h = 4 m, and M = 1, 2, 3, and 5.

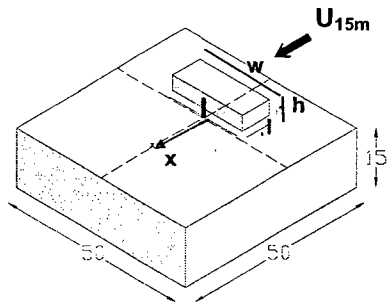

Symbol	RTS (w/h)
▲	2.5
■	5.0
◆	7.5
●	10.0
×	12.5
△	Flat roof

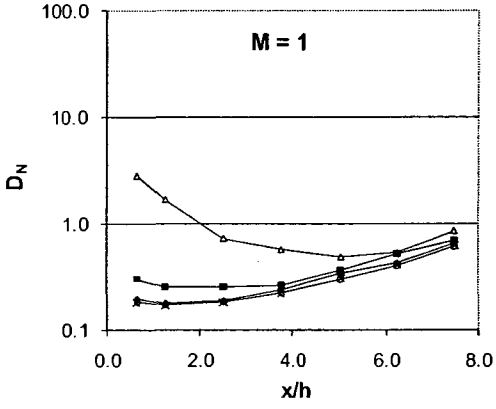

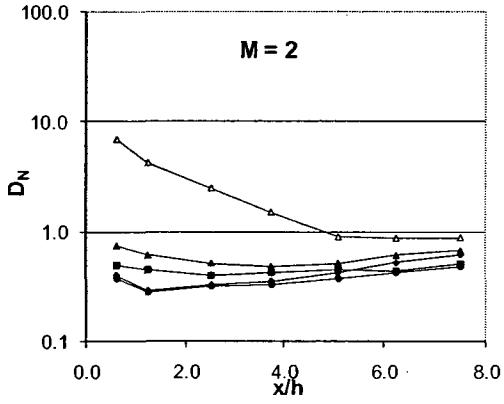

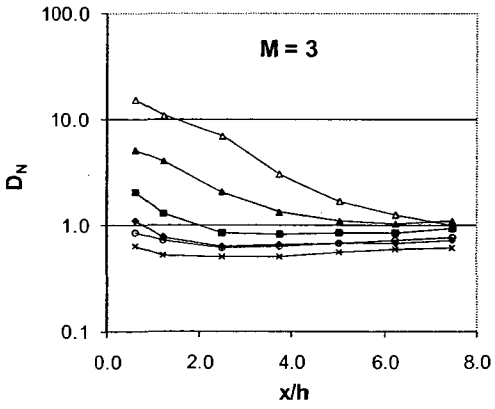

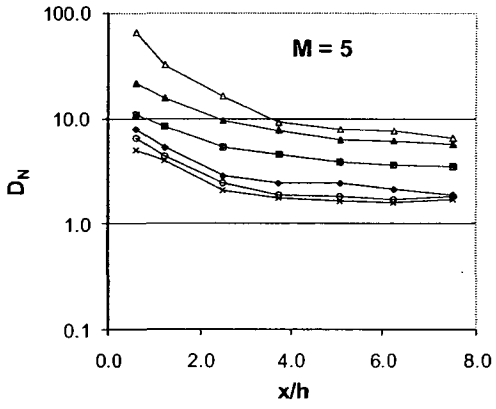

Figure E3 Effect of RTS cross-wind width on minimum dilution values for the low-rise building for stack height $h_s = 0.75h$, $\theta = 0°$, $h = 4$ m, and $M = 1, 2, 3$, and 5.

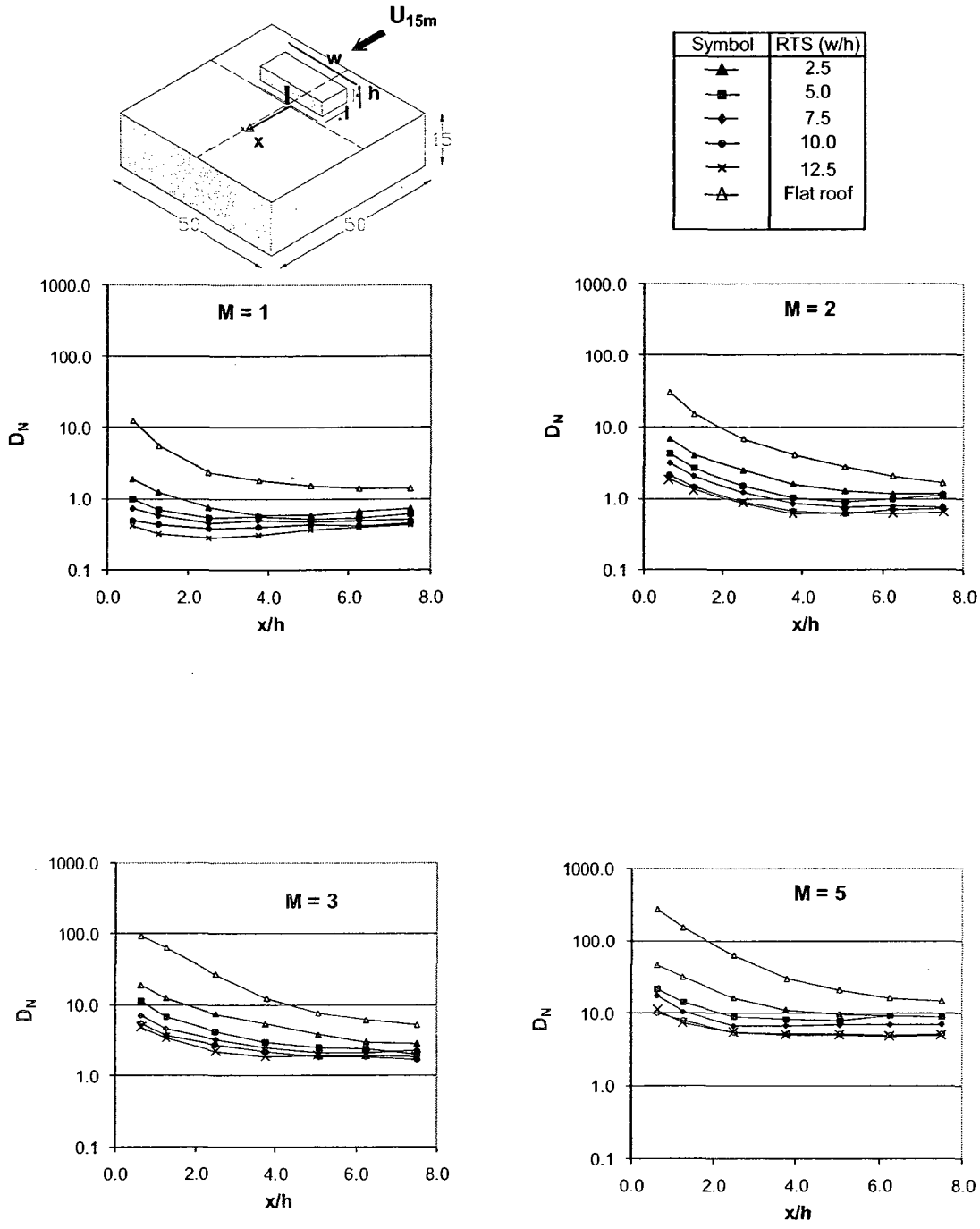

Figure E4 Effect of RTS cross-wind width on minimum dilution values for the low-rise building for stack height $h_s = 1.25h$, $\theta = 0°$, $h = 4$ m, and $M = 1, 2, 3$, and 5.

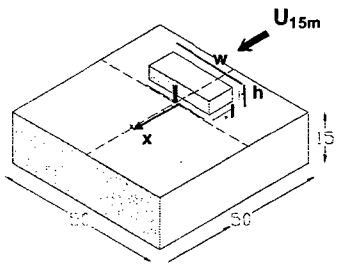

Symbol	RTS (w/h)
▲	2.5
■	5.0
◆	7.5
●	10.0
×	12.5
△	Flat roof

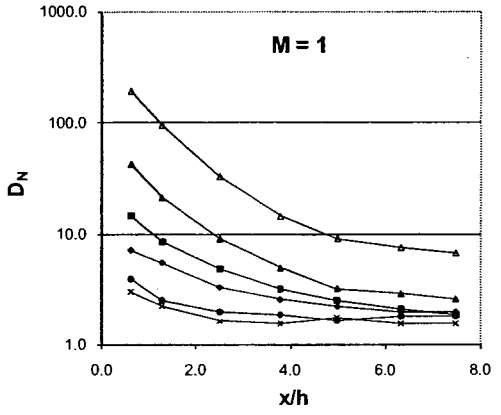

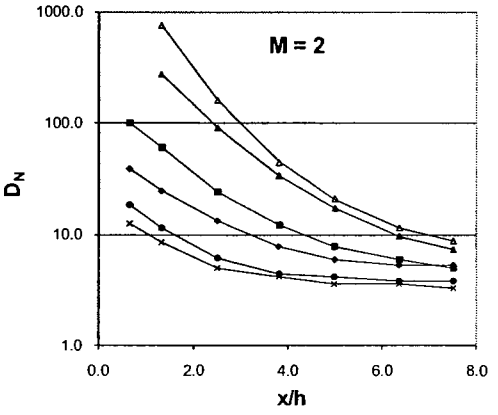

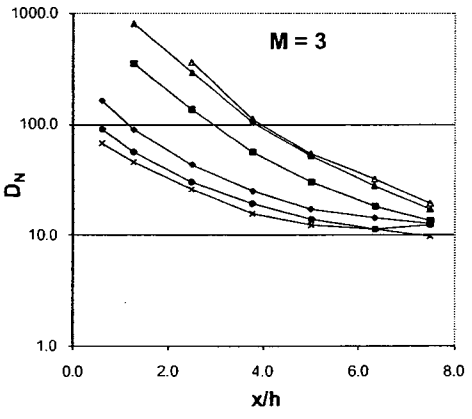

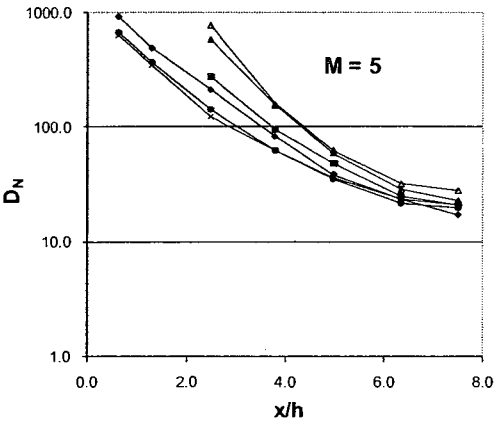

Figure E5 Effect of RTS cross-wind width on minimum dilution values for the low-rise building for stack height $h_s = 1.75h$, $\theta = 0°$, $h = 4$ m, and $M = 1, 2, 3$, and 5.

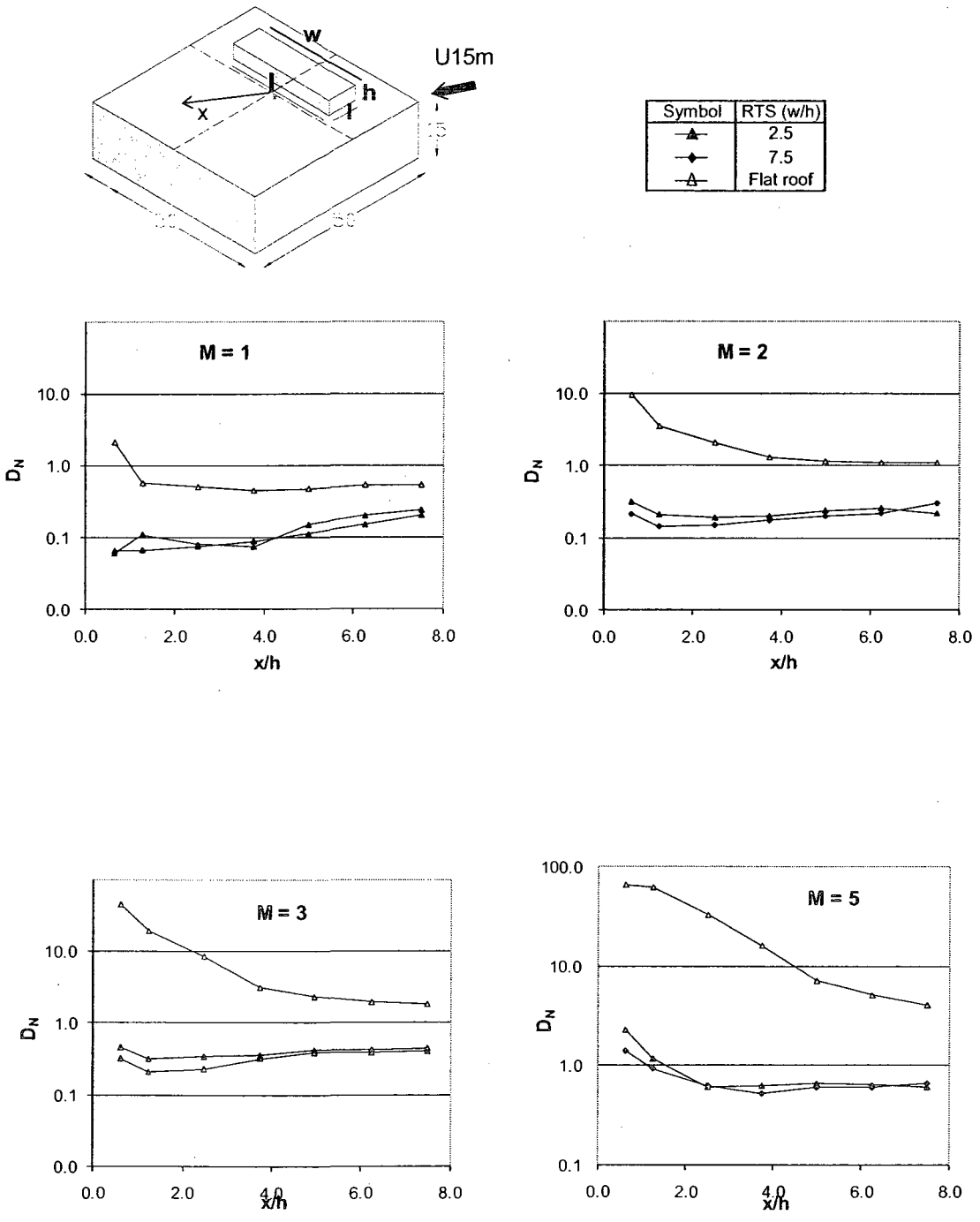

Figure E6 Effect of RTS cross-wind width on minimum dilution values for the low-rise building for stack height $h_s = 0.25h$, $\theta = 45°$, h = 4 m, and M = 1, 2, 3, and 5.

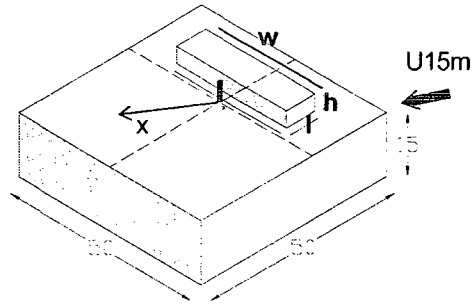

Symbol	RTS (w/h)
	2.5
	5.0
	7.5
	10.0
	12.5
	Flat roof

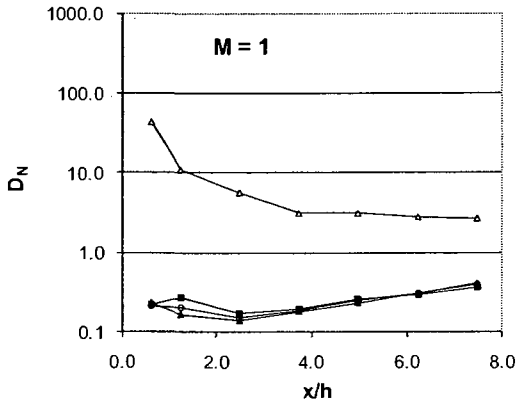

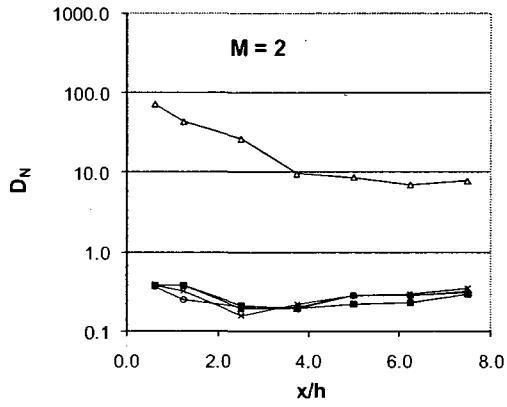

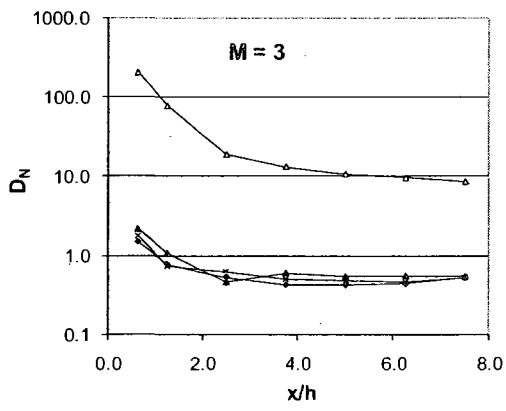

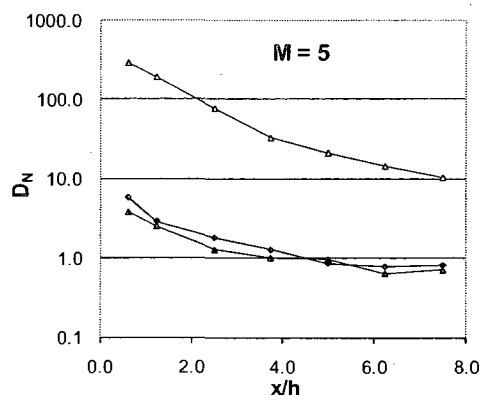

Figure E7 Effect of RTS cross-wind width on minimum dilution values for the low-rise building for stack height $h_s = 0.75h$, $\theta = 45°$, h = 4 m, and M = 1, 2, 3, and 5.

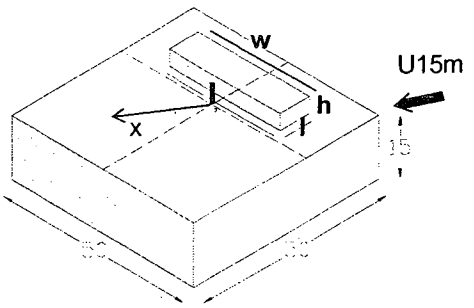

Symbol	RTS (w/h)
	2.5
	5.0
	7.5
	10.0
	12.5
	Flat roof

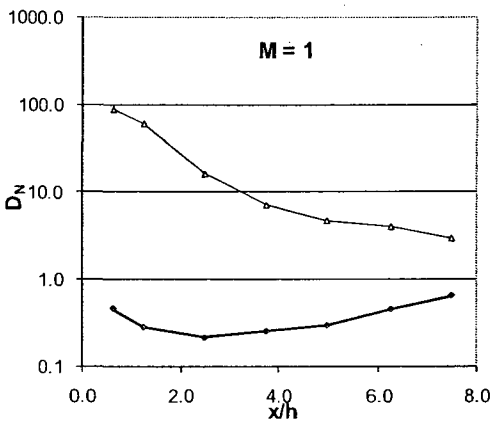

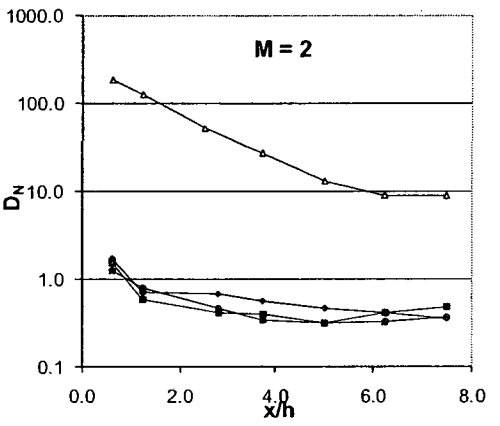

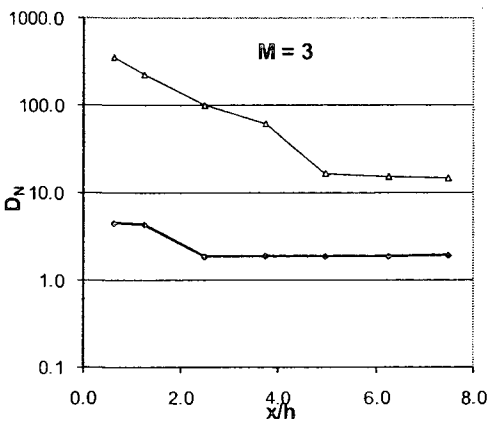

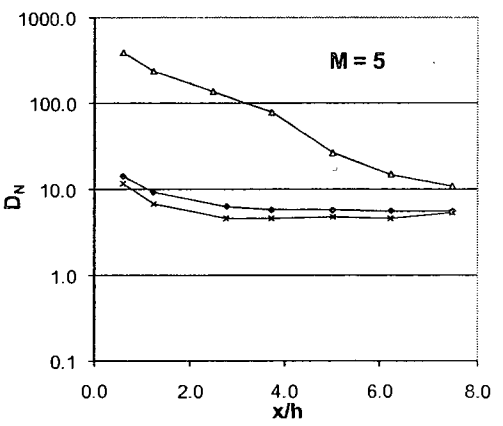

Figure E8 Effect of RTS cross-wind width on minimum dilution values for the low-rise building for stack height $h_s = 1.25h$, $\theta = 45°$, h = 4 m, and M = 1, 2, 3, and 5.

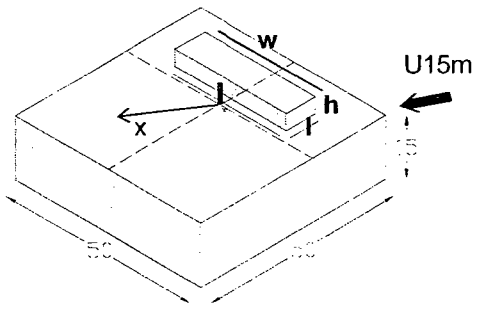

Symbol	RTS (w/h)
—◆—	7.5
—△—	Flat roof

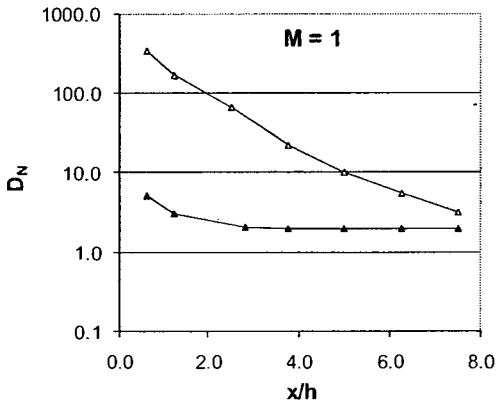

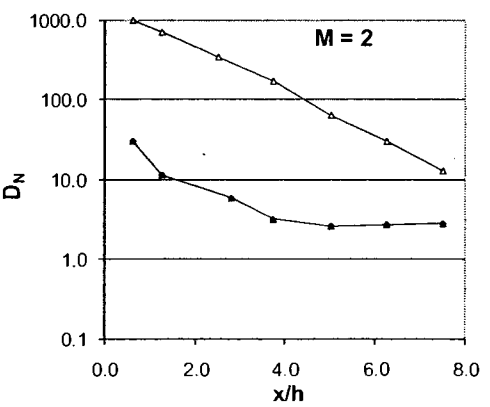

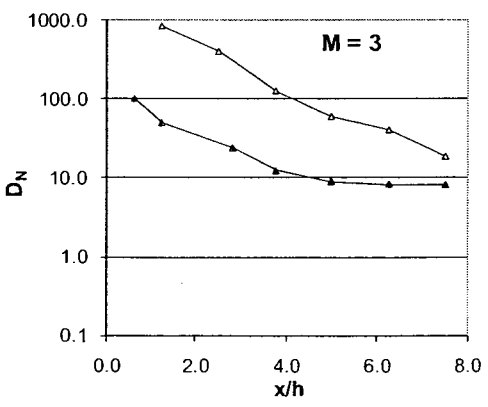

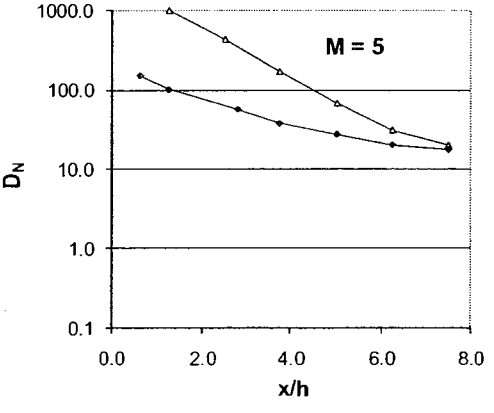

Figure E9 Effect of RTS cross-wind width on minimum dilution values for the low-rise building for stack height $h_s = 1.75h$, $\theta = 45°$, $h = 4$ m, and $M = 1$, 2, 3, and 5.

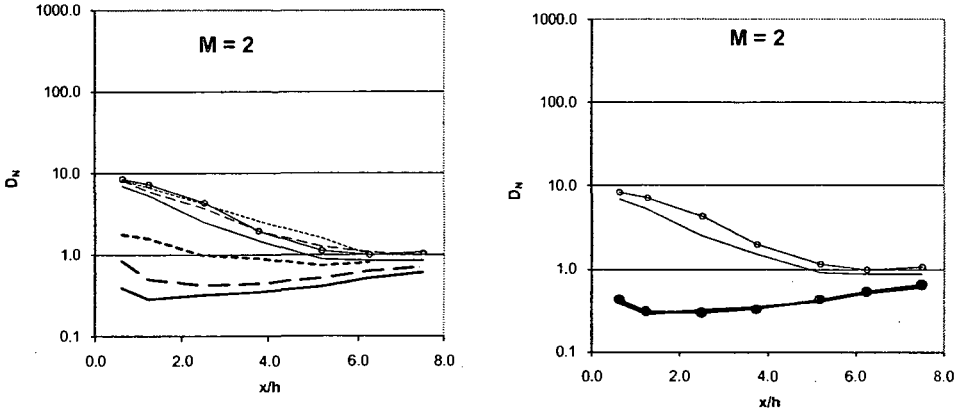

Figure E10 Effect of separation distance between stack and RTS for the low-rise building; $h_s = 0.75h$, $\theta = 0°$, w/h = 7.5, h = 4 m, and M = 2

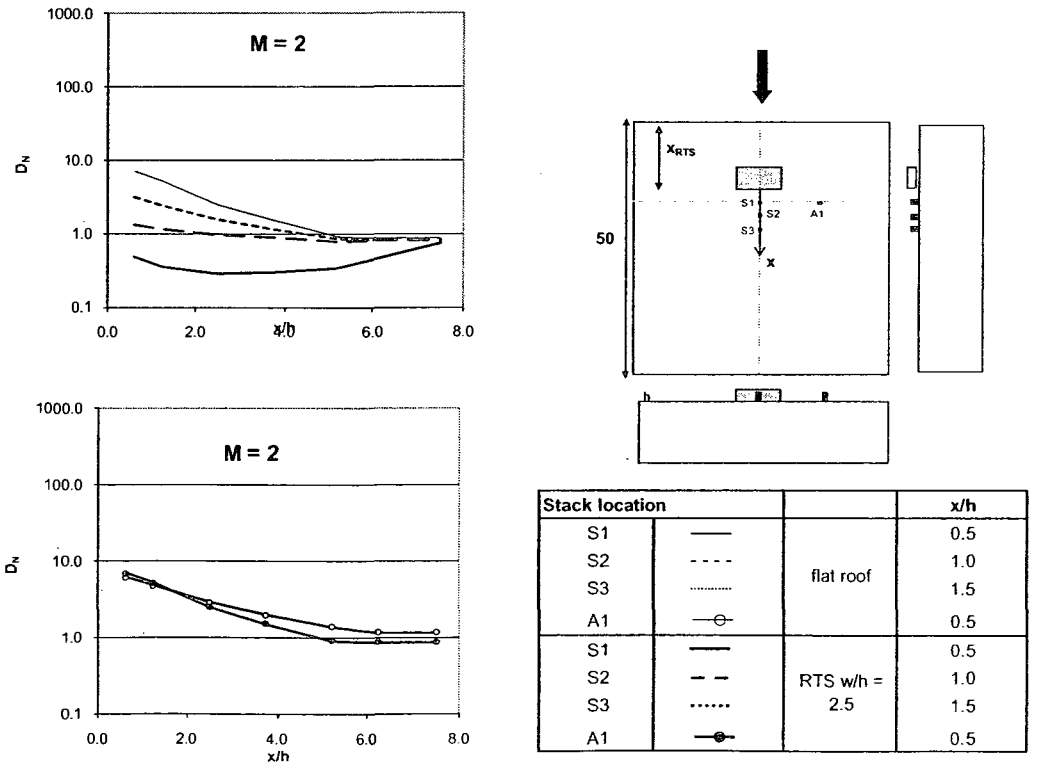

Figure E11 Effect of separation distance between stack and RTS for the low-rise building; $h_s = 0.75h$, $\theta = 0°$, w/h = 2.5, h = 4 m, and M = 2

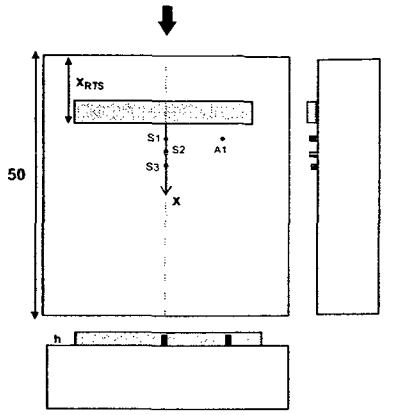

x_{RTS} = 18m

Stack location			x_s
S1	——	No RTS	0.5h
S2	- - - -		h
S3	.....		1.5h
A1	—○—		0.5h
S1	——	RTS w/h = 7.5	0.5h
S2	– –		h
S3	.....		1.5h
A1	—●—		0.5h

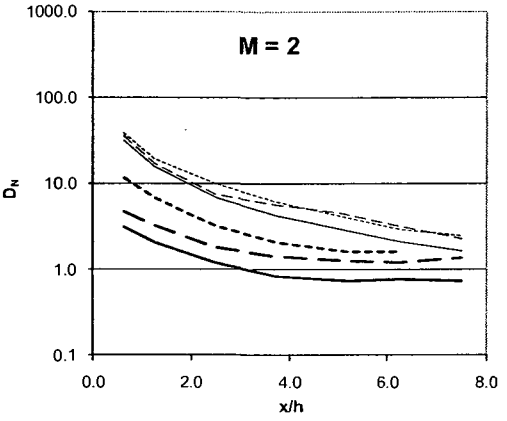

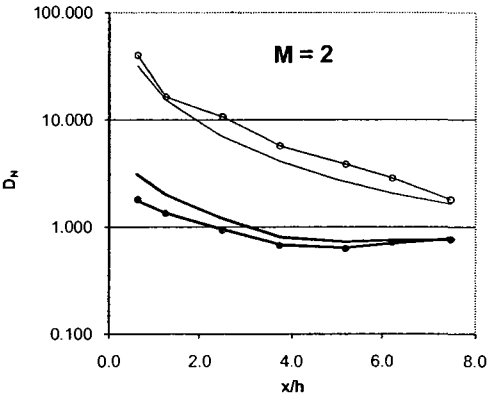

Figure E12 Effect of separation distance between stack and RTS for the low-rise building; h_s = 1.25h, θ = 0°, w/h = 7.5, h = 4 m, and M = 2

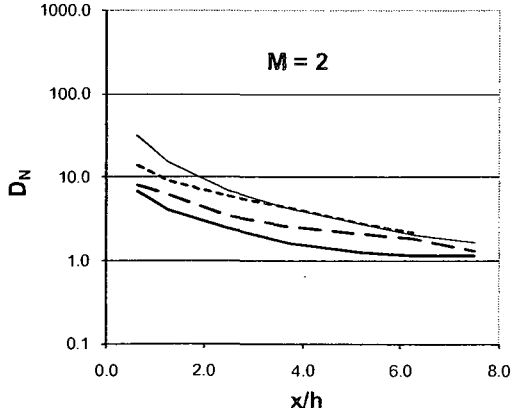

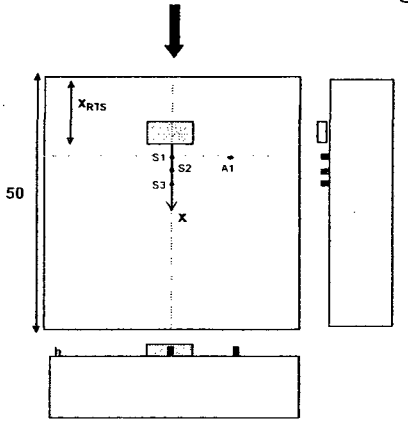

Stack location		RTS (w/h)	x/h
S1	——	flat roof	0.5
S1	——	RTS w/h = 2.5	0.5
S2	– –		1.0
S3	.....		1.5

Figure E13 Effect of separation distance between stack and RTS for the low-rise building; h_s = 1.25h, θ = 0°, w/h = 2.5, h = 4 m, and M = 2

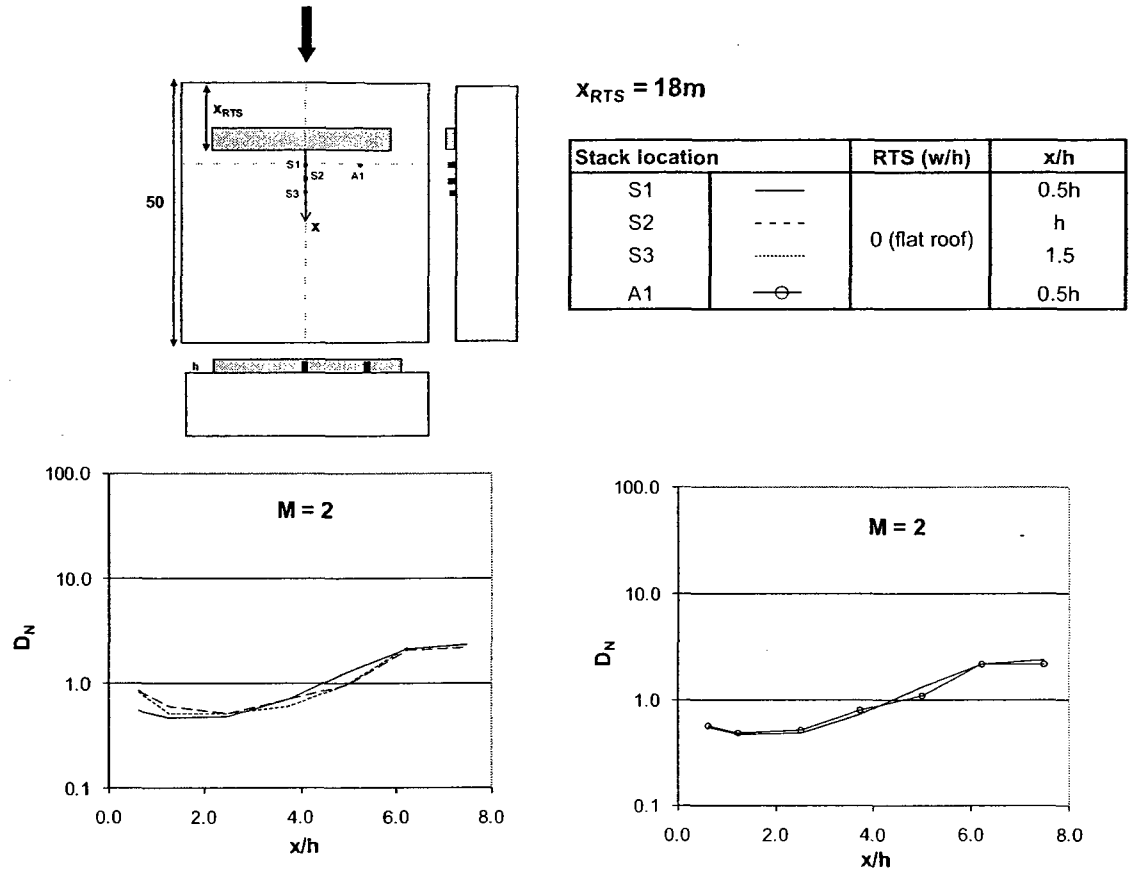

Figure E14 Effect of separation distance between stack and RTS for the high-rise building; h_s = 0.75h, $\theta = 0°$, w/h = 7.5, h = 4 m, and M = 2

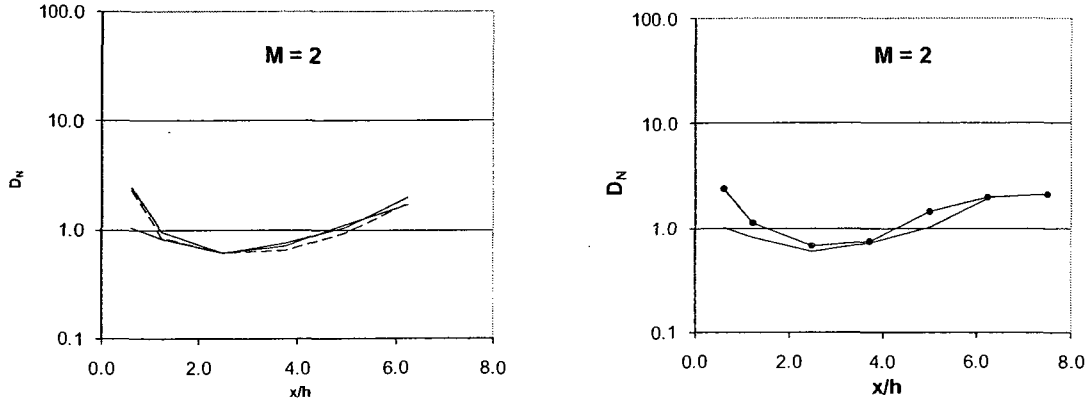

Figure E15 Effect of separation distance between stack and RTS for the high-rise building; h_s = 1.25h, 0°, w/h = 7.5, h = 4 m, and M = 2

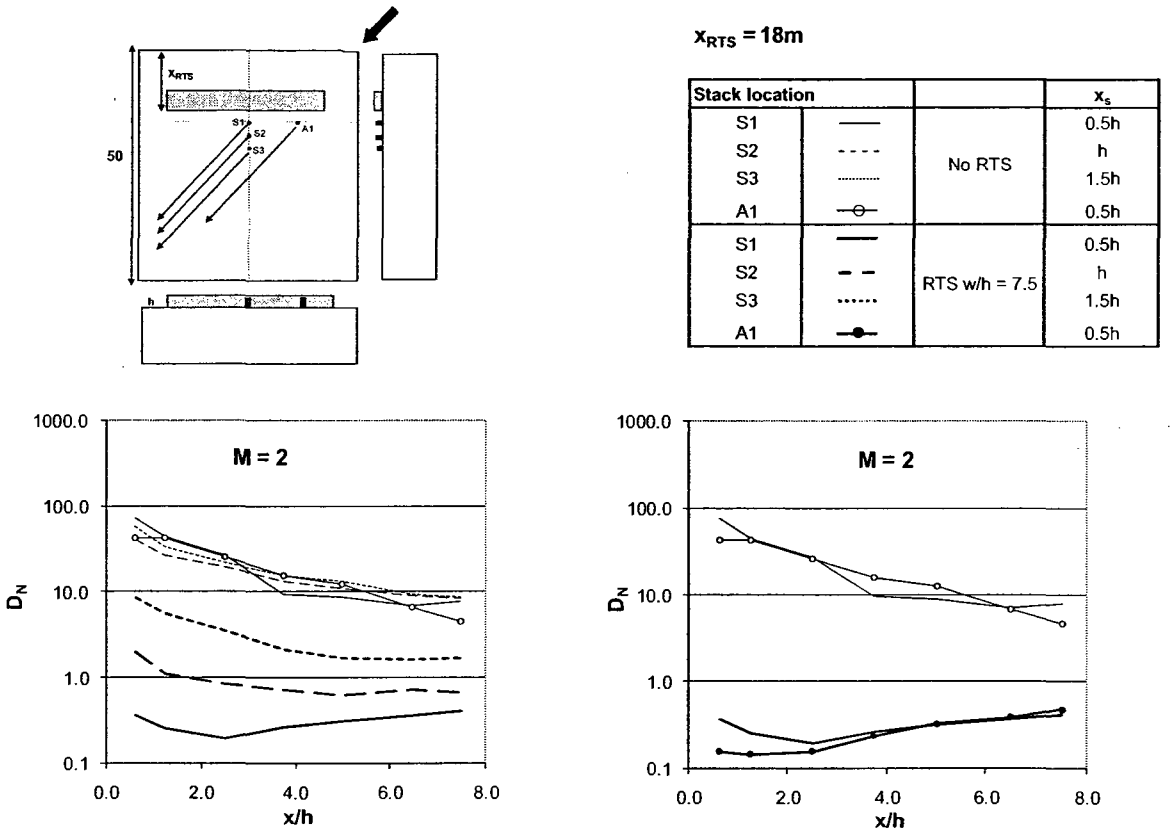

Figure E16 Effect of separation distance between stack and RTS for the low-rise building; h_s = 0.75h, θ = 45°, w/h = 7.5, h = 4 m, and M = 2

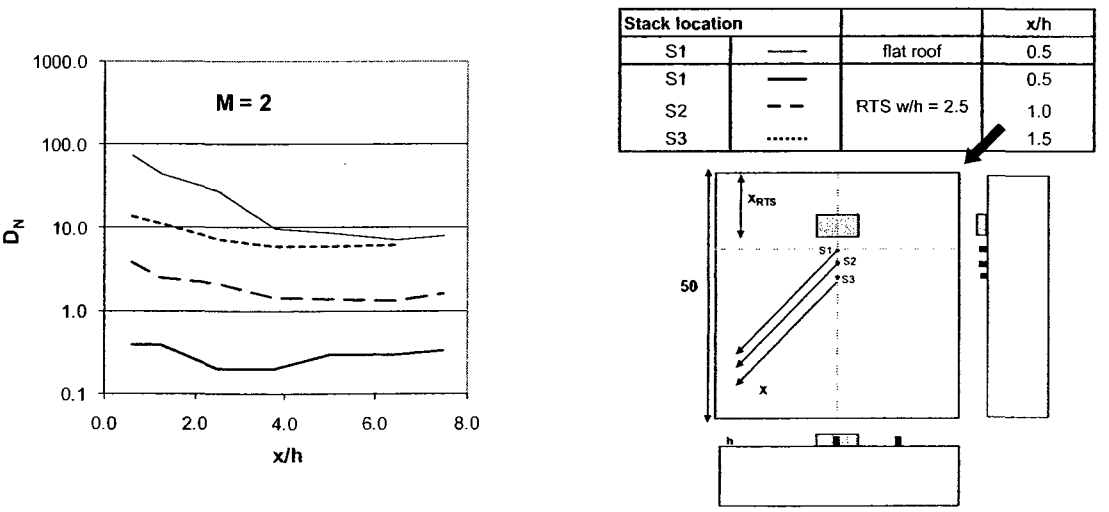

Figure E17 Effect of separation distance between stack and RTS for the low-rise building; h_s = 0.75h, θ = 45°, w/h = 2.5, h = 4 m, and M = 2

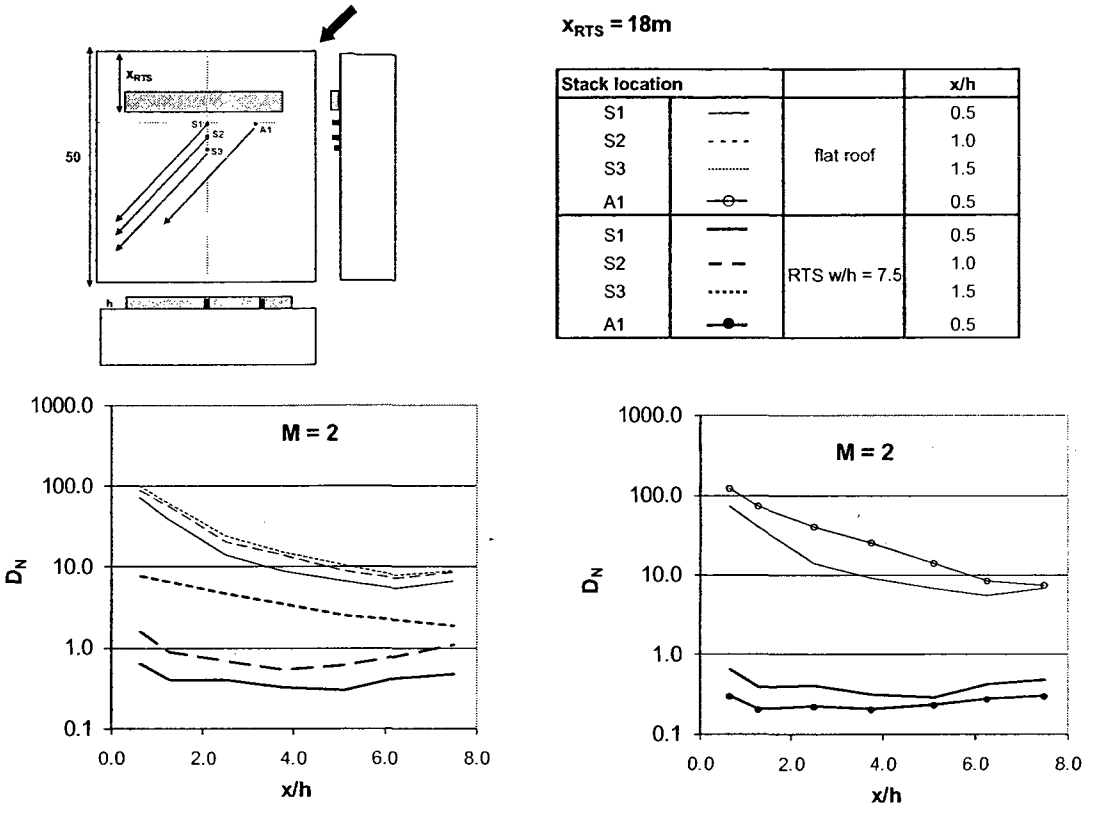

Figure E18 Effect of separation distance between stack and RTS for the high-rise building; h_s = 0.75h, θ = 45°, w/h = 7.5, h = 4 m, and M = 2

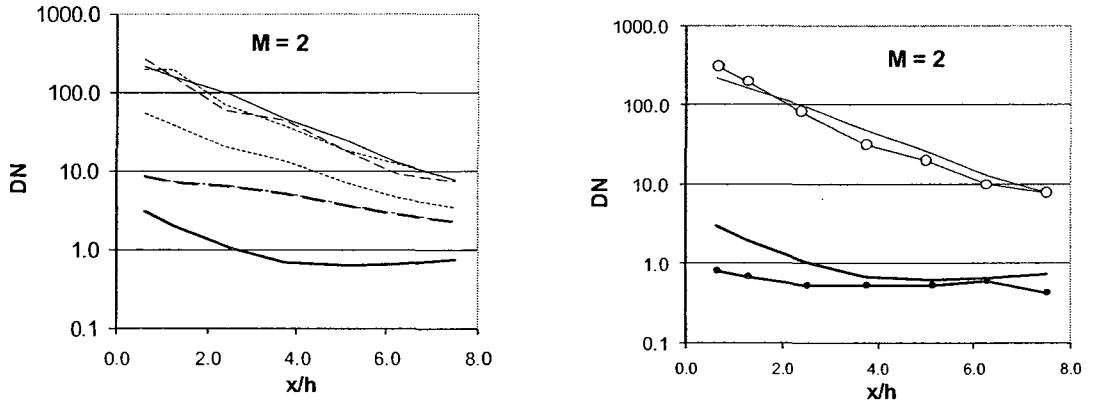

Figure E19 Effect of separation distance between stack and RTS for the high-rise building; h_s = 1.75h, θ = 45°, w/h = 7.5, h = 4 m, and M = 2

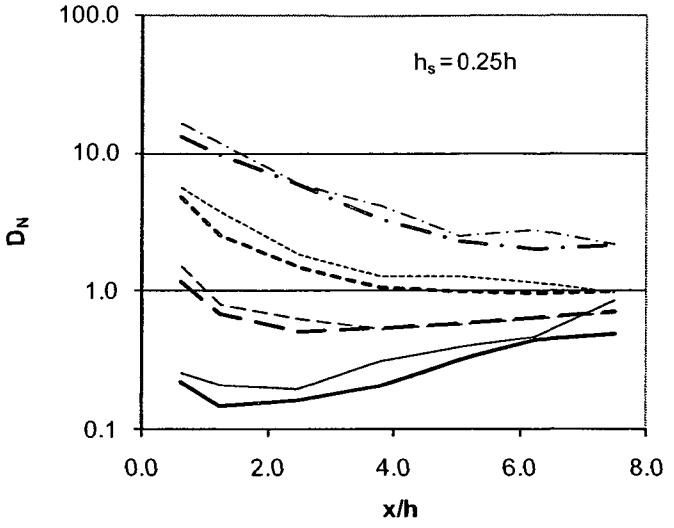

Bldg width	Symbol	M
W = 50m	———	1
	— —	2
	.....	3
	— · ·	5
W = 30m	———	1
	— — —	2
	- - - - -	3
	· · · · ·	5

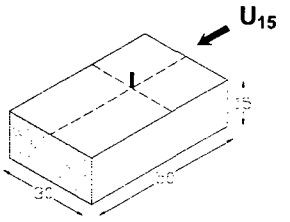

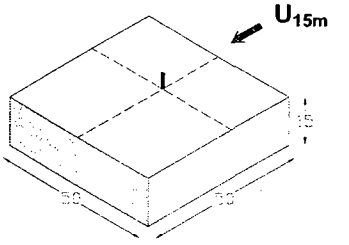

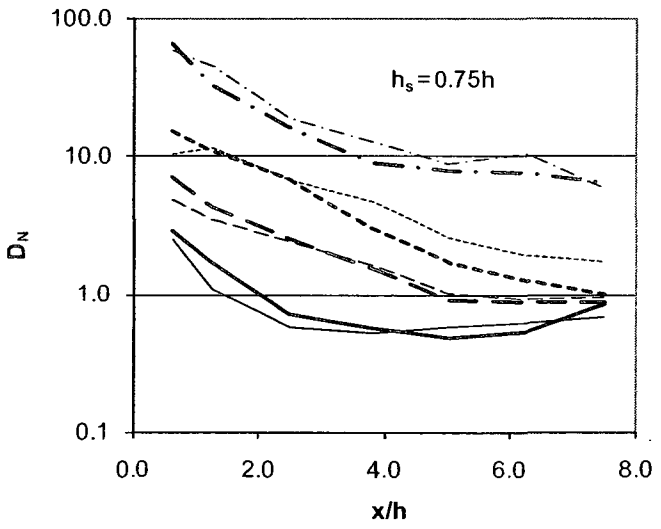

Figure E20 Effect of building cross-wind width on minimum dilution values for the low-rise building with no RTS for $h_s = 0.25h$ and $0.75h$: $\theta = 0°$, $h = 4$ m, and $M = 1, 2, 3$, and 5

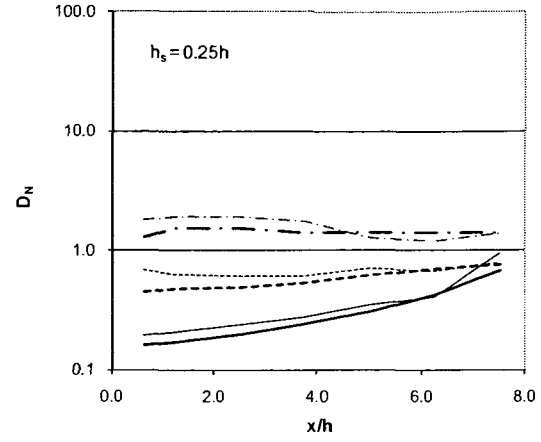

Bldg width	Symbol	M
W = 50m	———	1
	— —	2
	.....	3
	— · ·	5
W = 30m	———	1
	— — —	2
	- - - - -	3
	— · · ·	5

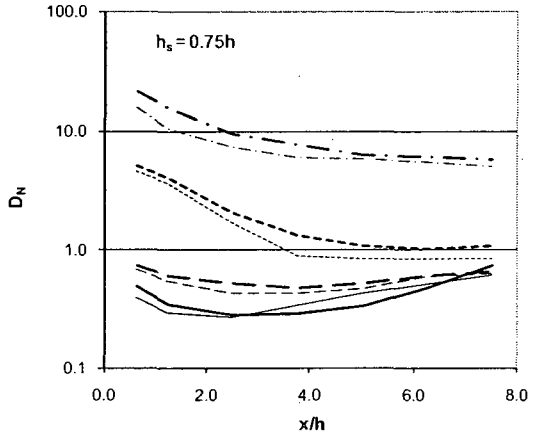

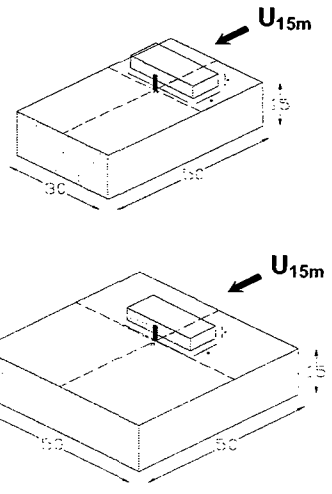

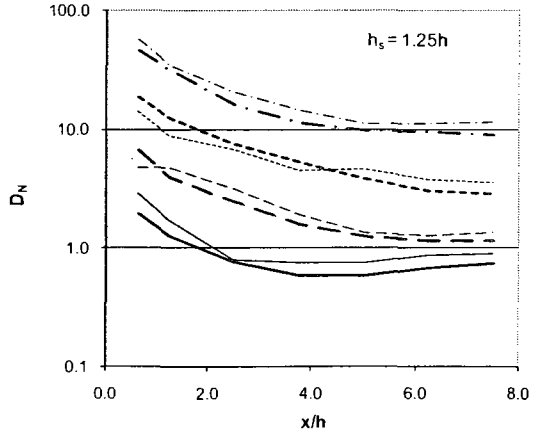

Figure E21 Effect of building cross-wind width on minimum dilution values for the low-rise building with RTS (w/h = 5) for h_s = 0.25h to 1.25h: $\theta = 0°$, h = 4 m, and M = 1, 2, 3, and 5

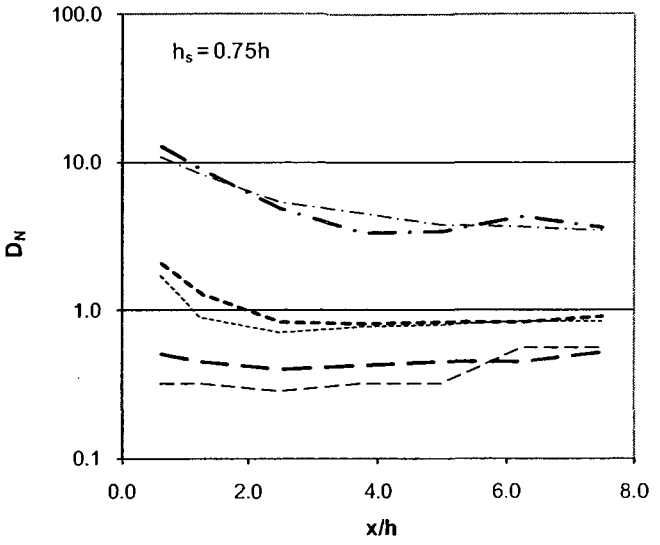

Bldg width	Symbol	M
W = 50m		
		2
		3
		5
W = 30m		
		2
		3
		5

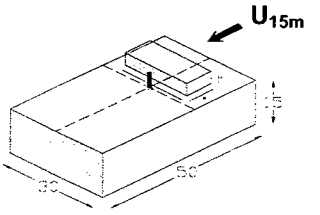

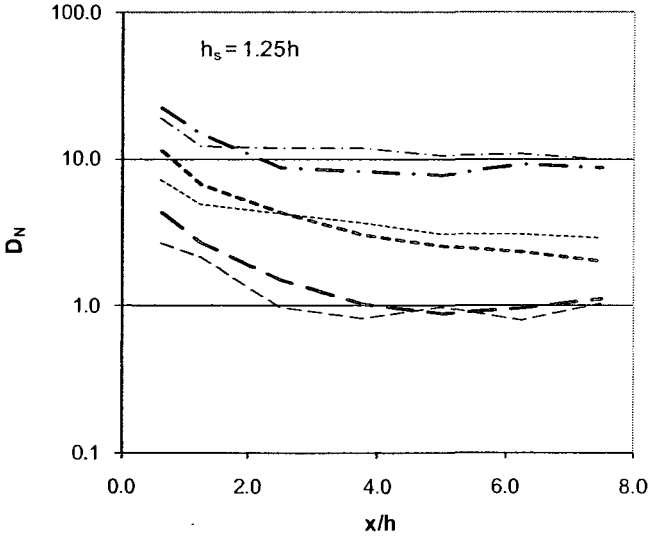

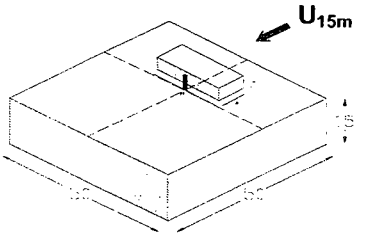

Figure E22 Effect of building cross-wind width on minimum dilution values for the low-rise building with RTS (w/h = 5) for $h_s = 0.75h$ and 1.25h: $\theta = 0°$, h = 4 m, and M = 2, 3, and 5

APPENDIX F

Validation of proposed model with results from previous studies for $M > 3$ and $h_s < 3$ m

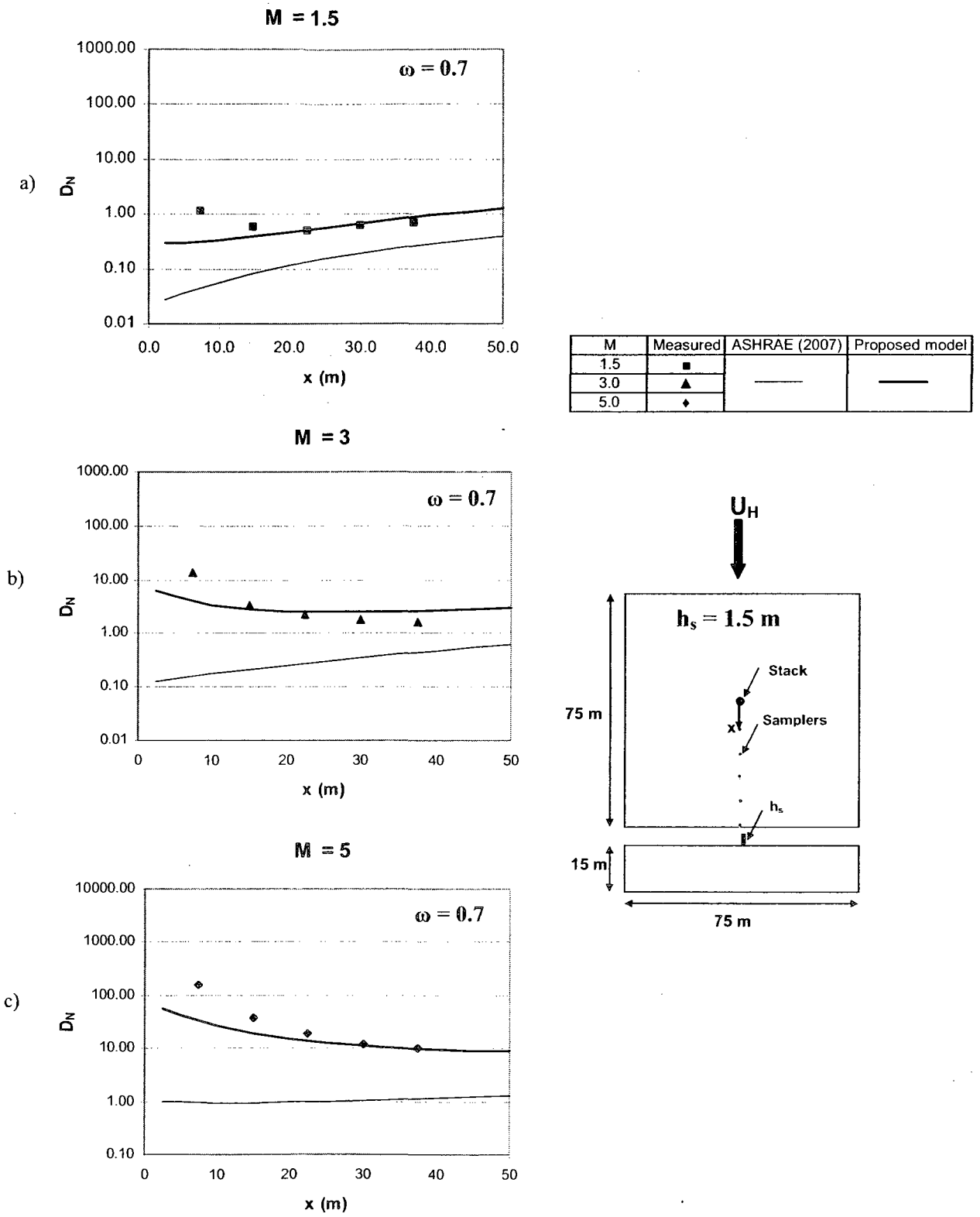

Figure F1 Model validations with Schulman and Scire (1991) wind-tunnel data for the flat-roofed low-rise building for h_s = 1.5 m and θ = 0°: a) M = 1.5; b) M = 3; and c) M = 5.

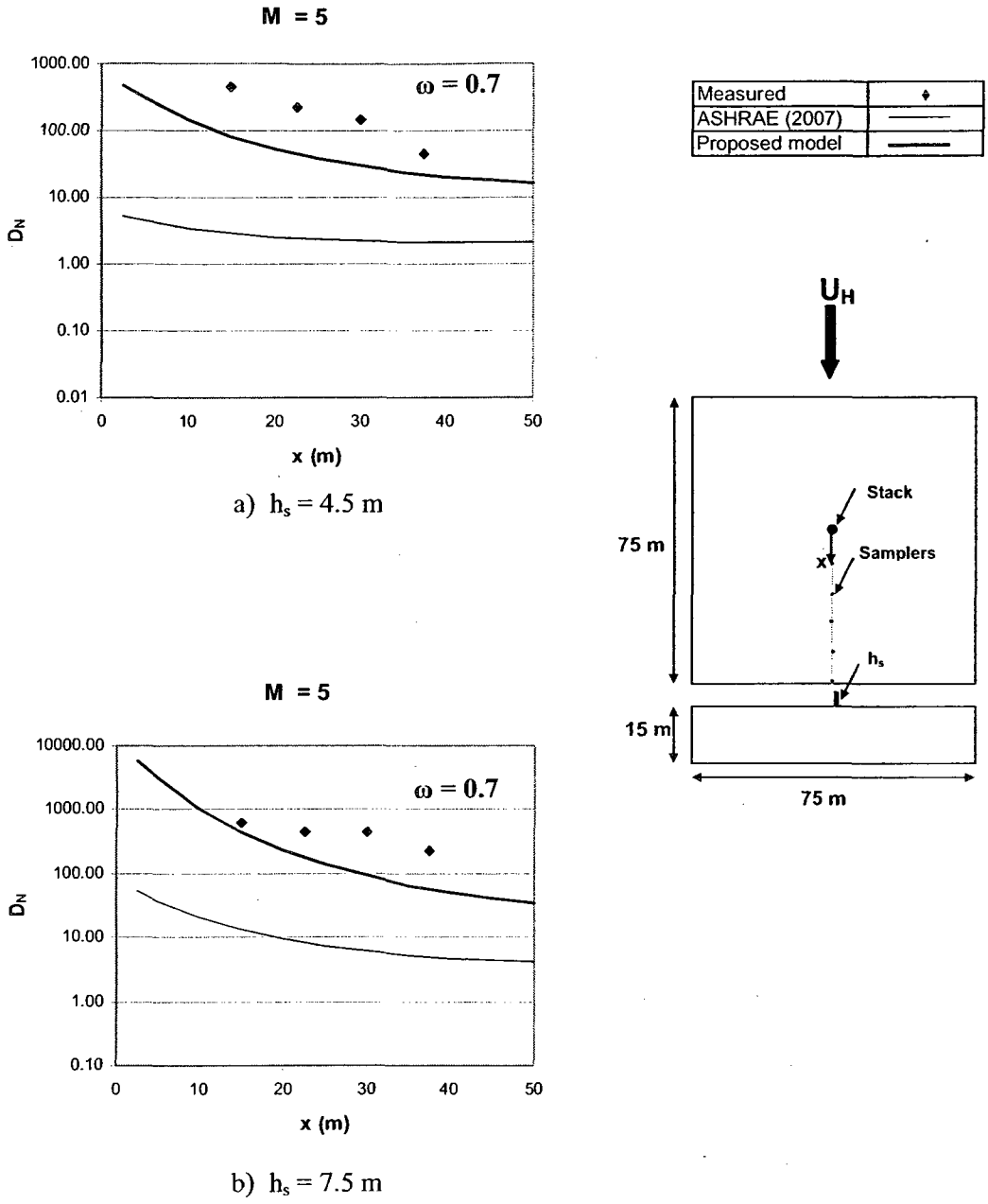

a) $h_s = 4.5$ m

b) $h_s = 7.5$ m

Figure F2 Model validations with Schulman and Scire (1991) wind-tunnel data for the flat-roofed low-rise building for M = 5 m and $\theta = 0°$: a) $h_s = 4.5$ m; and b) $h_s = 7.5$ m

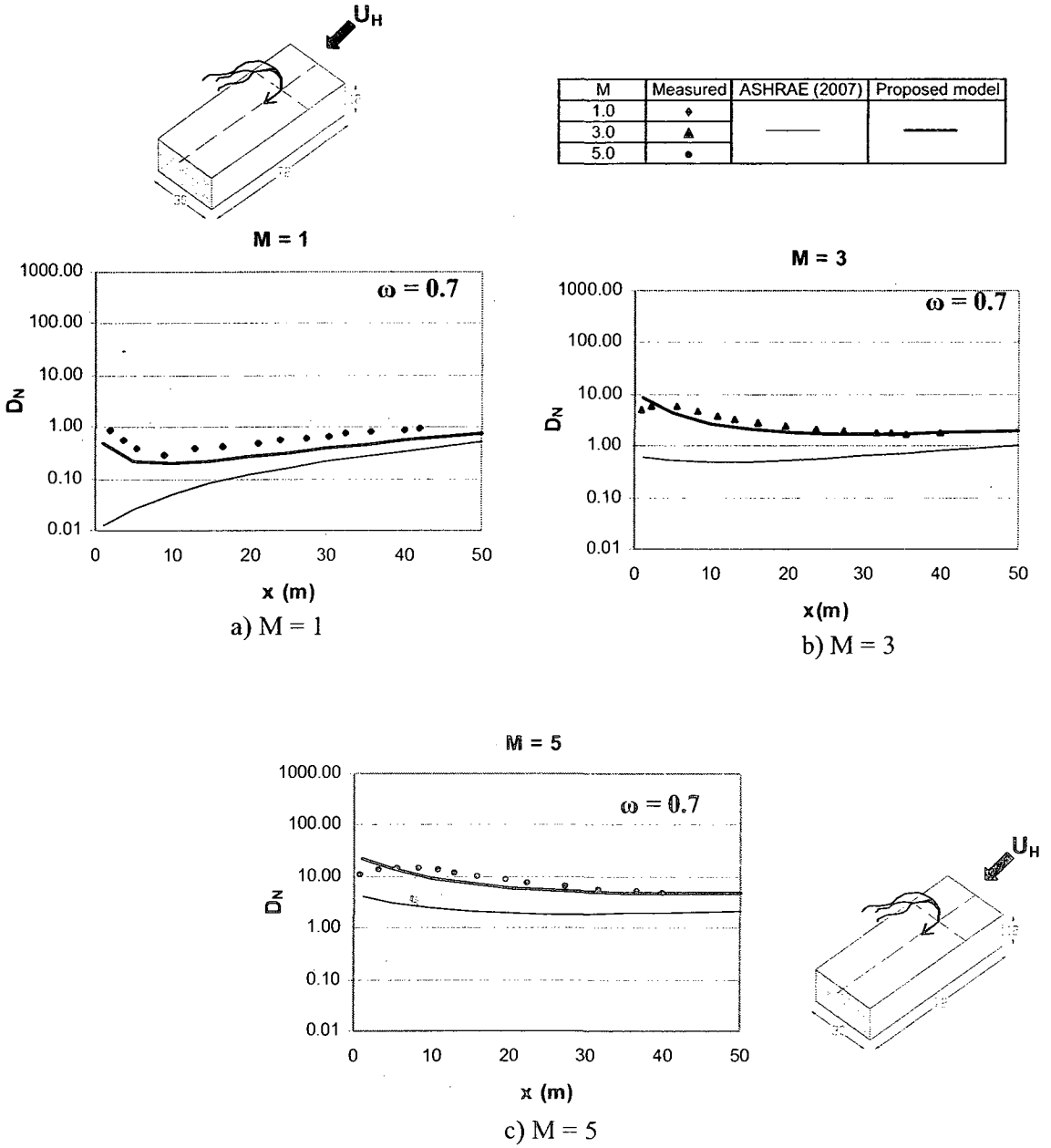

Figure F3 Model validations with Wilson et al. (1998) water flume data for the flat-roofed low-rise building for h_s = 2 m and $\theta = 0°$: a) M = 1; b) M = 3; and c) M = 5.

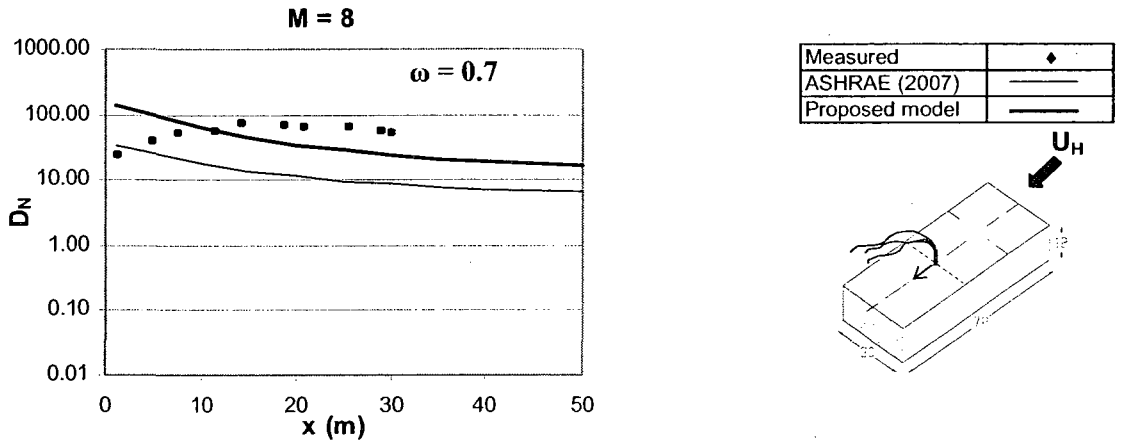

Figure F4 Model validations with Wilson et al. (1998) water flume data for the flat-roofed low-rise building for M = 8, h_s = 3 m, and θ = 0°.

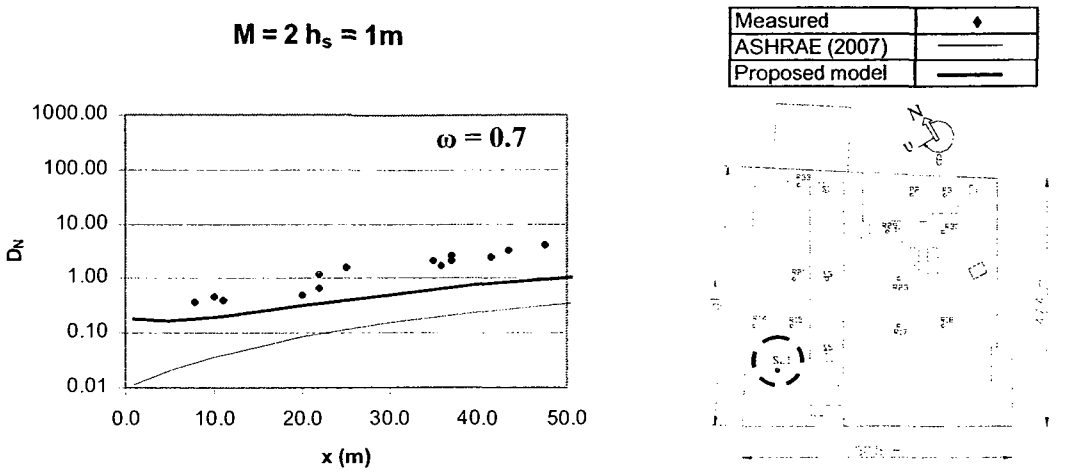

a) Oct. 12, 2000: θ = 291°–297°

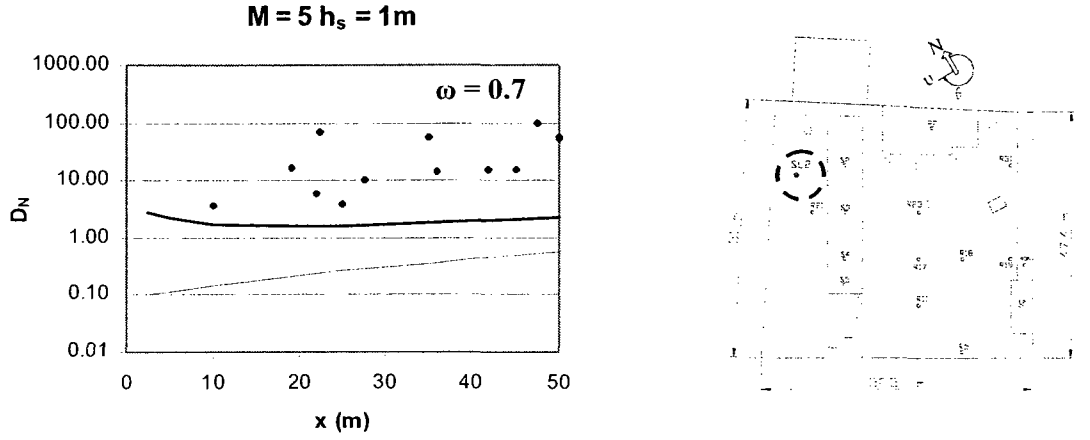

b) June 28, 2001: θ = 293°–300°

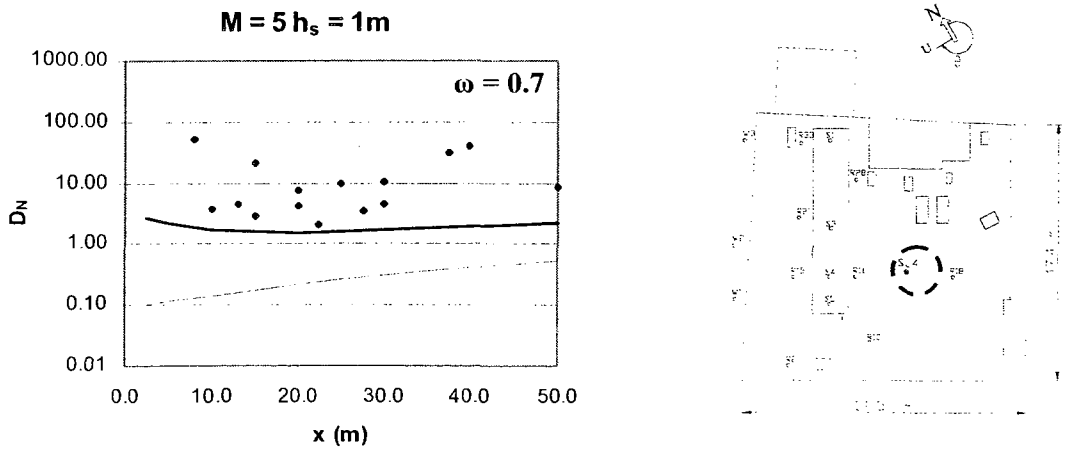

c) Nov. 21, 2003: θ = 150°–170°

Figure F5 Model validations with Stathopoulos et al. (2003) for the low-rise building for h_s = 1 m: a) SL1, M = 2; b) SL2, M = 5; and c) SL4, M = 5.

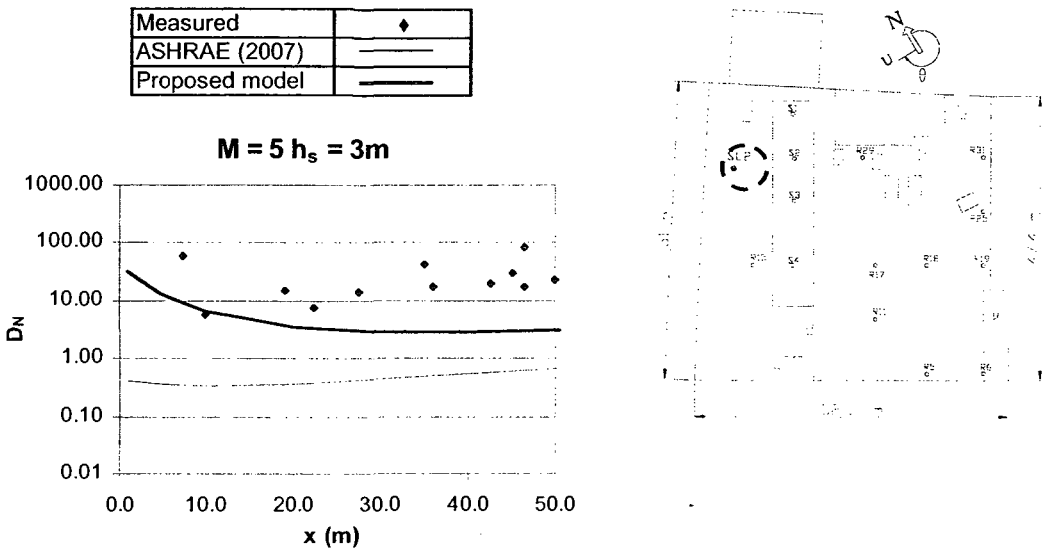

Figure F6 Model validations with Stathopoulos et al. (2003) field test Oct. 30, 2001: $\theta = 298°–313°$ f or the low-rise building for $h_s = 3$ m, M = 5, and SL2.

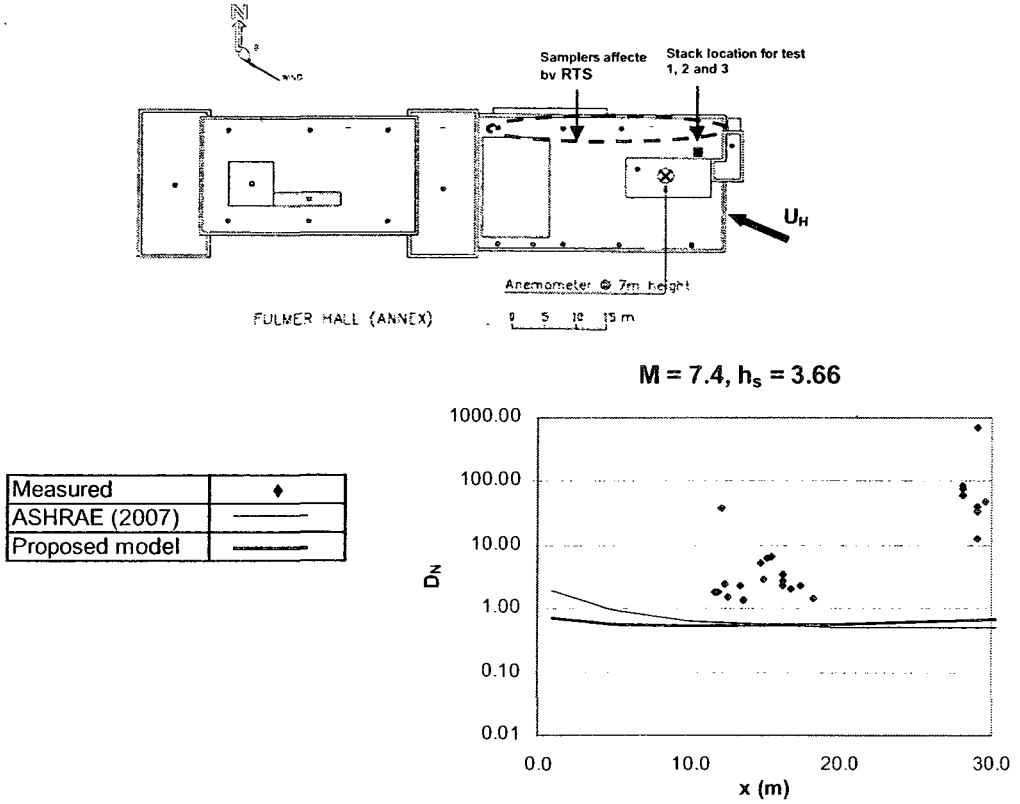

Figure F7 Model validations with Wilson and Lamb (1994) field test 3for a low-rise building with an RTS upwind of stack: $\theta = 113°–124°$, $h_s = 3.66$ m, and M = 7.4.

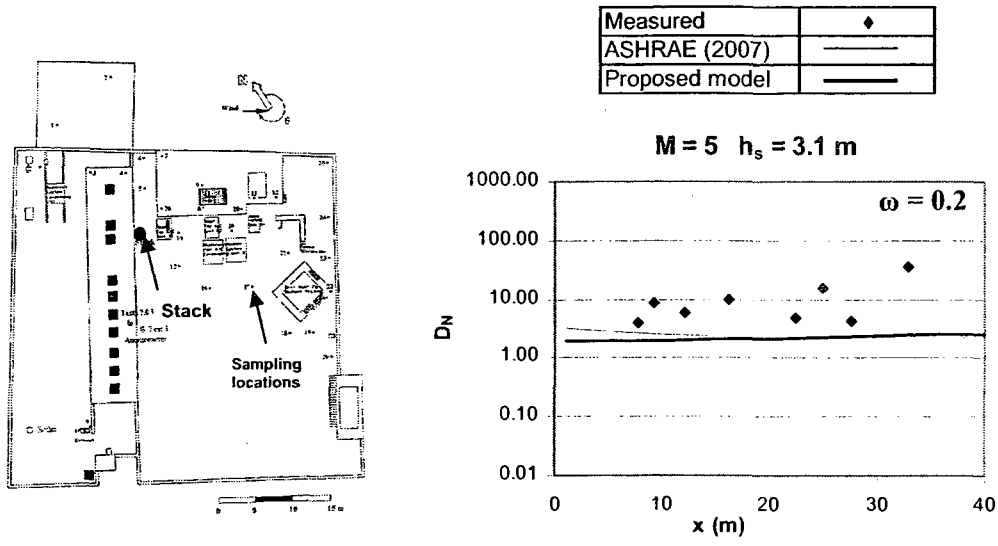

Figure F8 Model validations with field data from Saathoff et al. (2002) for a low-rise building, h_s = 3.1 m and M = 5.

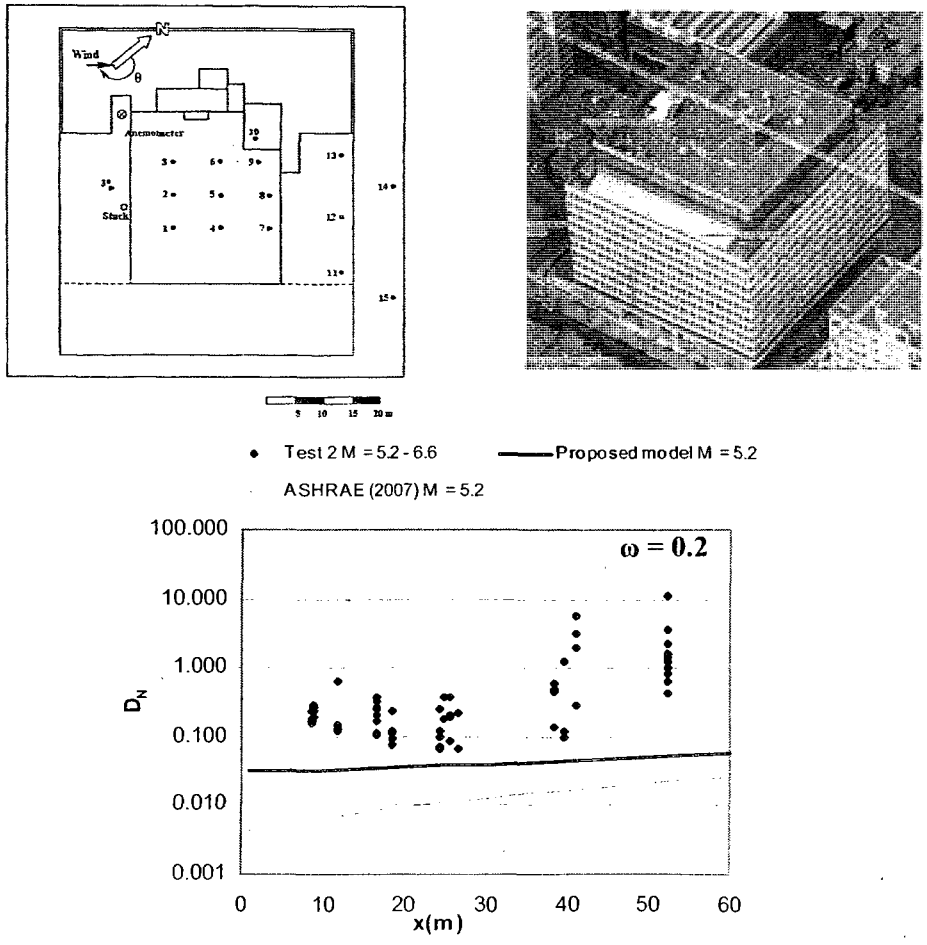

Figure F9 Model validations with Stathopoulos et al. (1997) field test 2 for the high-rise building: θ = 150°–170°, h_s = 0.5 m and M = 5.2–6.6.